Formula SAE Monocoque Chassis Development

KC Egger kdegger@calpoly.edu

Brian Ford bgford@calpoly.edu

Kyle Nagao ktnagao@calpoly.edu

Neal Sharma nrsharma@calpoly.edu

Donovan Zusalim dzusalim@calpoly.edu

Sponsored by:

Faculty Advisor: John Fabijanic

Project Advisor: Dr. Joseph Mello

Mechanical Engineering Department

California Polytechnic State University, San Luis Obispo

Statement of Disclaimer

Since this project was a result of a class assignment, it has been graded and accepted as fulfillment of the course requirements. Acceptance does not imply technical accuracy or reliability. Any use of information in this report is done at the risk of the user. These risks may include catastrophic failure of the device or infringement of patent or copyright laws. California Polytechnic State University at San Luis Obispo and its staff cannot be held liable for any use or misuse of the project.

This project was made possible by generous donations from companies and individuals alike. We would like to express our sincere gratitude to these sponsors, who have allowed our project to flourish by providing materials, services, and technical knowledge.

We would also like to thank the members of the 2019-2020 Cal Poly Racing team for their help. We hope that this report will help you succeed in future race seasons!

Abstract

Formula SAE is a collegiate competition hosted by SAE International with the primary goal being to design, manufacture, and race an open wheel race car. The Cal Poly Racing Formula SAE team strives for improvement every race season and has remained competitive as a result. The 2019-2020 management team determined that further research and development towards the chassis would yield the greatest performance benefit for future seasons, as the previous chassis platform limited packaging and mounting options for vehicle subsystems which interfaced with the chassis.

A redesign of the Cal Poly Racing Formula SAE team's carbon fiber reinforced polymer monocoque chassis was requested to improve subsystem integration, increase torsional stiffness, and reduce weight compared to the previous platform. Specifically, this senior project team focused on manufacturing process improvement and laminate design to meet these goals for the 2020 Formula SAE competition.

This report details the design and manufacturing of such a chassis. Specific emphasis was placed on the geometry, laminate, and manufacturing process design. The geometry was designed using subsystem input for satisfactory integration of all subsystem components while maintaining a high specific torsional stiffness. The team also developed numerous analysis tools including spreadsheets and finite element models to design the asymmetric laminate of the chassis. Modular, multi-piece tooling was designed to produce a single-piece chassis and to allow for easy geometric changes in the future.

Though two complete chassis were delivered to the Formula SAE team, the outbreak of COVID-19 prevented the collection of data that would have been used to validate the design. However, the Formula SAE team was made aware of the validation plan proposed in this report.

Table of Contents

List of Figures

List of Tables

Introduction

Formula SAE is an annual collegiate design series in which student teams design, build, and race open-wheeled race cars like the vehicle shown in **Figure 1**. The competition consists of both static and dynamic events, testing the team's knowledge of design, cost, and business as well as the vehicles' skid pad, acceleration, autocross, and endurance capabilities. The Cal Poly Racing Formula SAE (CPFSAE) team currently participates in the electric and combustion series and was scheduled to compete at Formula SAE California in Fontana for the 2020 season. The members of this senior project, Formula SAE Monocoque Chassis Development (MCD), sought to improve the team's overall performance in both the static and dynamic events by creating an improved chassis platform for the 2019-2020 and future teams.

Figure 1. The 2018 CPFSAE combustion car pictured during Formula SAE Lincoln 2018.

The previous chassis platform, pictured in **Figure 2**, was designed by the 2017 senior project team *Carbon Fiber Monocoque Chassis Platform for Formula SAE and Formula SAE Electric Race Cars* [1]. The platform was used for three seasons, by both the combustion (CP20C) and electric (CP20E) vehicles. The technical advancements of the previous chassis platform brought significant improvement to the CPFSAE team, but to further the growth of the team, new chassis and laminate development was requested. Refreshing the chassis geometry allowed for subsystem input, encouraging new and improved designs. In general, greater understanding of carbon fiber reinforced polymer (CFRP) laminate analysis aided in the design of the structurally regulated regions and allowed for the faster production of a race-ready chassis. Development of the manufacturing methods also greatly benefitted the team, both in the physical aspect of quicker manufacturing and a more efficient laminate design, and in the education of the members and the progression of the team's understanding of composite structures.

Figure 2. 2017-2019 chassis platform developed by *Carbon Fiber Monocoque Chassis Platform for Formula SAE and Formula SAE Electric Race Cars* senior project team.

Background

Though monocoque chassis are a common design in the automotive industry, their use in Formula SAE competitions is limited. Many Formula SAE chassis are constructed from metallic tubing as the fabrication and analysis are not as complex. The Formula SAE rules are well-governed for these tube-frame chassis, but an alternative set of rules is used for teams that wish to run a monocoque or a hybrid of the two. All teams must pass a pre-made document called the Structural Equivalency Spreadsheet (SES), but SES for monocoques is much more involved and requires a design to be equal in strength and safety to a metallic chassis. This arduous process, coupled with more difficult manufacturing and analysis, makes the concept of a monocoque chassis unappealing to many teams. However, if implemented successfully, a monocoque chassis can offer significant performance gains when compared to a traditional tube-frame chassis.

Points Analysis

The 2020 team targeted a top-three finish. Based on historical data and the trendlines included in **Figure 3**, this would require obtaining over 800 points with the combustion car and 750 points with the electric car.

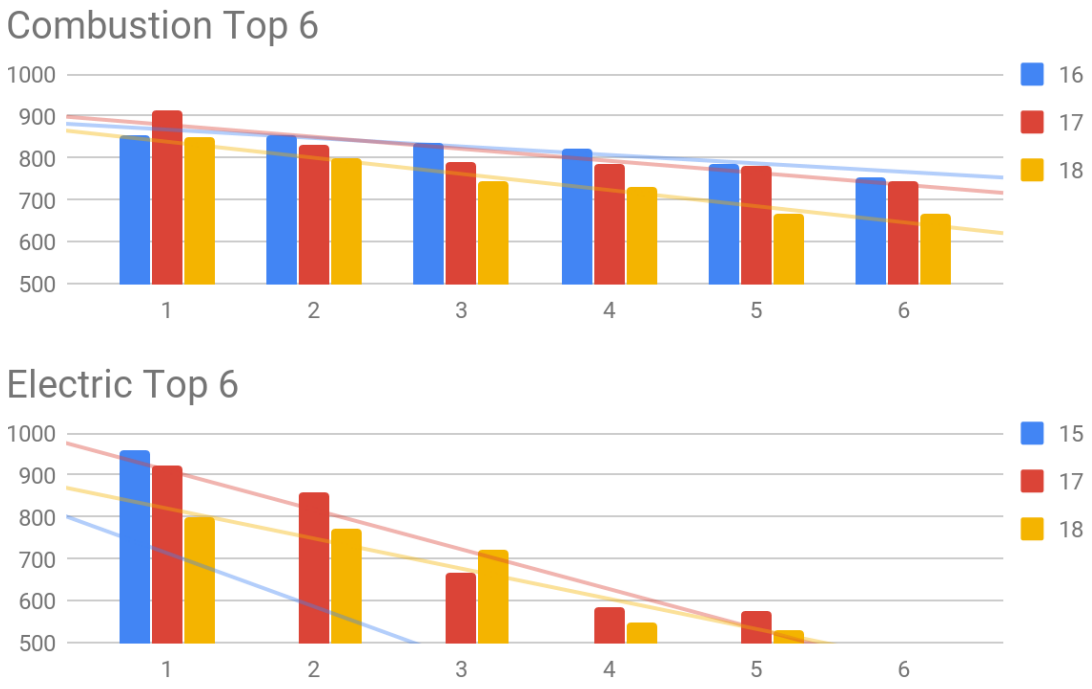

Figure 3. Historic points obtained per position in 2016, 2017, and 2018 Formula SAE Lincoln competitions.

Using the team's 2018 result as a baseline, this would require obtaining an additional 238 points and 558 points for the combustion and electric cars, respectively. However, it is important to know that in 2018 the combustion car did not complete in autocross due to a part failure, resulting in the loss of approximately 85 points. The 2018 electric car did not pass technical inspection in time and did not compete in any dynamic events, resulting in the loss of an estimated 540 points. Assuming the 2019 and 2020 cars could have competed in all dynamic events, the team identified 2 key areas requiring improvement to reach the point targets. The point sensitivities of each dynamic event are shown in **Table 1**.

Table 1: Team Point Sensitivities

Goal	Car	Sensitivity
Cut weight	Combustion	- Losing 33.4 lbs: 5 pts gained in endurance, 4 pts in autocross ~ 9 pts total
	Electric	-Losing 22.7 lbs: 3 pts gained in endurance, 2 pts in autocross ~ 5 pts total
Decrease dynamic times	Combustion	-Acceleration event: (47 pts/sec gained) -Skidpad event: (33 pts/sec gained) -Autocross event: (4.9 pts/sec gained) -Endurance event: (6.6 pts/sec gained each lap)
	Electric	-Acceleration event: (47 pts/sec gained) -Skidpad event: (41 pts/sec gained) -Autocross event: (4.5 pts/sec gained) -Endurance event: (5.5 pts/sec gained each lap)

Carbon Fiber Sandwich Panel Laminae

To produce a high stiffness to weight ratio, carbon fiber honeycomb sandwich panels are typically used in the design of monocoque chassis. Honeycomb sandwich panels like the specimen shown in **Figure 4** are also widely used in the aerospace industry due to the high specific stiffness that can be achieved with proper laminate design.

Figure 4. Example of a honeycomb core sandwich panel.

The honeycomb core between two fiber composite laminate skins acts like the web of an I-beam, taking the shear load and spacing apart the two outer skins. The two outer skins are subjected to bending stresses, with one skin placed under a compressive load and the other supporting the tensile loads. **Figure 5** visually shows the physical analog between a composite sandwich panel and a traditional I-beam made of an isotropic material.

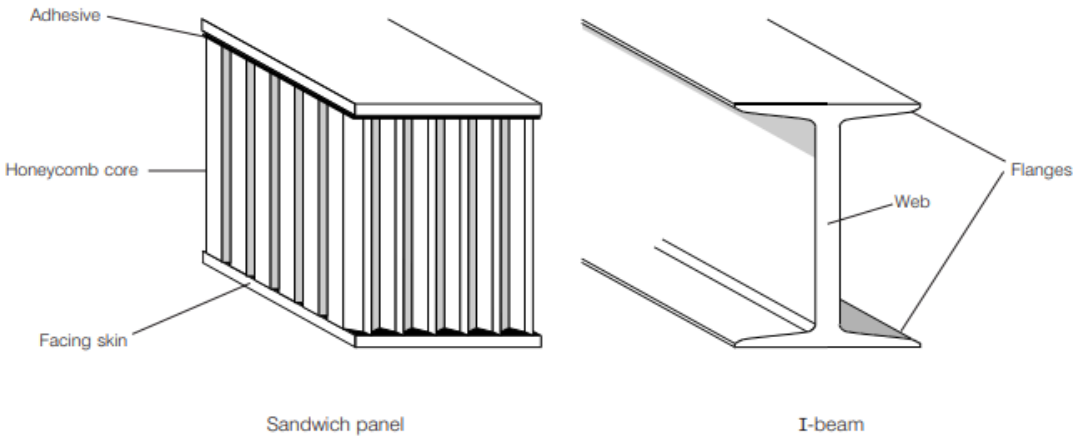

Figure 5. Figure from HexWeb ™ Honeycomb Sandwich Design Technology document supplied by Hexcel Corporation illustrating the analog between composite sandwich panels and a traditional I-beam. [2]

Since the bending strength and stiffness is highly dependent on the lamina and orientation chosen for use in the sandwich panel's skins, panels can be designed to produce the desired material properties in specific directions, which is more efficient than the standard behavior of an isotropic material. The benefits of this and the methods of manipulation will be discussed later in the report.

The benefits gained from using a fiber composite honeycomb structure entail their own specific design criteria. Since the materials are just many different elements bonded together, numerous modes of failure can occur in this type of composite laminate. Some of the failures that can occur with a composite sandwich panel laminate are skin failure, skin buckling, panel core shear, skin wrinkling, intracell buckling, and local compression and skin delamination. While the expected behavior of a sandwich panel can be modeled using plate theory, it is important to physically test all sample laminate designs with design loads as the failure modes of each panel vary greatly on the loading conditions and manufacturing quality.

Composite Chassis Laminate

The chassis laminate is heavily influenced by the Structural Equivalency Spreadsheet (SES), a rules-driven Excel sheet released by Formula SAE at the start of every competition year. In order to pass technical inspection and run the vehicles in dynamic events, the chassis must meet the strength requirements for each of the different sections, namely, Side Impact Structure (SIS), Front Bulkhead (FBH), Front Bulkhead Support (FBHS), Main Hoop Mounts, Front Hoop Mounts, Main Hoop Bracing Support (MHBS), and Shoulder Harness Attachments, shown in **Figure 6**.

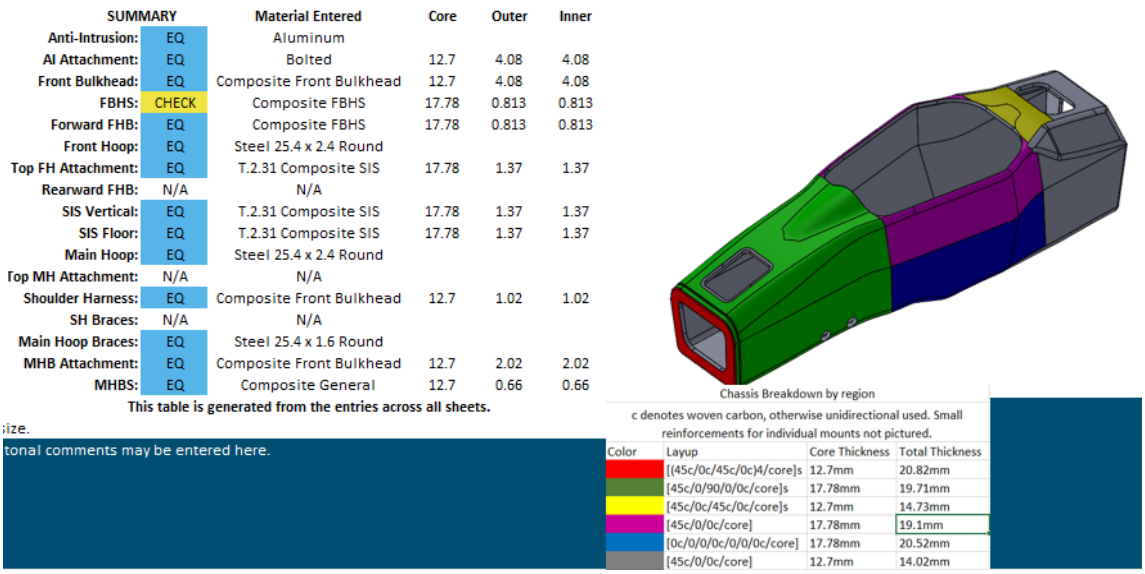

SUMMARY		Material Entered	Core	Outer	Inner
Anti-Intrusion:	EQ	Aluminum			
AI Attachment:	EQ	Bolted	12.7	4.08	4.08
Front Bulkhead:	EQ	Composite Front Bulkhead	12.7	4.08	4.08
FBHS:	CHECK	Composite FBHS	17.78	0.813	0.813
Forward FHB:	EQ	Composite FBHS	17.78	0.813	0.813
Front Hoop:	EQ	Steel 25.4 x 2.4 Round			
Top FH Attachment:	EQ	T.2.31 Composite SIS	17.78	1.37	1.37
Rearward FHB:	N/A	N/A			
SIS Vertical:	EQ	T.2.31 Composite SIS	17.78	1.37	1.37
SIS Floor:	EQ	T.2.31 Composite SIS	17.78	1.37	1.37
Main Hoop:	EQ	Steel 25.4 x 2.4 Round			
Top MH Attachment:	N/A	N/A			
Shoulder Harness:	EQ	Composite Front Bulkhead	12.7	1.02	1.02
SH Braces:	N/A	N/A			
Main Hoop Braces:	EQ	Steel 25.4 x 1.6 Round			
MHB Attachment:	EQ	Composite Front Bulkhead	12.7	2.02	2.02
MHBS:	EQ	Composite General	12.7	0.66	0.66

This table is generated from the entries across all sheets.

ize.

tonal comments may be entered here.

Chassis Breakdown by region

c denotes woven carbon, otherwise unidirectional used. Small reinforcements for individual mounts not pictured.

Color	Layup	Core Thickness	Total Thickness
	[(45c/0c/45c/0c)4/core]s	12.7mm	20.82mm
	[45c/0/90/0/0c/core]s	17.78mm	19.71mm
	[45c/0c/45c/0c/core]s	12.7mm	14.73mm
	[45c/0/0c/core]	17.78mm	19.1mm
	[0c/0/0/0c/0/0/0c/core]	17.78mm	20.52mm
	[45c/0/0c/core]	12.7mm	14.02mm

Figure 6. Representative excerpt of the Structural Equivalency Spreadsheet (SES). Each of the dimensions shown are the thicknesses of each material in mm.

Each of the sections has a specific set of requirements to pass, such as a minimal strength, minimal energy absorption, or minimal tear out strength. Representative panels with the same layup schedule are tested via 3-point bend and perimeter shear. However, the harness mounts have a specific test configuration, shown in **Figure 7**, where the harnesses are used to load the panel in tension to determine pullout strength. The motivation behind each test is to prove structural equivalency, ensuring the safety of the driver for any possible collision event.

Figure 7. Harness mount test panel.

One of the main tests required by the SES is a 3-point bend test, illustrated and photographed in **Figure 8** and **Figure 9**, respectively. The rules dictated by SES require that if a laminate is not considered quasi-isotropic, the 3-point bend test must be done along both the strong and the weak orientations of the laminate. The test does not specify which skin of the sandwich panel must be on top, and the test is only required to be in one orientation with respect to the top and bottom, whether the layup is considered quasi-isotropic or not. Because of this, the laminate for each of the controlled sections of the chassis that require a 3-point bend test to prove structural equivalency can be designed with an asymmetric laminate where the bottom skin can be made thinner than the top skin, since a carbon laminate can support more load in tension than in compression.

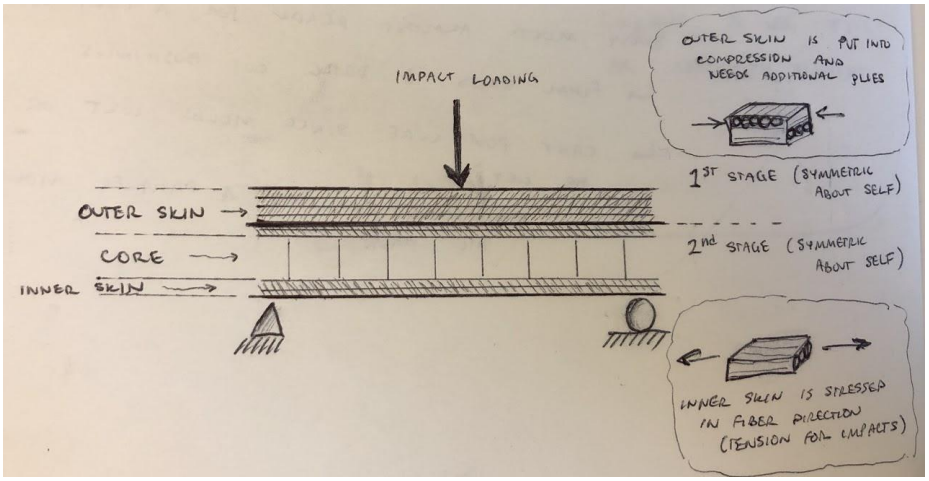

Figure 8. Example drawing of an asymmetric sandwich panel laminate.

An asymmetric laminate could be more mass efficient for achieving a given bending stiffness and strength target versus a symmetric laminate when tested in the configuration defined by SES. However, it will typically run into warping issues during manufacturing since the thermal stresses experienced by the outer and inner skin do not balance each other. This phenomenon is caused by the non-isotropic nature of the laminate fiber, most notably in unidirectional fiber lamina, as well as the different thermal masses between the skins if the ply count varies between the two skins. To counter this issue, an investigation into using a multi-stage curing cycle was performed to evaluate its effect on the overall warping of the part itself, as well as its effects on laminate properties. **Figure 8** shows an asymmetric laminate concept as well as the multiple symmetric stages within that laminate. Following this discovery, an asymmetric laminate for the CP20 generation of monocoque was investigated, designed, and tested against the standard symmetric laminate that has been used on previous vehicles.

Figure 9. 3-point bend test setup for SES.

Previous Chassis Designs

2013's *Formula Chassis Works* [3] researched the usage and benefits of using a hybrid monocoque-steel tube chassis for use in the chassis pictured in **Figure 10**. The goal of this project was to further develop the processes and technology of Cal Poly Racing's carbon fiber manufacturing processes. Much of the effort of this project was also spent on refining the laminate design using classical laminate theory.

Figure 10. 2013 *Formula Chassis Works* partial monocoque chassis at competition.

Frame Engineering Associates [4] was a 2015 senior project group that utilized the Alternative Frame rules, which allow for materials other than steel to be used for the side impact supports provided that extensive analysis in the form of FEA is produced. The result was a cut-and-fold chassis for the electric car comprised of planar sandwich panels bonded together and reinforced with wet-layups and microballoons, shown in **Figure 11**. The team managed to save approximately 40 lbs. versus the previous steel-tube frame but achieved a torsional stiffness of only 1200 ft-lb/deg, well below their target of 1800 ft-lb/deg, a number that was never validated.

Figure 11. 2015 *Frame Engineering Associates* cut-and-fold chassis.

The *Frame Engineering Associates* team utilized Abaqus CAE for their FEA model, with shell elements comprising the main frame and wire elements representing the suspension and roll hoop. The shell bodies were then partitioned by laminate schedule. Even though the MCD team's analysis was completed in ANSYS, the general FEA technique and process developed by the *Frame Engineering Associates* team is still utilized.

The 2016-2017 *Carbon Fiber Monocoque Chassis Platform for Formula SAE and Formula SAE Electric Race Cars* senior project saw the complete design and development of two full CFRP monocoque chassis, shown in **Figure 12**.

Figure 12. 2017 Formula SAE car produced by *Carbon Fiber Monocoque Chassis Platform for Formula SAE and Formula SAE Electric Race Cars*.

The 2017 team conducted an extensive study on chassis platform selection, quantifying the performance gains and losses of a monocoque, hybrid chassis, and steel tube frame, shown in **Appendix A**. In addition to designing the laminate and tooling, the team also performed detailed analysis on hardpoints and bolted joints connections to composite sandwich panels, developing potted inserts and pad-ups for increased localized stiffness.

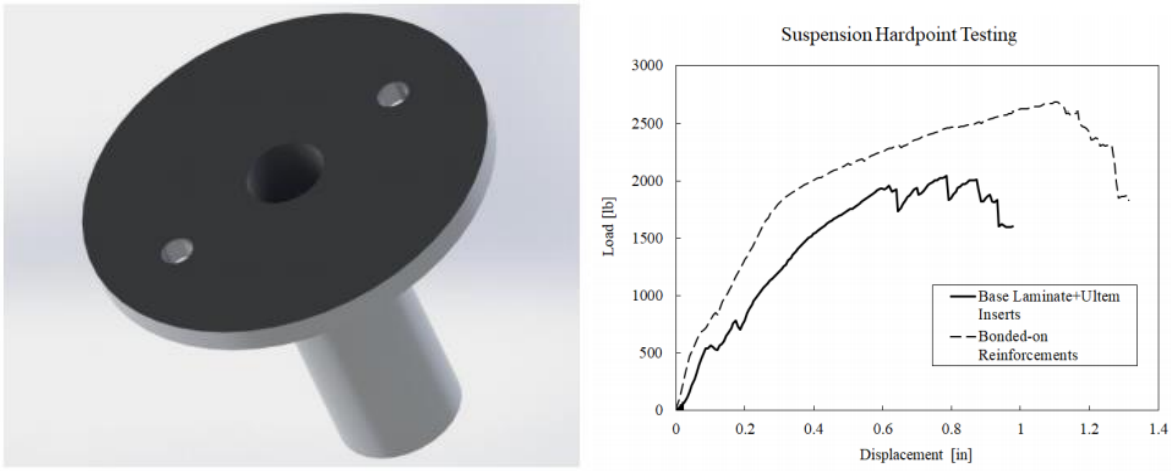

Figure 13. Half spool, potted insert geometry (left) and testing the two hardpoint designs (right).

Shown in **Figure 13**, the new half spool inserts proved to be effective, as they could carry more load that then bonded on reinforcements that previous chassis designs utilized. Furthermore, the 2017 project started the first full chassis torsional stiffness finite element model, shown in **Figure 14**. The suspension geometry and roll hoops are represented by line bodies, with the chassis modeled using surface elements. The rear uprights are fixed in all three degrees of translation and one front upright is simply supported while a load is applied to the remaining free corner.

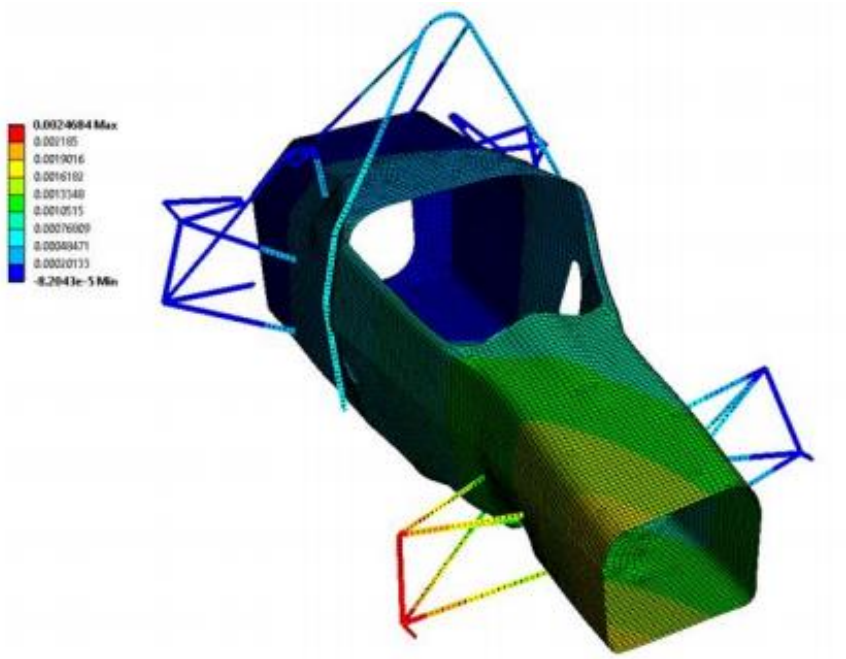

Figure 14. First iteration of the full chassis & rigid link suspension model.

This model is representative of how the chassis torsional stiffness is tested experimentally with three corners being supported by a steel I beam jig and a load applied at the free corner, shown in **Figure 15.**

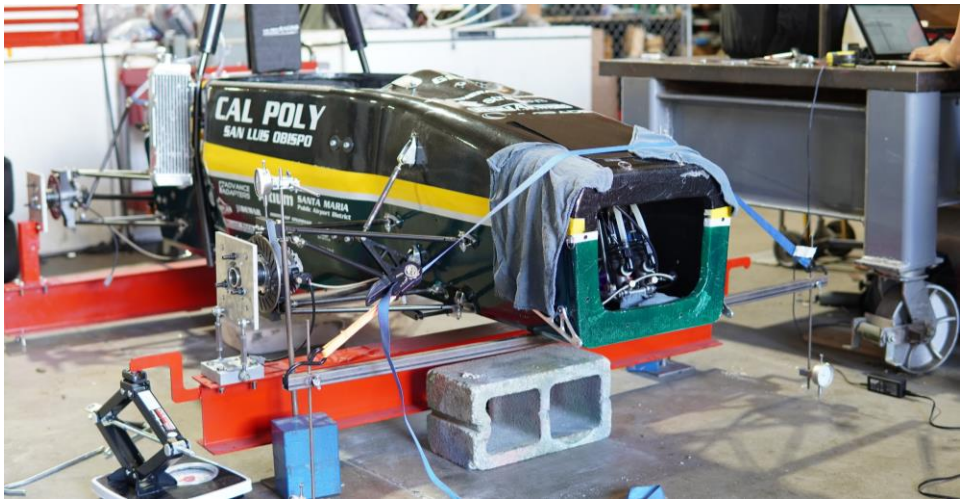

Figure 15. Chassis torsional stiffness test rig.

In addition to developing several detailed analysis tools, the 2017 team also developed a robust manufacturing technique for producing tooling for a monocoque type chassis. The process and technique were used as a basis for the manufacturing of the 2020 chassis.

Manufacturing Methods

The MCD senior project team investigated several manufacturing methods, including a half spool insert design, asymmetric layups, and multi-stage cures. As previously mentioned, potted half spool inserts are

an industry standard commonly used for bolted joint connections to sandwich panels. By removing core and potting the section underneath the insert flange with structural adhesive, the localized area is reinforced for any shear load due to bending or normal load applied at a bolted connection, shown in **Figure 16.**

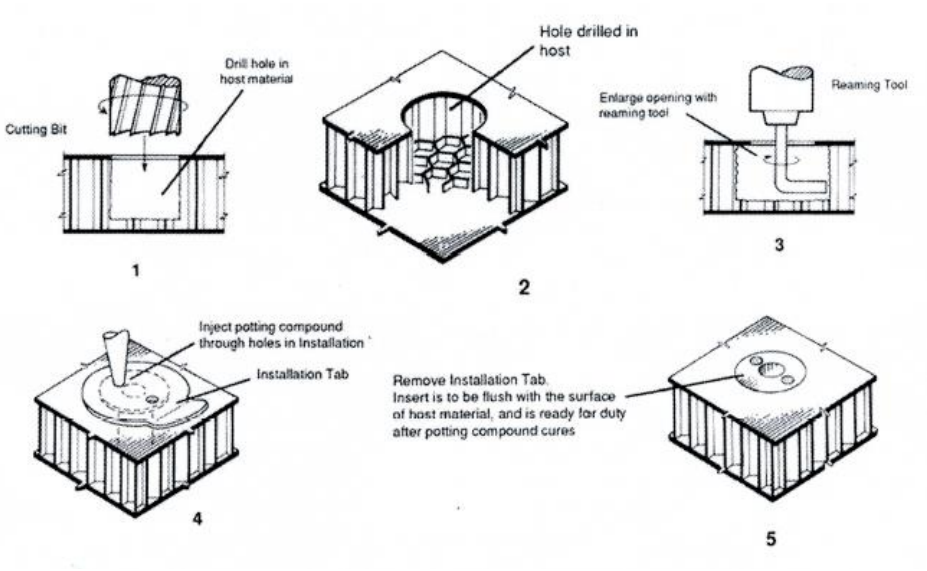

Figure 16. Industry standard for the insert potting process.

Improving localized reinforcement was beyond the scope of this project, and the 2017 configuration was successful. Therefore, the MCD chassis continued the same half spool insert design in the 2020 chassis. The MCD team also investigated the feasibility of a multi-piece mold and a single piece monocoque.

Figure 17. Ecurie Aix front quarters of four piece molds.

Shown in **Figure 17**, Ecurie Aix, a European competitor, utilized a four-piece mold and staged cure to produce a one-piece monocoque with an asymmetric laminate. This eliminates the need to bond the two chassis halves with a "strap joint," like the CPFSAE team has done in previous years. The strap joint has been a major source of excess weight, up to 8 lbs. Similarly, University of Washington used multi piece

molds, though their layup was done in one stage. By suspending their assembled two piece mold, pictured in **Figure 18**, they were able to lay up the part from the inside.

Figure 18. University of Washington one-piece layup.

In addition, the MCD team researched the performance benefits of a multistage cure. From *Formula 1 Composites Engineering* [5], a multistage cure allows one skin to remain flat against the mold during a cure cycle, whereas in a single stage cure the fibers get dimpled by the core under vacuum. The 2017 senior project did a study on this phenomenon with flat panel testing, shown in **Figure 19**. The 2020 MCD team did not pursue a staged cure since previous testing has shown the added manufacturing time outweighs the benefits of a staged cure.

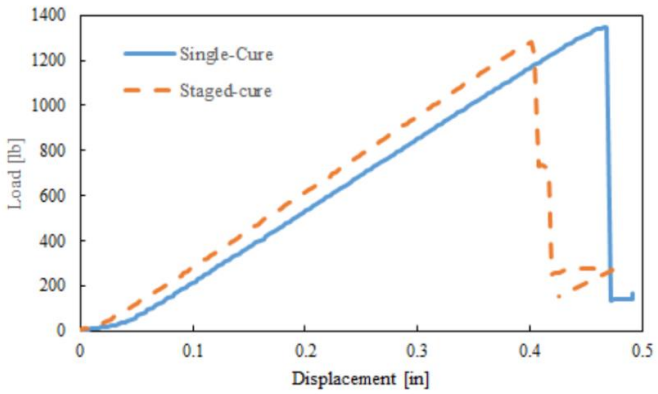

Figure 19. Flat panel properties for a single and multi-stage cure.

For the chassis to be successful, it must raise the team's overall score. One way to do this is to reduce overall weight, which has been proven to improve dynamic performance in Formula SAE competitions year after year. To achieve this from a manufacturing standpoint, the team investigated multi-piece molds to eliminate the need for an 8 lb. strap joint. Another way to reduce chassis weight is to reduce the total amount of core and carbon used on the chassis. The MCD team used FEA tools and sandwich panel testing to achieve stiffness and strength targets while using the minimum amount of material.

Existing Analysis Tool

To tune the laminate to meet rules requirements, previous teams utilized a computational model based on classical laminate plate theory. With this model, a very coarse study can be conducted to eliminate a variety of layup configurations, thereby eliminating unnecessary manufacturing and testing time. Ideally, the desired layup performance can be narrowed down to a few options via analytical models, then further eliminated based on experimental data, determining the final panel layup schedule.

Classical Laminate Plate Theory Model

A MATLAB script was previously created to quantify the stresses and strains at each lamina due to line loads, moments, and thermal loads using classical laminate theory. In addition, it generates the shape of a single laminate element, shown in **Figure 20**.

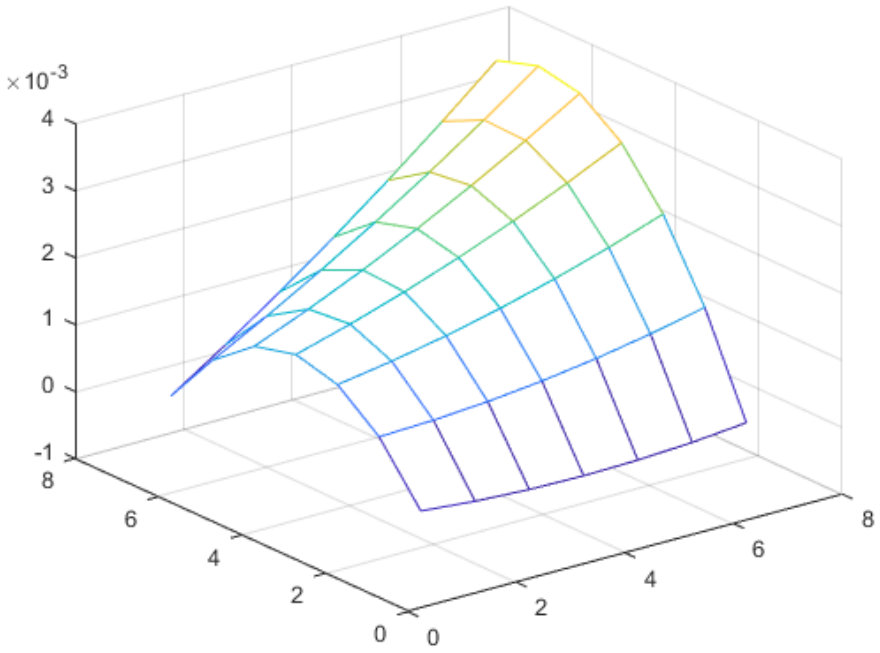

Figure 20. Mesh element of a laminate based on a given line load.

Currently, the model only quantifies the behavior of monolithic panels. To predict sandwich panel behavior, core shear stiffness can be added via superposition. With a complete sandwich panel model, the MCD team could predict both panel behavior subject to 3-point bend tests, as well as warping due to thermal loads from the prepreg cure cycle. In addition to developing this model, the MCD team created several new models discussed later in this report.

Objectives

For the project to be successful and worthwhile, the MCD team must have met or exceeded the high-level requirements set by the CPFSAE team with a finite budget. In addition to satisfying these requirements, the MCD team must have understood the risks and implications associated with achieving each specification so as not to put the CPFSAE team behind in its schedule.

Problem Statement

A redesign of the Cal Poly Racing Formula SAE team's carbon fiber reinforced polymer monocoque chassis was requested to improve subsystem integration, increase torsional stiffness, and reduce weight compared to the current platform. Specifically, the Formula SAE Monocoque Chassis Development team focused on manufacturing process improvement and laminate design to meet these goals. The team designed and manufactured a rules-compliant CFRP chassis, and its tooling, to compete in the 2020 Formula SAE competition.

Boundary Diagram

The 2020 CPFSAE team decided that two of the overall team goals were drivability and performance. These goals manifest in vehicle requirements, including increased torsional stiffness, decreased weight, and effective subsystem packaging. Based on these needs, the MCD team highlighted the key chassis parameters that could be improved to meet the team goals: laminate design and chassis shape. The relationship between the MCD and CPFSAE team is illustrated in **Figure 21**.

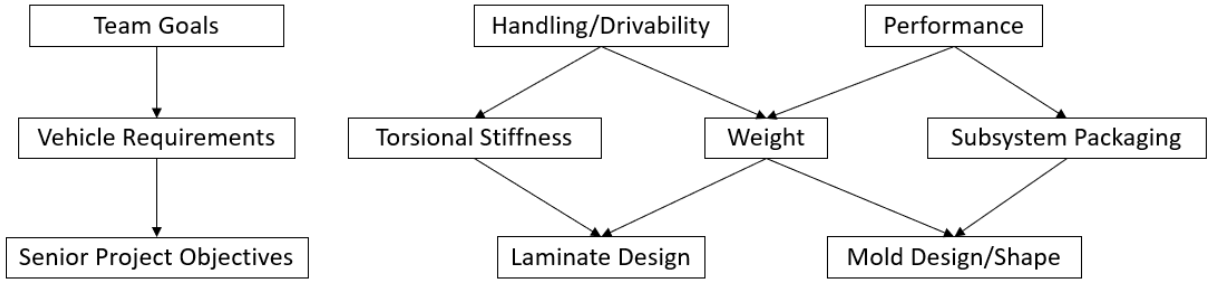

Figure 21. Boundary diagram describing relationship between team, vehicle, and senior project objectives.

Customer Requirements

The CPFSAE team and technical directors developed the specific project requirements necessary to obtain the points needed to achieve the desired podium finish at competition. The requirements include engineering specifications, a budget of $3000, and adherence to a strict timeline.

Specifications

The CPFSAE team laid out the specifications of the new monocoque, with emphasis on weight, torsional stiffness, and packaging modularity. **Table 2** shows the parameters and their respective target values for the chassis that were pulled from the Quality Function Deployment performed by the MCD team. A visual representation of the "House of Quality" is provided in **Appendix B** of this report.

Table 2: Parameters Developed using QFD

Spec #	Design Parameter	Target/Req.	Tolerance	Compliance	Risk	Notes
1	Torsional Stiffness	1700 ft-lbf/deg	+/- 200 ft-lb/deg	Analysis, Test	Medium	*See Note 1 Below*
2	Weight	45 lb.	+/- 5 lb.	Analysis, Test	High	*See Note 2 below*
3	Rear Packaging	3 ft^3	+/- 0.5 ft^3	Analysis, Inspection, Similarity	Low	*See Note 3 below*
4	Camber Compliance	0.4 deg/g	+/- 0.05 deg/g	Analysis, Test	Low	*See Note 4 below*
5	Toe Compliance	0.02 deg/g	+/- 0.005 deg/g	Analysis, Test	Low	*See Note 4 below*
6	Material Cost	$2500	Maximum	Analysis	High	*See Note 5 below*
7	Manufacturing Time	1000 man-hours	+/- 200 man-hours	Analysis	High	*See Note 6 below*
8	Rules-Compliant	Pass	N/A	Inspection	Medium	*See Note 7 below*

Note 1:

Torsional stiffness of the vehicle is measured with all suspension components on the car, and the target for torsional stiffness includes stiffness of the suspension members and mounting.

Note 2:

Chassis weight is measured after all post processing, including bonding joints (where required), all prep and paint work and reinforced mounting inserts.

Note 3;

Rear packaging accommodates the powertrain systems for both the combustion-powered car and the electric-powered car. While internal packing volume is a good indication of space, the difference in the geometry of the components to be packaged means that this is not a completely reliable metric for such a requirement.

Note 4:

Camber and toe compliance requirements are for the combined compliance of both the chassis and suspension systems combined, similar to torsional stiffness. This parameter is driven by localized stiffness of mounting locations for suspension, rather than the stiffness of the chassis structure as a whole.

Note 5:

Price reflects cost to team after sponsorships and donated material. The CPFSAE team gave the chassis subsystem a budget of $1640, but with emergency funding this number could rise to no more than $2500.

Note 6:

Manufacturing time for the chassis only includes the processes that are absolutely required to have a rules-compliant chassis; this excludes final assembly and painting.

Note 7:

The parameter "Rules-Compliant" encompasses any regulation required for the fielding of a CFRP chassis in a regulated Formula SAE competition. This includes SES regulations that may change from year to year, and any geometry restrictions such as template or any other geometry-based requirements.

Risk Analysis

The high-risk specifications were the weight of the chassis, cost of development and manufacturing, and manufacturing time. The chassis weight is very sensitive to other chassis parameters such as torsional stiffness. Generally, torsional stiffness and weight are proportionally linked since additional material may increase torsional stiffness. The weight is also sensitive to manufacturing processes, as lack of quality control can result in additional weight. The material cost is dependent on the sponsors and funding given to the club and is at the discretion of the 2020 CPFSAE Team Manager. If the CPFSAE team was not proactive with respect to procuring material and sponsors ahead of time, rushed shipping costs and the lack of availability could have driven up the price of otherwise free or discounted materials. The manufacturing time was also deemed high risk because it is reliant on the outsourcing of an already complex process. If a sponsor was forced to delay their involvement in the manufacturing process, alternatives would have been considered.

Required Timeline

The chassis needed to be manufactured as early as possible so the team could meet overall vehicle manufacturing milestones during build season. Other subsystems required a complete chassis well before testing season to fit up their components and test their parts. Since manufacturing a new chassis with new tooling requires long lead times, an aggressive schedule, shown in **Figure 22**, was adopted.

The previous senior project team ran into numerous delays with the manufacturing of the plug, which was outsourced to Zodiac Aerospace (now Safran) in Santa Maria. Their overall timeline was pushed back 5 weeks, forcing drastic changes to the club's timeline. Furthermore, the 2017 chassis mold failed to release from the plug, costing the team another 3 weeks to repair the mold surface. As a result, approximately 8 weeks of testing time was lost, and critical design validation data could not be acquired, resulting in the team dropping design points.

To meet the teams testing goals, both cars needed to be fully built and ready to test by Spring Quarter 2020. The subsystems needed to be given a minimum of 3 weeks to install and fit their parts, and the chassis required post-processing and painting. Thus, both chassis needed to be done at the latest by mid-Winter Quarter 2020.

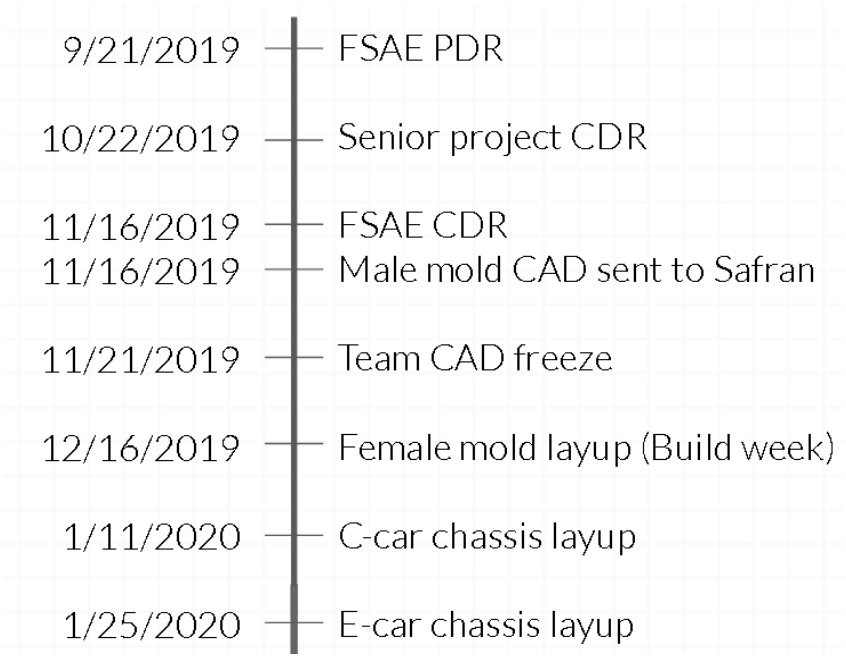

Figure 22. Team and class critical dates for Fall and Winter 2019.

Unfortunately, the outbreak of COVID-19 in early spring forced the MCD and CPFSAE teams to halt all operations. As a result, the race season was finished virtually. The effects and outcomes of this abrupt end are discussed later in the report.

Design

Several high level details were considered when designing the chassis. Aerodynamics, torsional stiffness, and subsystem integration roughly guided shape of the chassis. This idea of shape was iterated upon several times, often congruently with the analytical models found in the "Analysis" section of this report. The final car model is a culmination of the efforts taken by the MCD team and CPFSAE subsystem leads to create a high performance chassis.

Aerodynamic Concerns

Aerodynamic performance was factored into the design of the external geometry, but most of the aerodynamic design focused on improving the performance of the underbody aerodynamic devices (the "undertray"). An undertray, shown in **Figure 23**, creates a large low pressure region under the car, creating a net downward force. This is a very efficient way of producing more downforce with a lower drag penalty when compared to other aerodynamic devices such as wings. This downforce increases normal load on the tires, resulting in higher lateral force generation and faster lap times. The design of the aerodynamic components was beyond the scope of this project, but the senior project team worked with the relevant CPFSAE team members designing the components to ensure they performed as expected.

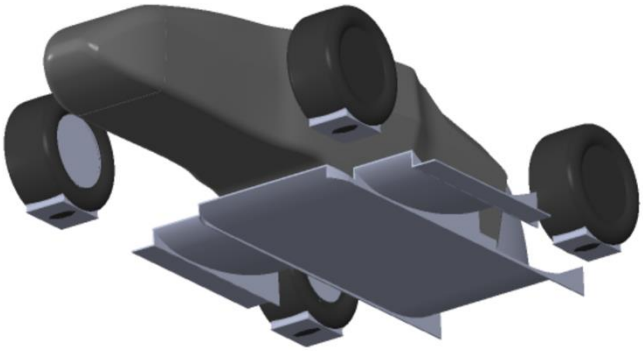

Figure 23. Preliminary undertray design mounted on the 2019 chassis.

To improve the performance of the undertray, two primary geometry changes were studied. The first is a diffuser section on the rear of the chassis. This allowed a larger, more aggressive undertray diffuser angle to fit with the chassis geometry, shown in **Figure 24**. A larger diffuser angle creates a stronger low pressure region under the car, increasing the net downforce created.

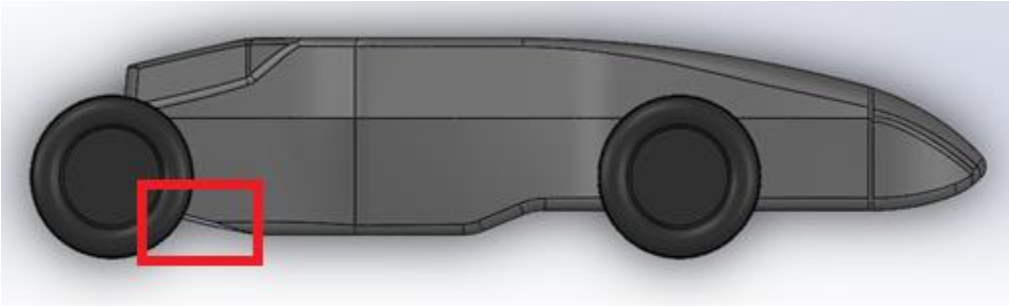

Figure 24. Diffuser section preliminary design.

Second, the effects of a raised nose section like the model in **Figure 25** were evaluated. This should allow more air to flow under the car and into the center section of the undertray. This increased mass flow would also increase the net downforce produced by the car.

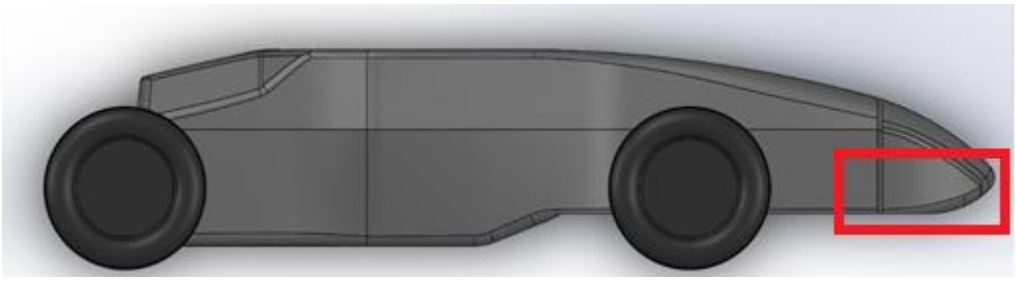

Figure 25. Raised nose conceptual design.

The proposed geometry changes were analyzed using computational fluid dynamics (CFD) so performance predictions of the proposed changes could be evaluated without the need to develop models for physical testing. Required mesh settings and domain size needed for grid independence found from previous work completed by the CPFSAE were applied to the preliminary chassis study. All analysis was performed on simplified geometry consisting of the chassis outer mold line and the spinning wheels. Performance was evaluated at 35 mph, the average speed of the car.

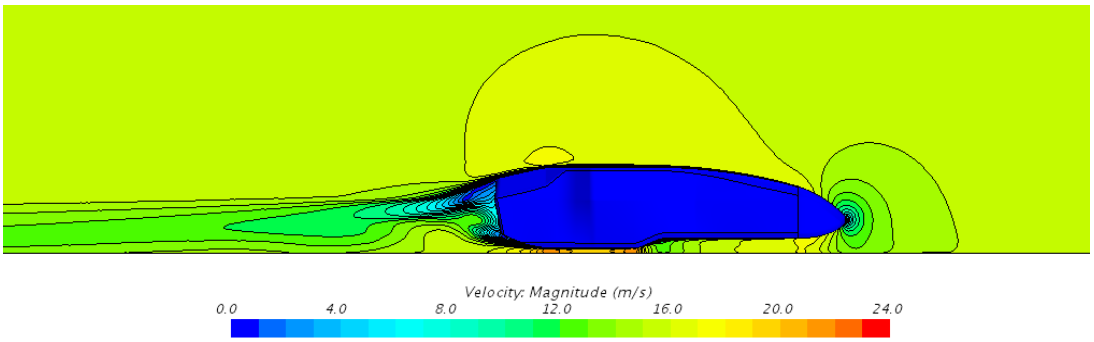

Figure 26. Preliminary CFD analysis of chassis with diffuser section. Wheels are not shown for clarity.

CFD results from **Figure 26** showed that there was minimal change in the net forces produced by the shape, so it was decided that aerodynamics would not be a driving design consideration for the geometry.

Torsional Stiffness Concerns

For optimal performance, the vehicles need to be predictable, respond quickly to driver input, and wield consistent handling throughout various operations. Chassis torsional stiffness, K_c, has a direct impact on vehicle handling, in both steady state and transient operating cases. Modeled as a spring in series, illustrated in **Figure 27**, the chassis acts as a torsional spring, deforming based on an equation where T is the torque applied, θ is the angular deformation, and J is the spring stiffness.

$$T = \theta * J$$

While the stiffness can be dependent on the laminate design, it is also influenced directly by the chassis geometry. Since geometric stiffness is a property that is easily adjustable early in the design phase, maximizing its effects early on can reduce the stiffness dependence on the laminate.

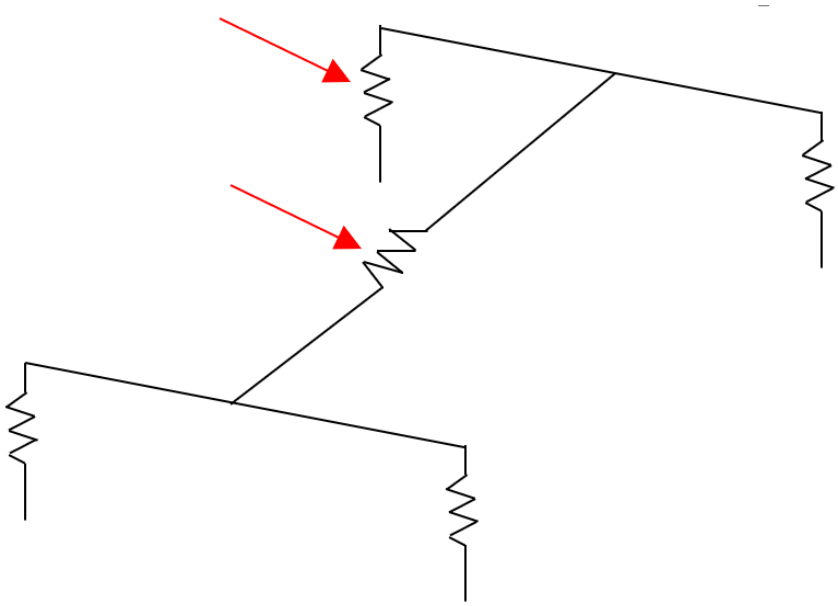

Figure 27. Simplified vehicle rigid link model including suspension links and chassis. The lower arrow points at the chassis as a torsion spring, and the upper arrow points at the quarter car suspension.

As shown in *Research of a Chassis Torsional Stiffness on Vehicle Handling*, chassis with lower torsional stiffnesses correlate to increased roll angle under cornering, akin to how a soft spring will deflect more than a stiff spring for a given load. [6] This has a negative impact on vehicle handling through cornering and any lateral acceleration case, as load is manifested in spring displacement as opposed to complete load transfer through the rigid links. Shown in **Figure 28**, a sweep through roll stiffness distribution with varying torsional stiffness was modeled. With lower stiffnesses, the lateral load transfer distribution is not a linear function of roll stiffness distribution. This results in inconsistent spring/damper actuation, leading to unpredictable handling through varying damper and tire forces.

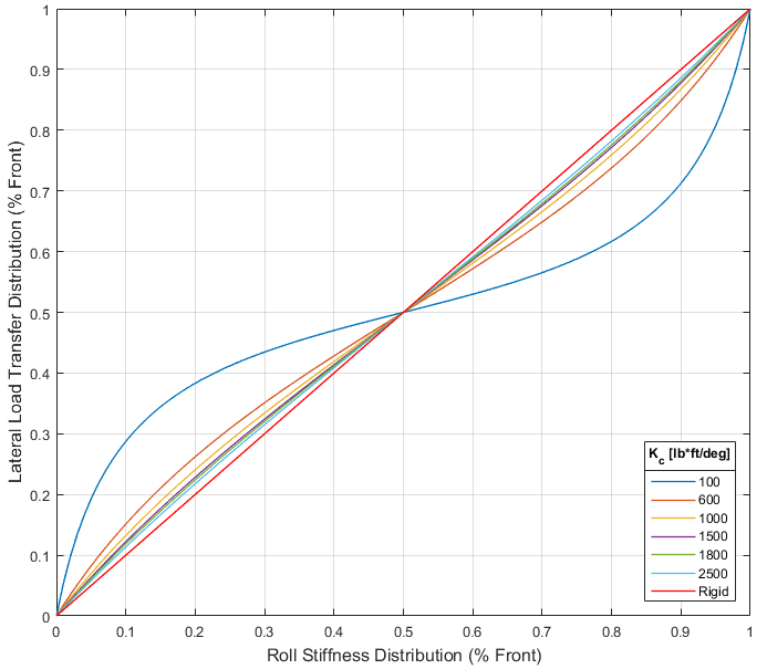

Figure 28. Lateral load transfer distribution as a function of roll stiffness distribution with varying chassis torsional stiffnesses. Non-linearity increases as torsional stiffness decreases.

Beyond lateral load transfer sensitivities as a function of roll stiffness distribution, torsional stiffness has a quantifiable effect on the transient response of the vehicle. Using preliminary 2020 vehicle parameters, a quasi-static four wheel vehicle model was created. Sweeping through K_c values, a step steer input was utilized to quantify the dynamic response of the vehicle. As shown in **Figure 29**, an increase in torsional stiffness decreases the peak oscillation of front lateral load transfer.

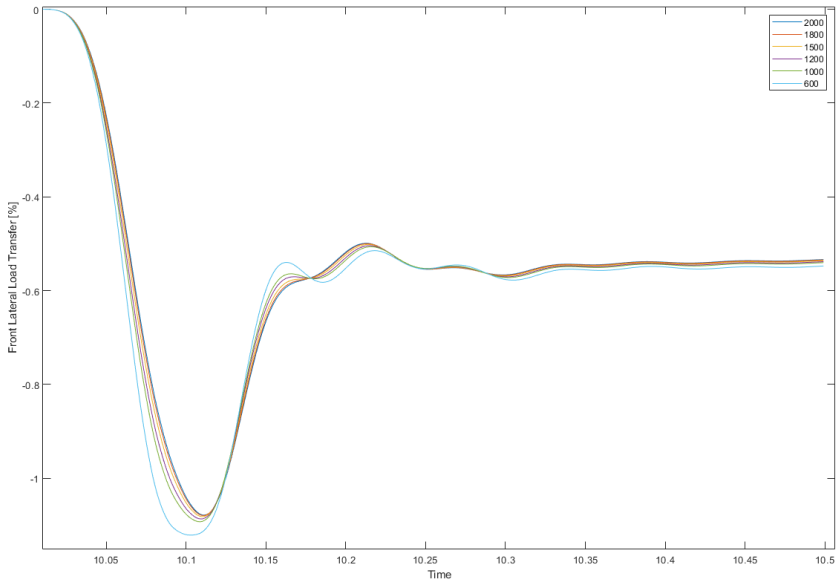

Figure 29. Step steer response of lateral load transfer with varying torsional stiffnesses. As stiffness increases, the dynamic response time and oscillation magnitudes are decreased, lending to quick vehicle response.

Because geometry will be altered to improve subsystem integration and iterative modularity, a sensitivity study was performed to quantify the effects of geometric changes specifically on torsional stiffness. Illustrated in **Figure 30**, the chassis was isolated and modeled as a spring in series with differing spring rates at major sections of the chassis, since torsional stiffness is not constant along the length of the chassis. Each of these sections was separated due to differing cross-sectional properties, namely rear bulkhead, rear powertrain bay, main hoop, cockpit, front bulkhead support, and front bulkhead. Rear bulkhead, main hoop, front bulkhead support, and front bulkhead were modeled as rectangular cross-sections, while the powertrain bay and cockpit were modeled as U-channels since the whole top section of the chassis was cut out in these sections for powertrain accessibility and driver fitment, respectively.

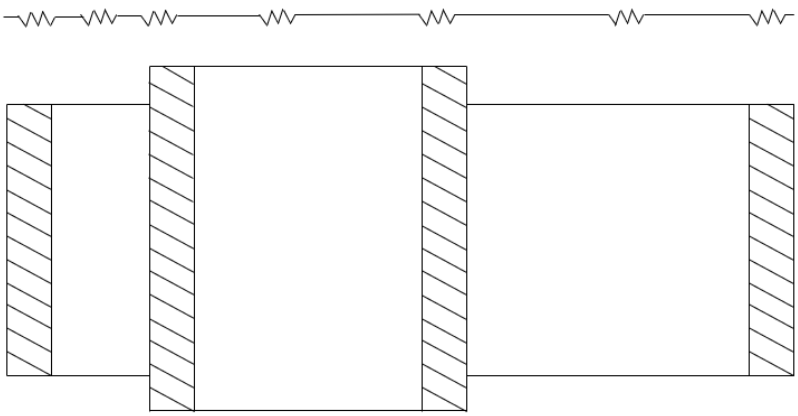

Figure 30. Top view of the chassis modeled as a spring in series. Each geometric cross-section has a different stiffness value.

Using the 2019 chassis dimensions as a base metric, parameter sweeps were conducted to quantify general trends of stiffness, displayed in **Figure 31**.

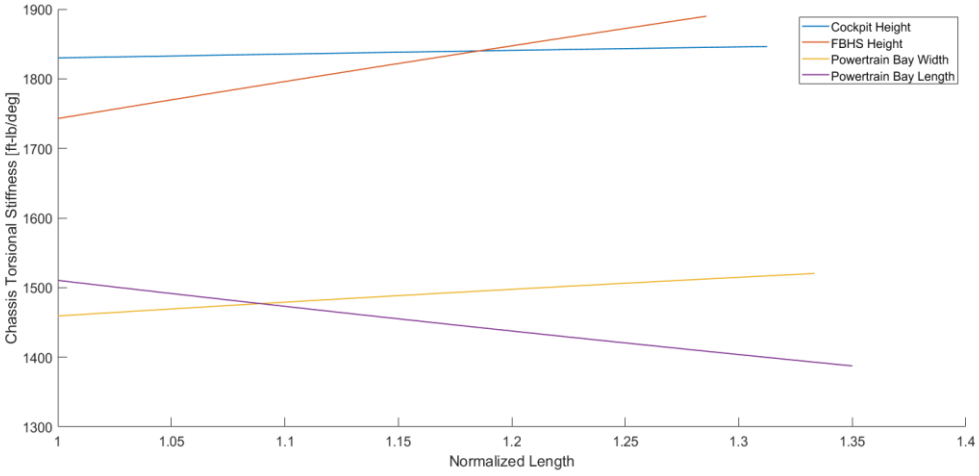

Figure 31. Torsional stiffness as a function of chassis dimensions.

Cockpit sidewall height, front bulkhead support height, powertrain bay width, and powertrain bay length were identified as areas of interest since they were changed to fit the needs for aerodynamics, driver

controls, engine, and accumulator. Dimension sweeps were normalized with the minimum value in the swept range to compare relative trends. Based on the study, the length of the powertrain bay had the largest effect on torsional stiffness.

Subsystem Integration

Another chassis requirement sensitive to the overall geometric design was subsystem packaging. Previously, the team had serviceability and packaging issues that stemmed from inadequate geometry. In 2017, when the overall shape of the chassis was being designed, the rear suspension architecture was designed with single shear rockers that mounted to the diagonal flats on the rear powertrain bay structure, shown in **Figure 32**. However, this geometry resulted in low torsional stiffness and poor load paths for the A-arms and pushrods, leading to heavy rockers, rocker mounts, and pushrods. Furthermore, the aft control arm mounts and tie rod inboard pick up points were limited by the end of the chassis, resulting in compound angle mounts, also shown in **Figure 32**.

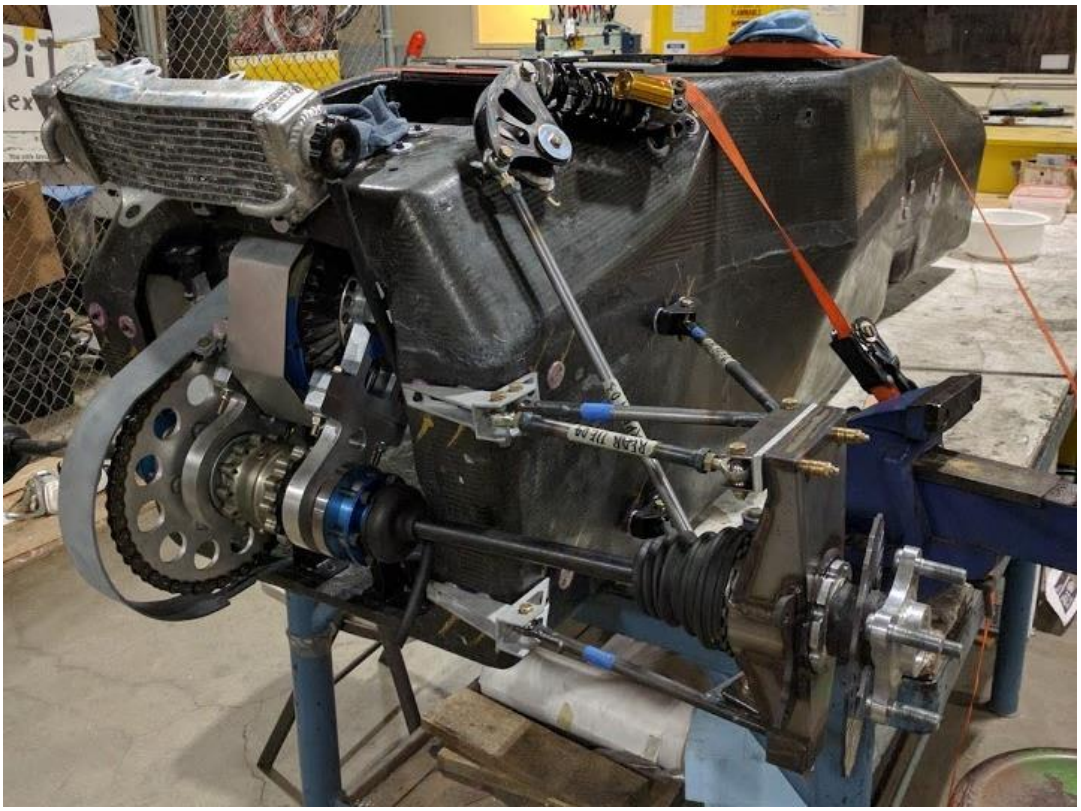

Figure 32. 2017 rear suspension geometry showing aft mount.

To extract the bottom half of the chassis from the female mold, the 2017 rear bulkhead surface and chassis powertrain bay side surface were designed with a draft angle, making the suspension mount difficult to manufacture and install. Due to compliance and serviceability issues, the rear suspension geometry was redesigned with in-plane pushrods and double shear rocker mounts. Shown in **Figure 33**, the 2019 pushrod geometry was designed for in-plane rocker loading, reducing weight and increasing overall stiffness.

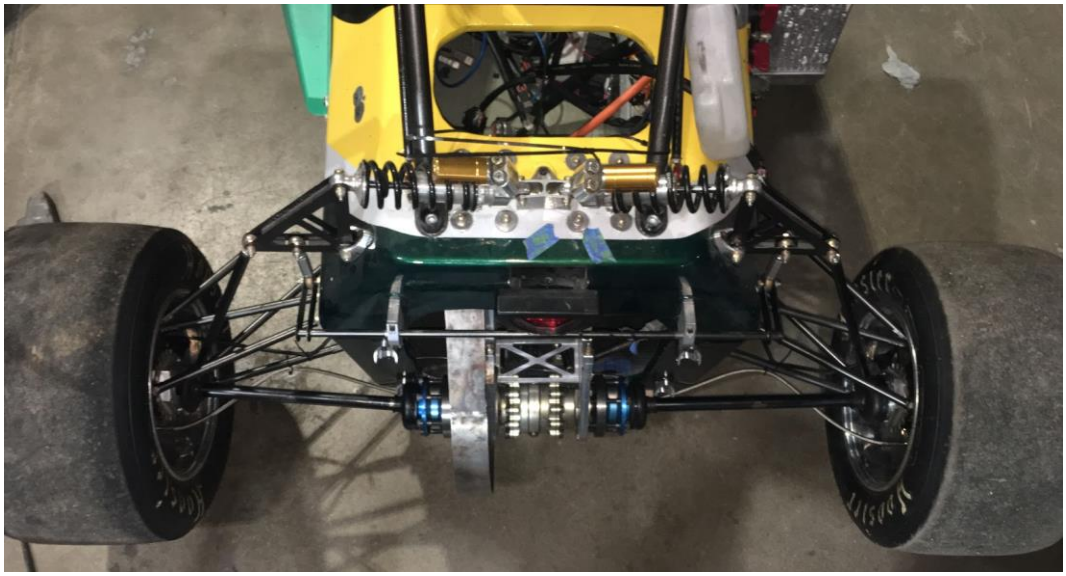

Figure 33. 2019 suspension geometry with in-plane rockers and double shear mounts.

However, the 2017 chassis geometry was only designed for that year's powertrain iteration, which has since been overhauled with major changes for both vehicles, specifically to the intake plenum, electric motor mounts, and motor controller location. Because of the chosen cutout locations with a small area at the top of the engine bay and a large cutout in the rear bulkhead, the powertrain components were very difficult to service and install, with assembly times of more than 2 to 3 hours. After gathering benchmark data from other teams at the 2018 competition and subsystem lead qualitative feedback, a large cutout located at the top of the chassis is more beneficial for accessibility. One example, shown in **Figure 34**, is the University of Washington rear packaging area, with a closed rear bulkhead and large cutout at the top for subsystem serviceability.

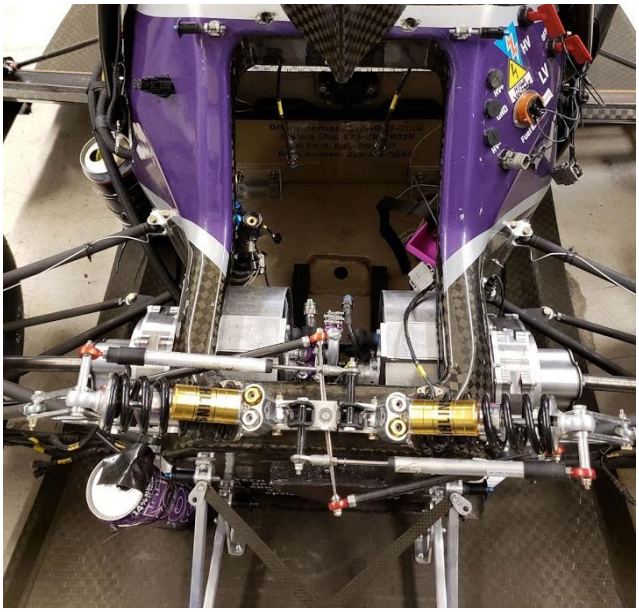

Figure 34. University of Washington rear packaging.

Furthermore, the previous chassis CAD was not easily editable, as most of the surfaces were generated by compound lofts and fillets. Whenever a subsystem wanted to interface with the chassis, a representative surface plane must be created, which is not accurate to the actual chassis. Because of this issue, the team had multiple subsystem assembly issues, including component to component interference and misalignment.

To improve iterative design, the chassis geometry was constructed with several front cross-sectional sketches a parting line, illustrated in **Figure 35**.

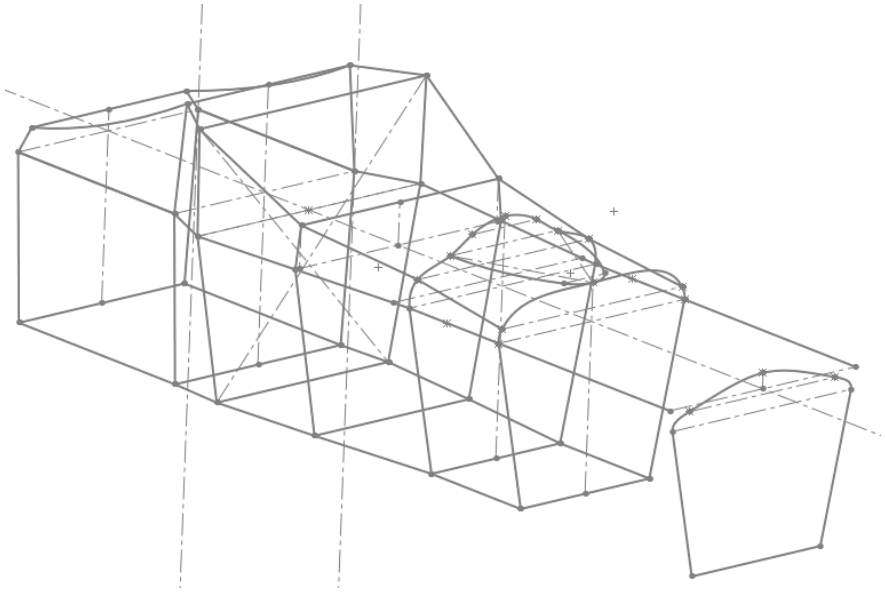

Figure 35. Preliminary chassis guide sketches including parting mold lines, template cross-sections, and rear bulkhead geometry.

Using specific cross-sections to create the chassis geometry makes chassis iteration alongside subsystem design iterations much quicker. Powertrain and suspension mounting can change very quickly, and accommodating those changes is a benefit. Furthermore, the parting line was easily adjusted based on the limitations of the manufacturing processes. A conceptual render of chassis geometry resulting from guide sketches is shown below in **Figure 36**.

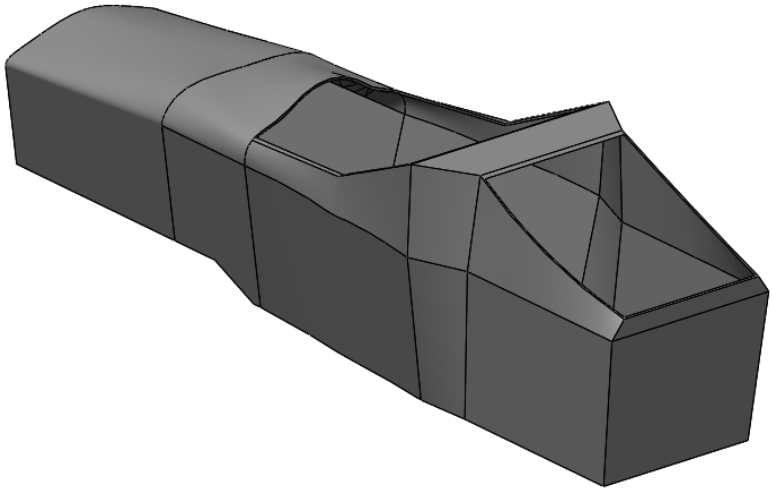

Figure 36. Conceptual chassis geometry, including planar faces.

Geometry

Two phases of design occurred for the monocoque, namely a preliminary iteration based on global vehicle requirements and a detailed iteration cycle in conjunction with detailed subsystem design.

Preliminary Iteration: Vehicle Requirements

The preliminary shape of the chassis was created using multiple loft sections, starting with the cockpit area, as this could be determined without any subsystem input. The cockpit width, length, and approximate sidewall height were all designed around a 95th percentile male, as dictated by the Formula SAE rulebook and general ergonomic design practices. At this point, the rest of the chassis was arbitrarily sized to get a reference point for subsystem input.

Once the preliminary chassis geometry was created, the model was imported into the full vehicle models for subsystem integration. Based on vehicle weight distribution requirements, the driver was placed in the x-axis center of gravity (CG_x) location. The chassis was then located using the driver's thighs, and the geometry was tailored to the suspension points and desired ride height, shown in **Figure 37**.

Figure 37. Preliminary iteration of the entire vehicle.

Detailed Iteration

Using the preliminary model as a basis, the geometry was then developed through numerous iterations, changing cross-sectional areas and draft angles as necessary to meet rules and subsystem requirements. Iterations occurred every team design night when subsystem representatives could be present to give feedback. The iteration process, visualized in **Figure 38**, spanned the entire duration of the design season, from week 0 of Fall Quarter 2019 until the Formula team CDR during week 8. Though there are 71 total logged revisions to the chassis geometry, the biggest changes are discussed in the following section.

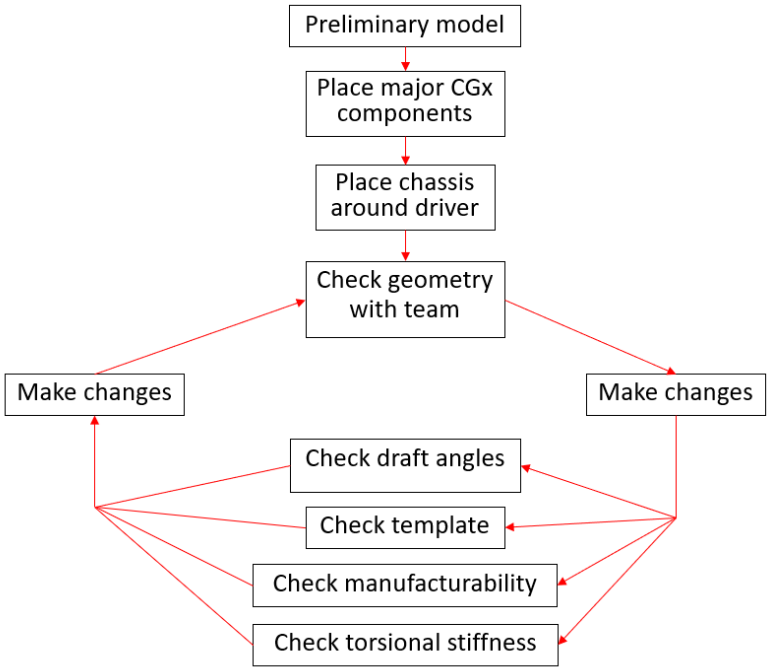

Figure 38. Iteration through chassis changes.

After the first few weeks of the quarter, subsystems understood their packaging requirements, and the chassis was modified to the shape shown in **Figure 39** to suit their preliminary needs. Among these initial changes included raising the front cockpit section height for steering and electronics packaging, adding front cutouts to improve access, and reducing the rear engine bay height to improve engine, drivetrain, and electronics access.

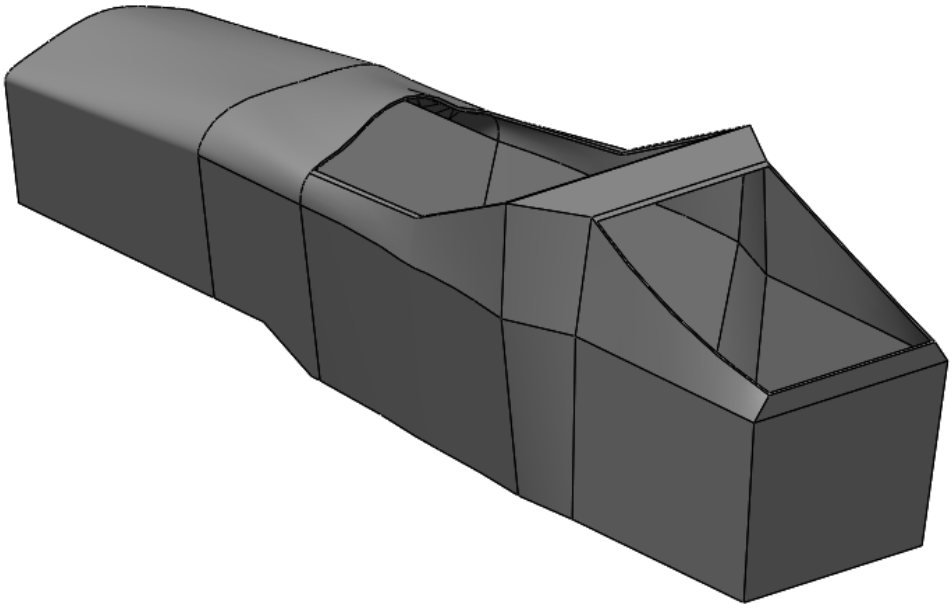

Figure 39. Preliminary geometry set by packaging and rules requirements.

One of the major considerations of chassis design was suspension packaging. There are several considerations, namely packaging feasibility, kinematic targets, link loads, and chassis loads. With respect to chassis, the optimal load path is in-plane loading, as sandwich panels are strongest in-plane relative to the fibers. The rear of the chassis was extended to allow suspension A-arm angles to widen, lowering loads. The aft A-arm mounts were moved further back along the chassis, reducing loads by 20% relative to the previous year's swept A-arm configurations.

For the front suspension, the change to 16" tires resulted the A-arm pickup points lowering by about 1" in Z. This resulted in an unideal mounting location, as the lower control arm pickup mount would have to mount to the lower chassis fillet, shown in **Figure 40**.

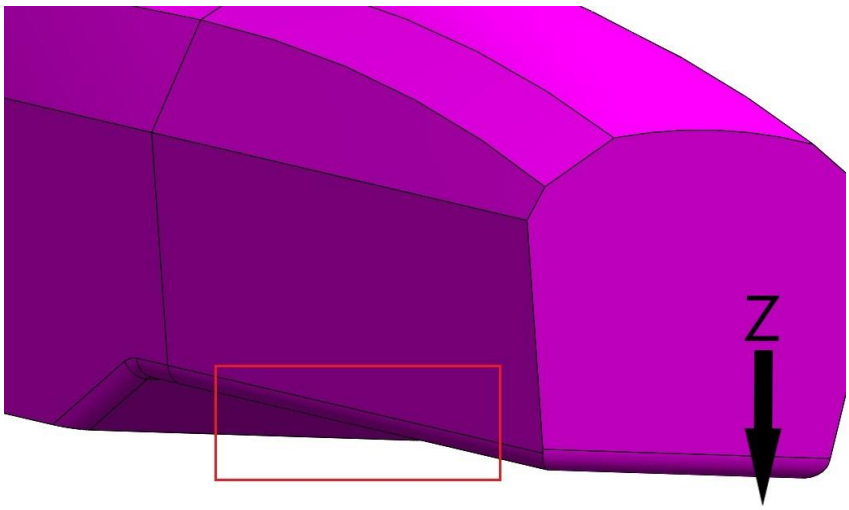

Figure 40. Lower control arm mounting location.

Furthermore, the inboard lower control arm pick-up points needed to be closer to the centerline plane to meet roll center migration targets. To avoid complex surface mounts, a flat boss was created at the mounting locations. Several considerations were considered when creating this geometry, namely front cockpit template, chassis loading, suspension link loads, and roll center goals. The most ideal location would be to place the mounts under the chassis to put all loads in-plane into the chassis, but this would hinder wheel travel, making it infeasible. An angled flat boss constrained by driver template and mount manufacturability was designed instead, shown in **Figure 41**. To reduce lower control arm (LCA) link loads and chassis out-of-plane loads, the length of the LCA boss was set to 17.35", allowing for wide A-arm angles. The angle and depth of the boss were determined by placing the boss as inboard as possible without encroaching on the pedal box and template area.

Figure 41. Refined preliminary geometry. Note the lower control arm boss added to the lower front of the cockpit and the flat shock "shelf" at the rear.

To lower shock CG height and to improve the shock load path into the chassis, a lowered shock mounting "shelf" was created, shown in the rear of **Figure 41** and **Figure 42**. This allows for a low shock angle, resulting in better load path for torsional stiffness due to higher in-plane loading. However, the placement of the shocks on the "shelf" requires the use of suspension rockers. To produce a mounting surface for the rockers, a chamfer was added to the sides of the "shelf".

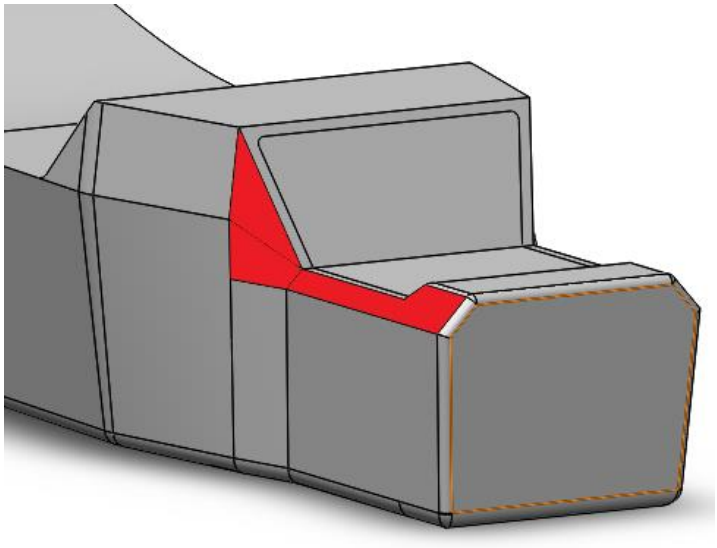

Figure 42. Refined preliminary geometry. Rear step-down rocker chamfer, highlighted in red, added for suspension mounting.

Adding the angled rocker chamfer produced non-planar geometry, shown in the leftmost part of the red area in **Figure 42**. At this point in time, the chassis parting line was in a horizontal plane that intersected this non-planar portion of the chassis. The tooling required for this geometry would have been difficult to produce. In addition, the team had already decided on designing a 4-piece mold to allow for modularity in future chassis, and maintaining a positive draft required splitting the chassis after the rear step-down, thus forcing future teams to have the same angle and size step-down pictured above. To mitigate this issue, the chamfer was terminated via a drafted cut, shown in **Figure 43**.

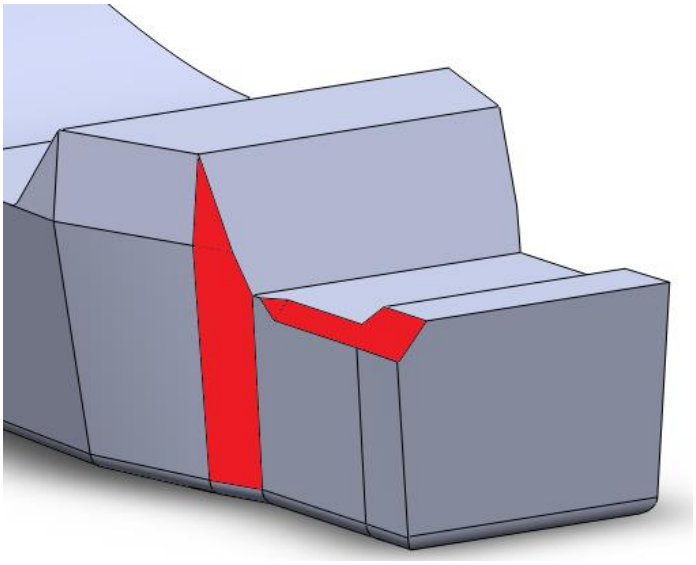

Figure 43. Rear step-down rocker chamfer terminated with drafted cut to remove non-planar geometry.

After this change, the torsional stiffness model was run and produced a stiffness well below the target. Most of the stiffness loss occurred due to the sharp step-down angle. After speaking with subsystems that require rear access, the MCD team decided to increase that angle. This step-down angle needed to be kept low so as not to hinder engine bay access. A study, detailed in the torsional stiffness analysis portion of this report, found the smallest rear step-down angle that produced the desired torsional stiffness. The result is pictured in **Figure 44**.

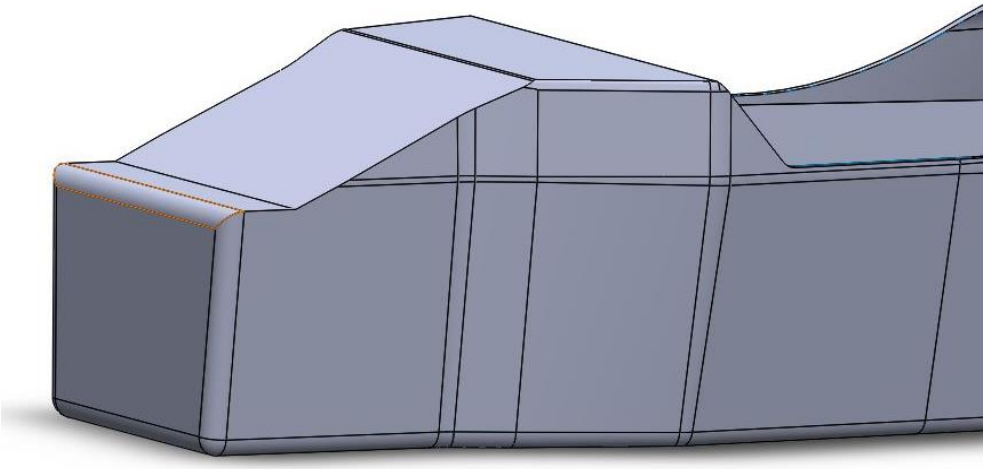

Figure 44. Rear step-down angle increase to improve torsional stiffness. The step-up to the rocker shelf was also eliminated. Note that the sidewall height was also raised to improve the torsional stiffness.

At this point in time, the MCD team made the decision to split the chassis tooling along a vertical plane instead of a horizontal plane. This decision was made to simplify the overall manufacturing process, since the horizontal split required disproportionate female molds, angled mating flanges between molds, and limited the ability to change geometry easily in the future. To achieve a vertical parting line, draft needed to be added normal to the centerline plane, shown in **Figure 45**. Fillets were also added, with the smallest fillet radius being 1” motivated by the moldability of flex-core around corners. In general, however, all

fillet radii were made as large as possible to make manufacturing easier and to limit the amount of flex-core used.

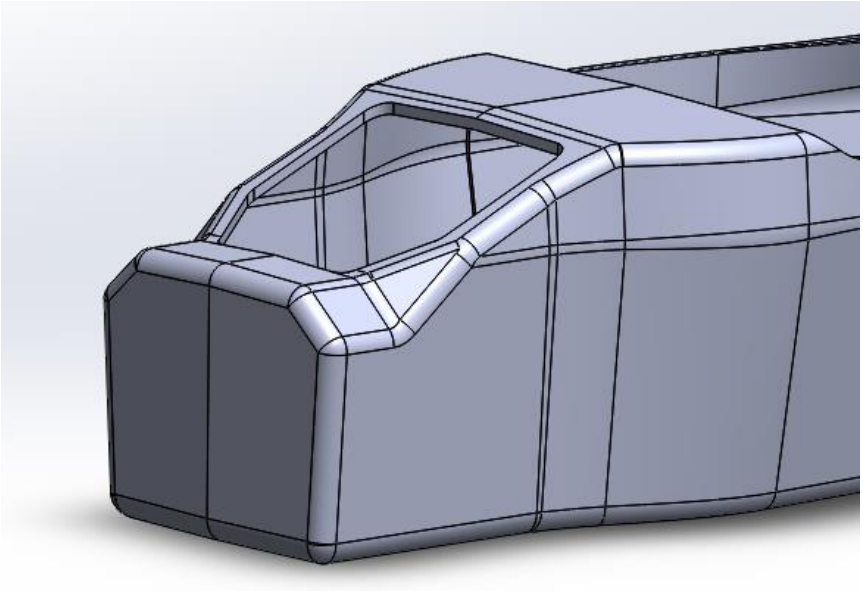

Figure 45. Draft, chamfer, and fillets added to rear section.

Following the CPFSAE team CDR, the suspension team decided to go from a front pull-rod setup to a push-rod setup. Not only would this improve suspension kinematics and vehicle handling, but it would greatly improve the overall torsional stiffness. However, this meant that the front shocks would need to be mounted on the top of the chassis along the vehicle centerline. Therefore, the top of the chassis was flattened to simplify suspension mounting, shown in **Figure 46.**

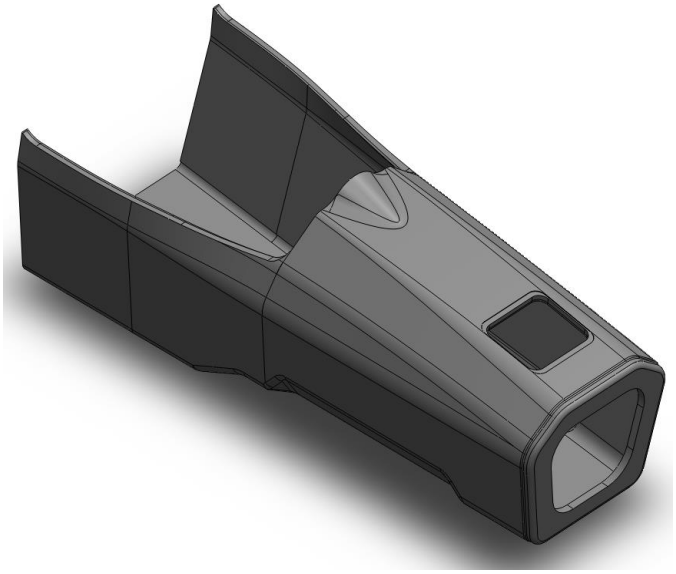

Figure 46. Top of front of chassis made flat to allow for top-mounted shocks. The sidewall height was also raised according to the torsional stiffness study discussed later.

However, after making the top flat, the steering wheel protruded above the chassis at full-lock, which is allowed in the Formula SAE rules as long as the steering wheel does not extend outside the front roll hoop

envelope [7]. This would have required the roll hoop to extend beyond the top of the chassis, adversely affecting aero and overall design aesthetics. The solution to this involved adding a “hump” or “swoop” in front of the front roll hoop as in **Figure 47** to allow for the roll hoop to protrude slightly higher and cover the steering wheel. The 2017 chassis had a similar feature for the same reason.

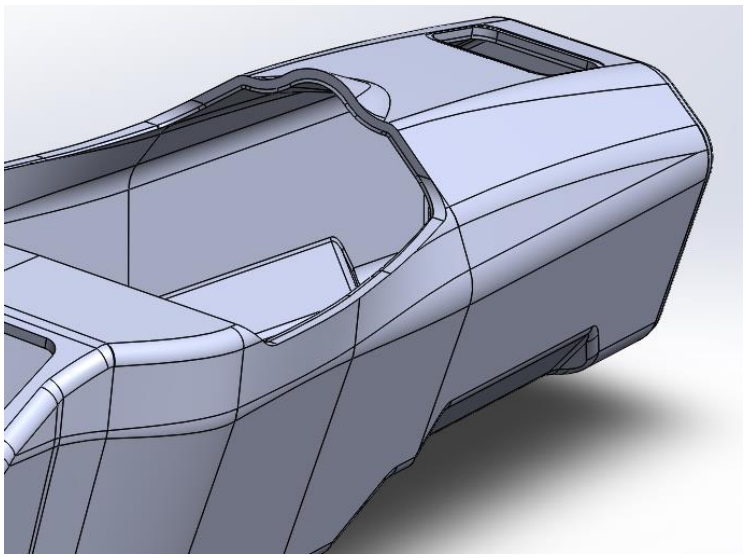

Figure 47. “Hump” or “swoop” in front of the front roll hoop to allow for steering wheel clearance per the rules.

Final Geometry

After all iterations were made, the geometry was finalized for a manufacturability check. This included a symmetry check, draft study, and near complete re-ordering of the features used to create the preliminary model. The preliminary chassis model included many fillets that were either not necessary or created geometry that would not be feasible to layup in, especially when considering core. To better understand the implications of creating a mold, SolidWorks models were created to mirror the actual manufacturing process. A final rules check (discussed later) produced the finalized geometry shown in **Figures 48-53**.

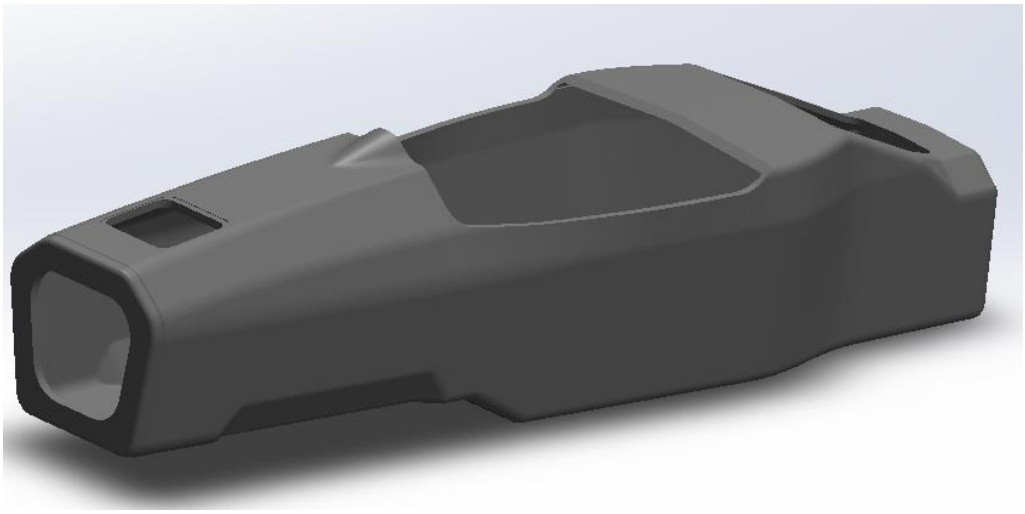

Figure 48. Final chassis geometry isometric view.

Figure 49. Chassis front and rear views, respectively.

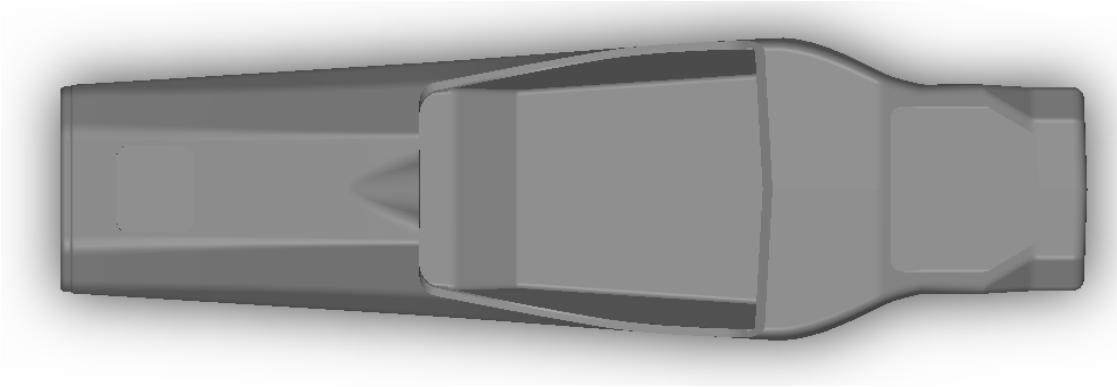

Figure 50. Chassis top view.

Figure 51. Chassis bottom view.

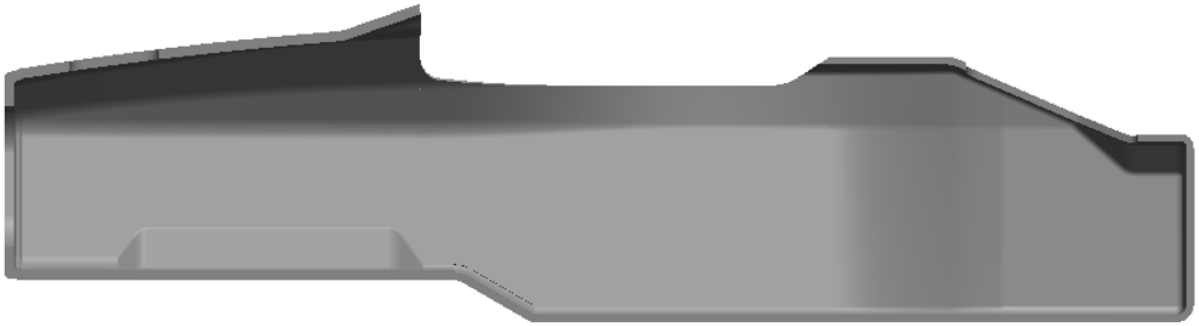

Figure 52. Chassis cross-section side view.

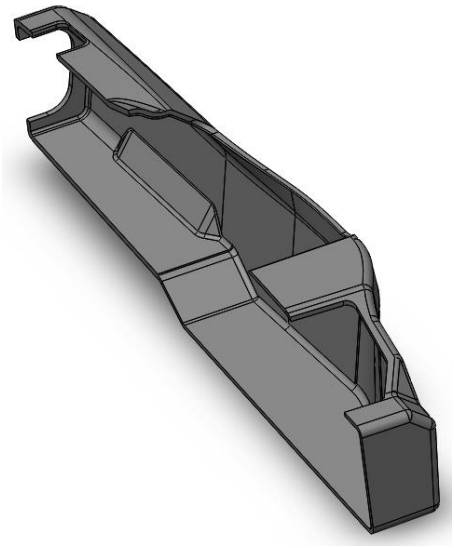

Figure 53. Cross-section isometric with edges shown.

Full Car Model

Whenever the chassis geometry changed, the full-car CAD assembly was automatically updated to incorporate those changes. **Figures 54-59** are taken from the full-car assembly after the final chassis revision was made.

Figure 54. Full-car assembly with final chassis design.

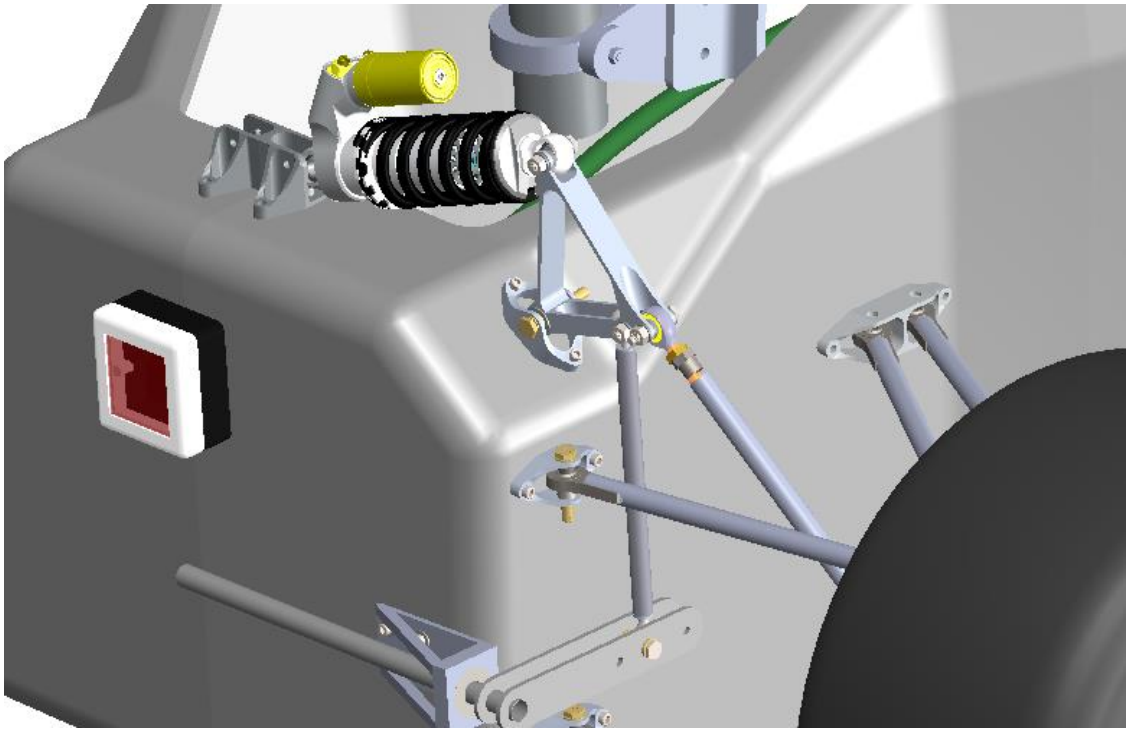

Figure 55. Rear suspension package. The rocker and shocks are mounted on the chamfered rocker "shelf".

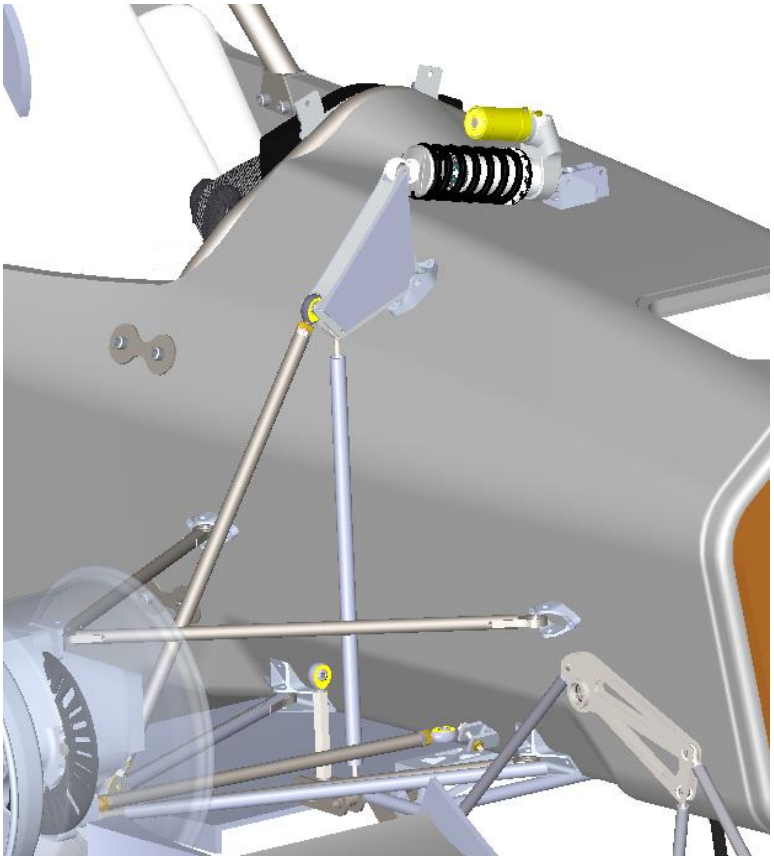

Figure 56. Front suspension package. Lower control arm is mounted to boss, rocker is mounted to planar surface, and shock is mounted to a flat top.

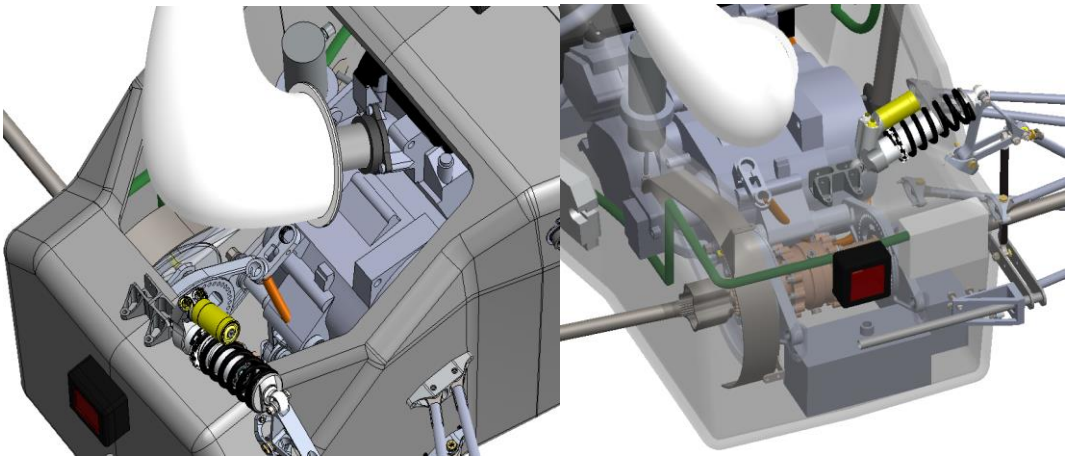

Figure 57. Engine and drivetrain packaging in combustion car.

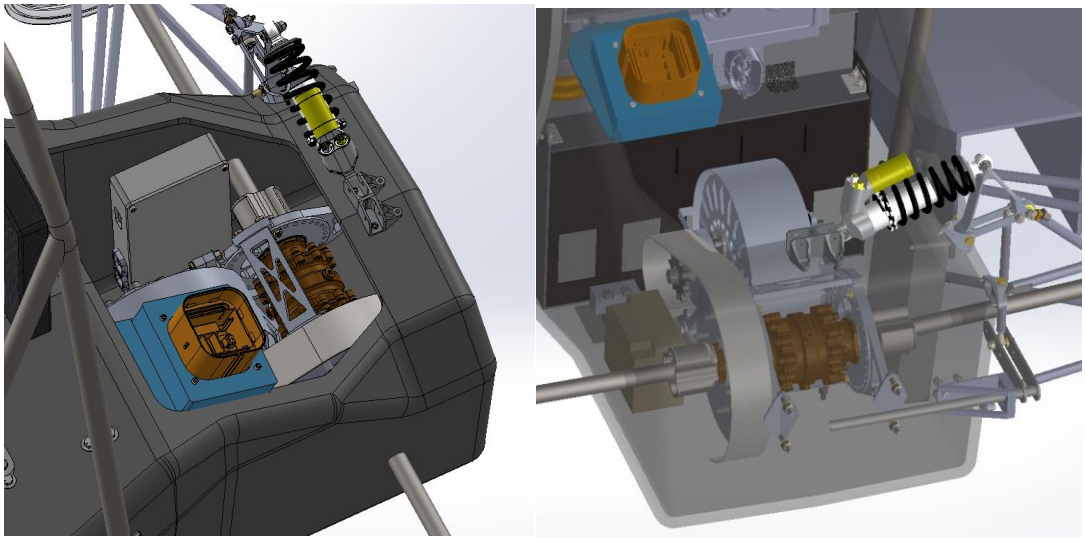

Figure 58. Battery box, motor, and drivetrain packaging in electric car.

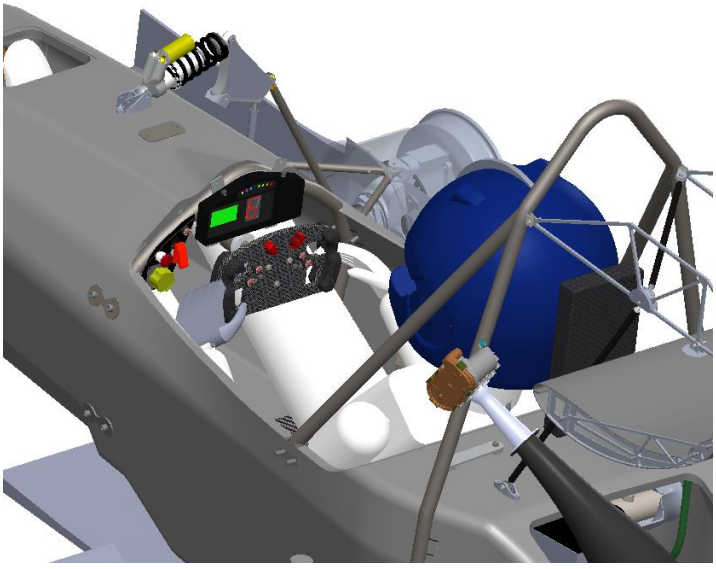

Figure 59. Cockpit with 95th percentile male model.

Analysis

In addition to the high-level geometric choices described in “Design,” the final chassis was designed using the following detailed analysis models. Preliminary tests explored asymmetric laminates as well as staged cures. Seven analytical models were created to define chassis laminate and specific shape. Torsional stiffness and energy absorption of the laminate were predicted and drove design decisions. Laminate strength and energy absorption predictions were tested using Formula SAE structural equivalency tests. Thermal analysis of the chassis during a cure cycle was done to predict manufacturability. Finally, cost and weight estimations were completed to set production goals for the chassis.

Preliminary Testing & Modeling

Early in the design process, test pieces were manufactured and tested for both warping and strength. This testing was conducted early-on to assess the physical feasibility and performance of asymmetric and stage-cured laminae. If the results were promising, they would warrant more computational analysis.

Warping in an asymmetric laminate occurs due to an imbalance in thermal stresses during the curing process. To mitigate this, the laminate can be cured in stages. In addition to studying the effects of stage curing, samples were also tested for strength and stiffness properties while loaded.

For the first test, an asymmetric laminate was cured using two separate cure stages. The geometry chosen for these panels was one corner of the pre-existing 2017 chassis molds. This was chosen to check an asymmetric laminate’s behavior in a fileted corner. These pieces were then checked against a control symmetric laminate cured in a single stage, shown in **Figure 60**. The maximum deformation in the single stage cure sample was 0.345”. The dual stage cure significantly reduced this deformation to 0.094”.

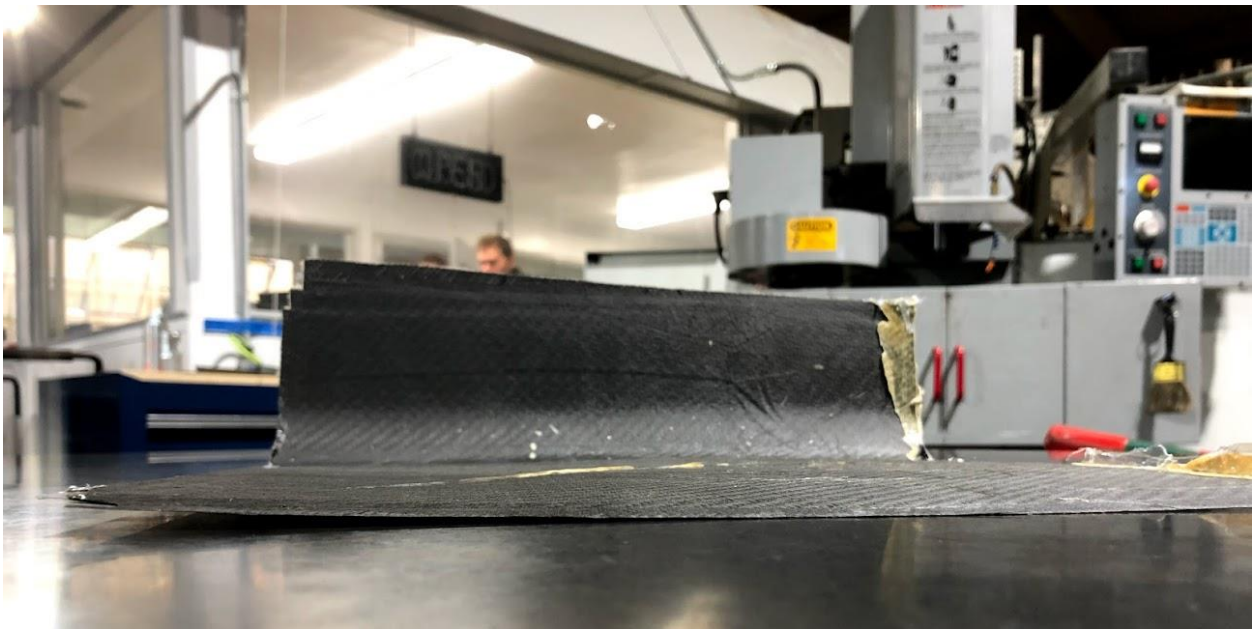

Figure 60. Symmetric Test sample being checked against a micro-flat reference table.

Another performed test involved small sandwich panel samples cured in a round corner section of the existing chassis mold. As in the previous test, a controlled symmetric laminate was laid up to establish baseline panel behavior. This test was designed to isolate the effects of multi-stage curing on a corner

sample's strength and stiffness characteristics, with special consideration given to the difference in possible failure modes. The multi-stage cure for these test samples was chosen to be a dual-stage cure, with the first being a full cure of the outer skin alone, and the second cure adding in the core, core adhesive and the inner skin of the laminate.

Figure 61. Images of single-stage cured sample pieces after destructive testing.

The samples manufactured using the multi-stage method were then compared to samples created using a traditional single stage cure, where the outer and inner skins were cured all at once along with the core and the core adhesive. The chosen method of testing for these samples was a standard compression test, where the geometry of the test created a loading scenario like a 3-point bend test, as pictured in **Figure 61**. By looking at the samples after they had failed under the compression test, the failure modes of each were found and compared to one another in **Table 3.**

Table 3: Stage-cured Samples and Failure Modes Under Compression

Sample	Failure Mode
Single-stage sample 1	Core failure
Single-stage sample 2	Core failure, inner skin delamination
Dual-stage sample 1	Core failure, outer skin delamination
Dual-stage sample 2	Outer skin delamination

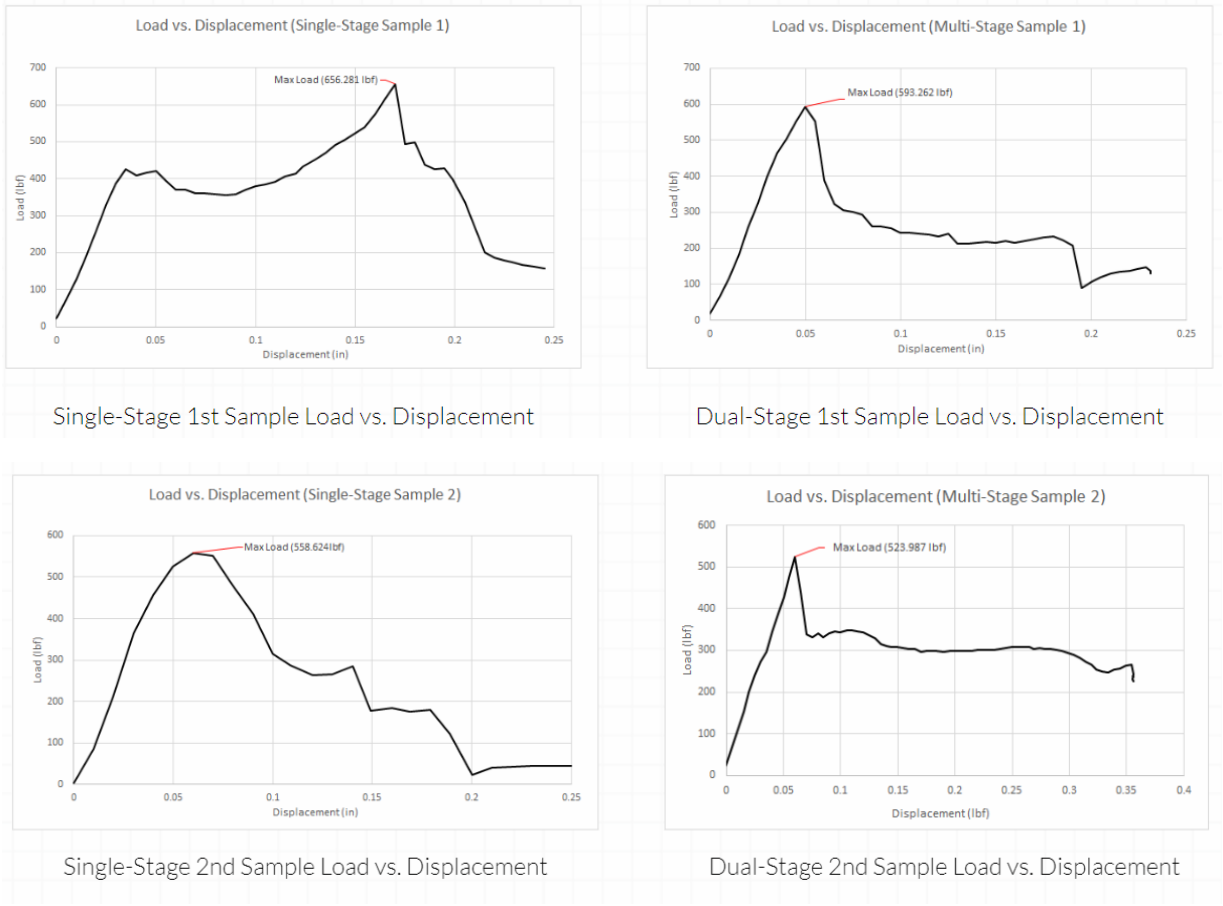

Figure 62. Comparison between single-stage and dual-stage load versus displacements.

From **Figure 62**, the single-stage cure pieces tended to have a larger failure load, with similar values for stiffness. However, the dual-stage samples were able to sustain loads at around 50% of their ultimate load for much longer after peak loading had been accomplished. The load carried by the single-stage samples tended to drop off significantly and dramatically after the peak loading was achieved. This follows the failure modes observed for each part, since the single-stage cure samples saw core shear failure issues far before the skins delaminated from the core, but the dual-stage samples experienced outer skin delamination first, and the core and inner skin laminate was still left intact enough to support a load after the initial failure. Though the structural benefits of multi-stage curing are evident, the MCD team decided that the added manufacturing time associated with additional cures threatened the project timeline. Instead, the MCD team decided to further investigate the use of a single-stage cured asymmetric laminate.

Finite Element Model

A basic finite element model was created to predict sandwich panel performance using ANSYS Workbench. Material properties and ply schedules for panels were inputted into an ACP (Pre) block in the Workbench, which then generates the A, B, and D matrices. Where available, material properties were taken from tensile testing done by the team. However, the properties for the new materials were taken from the data sheets included in **Appendix C**. The panel was then imported into the ANSYS structural analysis module and simply supported at the edges.

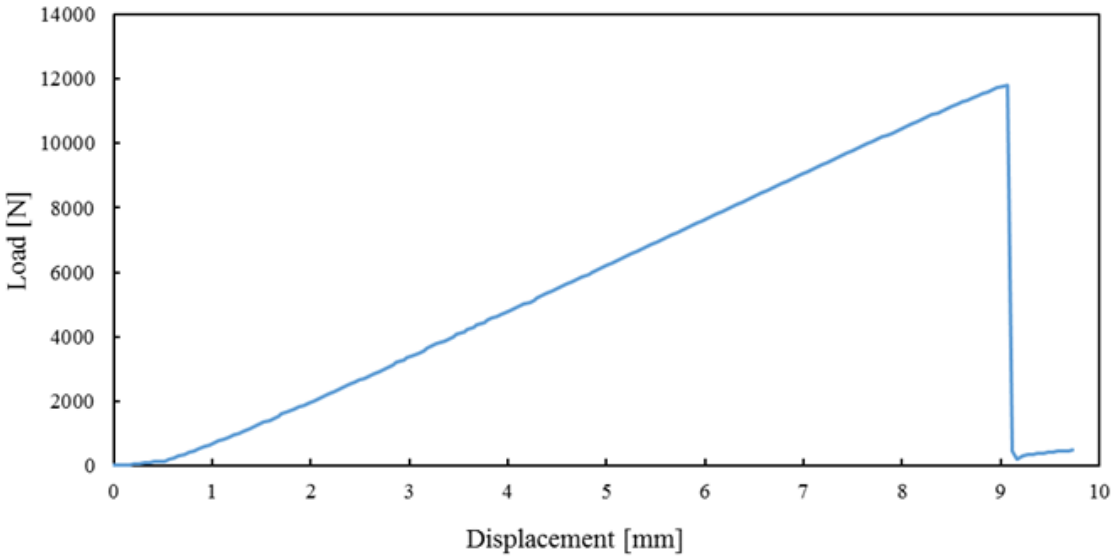

Figure 63. Test data from 2017 panel.

A line load was then applied to the center of the panel depending on the load requirement of the specific section. To validate the model within a certain tolerance, the model was compared to tested panel data from 2017, shown in **Figure 63**.

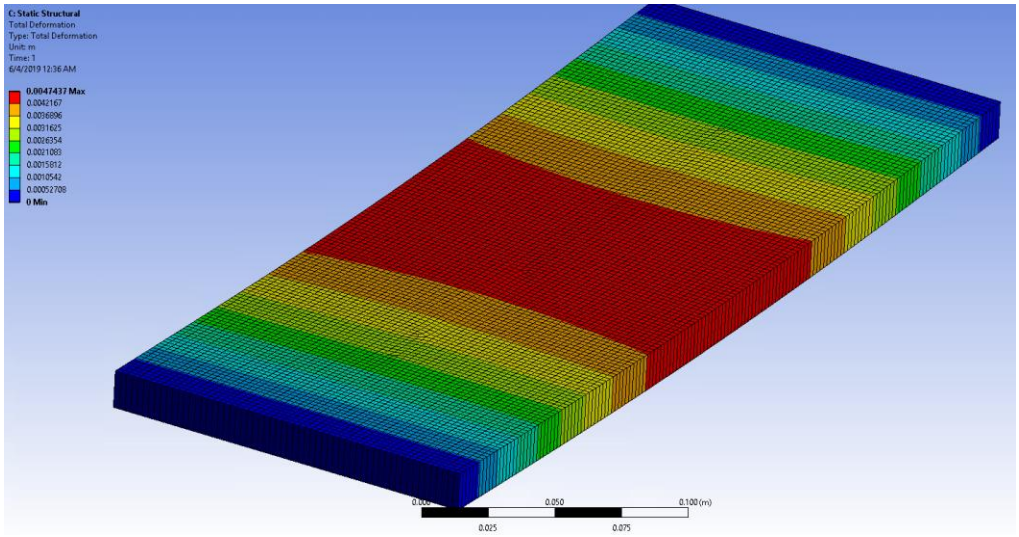

Figure 64. Resultant displacements after convergence study.

The existing model has a 40% error from the displacement of the tested panel, evident in **Figure 64**. The error is most likely due to the simplified boundary conditions and load application, as contact stresses and contact loads are not modeled. A model with these additions was created, discussed later in the analysis section.

Modeling & Laminate Design

To evaluate all the geometry changes and ensure high specific stiffness and strength, several global and local models were made to predict the stresses within the monocoque. In addition, models to predict panel performance for SES compliance were also created. A summary of each model and its purpose is included in **Table 4.**

Table 4: Model Summary

Model	Purpose	Model Number
Full chassis, rigid suspension model (ANSYS)	Quantify torsional stiffness Select ply angles Select roll hoop bracing orientation	(1)
3-point bend model (ANSYS)	Predict load capacity Predict displacement Predict energy absorption	(2)
3-point bend local failure modes (Excel)	Predict SES testing mode of failure	(3)
3-point bend CLT (MATLAB)	Predict panel properties	(4)
Local suspension: FLCA (ANSYS)	Characterize stresses at FLCA mounts	(5)
Local suspension: Hardpoints (ANSYS)	Size hardpoint puck for stiffness, strength	(6)
Full monocoque (ANSYS)	Predict thermal stresses during cure cycle	(7)

However, not all models were used due to material property inaccuracies for the T700 and HTS40 composite, namely (2), (3), and (5).

Structural Equivalency Spreadsheet

In order to run the vehicles at competition, the chassis must comply with the Structural Equivalency Spreadsheet (SES). Specifically, teams with composite monocoques must show that the chassis' respective sections can replace a given set of steel tubes in varying criteria, shown in **Table 5.** This was the most critical requirement is for chassis laminate development, as non-compliance would disqualify CP20C and CP20E from participating in competition altogether.

Table 5: SES Regulated Structural Areas and Equivalency Criterion

Section	Governed Parameters
Side Impact Structure (SIS)	Buckling modulus, ultimate tensile strength, peak shear load, energy absorption, directional stiffness, maximum 3 point bend force
Front Bulkhead Support (FBHS)	Buckling modulus, ultimate tensile strength, peak shear load, directional stiffness, peak 3 point bend force, maximum deflection, minimum EI
Front Bulkhead (FBH)	Buckling modulus, ultimate tensile strength, minimum EI, maximum deflection
Main Hoop Brace Supports	Buckling modulus, ultimate tensile strength, minimum EI, maximum deflection
Upper Harness Mounts	Buckling modulus, ultimate tensile strength, minimum EI, maximum deflection, peak 3 point bend load, representative panel test (with harness attachment)
Lower Harness Mounts	Buckling modulus, ultimate tensile strength, minimum EI, maximum deflection, peak 3 point bend load, representative panel test (with harness attachment
General Composite	Strength, stiffness, directional stiffness

The sections must pass a 3-point bend (3PB) test, where a test panel is manufactured measuring 500mm x 250mm is simply supported at two ends 400mm apart along the length of the panel, and a round load applicator with a 50mm radius is positioned halfway between the two supports. The test load data and position data are collected and compared to the data from a similarly conducted test of two steel tubes like those shown in **Figure 65**, with different tube sizes required depending on the evaluated structural area. Through these tests, panel performance properties can be acquired, including buckling modulus, ultimate tensile strength, peak shear load, energy absorption, directional stiffness, and maximum 3 point bend force.

The data yielded from the 3-point bend tests is inputted to the SES spreadsheet, which automatically calculates energy absorption and ultimate strength of the sandwich panel. It is compared to benchmark 3PB tests performed on two steel tubes and determines if the panel is stronger. As testing was performed, the panel failure modes were visually recorded, with written records and pictures accompanying each panel.

Figure 65. Steel tube baseline 3-point bend test setup.

The same layup must also pass a perimeter shear test, requiring a test panel measuring 100mm x 100mm to be supported by a flat plate with a 32mm hole at its center, shown in **Figure 66**. A 25mm punch aligned coaxially with the 32mm hole is then used to determine the load required to push the punch through the panel. The SES-regulated SIS and FBHS panels are required to support a set applicator shear load of 7.5kN and 4kN, respectively. These values are not directly dependent on the equivalency to a standard material and cannot be altered. The FBH, however, must have a peak applicator load equivalent to the load required to punch through a 1.5mm thick sheet of steel using the same load applicator and panel base.

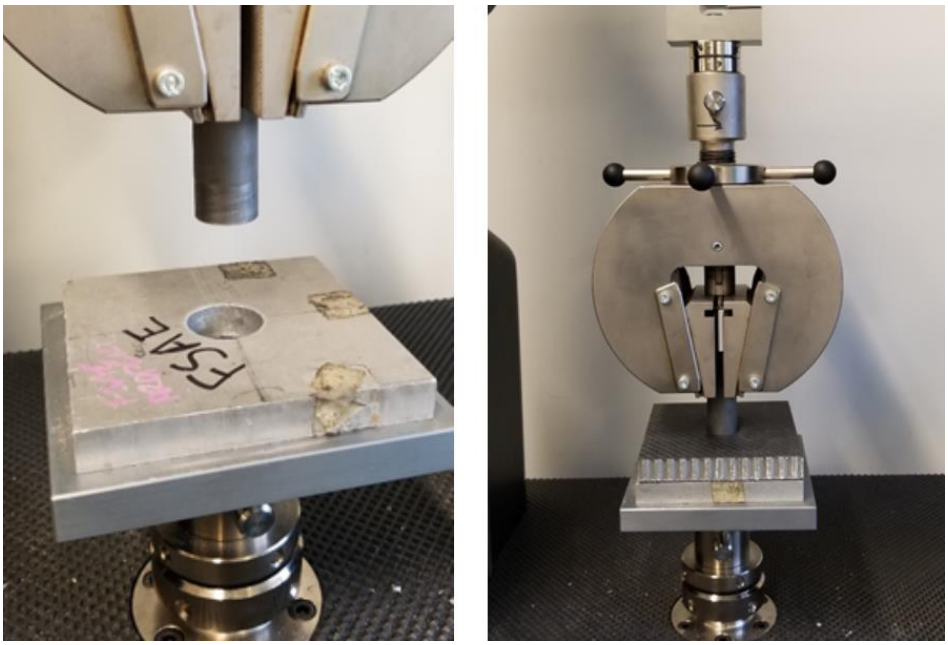

Figure 66. Perimeter shear test setup.

As previously mentioned, each 3-point bend section must pass tailored requirements based on tube properties qualified via ASTM standard 3-point bend testing. Using the resulting test data and panel dimensions, the SES spreadsheet calculates the properties of the panel and determines if it meets the requirements necessary. In addition to the physical tests, every chassis section must also pass a directional stiffness and strength requirement, stating that the fibers in the 0 degree direction of a panel must have at least 50% fiber in the 90 degree direction, evaluated by areal weight.

3-point bend models were made because panel performance can be predicted. This helped minimize the amount of time and resources required to develop a suitable sandwich panel layup as the team did not need to rely on excessive physical testing.

3-Point Bend Models

Test panel manufacturing consumes significant resources and time. To reduce time spent making panels, several 3-point bend models were made to predict panel performance and tune laminates for SES efficiently. A MATLAB script was made using Classic Laminate Theory (CLT) to quantify panel performance. The inputs included material properties, layup schedule, and an applied line load. However, this script calculates overall panel deflection and strength. It does not model local contact stresses, so typical 3-point bend failure modes cannot be predicted with this model. Instead, this model was used to eliminate most panels via SES stiffness and strength criterion, narrowing down test panel manufacturing to less than 10 individual panels per section.

To quantify contact stresses with more fidelity, a finite element model was created to model the panel. The facesheets were modeled using shell elements, as the shear deformation between the lamina did not need to be quantified. The core was modeled using solid elements to accurately represent the shear deformation and core shear stiffness, shown in **Figure 67**.

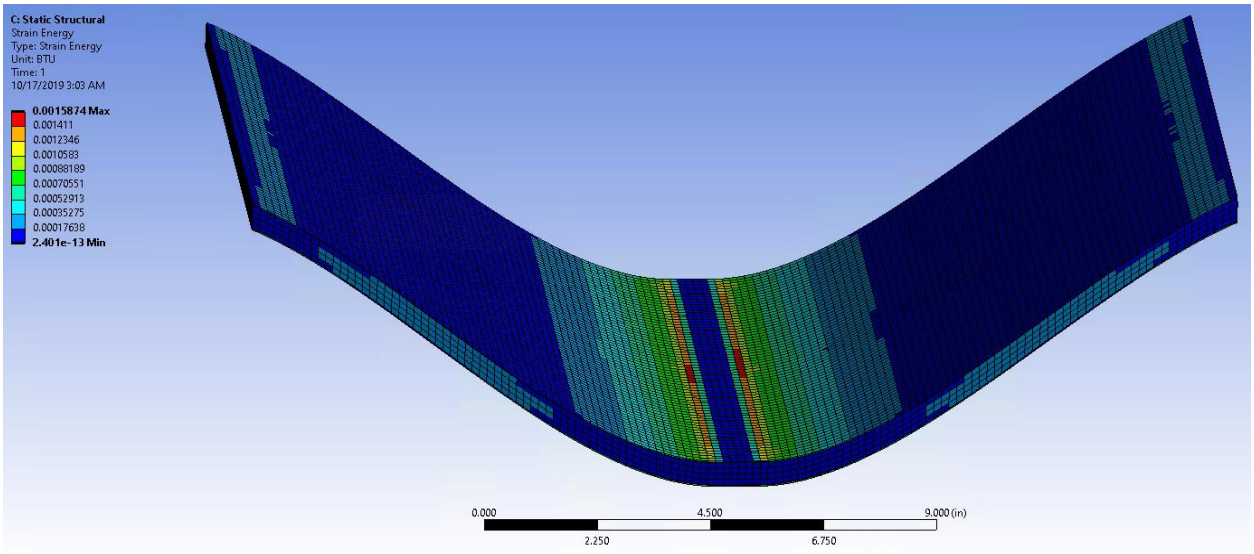

Figure 67. 3-point bend strain energy.

The load applicator was modeled as an infinitely stiff tube, and the load was applied to the applicator itself, resulting in a translated load from the applicator to the top facesheet. For the edge conditions, the panel was simply supported on both ends, as boundary conditions that included contacts was not needed at those areas. Most of the 3-point bend panels had local contact failures near the load applicator, usually due to the simultaneous core compression and transverse facesheet buckling, illustrated in **Figure 68**.

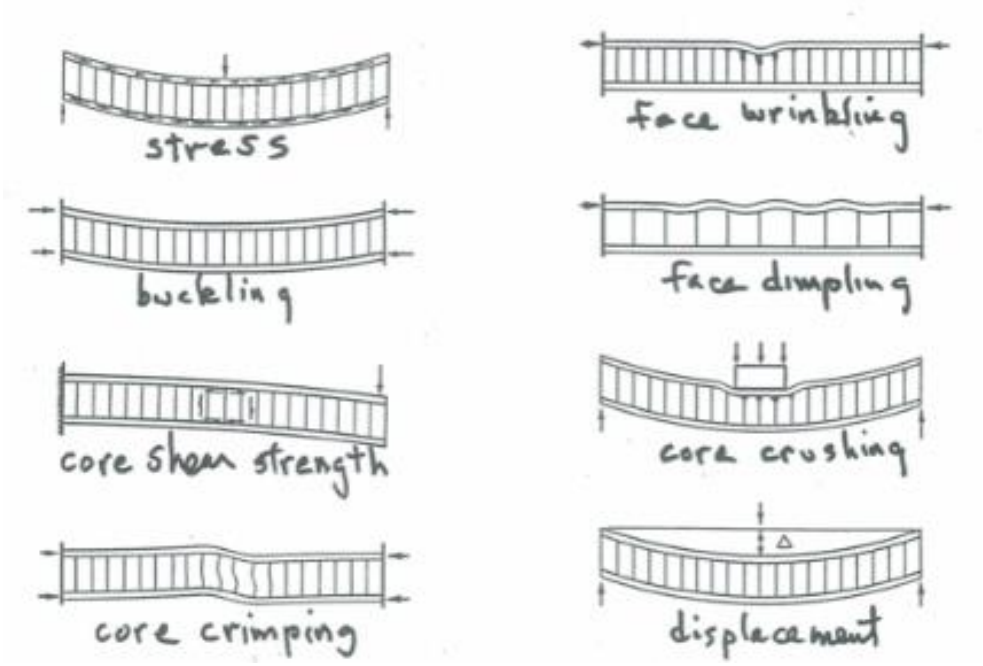

Figure 68. Typical sandwich panel failure modes.

Although complete, this model was not used to predict panel performance as the material properties were not representative of the actual materials used, specifically for the T700 composite. Resulting stress distributions looked reasonable, but the model's ability to predict failure modes cannot be verified until

multiple 3-point bend data sets are correlated with the FEM. However, if the model needs additional fidelity, the core near the load applicator could be modeled as individual shell elements. Furthermore, the load applicator should be replaced by nonlinear load functions applied to individual nodes along the midspan, replicating an elliptical load distribution from a tube applicator.

In addition, a 3-point bend failure mode spreadsheet was made to predict panel performance based on research published by Hexcel [8]. Inputs included panel dimensions and material properties, such as skin thickness and core shear modulus, respectively. The spreadsheet uses these parameters to calculate stresses and resulting safety factors for various failure modes, including facesheet yielding, core shear failure, facesheet dimpling, and facesheet wrinkling. This model was fully correlated to past test data, matching expected failure index criterion based on 2017 panel testing, which had known material properties. A snapshot of the most recent version of the spreadsheet used to predict local failure modes is included in **Appendix D** for reference. In the future, this script could be used as a quick method for predicting panel performance instead of a FEM, which requires significant effort to meet minimum accuracy for usable results. Additional failure mode criteria can be added to predict other modes of failure like core crushing, increasing versatility of the spreadsheet.

Local Suspension Model - Lower Control Arm Boss

With the new chassis geometry changes, stress concentrations can potentially be induced through small fillet radii and drastic angle changes needed to meet subsystem packaging. To meet the lower control arm suspension requirements, a boss was made, resulting in tight fillets and angle changes at the lower front bulkhead support corners. A local finite element model was created to quantify the laminate stresses in this section, as those are highly loaded areas due to suspension mounting, illustrated in **Figure 69**.

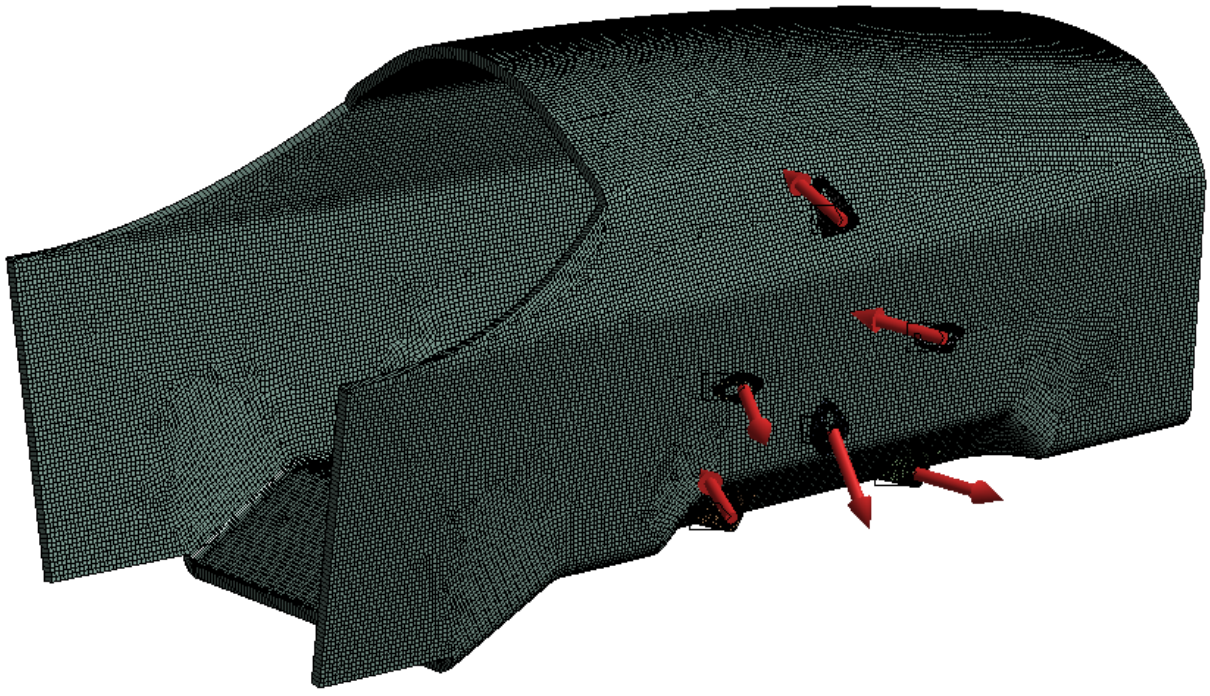

Figure 69. Chassis model and load paths.

This model included the front of the chassis, spanning from the front bulkhead to the end of the front bulkhead support section. Suspension mounts were included to model the behavior at the bolted joints. The

chassis surface was modeled using shell elements, with the suspension mounts modeled using solid elements. The front and rear edges of the chassis were fixed in space, spaced far enough from the loaded area such that their effects do not interfere with the stress distribution in areas of interest. An Excel-based steady state contact patch load calculator was used to define peak acceleration load cases, including braking, acceleration, cornering (lateral acceleration), and combined loading (braking and cornering), shown in **Table 6.**

Table 6: Acceleration and Contact Patch Load Cases

		Contact Patch Load (lb)					
		Front			Rear		
Operating Case	**Acceleration**	**Fx**	**Fy**	**Fz**	**Fx**	**Fy**	**Fz**
Braking	-2.3 long	-507	0	262	-118	0	58
Acceleration	1.7 long	163	0	79	471	0	241
Cornering	2.23 lat	0	474	276	0	487	285
Combined	1.8 lat, -1.0 long	-574	514	299	-426	374	217

Link loads were calculated using a MATLAB solver based on these contact patch loads and applied to the respective suspension mounts. A summary of the resulting link loads for the combined braking and cornering case is shown in **Table 7**.

Table 7: Link Loads Applied to Chassis Suspension Mounts

Link	ForcesX	ForcesY	ForcesZ	MAGforces
Fore Lower A-arm	-748.24	-1662.44	-163.65	1830.40
Aft Lower A-arm	-430.19	893.03	188.00	1008.91
Fore Upper A-arm	512.06	668.90	89.34	847.13
Aft Upper A-arm	261.91	-385.40	-109.01	478.55
Tie Rod	23.16	254.47	27.58	257.01
Push/Pull Rod	-3.71	-104.56	161.73	192.62

This model was not used to drive design decisions, as there was not enough time to evaluate resulting stresses using various failure criterion. To predict monocoque behavior subject to various load cases, normal and shear stresses can be evaluated using the Tsai-Wu failure criterion, with a sample normal stress distribution illustrated in **Figure 70**. Alternatively, since all the laminates used for the monocoque are fiber dominant (as opposed to matrix dominant), the maximum strain criterion is a more accurate method for layup evaluation [9].

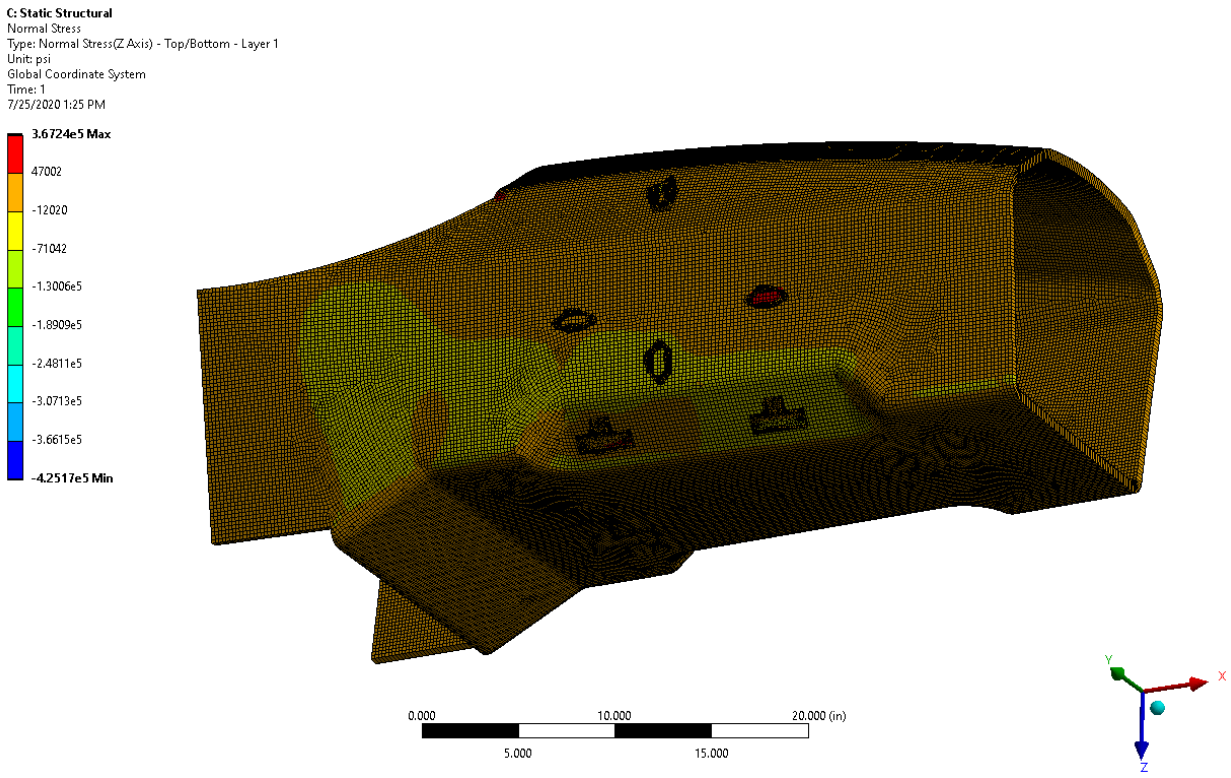

Figure 70. Normal shear stress, Z direction.

To analyze the panel using maximum strain criteria, strain magnitudes would need to be evaluated for each ply in the longitudinal and transverse directions, then compared to the material properties derived from in house tensile testing.

Local Suspension Model - Hardpoint Sizing

To account for high loads at suspension mounts and to meet camber and toe compliance goals, a hardpoint is manufactured at each mount. The hardpoint consists of a half spool insert potted with structural adhesive into a strong honeycomb core “puck”. To properly size the core puck, a local FEM was created, consisting of a suspension mount, the half spool inserts, and a representative panel. The panel is fixed at the outer edges, with an area large enough such that the boundary conditions do not have an effect on the area of interest. The panel was modeled using shell elements for the facesheets, and solid elements for the mount, insert, and core.

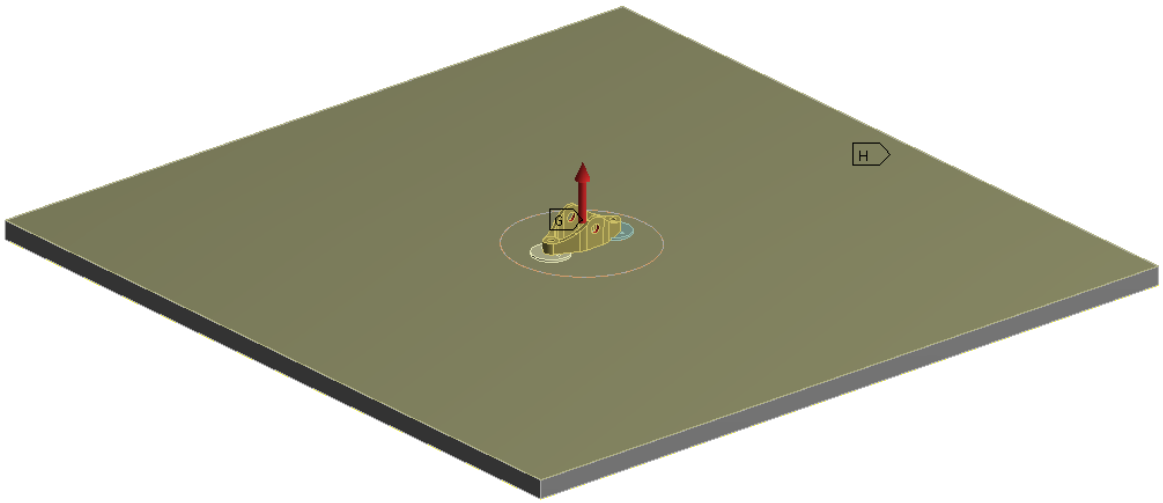

Figure 71. Hardpoint sizing model.

The panel components and inserts were constrained via bonded contacts, while the suspension mount was constrained via bushing joints to the inserts. To size these pucks, a representative suspension load was applied to the mount holes, as shown in **Figure 71**. A sweep through various puck diameters was performed to size the puck. However, this model did not utilize valid material properties, so no discrete conclusions could be made. Once the material properties are accurate, this model can be evaluated using maximum strain energy failure criterion to get safety factors for suspension loads. To further increase fidelity, representative volumes of the insert potting should be added to the model, as the structural adhesive plays a significant role in the subsequent load path from mount to global laminate. The ESA insert design handbook [10] can be referenced for statistical approaches to modeling adhesives. Additionally, stiffness can be evaluated via deflection distributions, as shown in **Figure 72**.

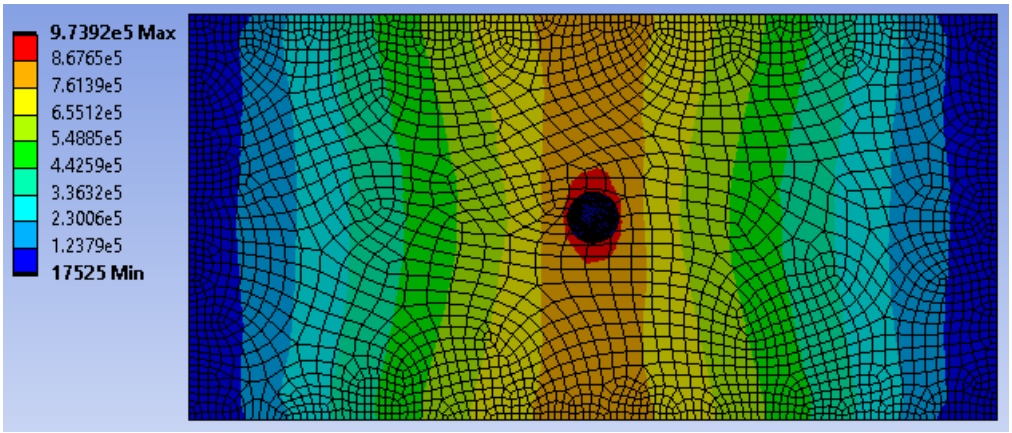

Figure 72. Local hardpoint FEM.

Torsional Stiffness Model

One of the most critical design parameters is chassis torsional stiffness. Lower chassis torsional stiffness correlates to increased roll angle under cornering, akin to how a soft spring will deflect more than a stiff spring for a given load. This has a negative impact on vehicle handling through cornering and any lateral acceleration case, as load is manifested in spring displacement as opposed to complete load transfer through

the rigid links. Shown previously in **Figure 28**, a sweep through roll stiffness distribution with varying torsional stiffness was modeled. With lower stiffnesses, the lateral load transfer distribution is not a linear function of roll stiffness distribution. This resulted in inconsistent spring/damper actuation, leading to unpredictable handling through varying damper forces and tire forces.

Based on this sensitivity, the target torsional stiffness was set to 1700 lb-ft/deg to eliminate any noticeable effects on handling. To achieve this goal, the major components to be evaluated include roll hoop bracing placement, layup schedule, and geometry.

Figure 73. CPFSAE 2019 main hoop bracing configuration.

The roll hoop may vary its mounting locations on the chassis, and be braced by either a forward swept brace, or a rearward swept brace, as shown in **Figure 73**. To finalize the roll hoop package, several items were considered including, driver egress and cockpit accessibility, weight, and rear powertrain accessibility. An ergonomic study was conducted in the current car to determine feasibility for driver egress, and it was found that the bracings had a minimal effect; therefore, this consideration was eliminated. The weight tradeoff between forward swept and rearward swept bracings were minimal, with a total weight difference of less than 5%, shown in **Table 8.**

Table 8: Forward Bracing versus Rearward Bracing Weight Difference

Forward Swept Bracing [lbf]	Rearward Swept Bracing [lbf]	Percent Difference [%]
10.51	10.04	4.5%

Due to this minimal difference, weight was also removed as a factor for consideration. Forward swept bracings would lend to easier accessibility in the rear for engine, differential, and other powertrain components, as the main hoop bracings in the past have typically hindered any access from the top of the chassis.

Furthermore, a finite element model was created to evaluate the performance of the forward swept main hoop bracing. In this model, the monocoque, main hoop with bracings, and suspension geometry were modeled. The hoops and suspension links were modeled using beam elements, and the monocoque was modeled using shell elements. For simplicity and solver speed, composite materials were not applied to the chassis, as that was not the focus of this model. Instead, the chassis and suspension were modeled using structural steel.

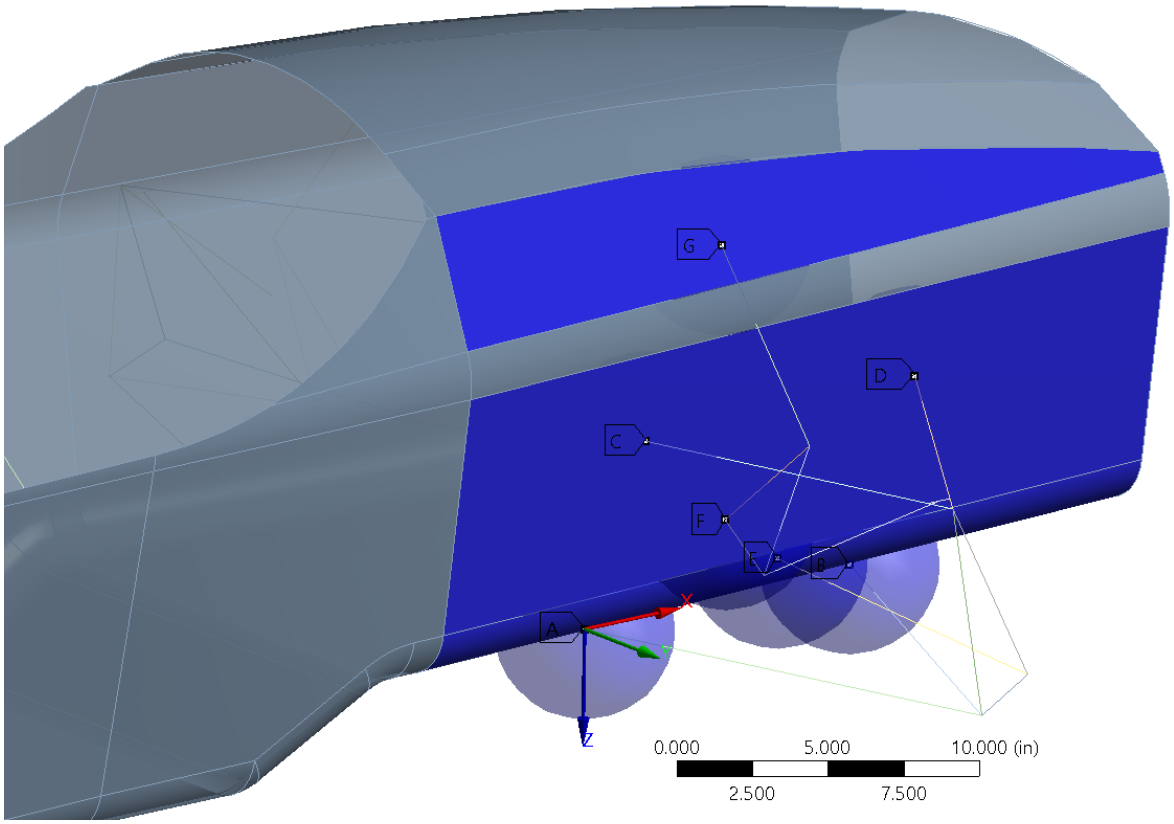

Figure 74. Sample inboard boundary conditions. Vertices are constrained to the chassis using pinball regions (shown in blue).

Shown in **Figure 74**, each of the links were constrained in translation relative to each other and left free in rotation, as each link joint has a bearing. The overall model was simply supported at three corners, and a load was applied to the fourth corner, shown in **Figure 75**.

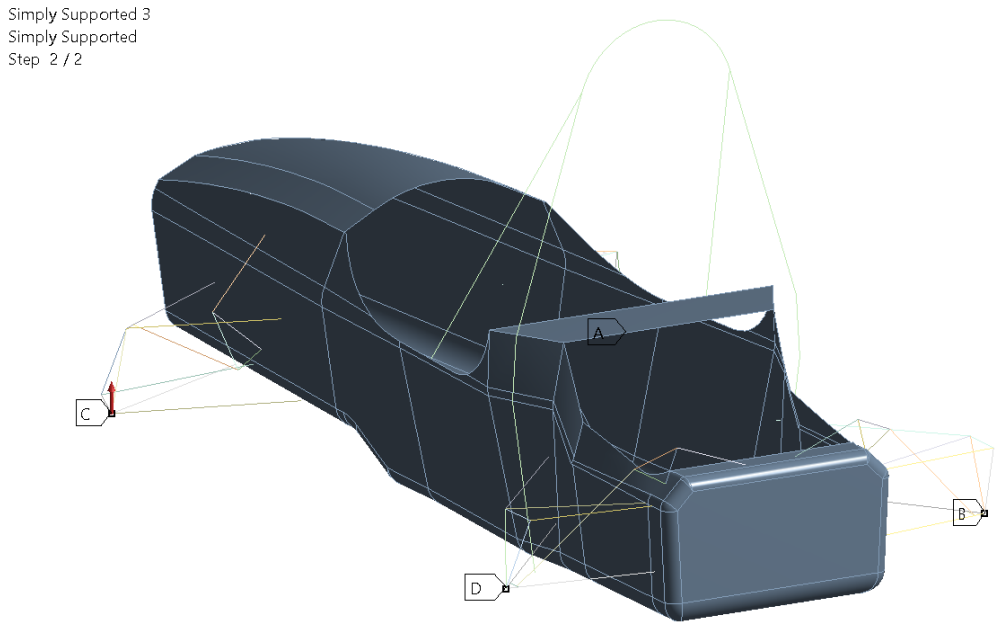

Figure 75. Torsional stiffness full vehicle constraints to model ground.

In addition, the main hoop was fixed in all three degrees of translation and rotation relative to the monocoque. After doing a coarse mesh convergence study, the model results matched predictions, with the forward swept bracings improving torsional stiffness and load distribution along the length of the chassis. Shown below, the principal stresses are less evenly distributed throughout the monocoque geometry without a forward swept bracing.

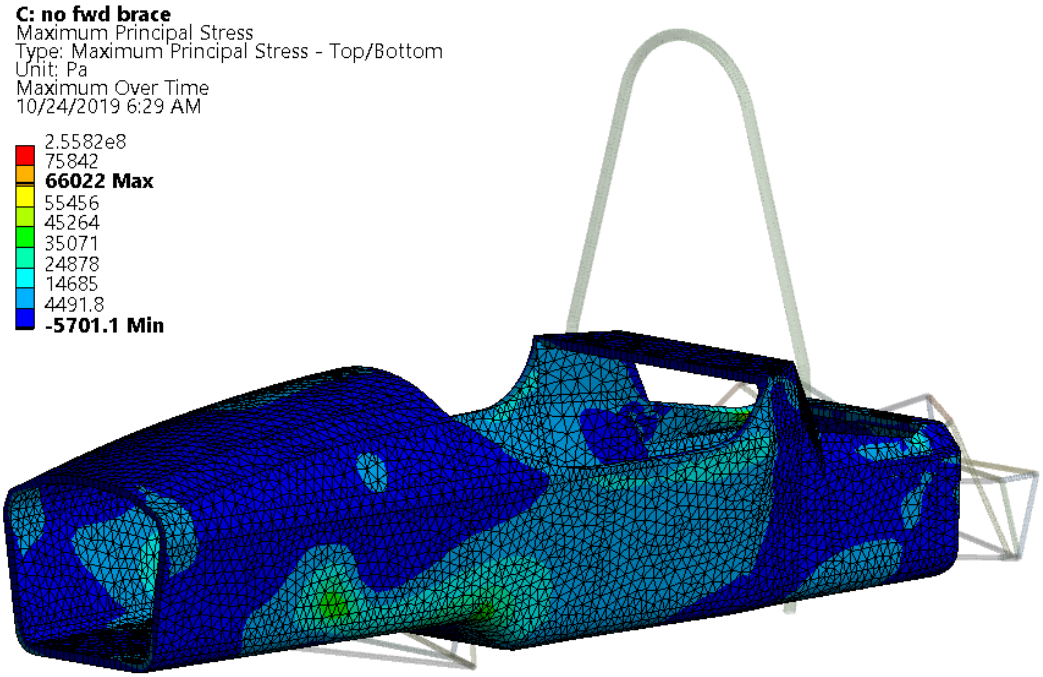

Figure 76. Maximum principal stresses, no forward sweep.

In particular, the sections by the lower control arms and change in chassis floor height have higher stresses than any other section of the car. Furthermore, most of the stress field only resides along the length of the cockpit, which is the worst section for torsional stiffness as it is not a closed tube section, unlike the rest of the chassis. On the other hand, the forward swept bracing, shown in **Figure 77**, distributes the load more evenly throughout the chassis, with peak stresses being significantly lower than its no bracing counterpart. The highest stresses are at the fixed points of the main hoop bracings, as opposed to the front lower control arm mounting locations.

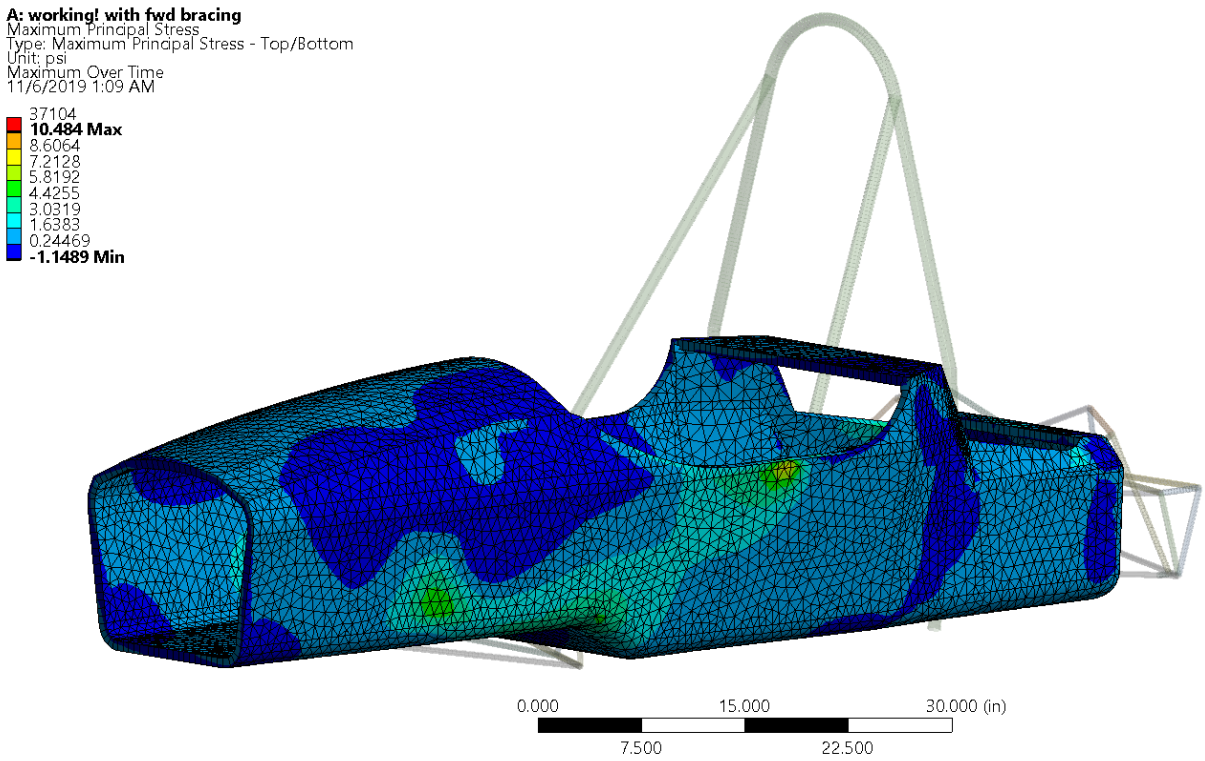

Figure 77. Maximum principal stress.

The forward swept bracing model showed a more favorable stress distribution, as the load is not concentrated in one section of the chassis. Illustrated in **Figure 78**, the floor shows a significant change in stress distribution between the two configurations, with the forward swept bracing configuration displayed on the right. Stresses are lower in the peak areas by about 6%, and more of the load is distributed throughout the floor. The difference in lower control arm stress distribution is even more apparent in the floor views.

With respect to total deformation, the forward swept bracing configuration results in lower deflection, specifically a 20% increase in torsional stiffness relative to the other bracing configuration.

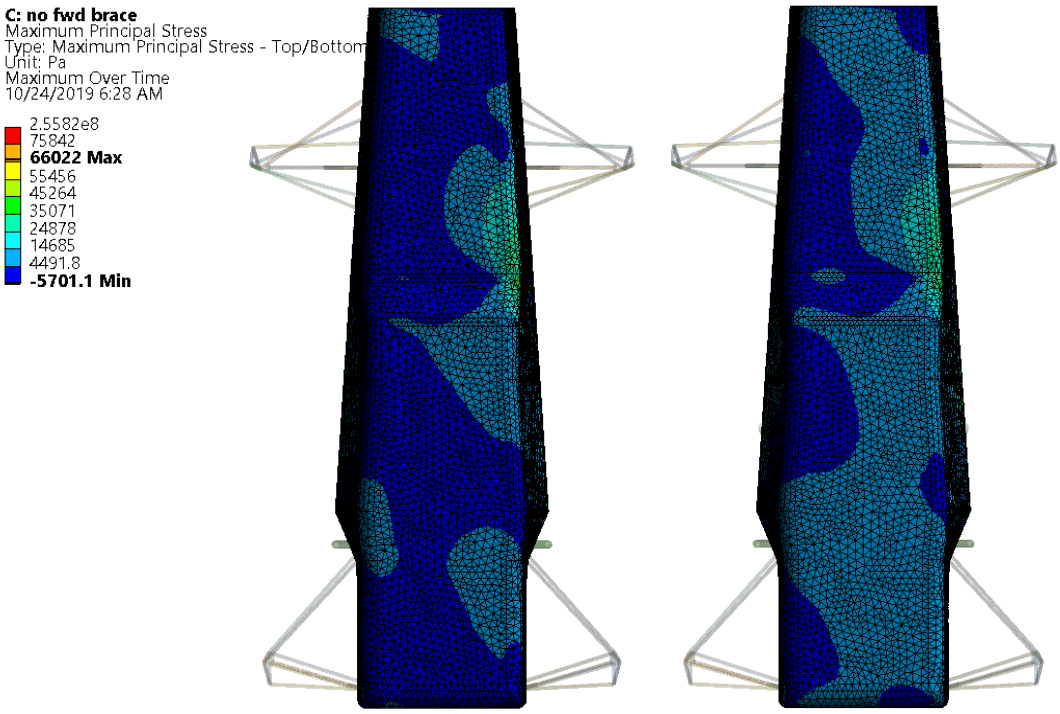

Figure 78. Maximum principal stress distribution, chassis floors.

This is evident in **Figure 79**, showing the deflection of the chassis without forward swept bracing. Without the forward swept bracing, the front section of the chassis tends to parallelogram, significantly deforming the local aft control arm sections.

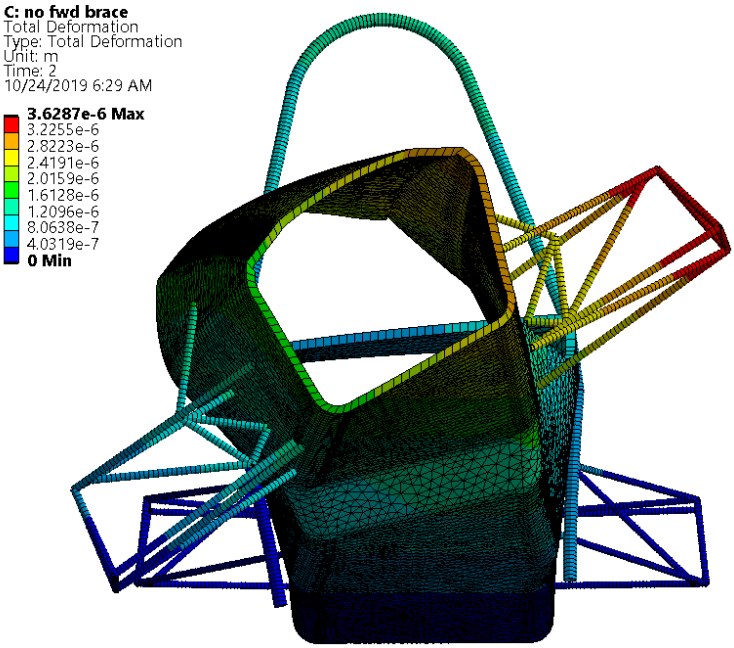

Figure 79. Total torsional deformation without a forward swept bracing.

The forward swept bracing had significantly less deformation since a portion of the torsional stiffness load was transferred to the main hoop bracings, shown in **Figure 80.**

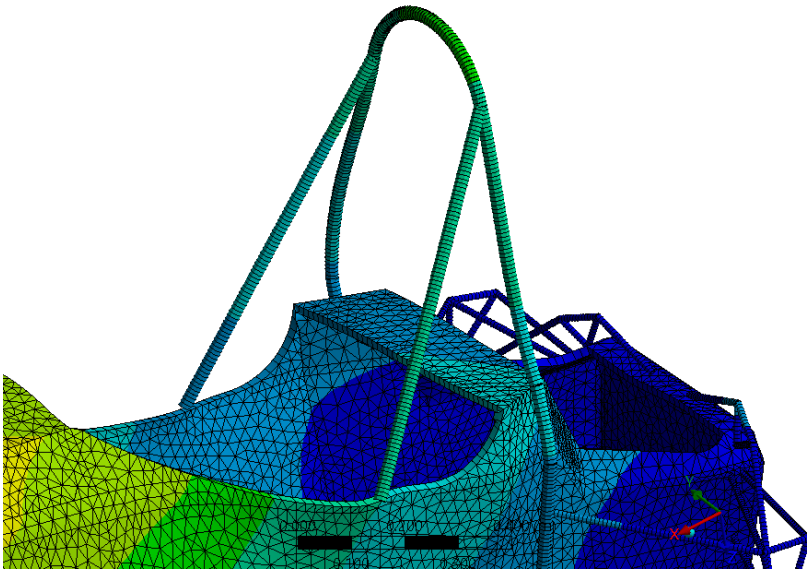

Figure 80. Deformation through bracings.

Total deformation is illustrated in **Figure 81**, with the parallelogram phenomena seen in the other model much less apparent. The magnitude of deflection is much lower, and the whole chassis deflects together as opposed to solely deforming the hardpoints around the suspension mounts. In addition, the main hoop has a higher deflection as the load distribution is more evenly spread out.

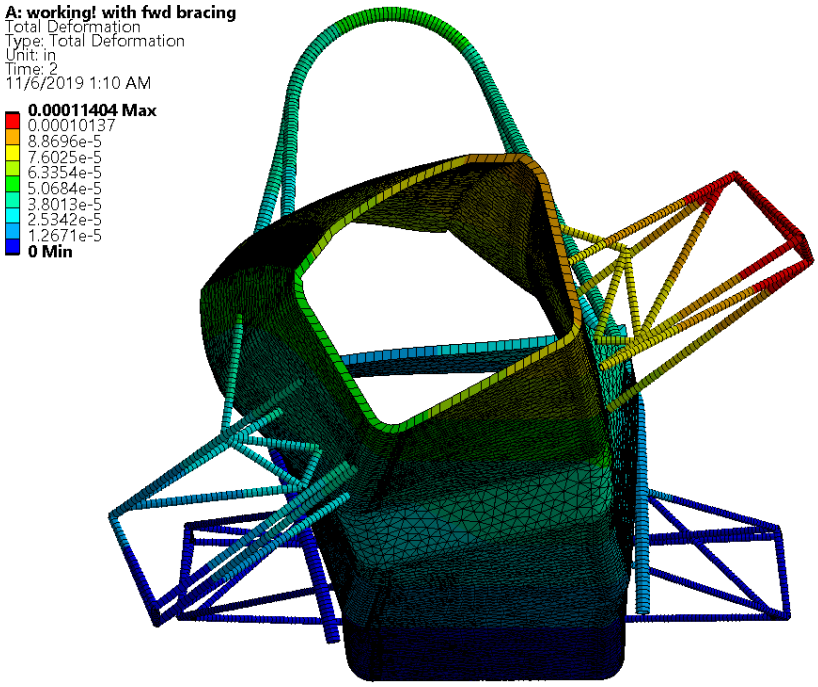

Figure 81. Total torsional deformation with forward swept bracing.

By evaluating these parameters, the forward swept bracing was found to be the best configuration, resulting in a better load distribution throughout the chassis and a higher torsional stiffness.

Once kinematics were developed to a near-final iteration, the torsional stiffness model was reconstructed using the updated points along with the expected layup schedule. The suspension links and roll hoops were modeled as beams, and the chassis was modeled using shell elements. The laminate was generated using ANSYS ACP Pre, the composites pre-solver module.

Table 9: Preliminary Layup Schedule with Color Code

	Description	**Layup Schedule**
	General	[45c/0/0c/0.5 Core/0c/45c]
	SIS	[45c/$(0)_3$/$(0c)_3$/0.7 core/$(0c)_2$/0/45c]
	FBHS	[45c/$(0)_2$/$(0c)_2$/0.5 core/0c/45c]
	Front Bulkhead	[$(45c/0/0c)_5$/0.25 core/$(0c/0/45c)_4$/0c/45c]
	Upper Harness	[$(45c/0c)_4$/0.5 core/$(0c/45c)_4$]
	Lower Harness *	[45c/$(0)_3$/$(0c)_3$/0.7 core/$(0c)_2$/0/45c]

* At the time of completion of this model, the lower harness schedule was not chosen. For manufacturing, the SIS schedule was used, with pad-ups laid near the harness bolt interface. The final, SES-confirmed laminate is included in **Table 14** in the "Structural Equivalency Testing and Summary" section of this report.

The laminate used for the final model is broken down by each SES section in **Table 9** and **Figure 82**.

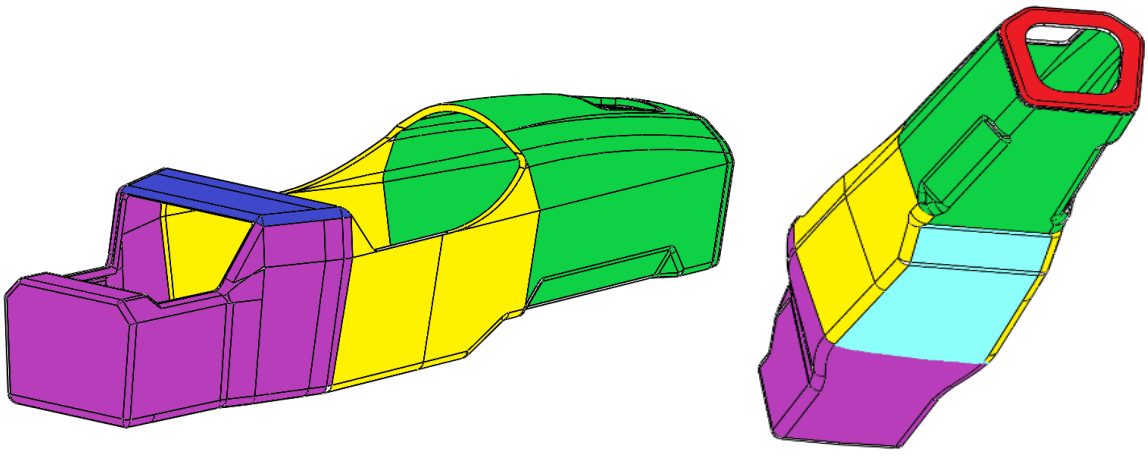

Figure 82. Color coded preliminary laminate breakdown as specified in Table 9.

The expected asymmetric layup was applied, and the same external boundary conditions as used in the bracing model were applied. With this geometry, the chassis is predicted to have a torsional stiffness of 600 lb-ft/deg, 60% lower than the desired minimum, illustrated in **Figure 83**.

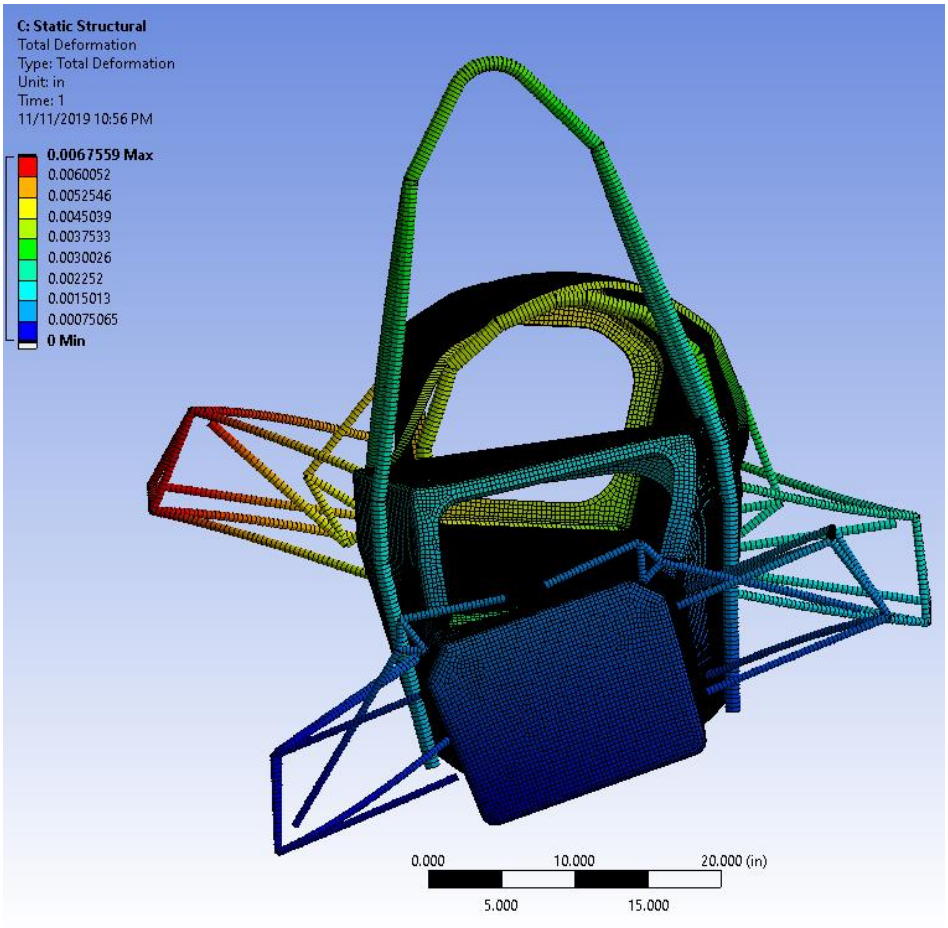

Figure 83. Initial torsional stiffness model with developed geometry, suspension points, and laminate.

Therefore, major geometry changes needed to occur to increase torsional stiffness. Based on the strain distribution shown in the initial model in **Figure 84**, several areas of interest were explored.

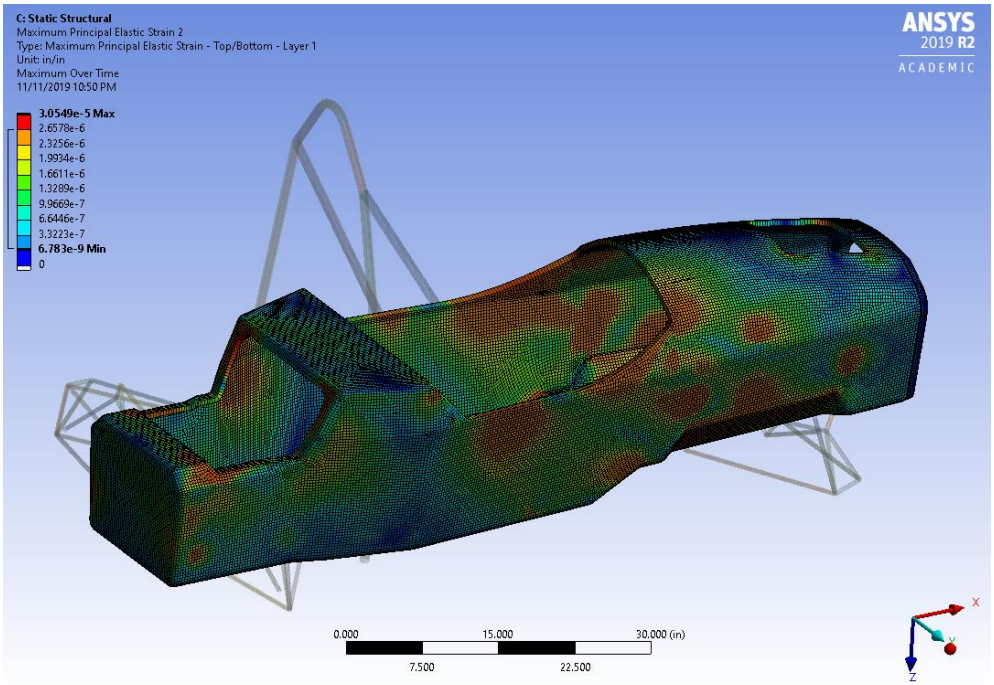

Figure 84. Strain distribution of initial model.

Notable locations include the transition from the front bulkhead support section to the cockpit sidewall as well as the rear stepdown. As displayed in **Figure 85**, there are high strain hotspots near the transition from the front bulkhead support to the cockpit area, near the edge and corner.

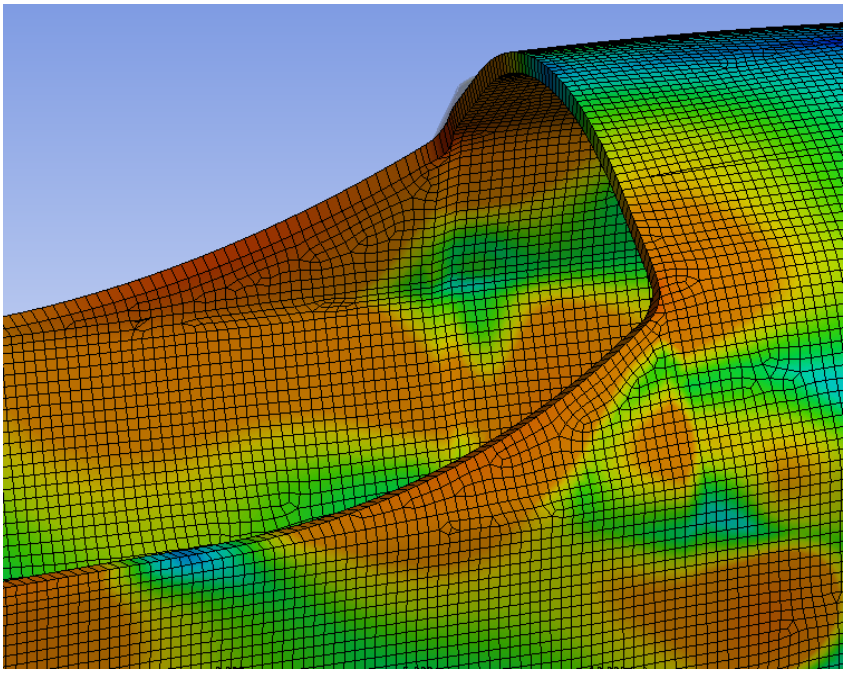

Figure 85. Strain hotspots at the cockpit transition from the front bulkhead support.

As expected, any sharp changes in geometry resulted in high strain areas, which were not captured by the initial springs-in-series model, particularly at the powertrain bay cutout. The rear shock shelf was moved up several inches and the transition from shelf to the upper harness panel was smoothed, shown in **Figure 86.**

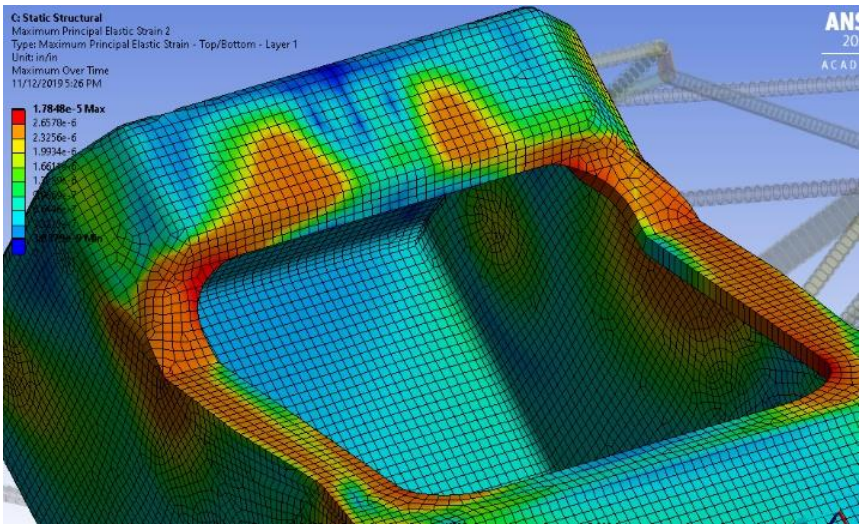

Figure 86. Strain hotspots at the rear stepdown.

Even after the geometry modifications, the rear powertrain bay was the largest contribution to compliance, thus explored in a torsional stiffness study, described below. Another area of high strain was the near the floor height transition, shown in **Figure 87**.

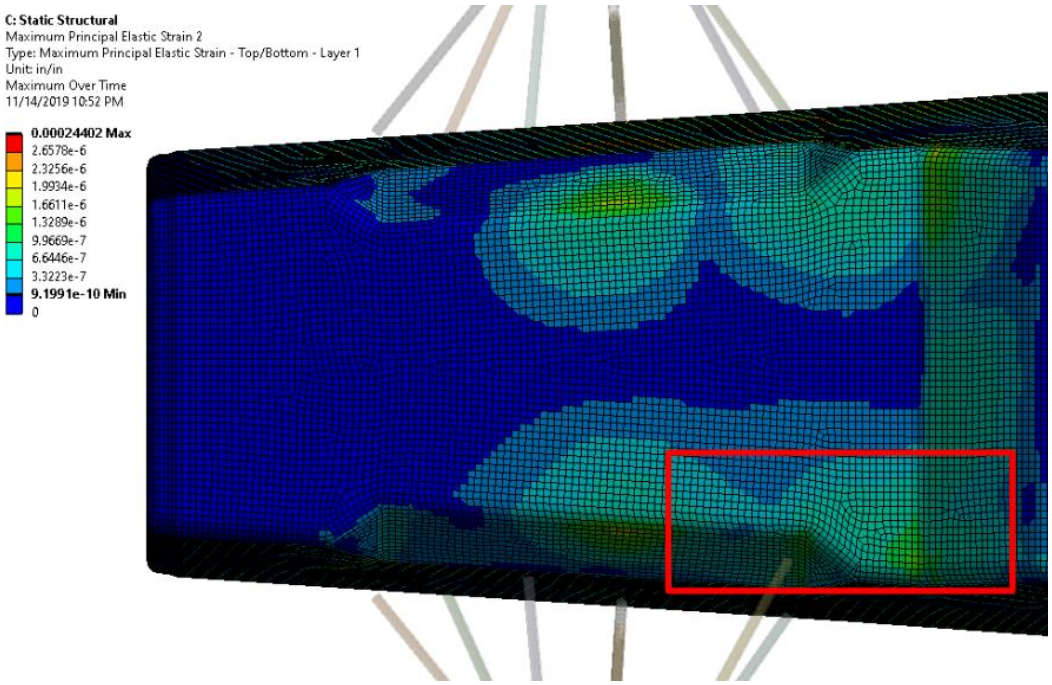

Figure 87. Strain at the monocoque floor height transition.

However, this model did not include any hardpoints at the suspension mounts, which is critical to local stiffness for camber and toe compliance. To nominally maximize stiffness, hardpoints consisting of an extra $[(45_c/0_c)_s]$ pad-up and stiffer core were applied to the laminate suspension mounts as well as the floor transition area.

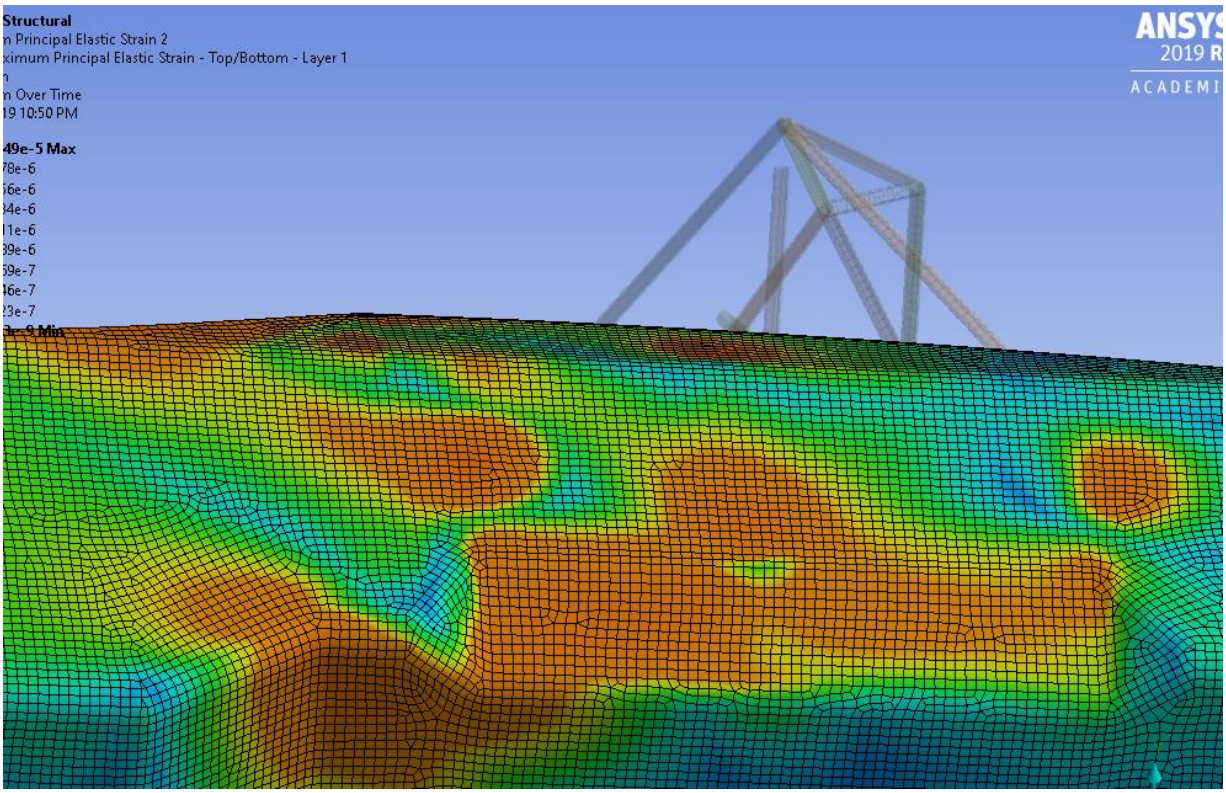

Figure 88. Strain hotspot at the rocker and control arm mounts.

Because torsional stiffness could be increased by adding material back to the cockpit sidewall height and rear stepdown, two sweeps were conducted to quantify the general trend of torsional stiffness as a function of geometry changes. Displayed in **Figure 89**, the cockpit sidewall was increased to the tallest possible height, then partitioned into 1" slivers.

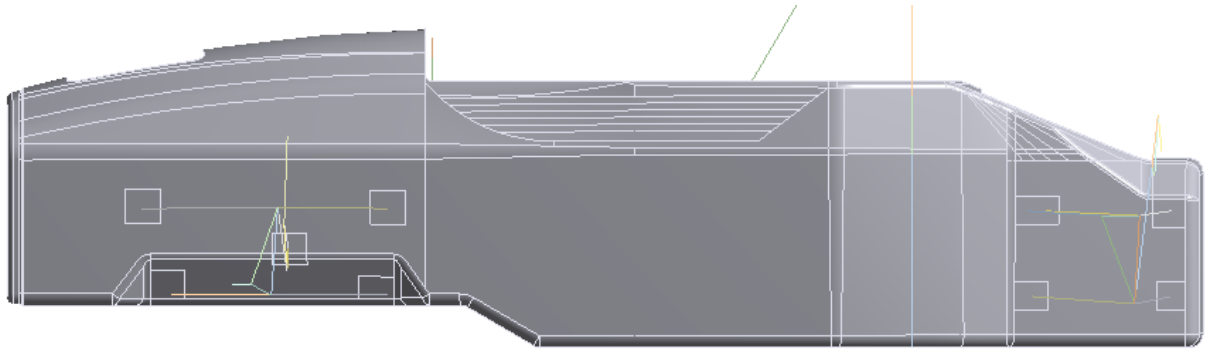

Figure 89. Partitioned cockpit sidewall height.

The first model was run where all the cockpit sidewall height was assigned as the SIS laminate material. Each sliver was then assigned to “air”- a material that has near zero stiffness, essentially unable to carry load. With this study, the torsional stiffness was linearly proportional to the cockpit sidewall height, decreasing as the sidewall decreases, shown in **Figure 90**.

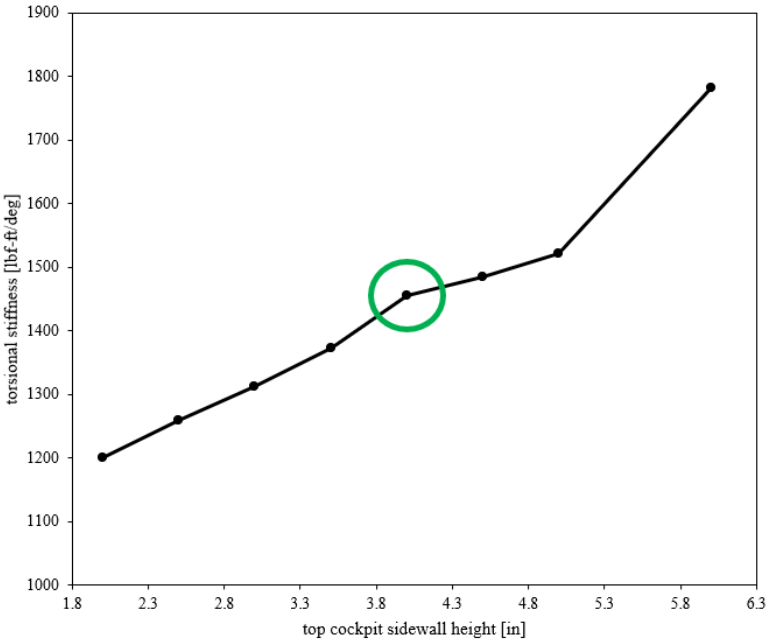

Figure 90. Torsional stiffness as a function of cockpit sidewall height.

To increase the torsional stiffness without increasing weight or decreasing accessibility significantly, a cockpit sidewall height of 4.0” was chosen. For the stepdown geometry, a coarse angle sweep was conducted in a similar fashion, illustrated in **Figure 91**.

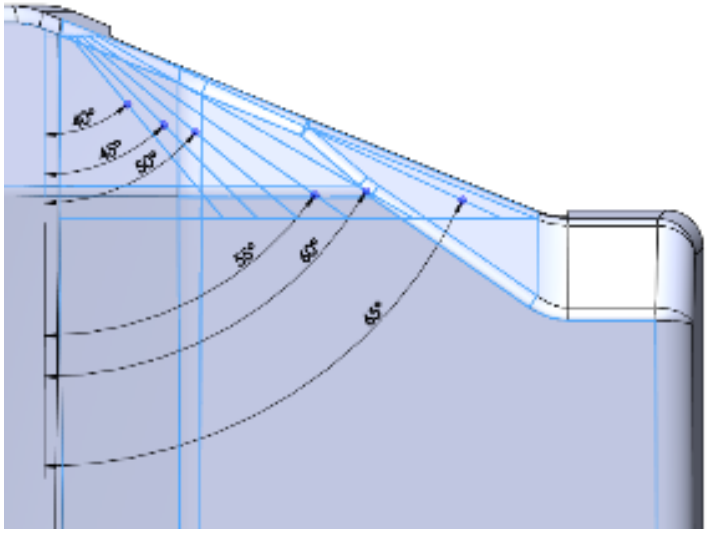

Figure 91. Rear stepdown angle sweeps.

Partitions in 5 degree increments were made on the chassis surface, minimizing sharp changes in form factor. Similarly, an "air" material was applied to the rear stepdown in increments, changing the effective amount of load carrying structure. Based on this sweep, shown in **Figure 92**, the monocoque torsional stiffness was extremely sensitive to the stepdown angle.

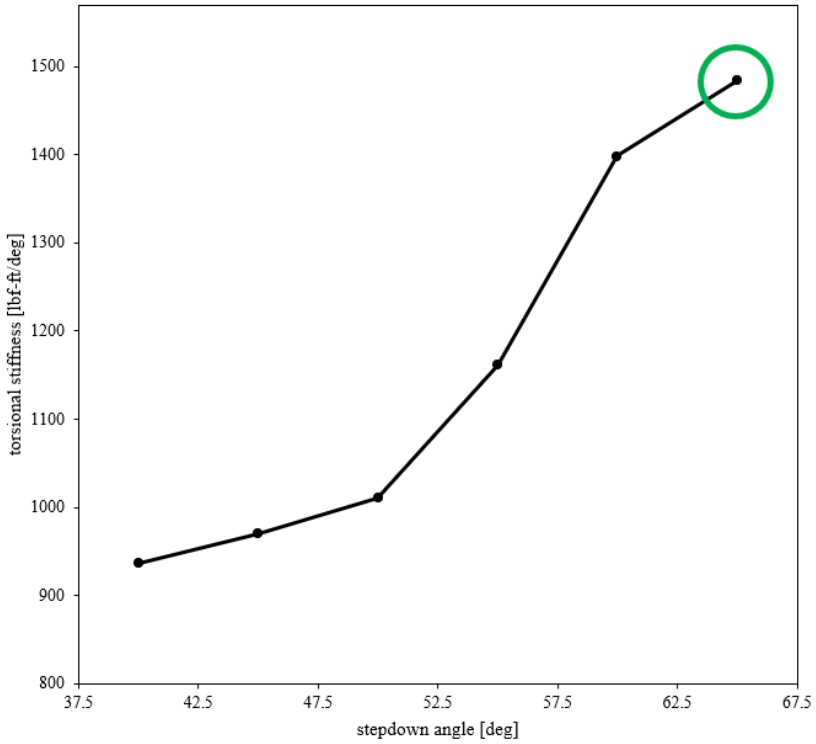

Figure 92. Torsional stiffness sensitivity to stepdown angle.

To meet the torsional stiffness goal, the largest stepdown angle of 67.5 degrees was selected. In the future, a better sensitivity study could be conducted with more seamless geometry changes, as this sweep did not include the overhanging material shown in **Figure 93** which reduces compliance significantly.

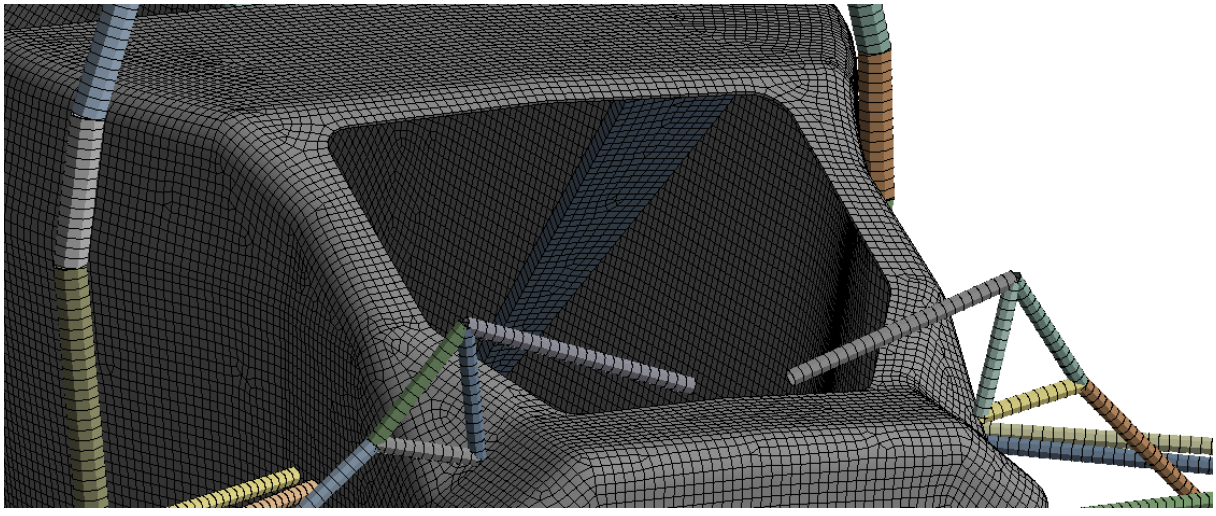

Figure 93. Overhang at powertrain bay access hole added to provide additional stiffness.

In the future, strain energy should be evaluated instead of strain for identifying areas of importance. Luckily, most strain energy hotspots overlapped with high strain energy for the monocoque, so improvements made to increase stiffness were still valid. As shown in **Figure 94**, the sections of high strain energy include the transition from the cockpit to the front bulkhead, the roll hoops, and suspension mounts.

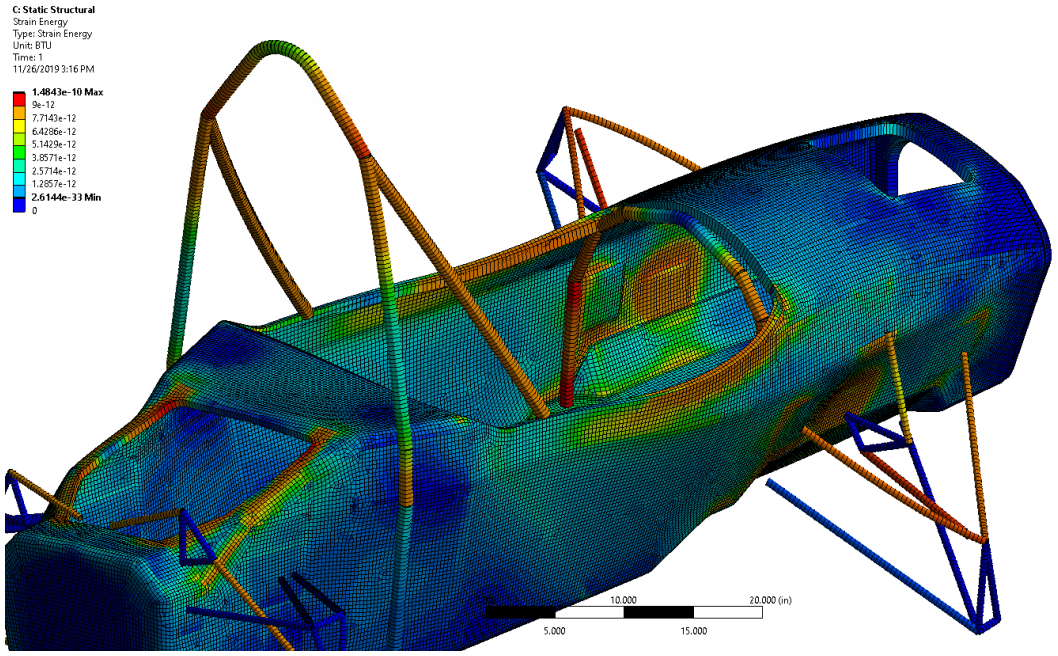

Figure 94. Full vehicle energy.

In particular, the shock and pullrod configuration had the largest strain energy compared to the rest of the suspension links, illustrated in **Figure 95**. With this suspension link configuration, the chassis was subjected to high plate bending loads at the shock. Furthermore, the low pullrod angle results in high link loads, making this configuration undesirable.

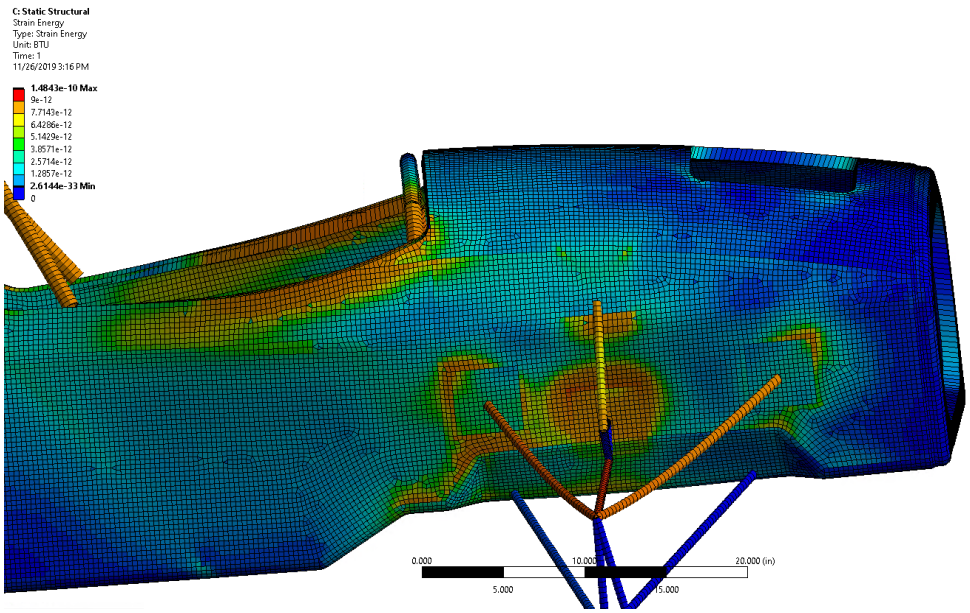

Figure 95. Front suspension strain energy.

Therefore, the suspension configuration was changed to top mounted pushrods to reduce chassis and suspension loads, pictured in **Figure 96**. By changing to the top mounted shock configuration, loads were reduced through the pushrod link and shock by 75%, a significant decrease in load which led to a link weight reduction of 7 lbs.

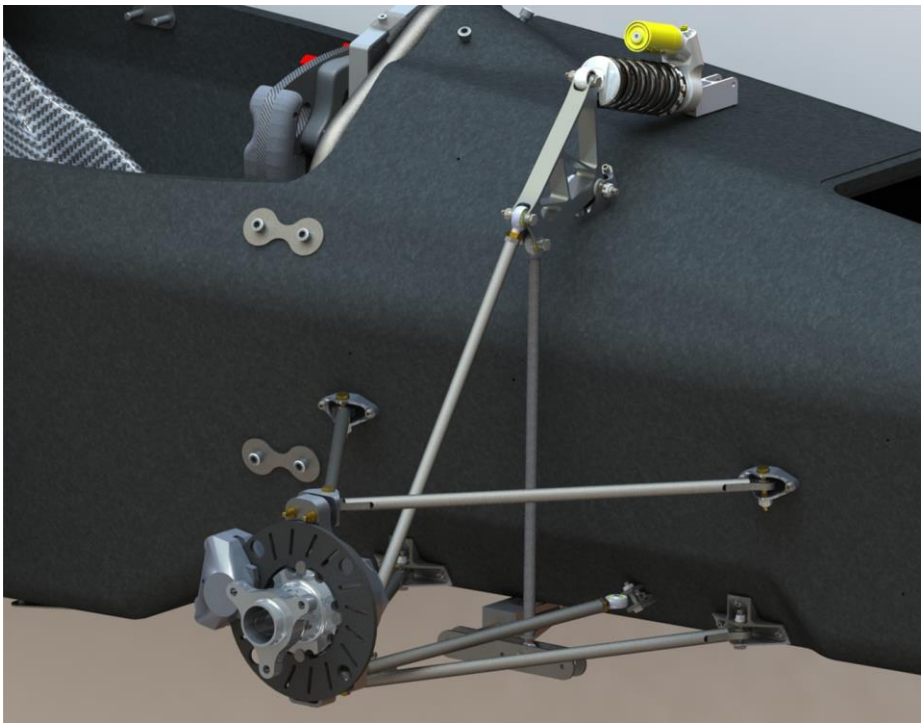

Figure 96. Final front suspension configuration.

Once the geometry was finalized to integrate the new front architecture, a final full torsional stiffness model was completed. Final SES laminates were assigned to each section, described later in the report, and hardpoint laminates with the finalized puck diameters were applied to each suspension mount section.

The resulting deformation plot, shown in **Figure 97**, is minimized with the change to the pushrod configuration. By changing to the pushrod configuration, torsional stiffness was increased from 1500 lbf-ft/deg to 1650 lbf-ft/deg.

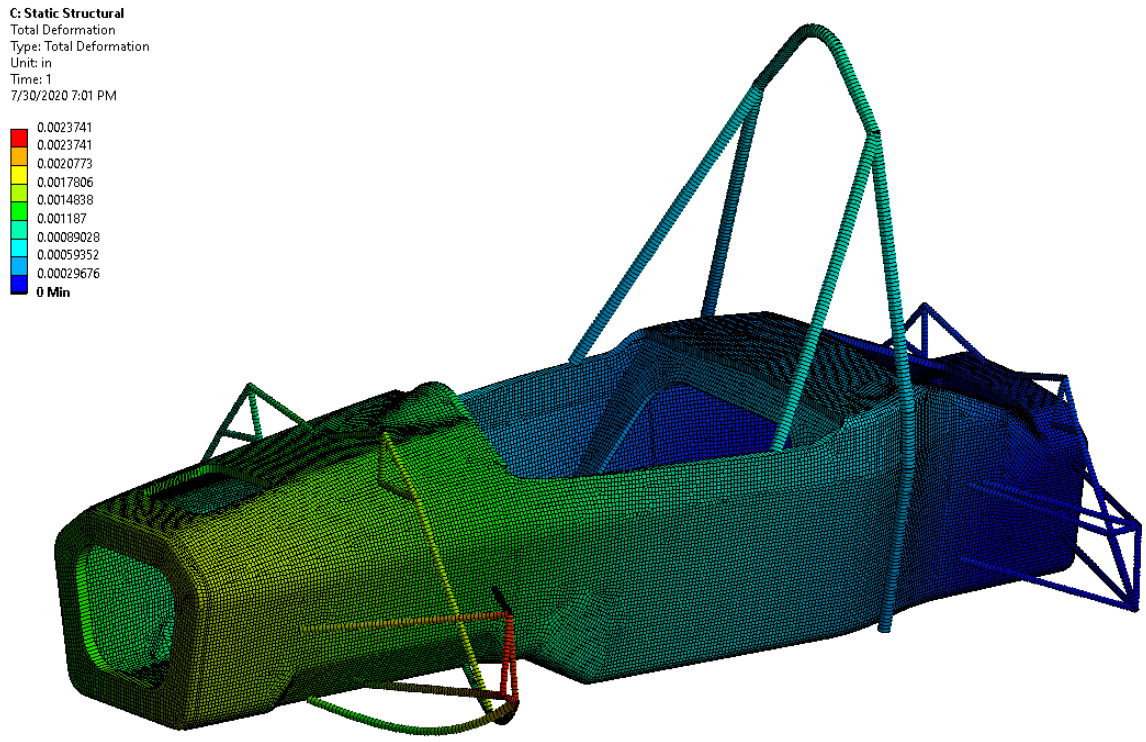

Figure 97. Completed FEM with updated geometry.

As expected, the strain energy at the front suspension decreased with the improved load path, shifting most sensitivities to the rear stepdown section and front bulkhead support transition, displayed in **Figure 98**. The cockpit floor transition region and surrounding FBHS areas also had high strain energy. Additional pad-ups in the form of unidirectional plies could be added to these areas to increase torsional stiffness for minimum weight gain.

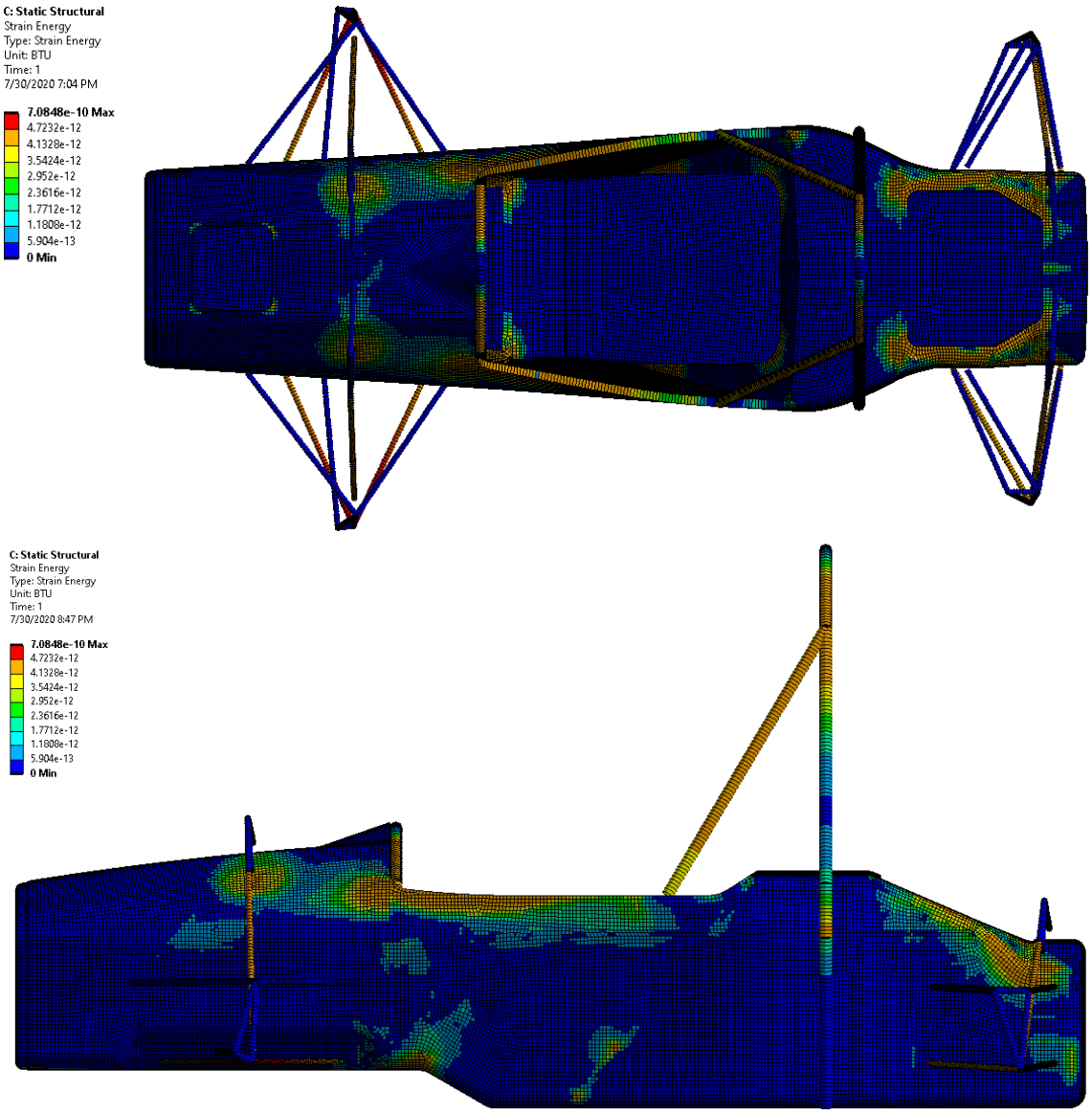

Figure 98. Strain energy distributions.

In the future, several changes should be made to the model to increase fidelity and improve model correlation. Each suspension mount should be included and modeled using plate elements, then connected to the chassis with appropriate CBUSH stiffnesses applied based on calculated joint stiffnesses, derived through the Huth equations or other equivalent joint stiffness model. Uprights should be modeled using plate elements with the correct material properties, instead of infinitely rigid links, as that is more accurate behavior of the structure in this type of reduced model. Rockers should also be converted to plate elements, as rockers behave more like a plate structure loaded in-plane than three rigid links. In addition, all major hole cutouts, specifically the axle slots, exhaust cutout and engine floor clearance hole, should be included to better model the stress distribution. In addition, the laminate edges should be constrained at the edges of the cockpit, front bulkhead, and rear powertrain bay to simulate closeouts as this is more representative of the physical chassis constraints.

Thermal Warping Model

With the introduction of an asymmetric layup to pass SES with low weight, thermal deformation occurs unevenly during the cool down portion of the cure cycle. For symmetric layups, the facesheets have equal coefficients of thermal expansion (CTE). However, with a thicker outer skin, the laminate will warp due to uneven CTEs, which could cause imperfections in the final part. Potential issues could include inaccurate suspension points, which leads to unbalanced handling left to right, and non-compliance with driver template. Therefore, the thermal deformation of the monocoque was quantified via a thermal finite element model. The purpose of this model was to identify the areas of deflection, specifically critical mounting locations, and quantify the magnitude of deflection. Using these trends, the mold layup can be tailored to stiffening the sections where it is needed, preventing warping in critical areas like suspension inboard mounting.

The chassis geometry was modeled using shell elements and constrained via two vertices at the cockpit cutout section to allow for free expansion in both directions. In reality, the chassis can freely expand in any direction during the cure cycle. However, this cannot be simulated as full free expansion in a finite element model will result in large deformations, and the solver cannot converge to a solution.

This model was run using a homogeneous asymmetric layup of [45c/0/0/0/0c/core/0c/45c], the preliminary Side Impact Structure laminate, as the laminate had not been fully defined for every section at the time. This layup is the most unbalanced layup that will be used in the chassis, as most SES regulated sections do not need to pass as high of an energy absorption requirement. A thermal load was applied to the body, ramping down from an initial temperature of 275 °F to 71 °F. As expected, the open edges tend to deform a significant amount, with up to .014” of deflection. In particular, the front bulkhead tends expand radially, shown in **Figure 99** and **Figure 100**, as it is the edge of a pseudo-closed tube.

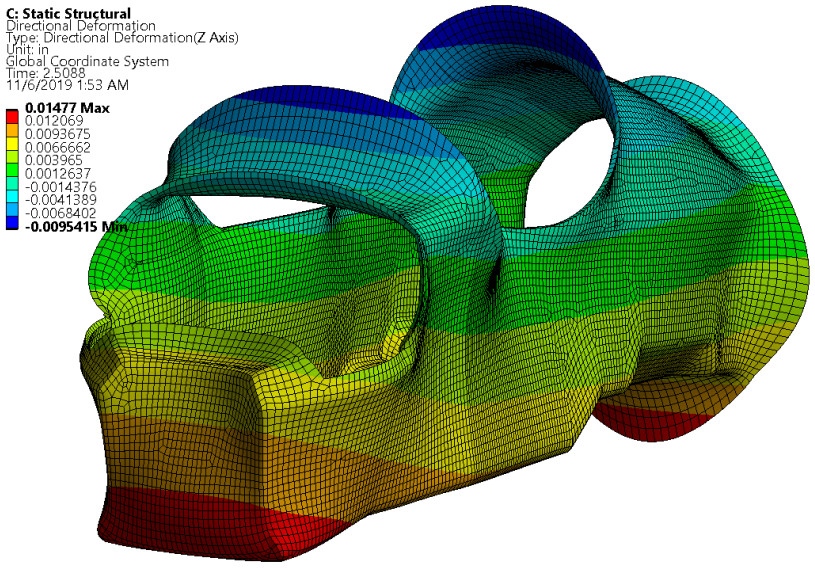

Figure 99. Total deformation from cure cycle ramp down.

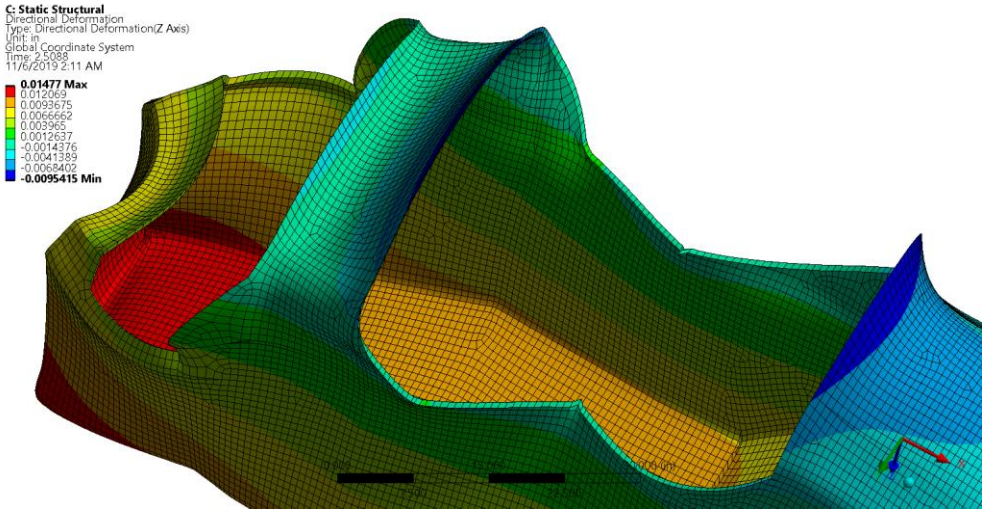

Figure 100. Second view of thermal deformation in the Z axis.

Furthermore, critical suspension mounting sections deformed up to 0.006”. This has a significant effect on kinematics, as tolerance stackups on top of suspension tolerances can lead to skewed roll center locations left to right, as well as uneven roll center migration through travel.

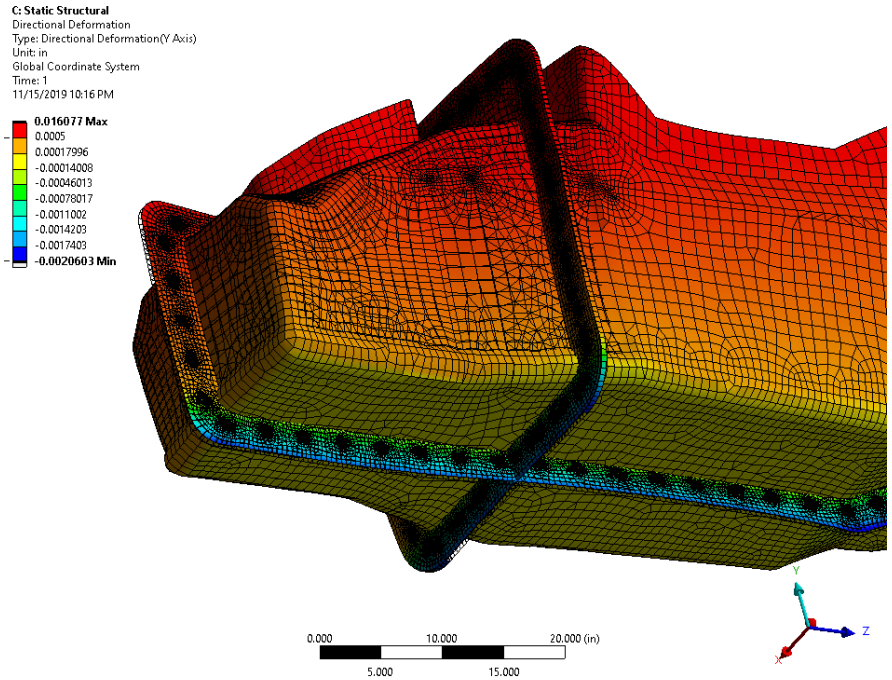

Figure 101. Thermal model with chassis and molds.

To accurately model the chassis thermal deformation, a second model including the molds was created. The chassis was constrained via a bonded contact to the mold inner surface, and the same ramp down thermal conditions were applied. A similar deformation distribution was produced, with the largest deformations existing at the cutout sections, as pictured in **Figure 101** and **Figure 102**.

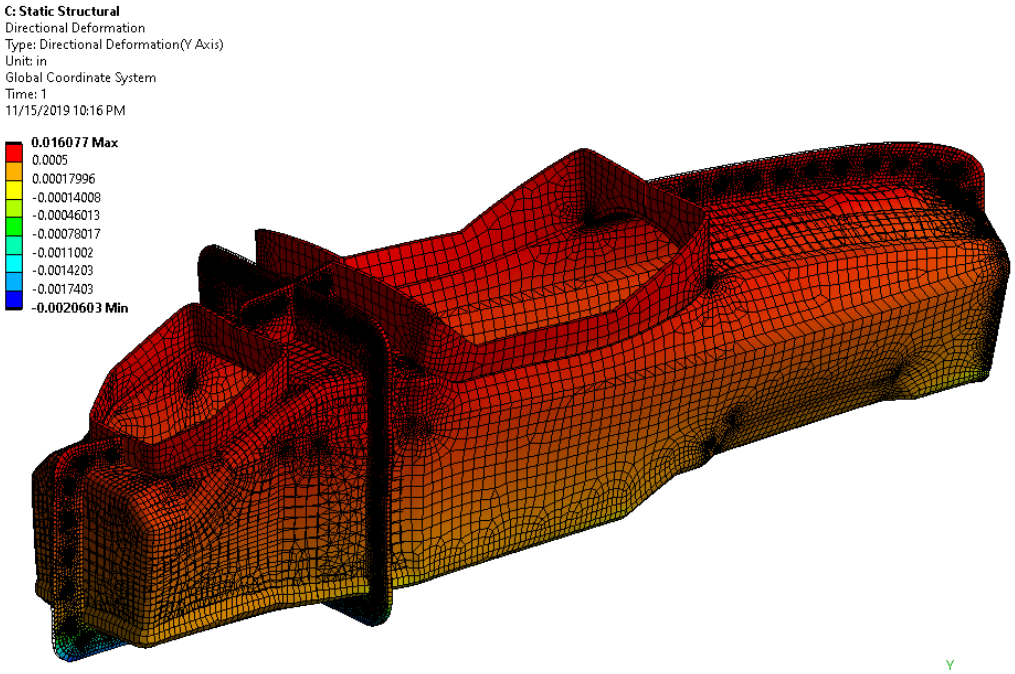

Figure 102. Vertical thermal deformation.

No major stress concentrations occurred due to the cure cycle, so any warping that could occur would be global. Probes were applied between suspension mounts to quantify the maximum expected deviation from nominal kinematics, and the resulting difference proved to be insignificant. The maximum change in location was less than 0.010", which is smaller than the tolerance for locating suspension mounts holes via drill jigs manufactured in house. Therefore, any monocoque deformations due to the ramp down portion are consumed in the tolerance stack up, and kinematics can be adjusted via shimming and tuning the conical washer stack up.

Chassis Weight Calculator

In addition to the ANSYS models, a simple spreadsheet was developed to predict the weight of the chassis. This spreadsheet, shown in **Appendix E**, uses each material's density in conjunction with the surface area of each local laminate to calculate the theoretical chassis weight. The calculator also includes core, core splice, film adhesive, hardpoint pad-ups and closeouts. A "ply overlap factor" is used to account for ply overlap and any excess material that may be added during the manufacturing process. Based on the final SES laminate discussed in the "Structural Equivalency Testing and Summary" section of this report, the chassis weight was predicted to be 43.6 lbs.

Cost Analysis

The CPFSAE team has given the chassis subsystem a preliminary budget of $1640 for the 2019-2020 season, which could increase to no more than $2500. However, this must include the cost of chassis details like roll hoop tubing as well as SES test materials. The MCD team and CPFSAE team have successfully established partnerships with numerous industry-leading companies, including Airtech, Chomarat, General Polymer Solutions, Henkel, Hexcel, PTM&W, Safran, and TenCate. Through these sponsors, the team has secured nearly every item required to make the actual chassis: including core, carbon prepreg and cloth,

adhesives, and release products. The team has also received $500 in funding from MESFAC for tooling resin, which was a significant cost.

Since composites and the products to make them are generally expensive, the MCD team made every effort to pick up materials and products at will-call wherever possible to eliminate shipping costs. Cheaper alternatives were considered wherever quality was not a concern, such as Harbor Freight brand consumables. A detailed cost breakdown and list of discounts is tabulated in **Appendix F**, and a cost summary is included in the Project Management section of this report.

Manufacturing

Carbon fiber reinforced polymer (CFRP) composites are made by curing a carbon fiber/matrix laminate around a tool which represents the desired geometry of the part. Uncured lamina may be either dry cloth or pre-impregnated (prepreg) unidirectional fibers or cloth with thermoset matrix. Curing can be achieved by applying hardening agents to resin (in a wet layup) or by baking the CFRP laminate (from a prepreg layup) in a composites oven.

To understand the philosophy of the 2020 manufacturing, the 2017-2019 manufacturing processes should be discussed. Typically, to create a master geometry, CNC material removal machines are used to take advantage of their accuracy and repeatability in 3D space. Additionally, CNC machines allow locating holes to be drilled into the master geometry. The male master geometry for the 2017-2019 was machined into foam using Zodiac Aerospace's (now Safran) 5th axis router. A durable female tool was then created. The tool was created in a wet layup using high temperature resin and dry carbon fiber cloth. These materials were chosen to withstand the elevated temperatures necessary to cure thermoset prepreg mats, and to closely match the coefficient of thermal expansion for thermoset prepreg mats. The female tool was used to cure prepreg parts, which are more uniform and repeatable than wet-laid parts.

For the 2017-2019 seasons, the CPFSAE chassis were manufactured from prepreg in two halves. Once the two parts were cured and trimmed, they were bonded together with a microballon-resin adhesive and sealed with a wet layup strap joint. Upon weighing the chassis halves before and after applying the strap joint, it was found that the strap joint added 8 lbs. to the total chassis weight.

Objectives

Aside from yielding a usable part for the CPFSAE team, the MCD team's objectives were to eliminate the strap joint, increase modularity of the chassis tooling, withstand elevated temperatures seen in prepreg curing cycles, and create durable tooling. Removal of the strap joint reduced chassis weight, which aligns with the team's performance goals. The 2017-2020 tooling was not designed for modularity, so the entire chassis geometry required a re-design if the platform needed tuning. While it was not in the scope of the project, future CPFSAE teams could manufacture new tools that interface with the ones created during the 2020 season. For instance, if powertrain packaging direction changes, two new rear tools might be manufactured that mate with the front tools. The tools were manufactured using resin that would not re-enter the plastic state at elevated temperatures. The tooling was designed to yield 50 parts, allowing the CPFSAE team to make many season's worth of chassis from one investment of capital. Additionally, this report details the design and modelling process used to make the tooling so that future teams have a solid foundation for future redesigns.

Manufacturing Concept

The MCD team manufactured the chassis utilizing 4 female molds that created a single CFRP chassis, with no requirement for a strap joint. The master geometry was created by machining a foam plug similar to 2017 senior project team *Carbon Fiber Monocoque Chassis Platform for Formula SAE and Formula SAE Electric Race Cars.* The durable female tool was wet laid over the foam and was able to produce thermoset prepreg parts. Drill bushings were built into the durable tooling for positioning critical components such as the suspension or engine mounts. Unlike the 2017 project, the molds bolted together so the entire closed chassis was laid up inside the tool, and there was no need for a strap joint. The last notable difference in

manufacturing was the mold geometry, which split the chassis using two planes, giving the molds 4 different tools.

The full production steps are outlined in **Table 10.** Research, discussing ideas with Safran, PTM&W, and performing small scale tests led to the development of this process.

Table 10: Chassis Manufacturing Steps

Subsystem	Step	Process	Product Used	Note
Male Master Geometry	1	Machine Foam	-	Machine foam to net shape of master geometry; Include locating holes and datums
	2	Prime Foam	White High Build Primer	Fills voids & prevent over-sanding
	3	Guide Coat	Blue Paint	Acts as a guide coat to show low spots
	4	Sand	180-240 Grit Sandpaper	Creates a smooth surface on master geometry
	5	Body Fill	Axson APF-7	Fills voids, scratches, over-sanded areas
	6	Seal	REN RP802 PVC Lacquer Sealer	Acts as final seal of the foam tool
	7	Final Sand	800-1500 Grit Sandpaper	Creates a smooth surface on master geometry
Female Mold	1	Mold Release	PTM&W PA0828	Creates a barrier between foam male and CFRP female
	2	Place Datums	Brittle Resin Pins and Steel Drill Bushings	References subsystem parts and jigs
	3	Surface Coat	PTM&W PT1995	Creates smooth, hard surface on female mold. Apply thinly (0.030” thick maximum)
	4	Wet Layup	Carbon + PTM&W PT2520, Aluminum Core	Creates female mold structure
	5	Cure	Peel-Ply, Breather, Vacuum Bag	CFRP cures tightly against foam tool
	6	Drill Holes	-	Flange holes drilled for tool assembly
	7	Trim	-	Access holes trimmed; Front bulkhead cut out
	8	Repair	-	Voids filled with PT1995 or high temperature body filler; Re-sanded to 1500 where necessary
	9	Post Cure	¼” Bolts, Support Structure	Post cured female tooling in oven at 250°F while assembled and supported via. “eggcrate”
Male Chassis	1	Install Boss Inserts	Ultem Printed Bosses, Plasticine	Affixed boss inserts using silicon; Filleted any gaps using plasticine
	2	Mold Release	Frekote 710	Creates barrier between female tool and male chassis

Table 10: Chassis Manufacturing Steps Continued

Male Chassis	3	Outer Skin	Prepreg	Applied outer skin per layup schedule
	4	Pad-up	Prepreg	Applied outer skin pad-ups according to location
	5	Film Adhesive	Film Adhesive	Film adhesive applied all over
	6	Core	Core + Core splice	Core applied per layup schedule
	7	Repeat Steps 5-2	-	Use reverse order (ex. #5, #4, …)
	8	Cure	Peel-Ply, Breather, Vacuum Bag	CFRP cures tightly against female tool
	9	Drill Holes	-	Drilled out locating holes while in assembled female tool
	10	Repair	-	Delamination addressed using structural adhesive; Sanded as needed

Many of the products were procured through sponsorships. Safran donated one of the largest production costs, their manufacturing time and most of the consumables needed for the foam tools. Another large donation was the raw foam from General Polymers. The PTM&W products were purchased using a collegiate discount with MESFAC funding. The dry carbon was donated by Chomarat, and the prepreg carbon was donated by TenCate and Toray. Finally, the core was donated by Hexcel.

Baby Mold Proof of Concept

The MCD team prototyped multi-piece mold manufacturing using a 1/4th scale model of representative chassis geometry. This project was called the “baby mold,” which was a 4-piece carbon mold that could be used to verify that parts can be pulled from a multi piece mold. Additionally, it confirmed the compatibility of certain products with each other. Bondo, Frekote B15 sealer, and Frekote 710 LV wipes each performed as expected while in contact.

To create the baby mold, geometry from the 2017 chassis was modified to create the most “difficult” small scale mold possible. The mold included corners, lofted features, and a recessed border to represent features that could be on the final chassis geometry. Then, the geometry was cut by two planes to produce quarters like the front upper plug shown in **Figure 103**. A bottom flange with drill holes was added so that holes could be drilled into the carbon mold for assembly. The plug geometry featured a minimum draft of 3 degrees in the part pull direction.

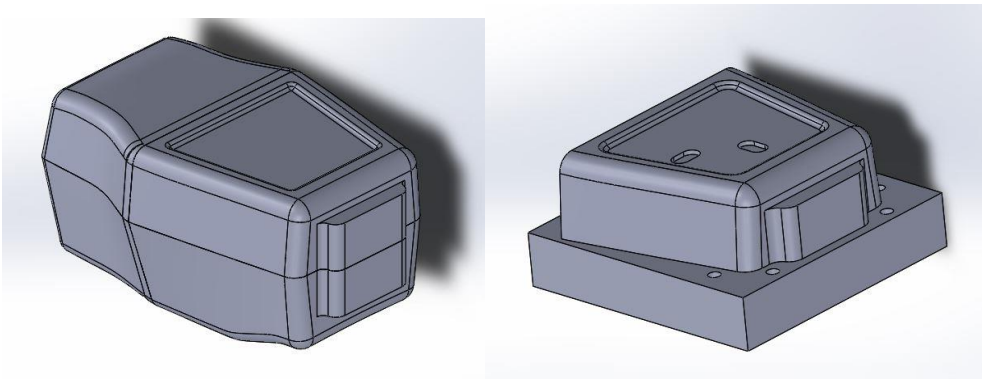

Figure 103. The geometry of the intended "baby chassis" on the left, and the sliced "baby mold" plug with bottom flange on the right.

The initial baby mold was to be made using the Hangar's 3-axis CNC router shown in **Figure 104**. The assumption made was that if this concept worked, the full-scale molds could be made easily on a 5-axis router.

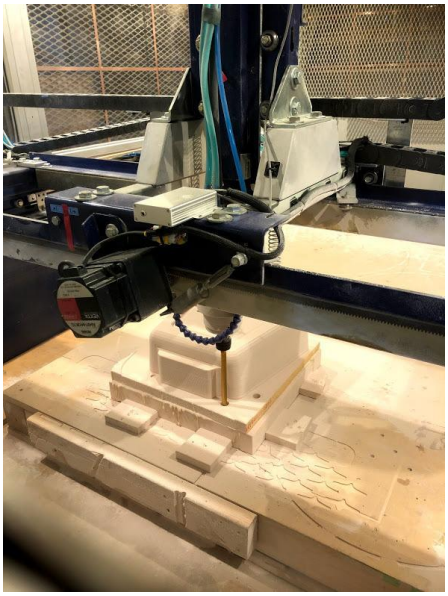

Figure 104. The machining of one of the baby mold plug quarters done on a 3-axis router.

To assemble the 4 baby mold quarters together, one more flanged surface with bolt holes needed to be included. Since this part could not be machined in one setup on the ME department's router, a second piece was added to each of the baby mold quarters. This piece was a vertical flange with mounting holes and a machined register to align the part to the quarter plug. The assembled quarter plugs are shown in **Figure 105.**

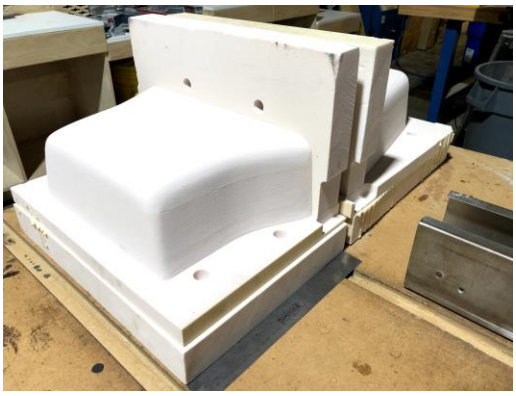

Figure 105. Foam mold quarters with their added vertical flanges. Notice the machined registers in the bottom corner of the flange to align the parts for gluing.

After machining and gluing, drill bushings were inserted into the bores, and the foam plug quarters were sealed using PT2520 resin. At this point in the baby mold manufacturing, the MCD team decided not to sand the resin coated foam in the interest of time. It was noted that sanding is an extremely important step in any mold-making process and was not be neglected when creating the final chassis mold. See **Figure 106** for a close-up shot of the rough, undesirable surface left just after sealing the foam with resin.

Figure 106. The resin sealed foam plug with drill bushings (left). The orange bits are earplugs used to keep resin out of the drill bushing holes. The rough, undesirable resin surface is shown on the right.

After the resin hardened, Frekote 710 LV wipes were used to apply mold release. Then the MCD team laid up tooling carbon with West Systems 105 since these products were readily available. The baby mold cured under vacuum for two days in the configuration pictured in **Figure 107**.

Figure 107. Each of the baby mold quarters curing under vacuum.

Upon removal of the vacuum bags an attempt to release the part was unsuccessfully made. The MCD team attributes this to the lack of any sanding done to the resin sealed. To release the plugs, the foam had to be chiseled out of the cured mold. This left an internal surface unfit to layup a part, which required extensive time spent sanding to yield a male part. The attempt to release the part is pictured in **Figures 108-110**.

Figure 108. Cured carbon molds not yet released from the plug.

Figure 109. “Releasing” the carbon mold from the plug.

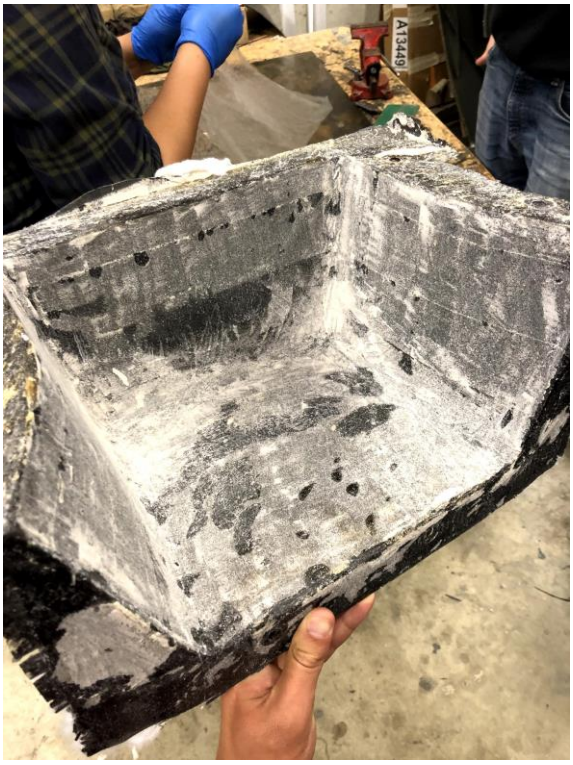

Figure 110. The inside of the carbon fiber baby mold quarter.

To produce valuable insights, it was decided that two of four of the baby mold halves would be salvaged and used to test the multi piece mold theory. The carbon was trimmed, mechanically sanded, and then hand

sanded to a 600-grit finish. Bondo was used to fill voids left from mechanical sanding and chiseling in previous operations. The finished mold is shown in **Figure 111**.

Figure 111. Sanded and cleaned female mold halves of the baby mold.

After sanding, the mold halves were assembled using C-clamps and the bolts through the bolt holes that had been drilled into the baby mold using the drill bushings. The resulting assembled part had a gap in the seam that had to be filled if a smooth part was to be produced from the mold. As pictured in **Figure 112**, the gap was filled with Bondo.

Figure 112. Seam gap shown on the left. Bondo body filler was used to fill the gap on the left.

After another sanding to get the Bondo joint to 600 grit, Frekote B15 mold sealer was applied to the entire inside surface of the baby mold. Then, Frekote 710 LV wipe on mold release was applied, and the baby mold was fully prepared for a layup. Tooling carbon wetted with West Systems 105 was laid up, vacuumed, and successfully pulled from the baby mold.

Figure 113. Successful male part pulled from two baby mold halves.

While pulling the part shown in **Figure 113**, it became clear that Bondo should be reconsidered as a solution to filling the seam gap between molds. The Bondo had to be chiseled and broken to separate the two baby mold halves. However, it did eliminate any sharp cusps on the male part because of the seam gap. It was determined that plasticine could be used as a gap filler, which molds easily, does not adhere to the tooling, and does not burn at elevated temperatures. These findings are shown in **Figure 114**.

Figure 114. Bondo seam had to be broken using a chisel to disassemble mold halves (right). No cusp exists on the final part (left).

The baby mold did show the MCD team that the multi-piece mold manufacturing was feasible. The importance of sanding and chemical compatibility was emphasized as a critical step during the creation of the female molds.

Plug and Mold Design

To begin the mold design, the finalized chassis model and geometry as required by other subsystems was analyzed for manufacturability. This included a feature check, symmetry check and draft study of the model. It was found that the model included many fillets that were either not necessary or created geometry that would not be feasible to layup in, especially when considering core. Multiple zero-thickness surfaces were also discovered in this chassis model. These issues were fixed, and the chassis model finalized for manufacturing was sent to subsystems for final fitment confirmation.

To better understand the implications of creating a mold, SolidWorks models were created to mirror the actual manufacturing process, meaning that the master plugs were first modeled from the chassis model, followed by the female molds. To easily account for any future changes in geometry, the molds were created as a configuration in the actual chassis part so that they automatically rebuilt any changed geometry or features when the chassis was changed.

Male Plug

The plug design began by splitting the geometry of the chassis by two planes. The first plane was perpendicular to the axial axis of the chassis near the harness bar area (aft of the driver's shoulders), and the second was perpendicular to the wheel axis, located at the chassis centerline. The first plane was dictated by the assumption that tool modularity would benefit by splitting the geometry between the cockpit and powertrain area. The second plane was chosen for its zero or positive draft angles when releasing the part from the tool. These planes are shown in **Figure 115**.

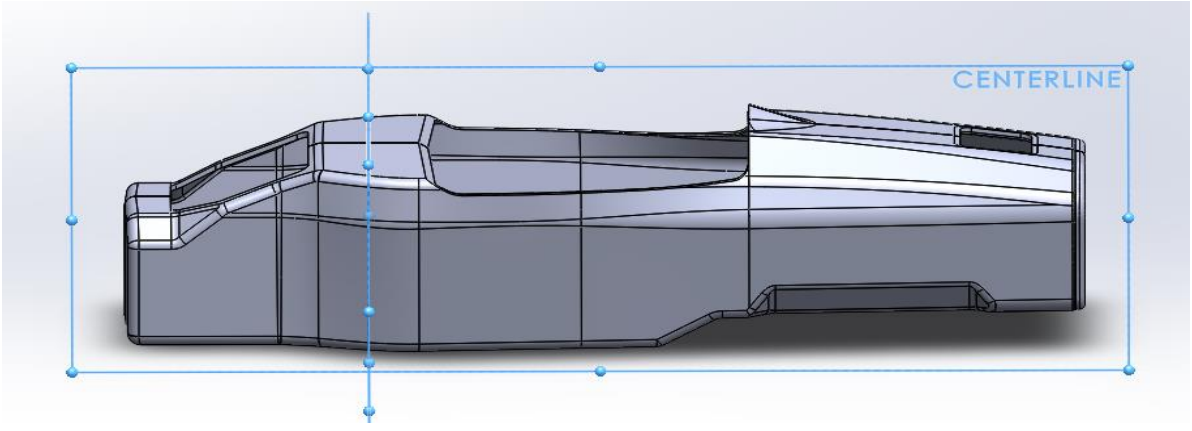

Figure 115. Final chassis geometry with split lines.

After splitting the geometry, four SolidWorks configurations were made, one with each quarter of the chassis unsuppressed. This allowed for each quarter of the tooling to automatically update if geometry changes were made to the chassis in the future. With each quarter, the "shell" feature used to hollow out the chassis model was suppressed. The result was a solid model from the outer chassis surface to the center plane. A rectangle was sketched around each part on the centerline plane to represent the foam stock on the plug. The rectangle was then extruded down from the centerline to create the flange bosses.

These flange bosses allow for mating surfaces with locating holes to be added to the master geometry. Locating holes were also added to every planar surface of the master geometry near, but not at likely mounting locations on the chassis. The flange extended 3” all around, except between the front and rear cockpit openings to provide drilling clearance. Large extrusions were added coming out of access holes such as the cockpit and rear powertrain to create openings. The resulting shapes were the master geometries used when machining the foam tool.

The design for the front suspension of the CP20C and CP20E cars requires a planar surface on the lower corners of the front monocoque in order to mount the front lower control arms (FLCA). To increase the modularity of the mounting possibilities, these were created using a standalone boss manufactured separate to the chassis molds themselves. This will allow for future teams to reuse the front chassis molds and still have some freedom with lower control arm mounting position. The boss is pictured in **Figure 116**.

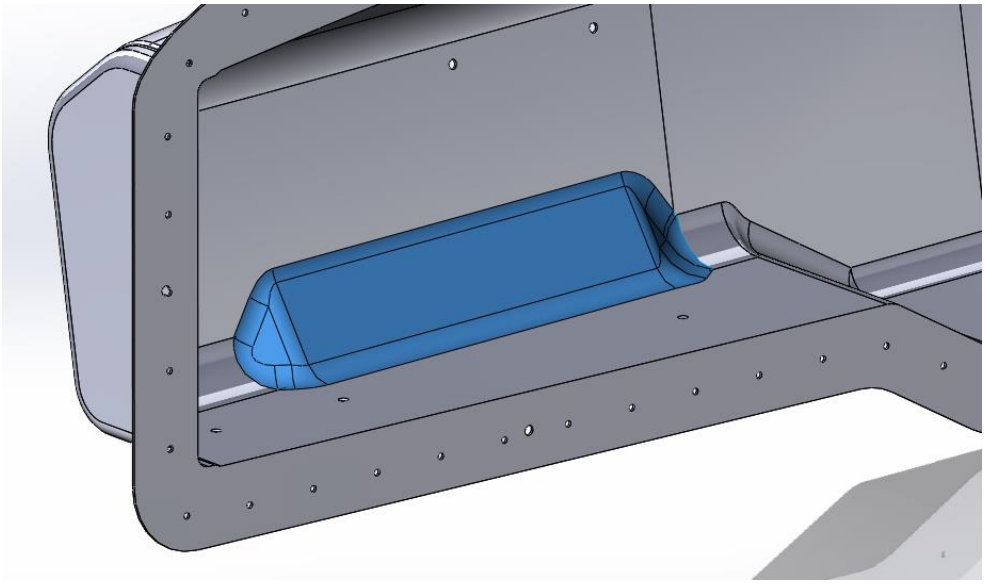

Figure 116. Separate FLCA mounting surface boss highlighted in blue.

The team has used this method previously for altering geometry on the previous monocoque molds, typically to allow for more freedom in choosing suspension architecture and mounting locations. These bosses have typically been 3D printed out of a high temperature thermoplastic provided by Stratasys, Ultem 1010, which is often used for composite tooling and manufacturing. However, Stratasys was unavailable to print the bosses this year, and they were instead machined in-house from RenShape high temperature tooling foam, discussed in more detail later in the report.

The finalized plugs are shown in **Figure 117**.

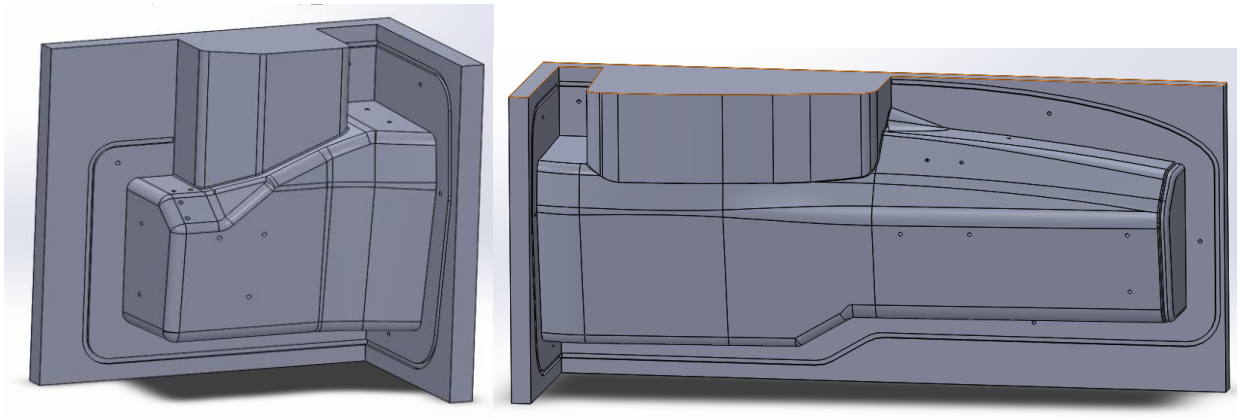

Figure 117. Rear RHS plug (left) and front RHS plug (right). Notice the large bosses at the centerline, harness bar line, and extending from the cockpit opening and the matching mating holes on the harness bar bosses between the front and rear geometry.

The pockets on the transverse flanges shown in **Figure 118** (perpendicular to centerline plane) are impossible to machine, even on a five axis, so the foam for these flanges had to be machined separately and then bonded on using locating features. After consulting the tooling team at Safran, it was decided to machine the plugs in 4”- 6” step increments. Instead of delivering a full block of raw stock, the first 5” thick slice of the plugs could be laid and machined on the router, and then the next 5” section could be glued on top of the machined surface. Doing this reduces the amount of 5 axis work required from the machinist, which adds time to the job. Additionally, it alleviates some of the difficulties of the geometry for the machinist. Stock foam “slices” are shown on the last pages of each of the plug part drawings in **Appendix G**.

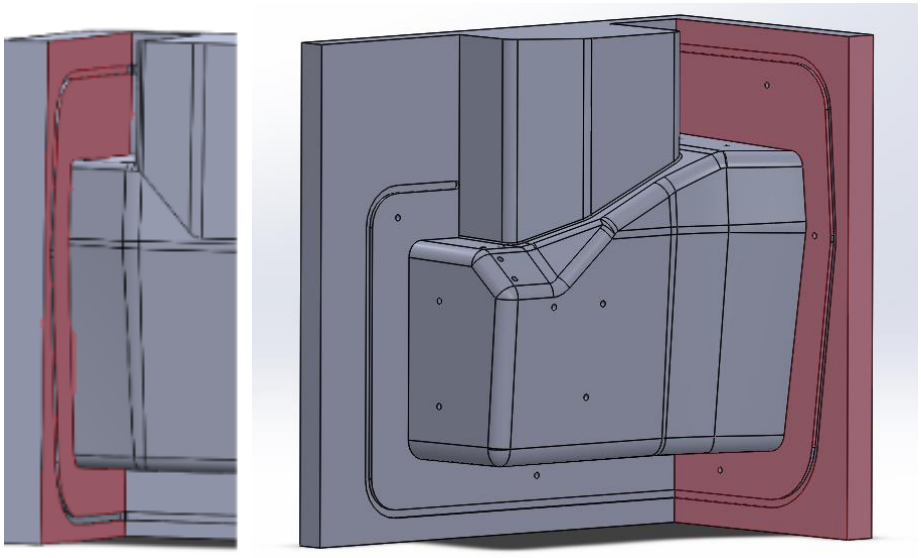

Figure 118. Transverse flanges that may need to be machined separately.

14 total locating pin holes were added to various locations around the flange to provide the initial lining up of the molds before we can match-drill the remaining holes around the flange. There are also pin holes on subsystem critical chassis planes, to ease in the creation of locating jigs. Bushings with a mating pin like the one shown in **Figure 119** will be placed in the plug before laying up on the female mold, so that they

can exist as holes in the female mold. These bushed locating holes could then be used to drill locating holes into the chassis before de-molding.

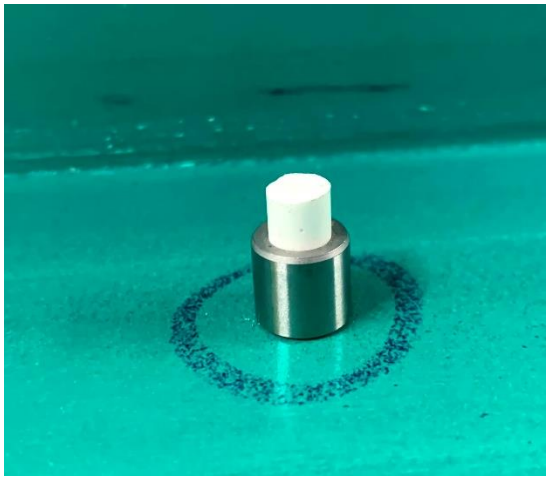

Figure 119. Resin pin and steel bushing in male plug before layup of female mold.

These bushings and pins were supplied by Safran but would be simple to construct in-house. Resin is poured into tubular molds to form the easily-breakable pins shown in white in the **Figure 119**. The pins are then inserted into locating holes machined into the plug. The steel bushings are then placed over the pins before layup of the female mold. When the female mold is pulled from the male mold, the pins break off and any remnants of the resin pin still stuck in the bushing can be drilled out.

Flange Mating Between Molds

As previously mentioned, the female molds needed to be flanged with bolt holes for mating. Mating the molds would then create one female mold for the entire chassis. Based on a gasket equation from *Shigley's Mechanical Engineering Design* [11], about 200 fasteners should be used to assemble the molds together in total, where D_b is equivalent to the perimeter of the chassis, d is the bolt diameter (0.250”), and N is the number of bolts.

$$3 \leq \frac{\pi \cdot D_b}{N \cdot d} \leq 6$$

However, since this is not actually a gasket, fewer fasteners were used. Since they are not subjected to large loads, cheap bolts will suffice, reducing the manufacturing cost. The hole pattern along the flange in the model was created by offsetting the flange outline and converting the outline to a spline using the SolidWorks “Spline Tool > Split Fit” feature to create a curve pattern. Since these holes were match drilled on the final part, the holes in the model were intended to be representative except for the 14 locating holes where bushings were installed. Ultimately, approximately 70 total flange holes would end up being drilled.

A potential issue that the MCD team considered is that upon mating the chassis molds together, a small void will be created due to non-zero radii in the flanges of the molds. This void would lead to a sharp cusp in the final part. To combat this, plasticine was used to fill the void and layup prepreg over it as shown in **Figure 120**. The plasticine was tested at cure temperatures and did not melt.

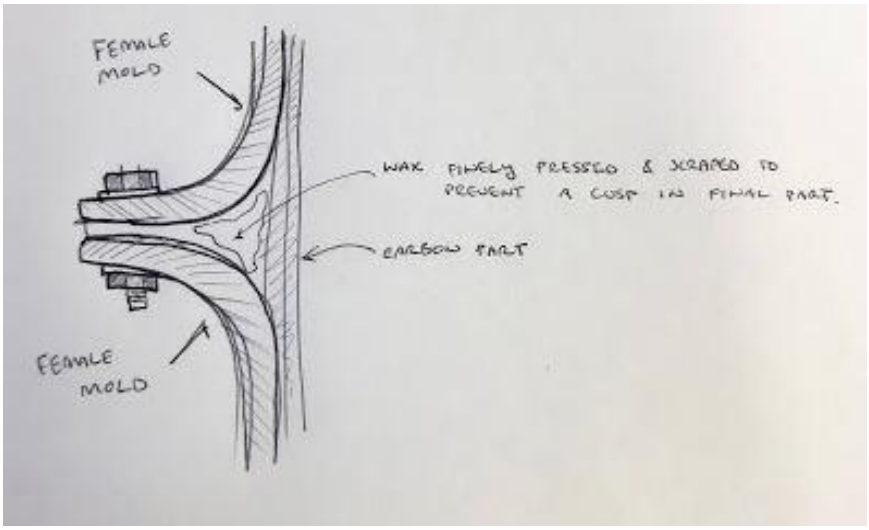

Figure 120. Plasticine illustration. “Wax” refers to plasticine.

Female Molds

The female molds were created by pulling the mold surfaces from the plugs using the “Offset Surface” tool in SolidWorks. The surface was offset to 0”, and then thickened outwards to a width corresponding to the laminate thickness. Due to the fragile nature of the “Thicken” tool, this took many attempts to get right. In the end, multiple iterations of using the “Evaluate > Check” tool for finding open surfaces and minimum radii resulted in a surface that was able to be thickened to the desired width. To get the cockpit and rear opening cutouts right, split lines were added to limit the height of the flange around those openings. In the plug, the boss may go up to the top of the mold, but actually laying up cloth to the top would inhibit accessibility and waste material.

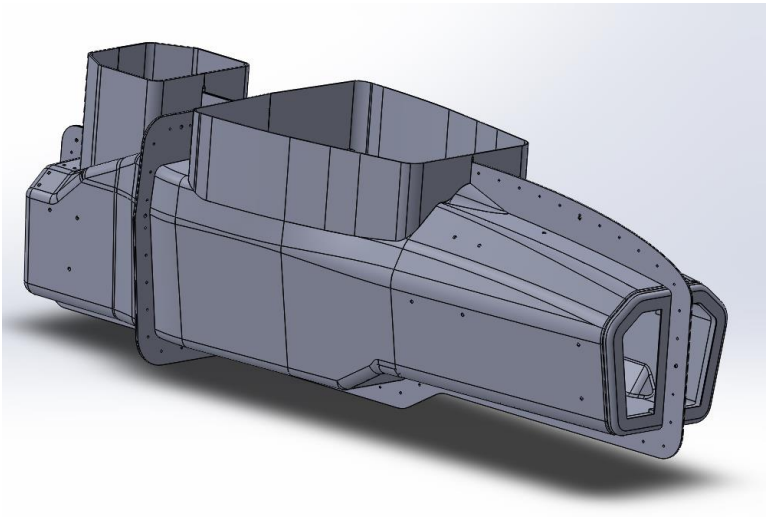

Figure 121. Female mold assembly.

An assembly of all the female molds, pictured in **Figure 121**, was created to visualize the chassis layup. From this visual inspection, various fillets increased in radius to ease in the layup. Additionally, the mold assembly would be used in the thermal model to determine the mold laminate to thwart warping. The finalized molds are shown in **Figure 122** and **Figure 123**.

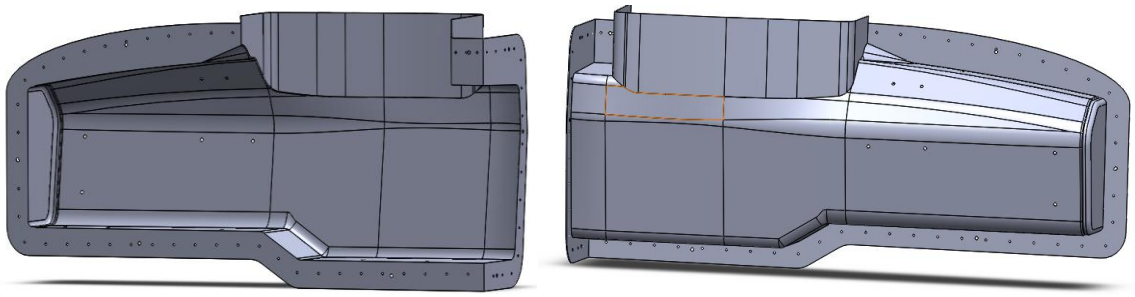

Figure 122. Front RHS female mold inside view (left) and outside view (right).

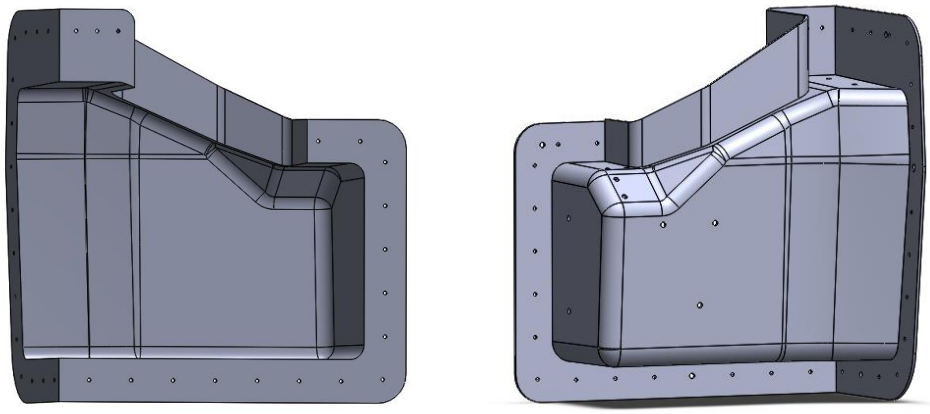

Figure 123. Rear RHS female mold inside view (left) and outside view (right).

Since the openings that allow access are relatively small, it would be hard to actually layup inside the molds, especially in the front section. A solution to this without compromising mold stiffness was proposed in **Figure 124**.

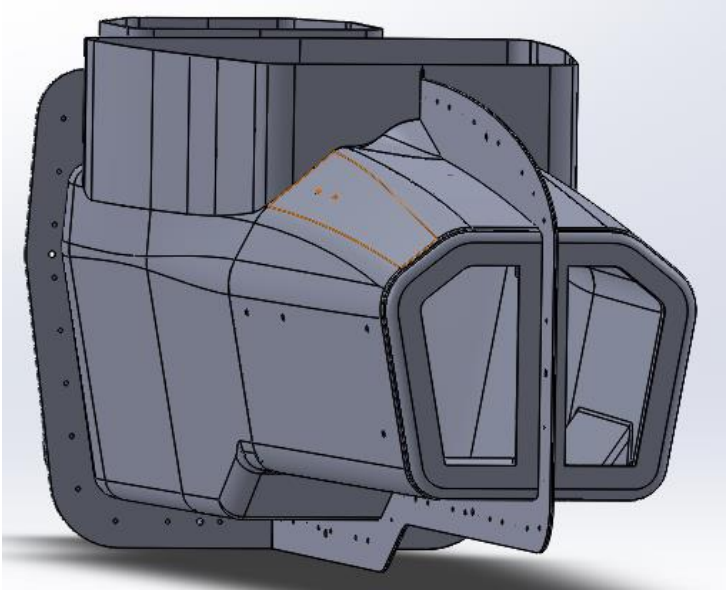

Figure 124. Front cutout for front access in mold.

This frontal cutout would be manually cut out of the female molds after they are pulled from the plugs. Any sort of extruded boss in the plug at this location would create negative draft and would result in the mold being unable to be released. However, once the mold is released from the plug, a Sawzall or similar tool can cut through and create two openings on either side of the flange without compromising mold stiffness or draft. Extra care must be taken to prevent any carbon or core from protruding out of the mold when doing the actual chassis layup, since even the slightest protrusion will make it difficult to release the part.

Draft Analysis of Molds

The SolidWorks "Draft Analysis" tool was utilized to ensure that the part would have at least one pull direction capable of releasing the part with all positive draft. Though many teams can pull parts with no draft, adding some draft on at least two of three surfaces will greatly increase our ability to release the final part. Since the female mold comes apart in four sections, we are not limited in terms of pull direction to a direction vector.

There is zero draft on the lower chassis surface due to concerns with engine mounting. If we were to add draft, the engine, drivetrain, steering, and brakes assemblies that mount to the chassis floor would increase in complexity, as will their respective locating jigs. Other teams pull parts with zero draft on multiple surfaces by prying and deforming the mold until it releases. Since the mold is essentially cantilevered along the bottom split line, it should be easy to deform, even with core. Another proposed solution was to use a compressed air nozzle to force the mold off the part, which ultimately proved to be ineffective. Upon sweeping through a range of pull directions, a small range of angles was found that results in even the bottom surface having positive draft. A screenshot is included in **Figure 125**. This draft analysis, combined with the previously mentioned release methods, were sufficient solutions to go through with the flat chassis bottom.

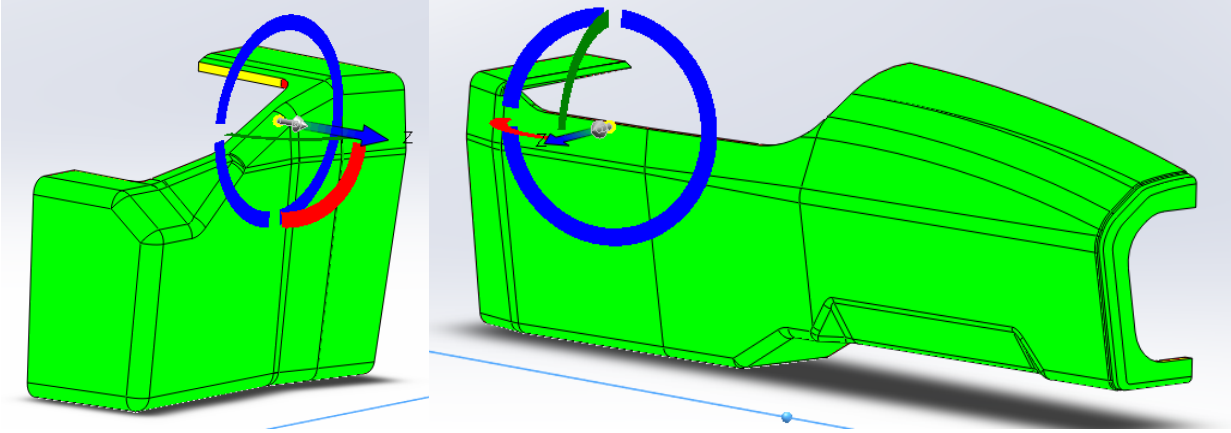

Figure 125. Draft analysis of molds. Green indicates positive draft of 2 or more degrees. Flanges are hidden for clarity. Note that though not visible, the bottom surfaces are green.

Mold Laminate

The female mold laminate was designed using a combination of the thermal model discussed previously and historic female molds. The laminate was $[(45_c / 0_c)_2 /45_c/ \text{core}]_s$, with 3/16 cell, 3.1 lbs/ft^3 0.5" thick honeycomb core and 12k 2x2 twill. To save core material and simplify the layup process, only large planar areas of the master geometry were cored. The core was also beveled at the edges to reduce bridging. The resin was PTM&W PT2520/B1, a high-temperature resin. The inner most surface coat was PTM&W PT1995 high temperature surface coat. After the layup, the molds cured at room-temperature. They were then released, assembled, and post-cured according to PTM&W post cure for PT2520 resin. Access holes were then cut, such as the front bulkhead access holes for the front of the chassis. The cure cycle and cored locations are shown in **Figure 126** and **Figure 127**, respectively.

SUGGESTED POST CURE CYCLES		
HARDENER	Initial RT Cure Cycle	Post Cure Cycle
Part B	Gel 18-24 hrs. @ 77°F	Post Cure for 3 hours each @: 150°F, 250°F and 300°F
Part B1	Gel at least 24 hrs. @ 77°F	Post Cure for 3 hours each @: 150°F, 200°F, 275°F and 325°F
NOTE: if the expected service temperature is to be higher than the final cure temperature listed, then an additional 2 to 3 hours at 25°F above the expected service temperature is recommended.		

Figure 126. PTM&W 2520 resin suggested post cure cycle

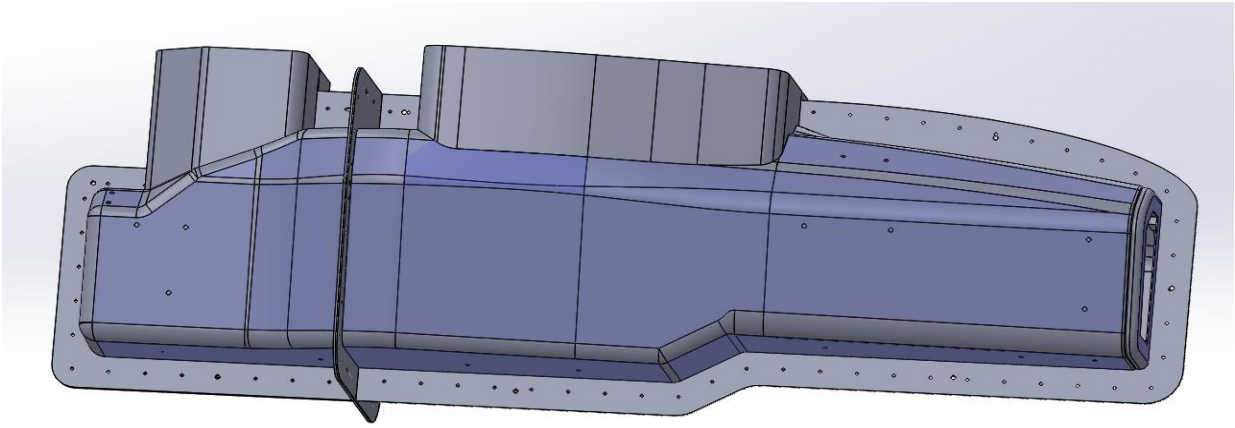

Figure 127. Locations to add core on the chassis mold.

Mold Manufacturing

For the reader of this report, it should be noted that mold production is no insignificant task. To illustrate this point, **Table 11** compares the initial target completion dates (set prior to manufacturing) to actual completion dates for the front right (FR) female mold. The initial time estimates were far too optimistic, as well as not motivated accurately. For instance, too much time was allotted for foam gluing, and machining at Safran. It is beneficial to set aside significant time for a process that is at the mercy of an independent manufacturer, but Safran was a generous and speedy manufacturer. In contrast, far too little time was allotted for repairing and sanding the cured female mold.

In creating the chassis, each major operation in manufacturing diminishes geometric accuracy, so significant care must be taken during the production of the durable tooling. In this case, the female molds required far more production time than what was originally allotted. The MCD team created durable tooling, but stresses that the final product demanded significant time and effort from the MCD and CPFSAE team alike.

Table 11: Comparison Between Target and Actual Completion Dates

Deadline (FR CFRP Mold Piece)	Target Completion Date	Actual Completion Date
Foam glued & delivered to Safran	11/22/2019	12/03/2019
Foam Machined	11/29/2019	12/12/2019
Foam Fully Sanded (Post PVA Sealing)	12/15/2019	12/14/2019
Female Mold Layup	12/16/2019	12/18/2019
Female Mold Trimmed and Repaired	12/20/2019	01/20/2020
Female Mold Post Cure	01/08/2020	01/20/2020
Female Mold Final Sand	01/10/2020	02/08/2020
First Chassis Produced (Unfinished)	01/16/2020	02/26/2020

Should new tooling be manufactured, this section will describe blunders experienced during the MCD project manufacturing and make recommendations for future manufacturing. The aim is to create a stronger tool in less time than shown above. The mold pieces will be referred to as front right (FR), front left (FL), rear right (RR), and rear left (RL).

Plug Manufacturing

The first step for creating the plugs was designing the foam stock. To maximize the time spent machining the foam using 3 axes, machining would be done in 4”-6” thick layers at a time. This allowed shorter tools to be used, and only necessitated 5^{th} axis work to drill locating holes on skewed planar surfaces of the master geometry. **Figure 128** shows a concept for a 4 layer design that surrounds the FR plug. See **Appendix G** for detailed drawings of the foam stock created. One last consideration for designing stock is to position any bond lines between homogenous boards of foam away from sensitive areas such as locating holes or large planar surfaces parallel to the bond lines.

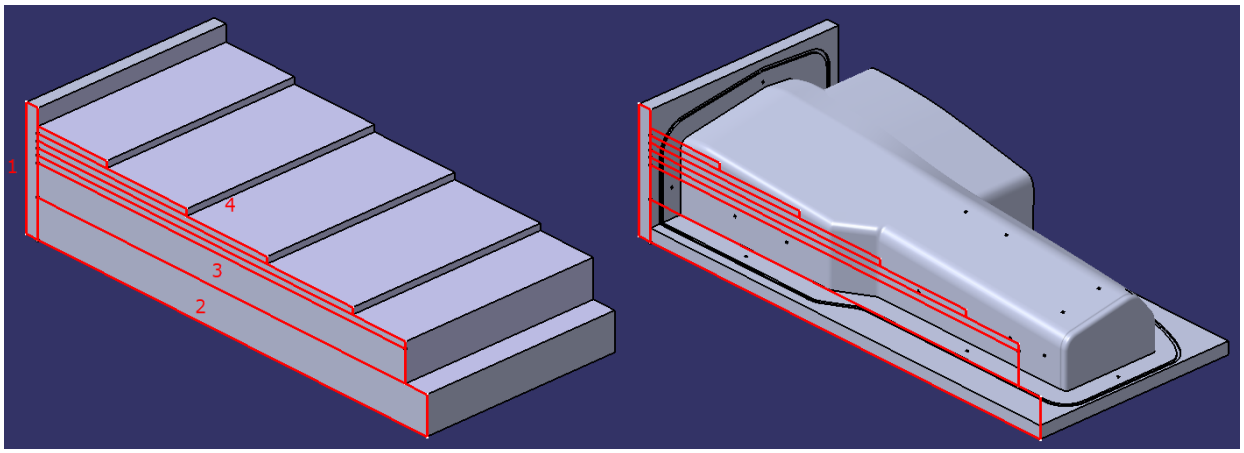

Figure 128. 4 layer stock design concept (left) projected onto the master geometry (right). Order of machining: 2, 3, 4, 1. Notice that the flange surface at the bottom of the geometry does not align with the bond line between layers 2 and 3.

At the time of production, foam sheets ranging from ¾" to 4" thick were available, in weights ranging from 10 lbs/ft^3 to 40 lbs/ft^3. It has previously been determined that foam which is at least 15 lbs/ft^3 is resolute enough to use for chassis production. The layers were created by gluing together the available stock using gorilla glue spread using metal spreaders. The board to be adhered to the already glued board was lightly misted with water to activate the gorilla glue, and then clamped to the glued board. One issue the MCD team experienced was delamination or voids at the bond lines due to inadequate clamp distribution across bond lines. Shown in **Figure 129**, this resulted in voids visible on the machined walls, and at its worst, delaminated layers which had to be completely remade on the router. The MCD team recommends gluing the foam together in smaller batches to use every available clamp or ballast weight on individual stock boards, rather than having these tools spread thin since all the stock was getting glued in one day. The tighter and stronger the bond line, the less sanding and body filler applications will be required to create the foam plug.

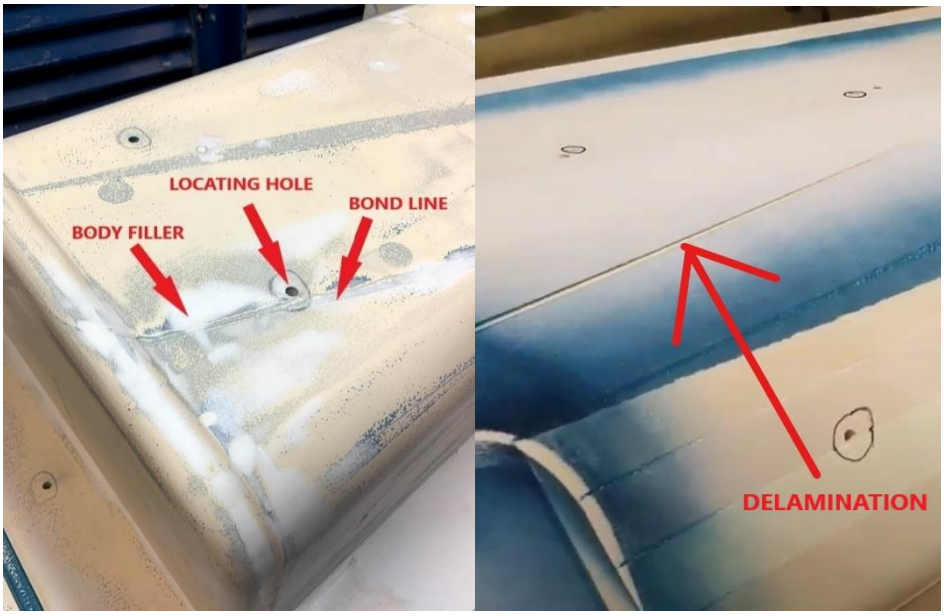

Figure 129. Large bond lines near important features (left) and delamination (right) only revealed after machining.

After machining, the rough plugs were sprayed with a thick coat of sanding primer, and a colored coat as a guide coat. The guide coat provided high contrast visual cues as to what areas of the plug were deeper than their surroundings. When sanded evenly using a rigid sanding block, the deep areas disappeared and blended into the sanding primer coat. It is important to not over sand, as this exposes the porous raw foam, which can disrupt surface finishes and prevent release of the female mold from the plug. Over sanded areas or voids at the bond lines were filled with body filler and re-sanded. The molds were sanded to 240 grit. From foam stock to sanded plug, each plug took about 5 days of work, with 5 people working. Safran's sanding facilities and the unsanded FR mold are pictured in **Figure 130**.

Figure 130. MCD team and CPFSAE team volunteer beginning to sand the FR foam plug.

Next, the PVC Lacquer sealer was sprayed, which helped fill fine pitting. This layer was sanded starting from 600 grit, to 1500 grit. At this point, the plugs were ready for wet layups, but the MCD team wanted to test sample areas of the plug to reduce the chance of a failed release.

Figure 131. Sealed and sanded PVC Lacquer layer on the FR plug.

Mold Layup Test Samples

If a CFRP part does not release from the foam plug, the only way to salvage the CFRP part is to carve out the foam plug. To avoid this large waste of foam and time, test samples of 1" x 4" strips were laid up on the foam plug. The resin (PTM&W PT2520), carbon (2x2 Twill from Chomarat), and surface coat (PTM&W PT1995) were laid up onto varying releases and conditions. The results are included in **Table 12.** Although the PTM&W PA0828 and car wax samples both released (shown in **Figure 132**), the more convenient and consistent PA0828 release was chosen for the remainder of the parts.

Table 12: Test Sample Results

Release Product	Result	Note
Frekote 710 LV Wipe	FAIL	Not on sanded region, cured in 50°F.
Frekote 710 LV Wipe	FAIL	On sanded region, cured in 50°F.
PTM&W PA0828	RELEASE	On sanded region, cured in 80°F. Resin and surface coat warmed to 100°F prior to application.
Turtle Wax	RELEASE	On sanded region, cured in 80°F. Resin and surface coat warmed to 100°F prior to application.

Figure 132. MCD members moments after discovering the 3rd and 4th tests released.

While the test was not exhaustive of the layup possibilities, the temperature in the room during the cure was deemed critical, as was using a warmer for the resin and surface coat. The warmer was a box constructed from insulation with a 100W lightbulb mounted within. Warm resin and surface coat allowed for easier wetting and spreading. Warm air temperatures allowed the resin to cure fully. For each of the wet layups, the room temperature would be maintained at 80°F using electric heaters. The room doors were insulated from the winter air using thick cardboard, though it was evacuated of fumes and heat at least every 8 hours to reduce explosion or asphyxiation hazards. Probed temperatures are included in **Figure 133**.

Figure 133. Room temperature determined by measuring thermocouples inserted within the foam (left), warmer box temperature determined by measuring thermocouples inserted into the box (right).

Mold Layups

After warming the room, a tack cloth was used to wipe dust off the sanded plug surface. Then PA0828 was applied using a rag in 5 coats. The release off-gased for 1 hour before the locating pins with drill bushings were inserted into the plug. After the pins, the warm surface coat was poured on in one thick coat then spread using popsicle sticks by the volunteers, shown in **Figure 134**.

The MCD team would like to note that a much more effective technique for spreading surface coat is to paint it on using high quality brushes so that the bristles do not fall out. This technique yields a thin layer of surface coat, with fewer air bubbles, which will harm the surface (more on this in "Release & Damage"). PTM&W technicians recommend one 0.030" layer applied with a brush, followed by a touching up with a brush. The MCD team's surface coat was as thick as .125" in some areas.

Figure 134. Application of the surface coat in a thick layer.

Following surface coat, the wet carbon fiber was laid according to the layup schedule. The MCD team chose to set up two folding tables covered in disposable drop cloths for wetting out carbon mats, and one table to organize tools, the scale, mixing sticks/cups, and a laptop for recording resin usage. The mats were pre-cut by volunteers and had masking tape along the edges which could be removed after wetting the mats. The wetting was accomplished by pouring resin over the dry mat and spreading it using squeegees. This process is pictured in **Figure 135**.

Figure 135. Wetting out carbon and removing masking tape (left), applying wet carbon and squeegeeing out air (right).

The MCD team would like to note that during the layup any air bubbles trapped in the laminate will cause voids which will damage the tooling. When laying down wet fibers, squeegee air bubbles out after each layer and debulk plies if possible. After the first skin was laid, it was debulked as in **Figure 136** for 45 minutes.

Figure 136. FR mold inner skin being debulked.

Core was cut to match each planar surface of the geometry, and single beveled using sanders. This allowed the outer skin of carbon to reattach to the inner skin along the edges with minimal voids or sharp radii. After debulking, the core was laid onto the carbon, shown in **Figure 137**.

Figure 137. Beveling the core using a sander (left), beveled core on skin (right).

Following core, the same process for laying up the inner skin was repeated for the outer skin. No other adjustments were made. The mold cured for about 2 days at around 80°F. Each mold was given the same treatment, but the FR mold remained on the plug for 2 weeks, whereas the other three molds were released almost immediately after cure. It is not known whether immediate release is required, however the FR mold took significantly longer, and was more damaged after release than its mating molds.

The MCD team recommends performing a closeout along the flange during the wet layup. This would prevent edge delamination due to wear and help increase user comfort while handling. One possible design is shown in **Figure 138**. The first ply should extend 3 inches out from the flange and folded onto the final layer right before allowing the mold to cure.

Figure 138. Closeout concept to increase durability and comfort.

Release & Damage

While releasing the molds, the FR plug was severely damaged due to adhesion along the vertical flange and along the right side of the chassis. The mold was forcibly removed using plastic furniture wedges, prybars, and in some areas a metal scraper. The plug, shown in **Figure 139**, should not be reused, but it was saved for future teams. The damage to the mold was less significant. Where the adhesion occurred, large areas of foam were stuck to the surface coat. It was unclear as to why adhesion occurred for this mold only. The edges near where wedges were used became delaminated and frayed because of mallet impact and wedges penetrating between layers. This type of damage was common to the molds, which is why it is recommended to include closeouts in the wet layup on future tooling.

Figure 139. Removal of the FR mold from the plug. Notice the severely damaged plug and adhered foam on the surface coat.

Each of the rear molds suffered from cracking along the rearmost flanges due to forceful removal, pictured in **Figure 140**. The vertical flanges were removed and then separating force was applied between the plug and the side of the chassis. This pinched the flanges and caused the surface coat and laminate beneath to crack. For future mold manufacturing, it is recommended to apply separating force evenly, using a combination of wedges and inflatable bladders.

Figure 140. Surface coat cracking along the rearmost flange on the rear molds.

The least damaged mold was the FL mold, which had no major issues due to the removal method. Every mold had minor voids and cracks along the flange corners, where the flange intersected chassis geometry. This was likely caused by air bubbles originally present in the surface coat during the wet layup. Every mold also had voids in the surface coat where bubbles existed in the wet layup. These voids, shown in **Figure 141**, would further crack and widen, demanding repair before any prepreg layup. For future production, voids could be avoided by applying the surface coat in thin layers while ensuring all bubbles are squeezed out.

Figure 141. Voids in the surface coat crack along planar faces (left) as well as corners (right).

The less common types of damage were drill bushings falling out or spinning in the laminate. During post-cure processing, the drill bushings would fall from place, so it was suspected that the basic bond between wet carbon and steel bushing is not durable. It is recommended to pot the areas around the drill bushings within the sandwich panel with structural adhesive if they are found to be damaged.

After release, the molds were placed back on the plugs to begin their post-cure bake. Since the foam plugs could withstand 150°F, they were used as supports for the first oven soak at elevated temperature. The successive soaks were performed with the 4 mold pieces assembled and supported by a wooden "egg crate."

Assembly & Egg Crate

After the first soak, the molds were removed from the plugs and assembled. The molds were assembled by aligning 3 locating bushings on each flange, and match drilling about 70 .25" holes along the flange perimeter. The fasteners were then inserted and tightened "snuggly." The assembly was then placed onto a holding structure, called an "egg crate". The egg crate consisted of numerous wooden rib sections spanning the length of the molds connected at the base by 2x4s. These ribs were sanded and band-sawed until they matched the shape of the mold. As shown in **Figure 142**, The egg crate fully supported the semi-cured female mold to prevent any warpage or sagging during the post-cure.

The egg crate was not modeled or designed ahead of time because the as-manufactured female molds would not match the CAD model exactly. Thus, any ribs modeled to fit up to them would likely need to be sanded or cut to fit anyways. The entire egg crate and assembly was soaked at the PTM&W recommended post-cure temperatures.

Figure 142. Egg crate structure (left) and female mold supported by egg crate (right).

Mold Sanding & Finishing

The final step in mold processing was to repair the damages and smooth every mold surface for the prepreg layup. The edges around the flanges and access holes were trimmed and smoothed using abrasive saws. The access hole in the front bulkhead was cut using abrasive saws. After the holes were cut, delamination between the skins and core was discovered. To repair this, Loctite 9396 structural adhesive was injected while clamping the sandwich panel together. Each part of the mold where delamination occurred was fixed using structural adhesive and clamps, pictured in **Figure 143**.

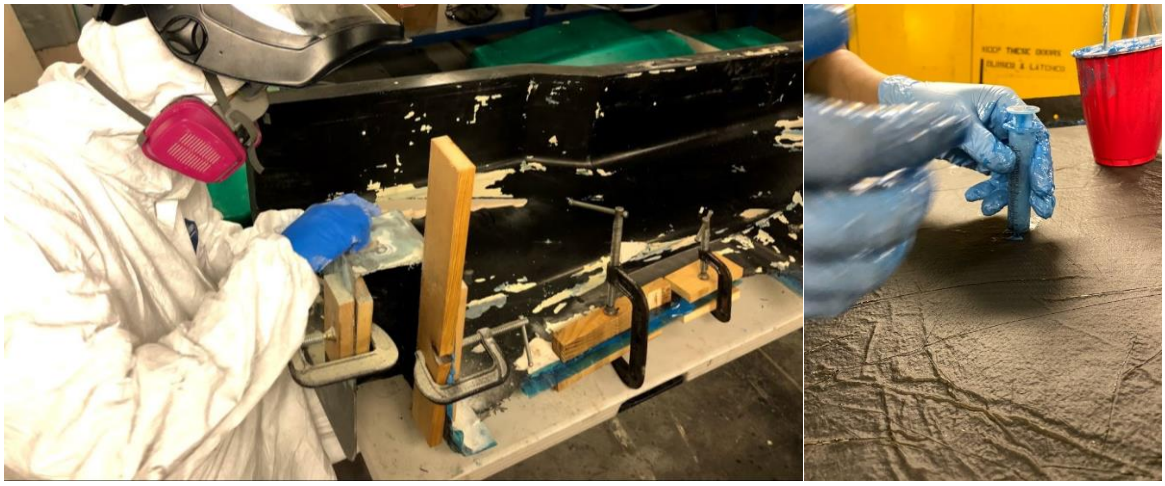

Figure 143. Injecting structural adhesive between laminate(right) and curing under clamping pressure(left).

Voids on planar and cornered surfaces were filled at first using additional PTM&W PT1995, and later filled using PTM&W Poly Filler HT due to ease of sanding and quick cure time. No significant difference was found between either filler. Fillers used during this step must be high temperature rated to withstand the prepreg cure cycle. **Figure 144** and **Figure 145** show the types of damages repaired, including surface voids and mating lines.

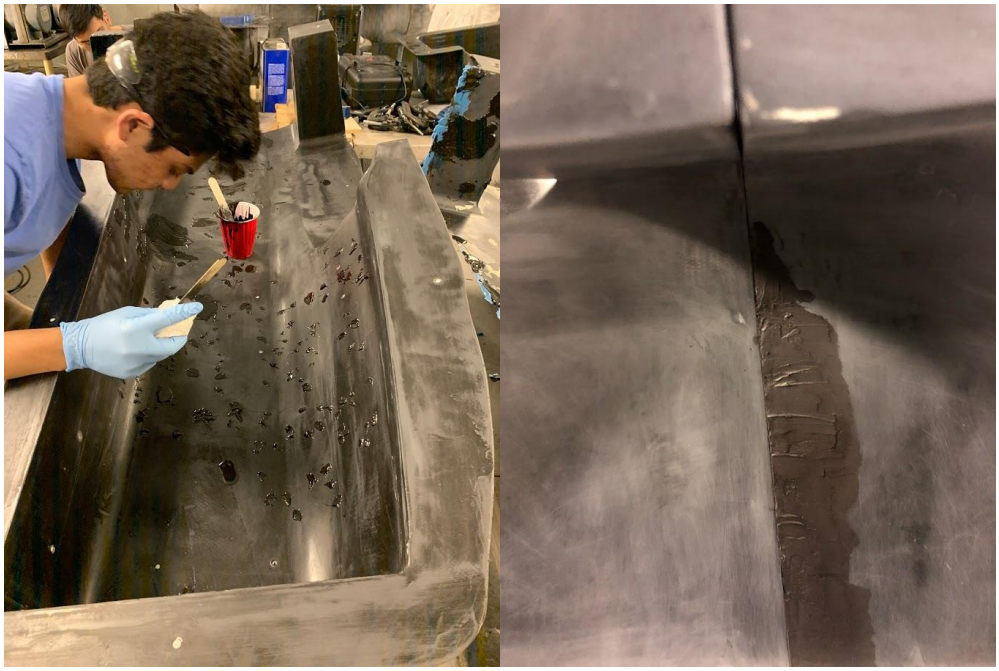

Figure 144. At first, voids were filled using PTM&W PT1995 (left) but PTM&W Poly Filler HT (right) was later favored for its ease of sanding and quick cure time.

Planar surfaces were checked for straightness using a straight edge. The mating lines between molds were checked using a straight edge, although sharp corners would be broken during normal handling. For mating lines, flash tape should be used under the outer skin of prepreg to prevent bulges into the mating line. The normal faces of the flanges were checked using a surface plate, and marking low areas where light shone through. Once the features were as straight as possible with the time allowed, they were sanded to 1500 grit, and hand buffed.

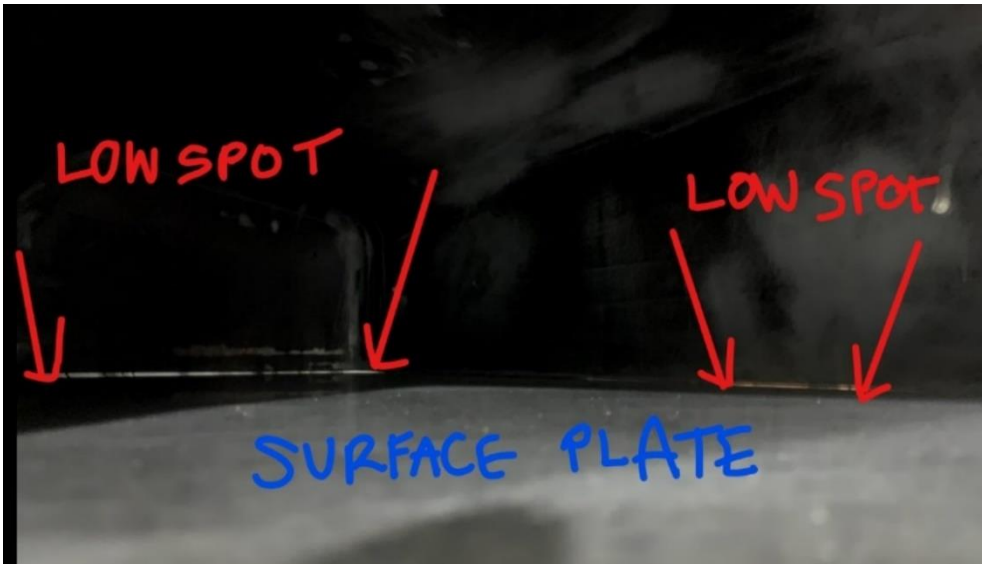

Figure 145. Finding low spots on the normal face of the flanges between mating mold pieces.

Repairing each of these features took substantially longer than the team originally planned for. Preventing the damages to each of the molds during their production should be a top priority when creating new tooling.

Additionally, the vacuum bag cutouts in the front bulkhead were made slightly too large, so a mix of Loctite 9396 and chopped fiber was used to fill material back in. The front molds were positioned with the front bulkhead surface parallel to the ground, and flash tape was applied to the front bulkhead surface. Backing plates were used to ensure a flat surface. The repair is visualized in **Figure 146**.

Figure 146. Front bulkhead fill in procedure. Loctite 9396 was first applied and cured, then a mix of Loctite 9396 and chopped fiber was added for extra structure.

The final touch on the molds was to bond in the FLCA surface into the bottom corners of the Front Bulkhead Support area. For the past few years, the team was sponsored by Stratasys, who provided Ultem 1010 and manufacturing support. However, they did not have the bandwidth to help this year, so inserts were made in house. FLCA inserts were manufactured out of RenShape 440 found in the CPFSAE scrap materials pile, originally misidentified as RenShape 5169. This caused major concerns, as the RenShape 440 glass transition temperature is 203ºF. A RenShape representative predicted that deflections could occur during the peak temperature hold, so the inserts were coated with Loctite 9396, a high temperature structural adhesive, pictured in **Figure 147**.

Figure 147. Coated FCLA boss.

The finished insert was bonded into the molds using silicon, and plasticine sealed the edges. To locate the FLCA boss inserts, a tape measure was utilized to check dimensions to CAD, shown in **Figure 148**. A

better locating method should be utilized in the future, but this method sufficed as the inserts “snapped” into place. Equal edge distances from the insert to the mold were verified, a final check to ensure the mold was in the correct location.

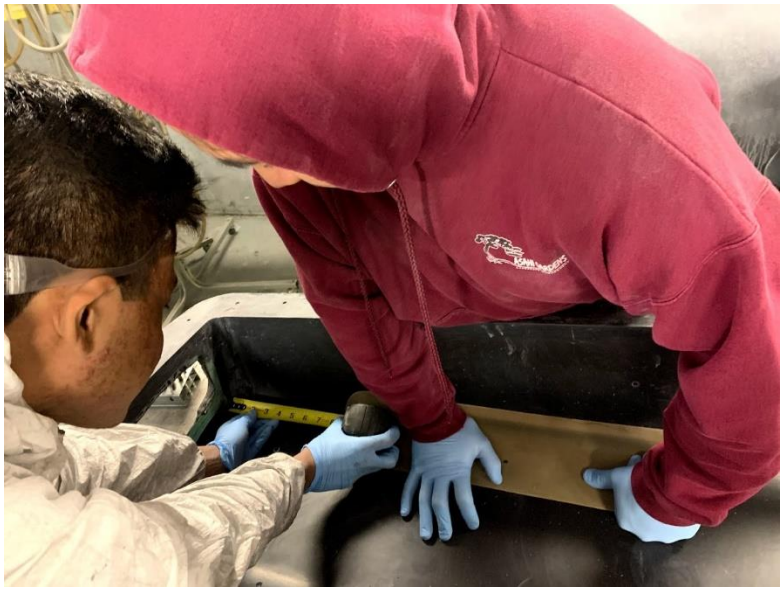

Figure 148. Bonding in the FLCA insert.

Chassis Manufacturing

Once the molds were fully prepared, chassis manufacturing began. To ensure the molds followed the correct cure profile and to test the four piece mold proof of concept, several test layups were conducted. The tests and actual layup were somewhat issue free, but there are a few recommendations for improving the process for future seasons.

Test Layups

The first test consisted of a 2’ x 1’ single 0_c ply across one of the mold seams. This sample was made to ensure proper part release, to check mold performance with the specified cure profile, and to assess the resulting seam geometry. A portion of the seam area was covered with plasticine (pictured in **Figure 149**) while another section was left bare. Five coats of Frekote 710 LV were applied to the surface to ensure easy release. When the ply cured, it released, but some plasticine remained the outer surface. Based on the goal of starting the layup in four separate pieces, plasticine was not included in the next test layup.

Figure 149. Plasticine filled and unfilled mating lines (left) lie underneath the test layup (right).

The second test layup was a full layup comprised of a single ply such that all of the molds were tested. This test was conducted to verify the one piece layup process, find any issues with mating the four molds, and to test the flash tape as a method for filling the seam. The skin was to be laid up with the mold separated, but in the interest of time, the rear halves were bolted together for this process.

Figure 150. Flash tape as a bridge between mating mold pieces (left), verifying function of the access holes during a layup (right).

Flash tape was applied at the seams (shown in **Figure 150**) to prevent resin from seeping through the mold during cure and to prevent seam lines from appearing in the part, as seen in the baby mold test. Laying up in four pieces was successful, but mating the four quarters proved to be difficult, as tape was applied to all four mold edges, pictured in **Figure 151**.

Figure 151. Unmated seam between the front quarters (left) and attempt to apply flash tape under overlapping plies.

The flash tape kept getting stuck between the mold surfaces when the team tried to mate the molds together, but eventually successful assembly occurred. The total mate time took about 1.5 hours, which is less than desirable for a single ply layup. Only using a single piece of flash tape for every mating edge was predicted to solve the issue. Furthermore, attaching the release ply to the skin and ensuring breather covered all surfaces for sufficient compaction was difficult, as the release ply and breather kept during application, shown in **Figure 152**.

Figure 152. Attaching breather and release ply.

To prevent the bag from ripping on sharp corners, tacky tape was applied to all outer seams and bolts. Once the mold was fully prepared, a large “donut” style bag, visualized in **Figure 153**, was made to get sufficient compaction on the inside of the mold.

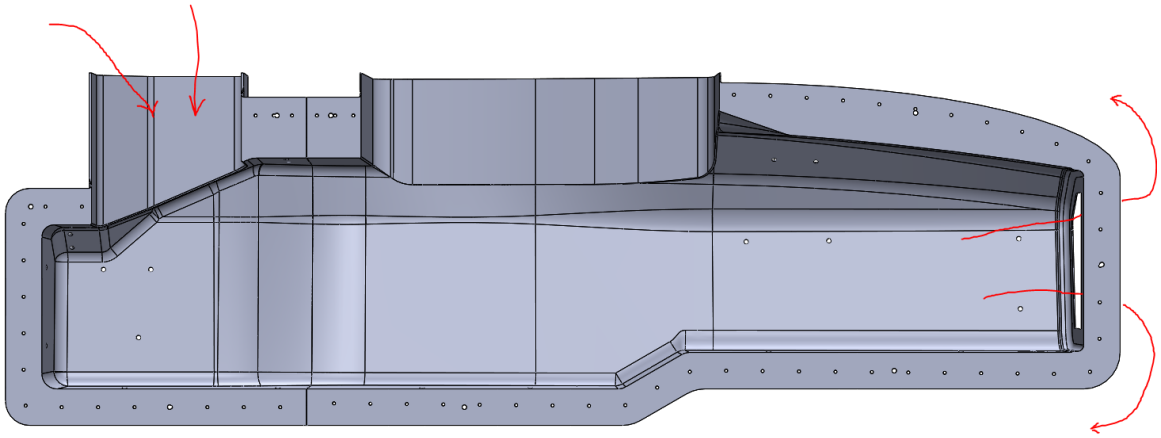

Figure 153. Donut bag feed direction through rear powertrain bay and out through hole in front bulkhead section. Though effective, the bag was difficult to manufacture and was an inefficient use of bagging material.

A 20’ x 15’ bag was made, which was necessary to prevent bridging in corners like in the rear powertrain bay. Even after fine adjustment of the breather and release ply over the material, the final result was still not perfect. Due to the nature of the bag, adjustment was very difficult in the cockpit region since team members could not access all surfaces through the powertrain bay hole. In addition, the hole through the front bulkhead section was also too small to reach all surfaces near the floor height transition, leading to improper application of breather material, pictured in **Figure 154**.

Figure 154. Donut bag through powertrain bay (left) and vacuumed bag (right).

Once the part was cured, releasing the skin proved to be difficult, which was expected due to tight geometry. The mold quarters were initially separated using Home Depot plastic wedges, then the rear molds were pulled apart using the large flanges on the molds at the powertrain bay section.

Figure 155. Released single ply skin at the rear mold.

The front mold quarters came off after using more plastic wedges between the skin and mold. Once released, the skin was inspected at the various mold seam interfaces. The flash tape stuck to the skin, and the part shown in **Figure 155** had ridges in some seams due to a lack of filler, which were both undesirable results. However, the test layup was successful in proofing most manufacturing processes before the final layups.

Chassis Layups

Before any chassis manufacturing was started, carbon and core templates from the geometry shown in **Figure 156** were made for assisting with cutting plies and core. Template design is critical and should be well thought out since poorly cut plies can produce a poor final part. To speed up the actual layup process, all carbon and core should be cut beforehand so plies can be directly applied to the mold in an efficient manner.

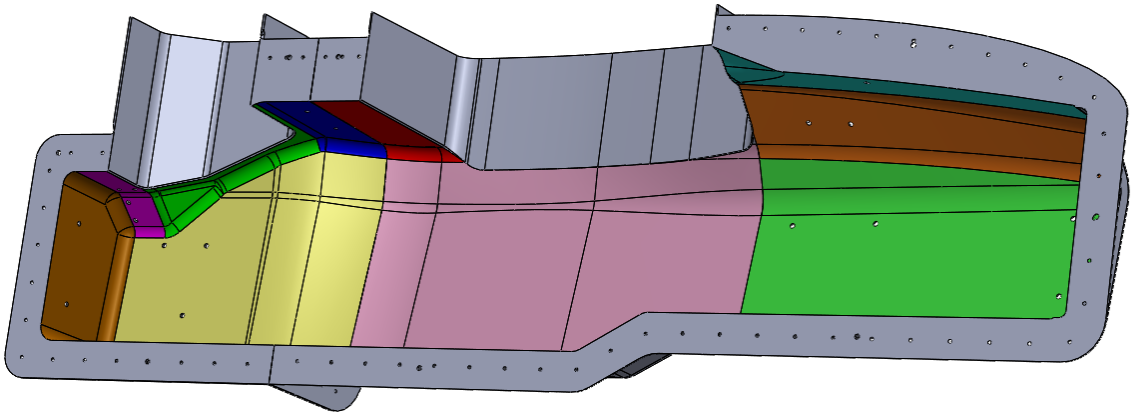

Figure 156. Carbon templates broken down by section. The cockpit floor (not pictured) consisted of three templates.

The carbon templates were designed such that plies were divided by planar surface, shown in the previous figure. Plies were divided such that they overlap in corners to prevent bridging, as the edges have freedom to slide into the corners. Core templates were similarly divided by planar section, but each corner had a separate template that extended beyond the radii, shown in **Figure 157**. Core spanned across the fillets such that no edges met in corners, as those interfaces would need to be heavily filled in with core splice. In addition, flex core could be used in each corner, which is designed for molding to complex contours. Standard honeycomb hex core was used only on planar surfaces, as the team could not produce a reliable core forming procedure. If hex core is used in corners without core forming, the core cells would be buckled into place, significantly reducing the effective strength of the material.

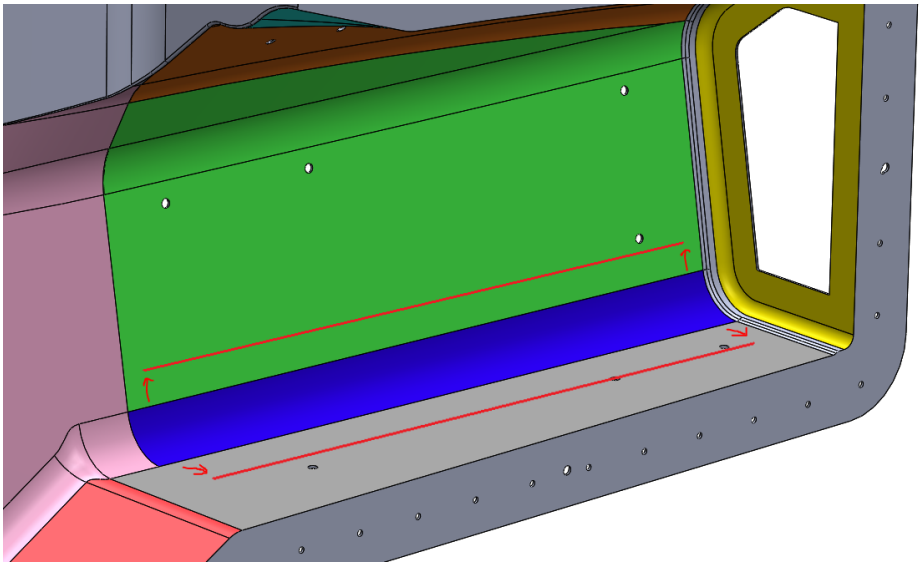

Figure 157. Core template example.

To begin the first chassis layup, all mold seams were lined with flash tape in an attempt to make mating the molds easier. 5 coats of Frekote 710 LV mold release were then applied to all inner surfaces and flanges and allowed to outgas. The first 45_c ply was then placed on all four molds and debulked to minimize defects on the outer surface and prevent bridging. Debulking was first attempted with the vacuum bag only spanning the part surface, pictured in **Figure 158**, but that proved to be insufficient on two of the molds since they had voids, aerating the bag.

Figure 158. Localized vacuum bag on the inner surface.

Once the first ply was debulked, subsequent plies were laid up in groups of three and debulked accordingly. A sample of the layup process is pictured in **Figure 159**. Each ply was separated at the edges using flash tape, so the plies were easy to separate for mating the quarters together. All future debulks utilized full bags around the mold. The first skin layup took about 12 hours, with a total ply count of 71.

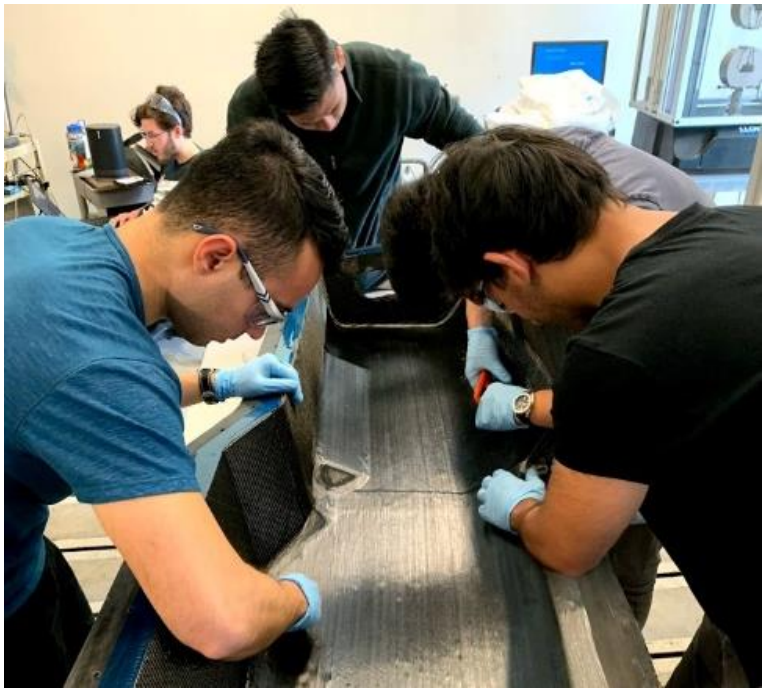

Figure 159. Team members laying up a unidirectional ply in one of the quarters.

With all the global laminate applied, local pad-ups were added to each suspension mount, harness mount, and engine mount location. These are seen in **Figure 160**.

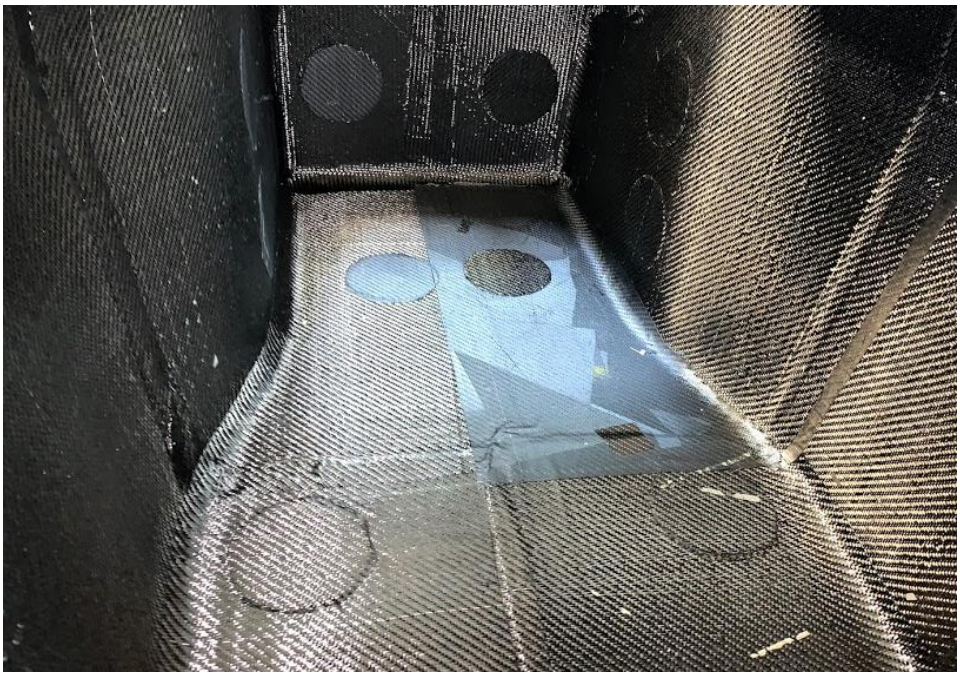

Figure 160. Pad-ups at suspension, engine, and harness mounts.

Once all the plies were placed, film adhesive, pictured in **Figure 161**, was applied to all surfaces to ensure a sufficient bond to the core. The part went through a final debulk once the film adhesive was applied.

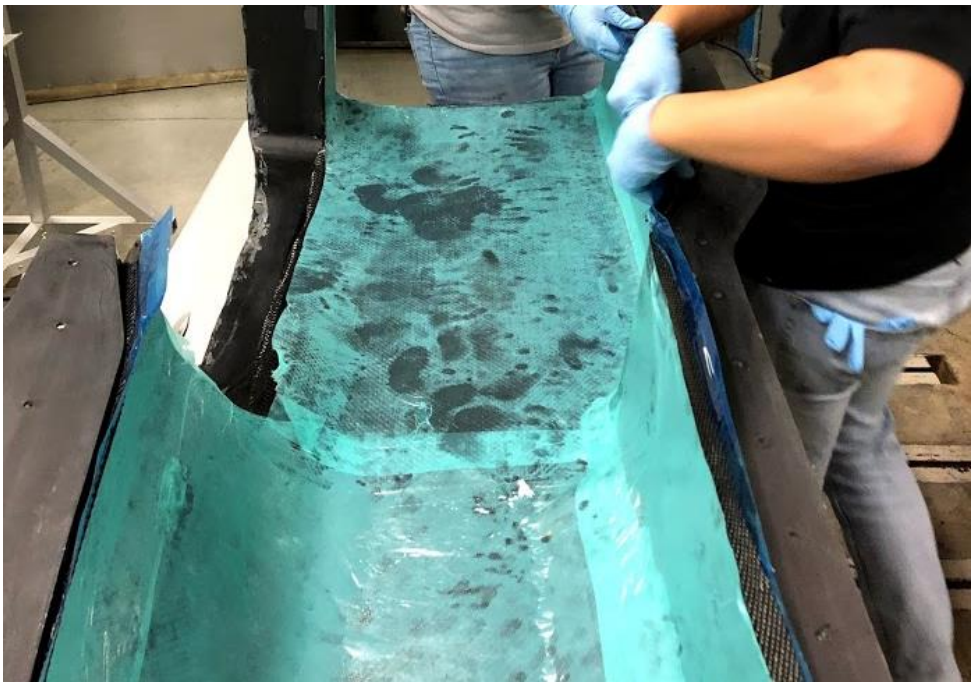

Figure 161. Film adhesive applied to one quarter.

The most difficult part of the layup was mating the four mold quarters. The team attempted to mate the front quarters first and encountered a multitude of issues. The flash tape stuck to the plies (shown in **Figure 162**) and was hard to remove, making interweaving the plies difficult. Since the plies were debulked in quarters, the flange pieces were laid up around the edges, so a protrusion in the laminate formed when it was straightened for mating.

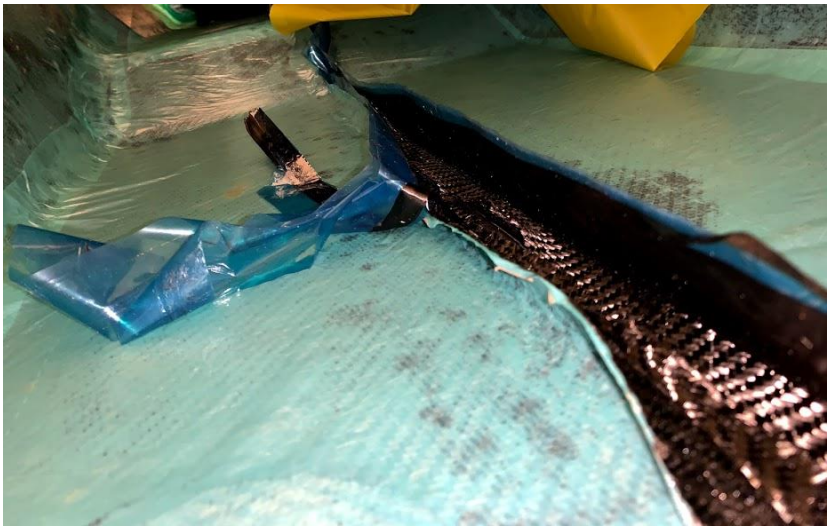

Figure 162. Struggling to remove flash tape and interweave layers.

The corners of the laminate proved to be nearly impossible to mate, namely the front bulkhead (pictured in **Figure 163**) which had 15+ plies. The total mating process took about 3 hours for a somewhat mediocre result. The team was not able to interweave individual plies since they were difficult to separate, so plies were interwoven in groups of three.

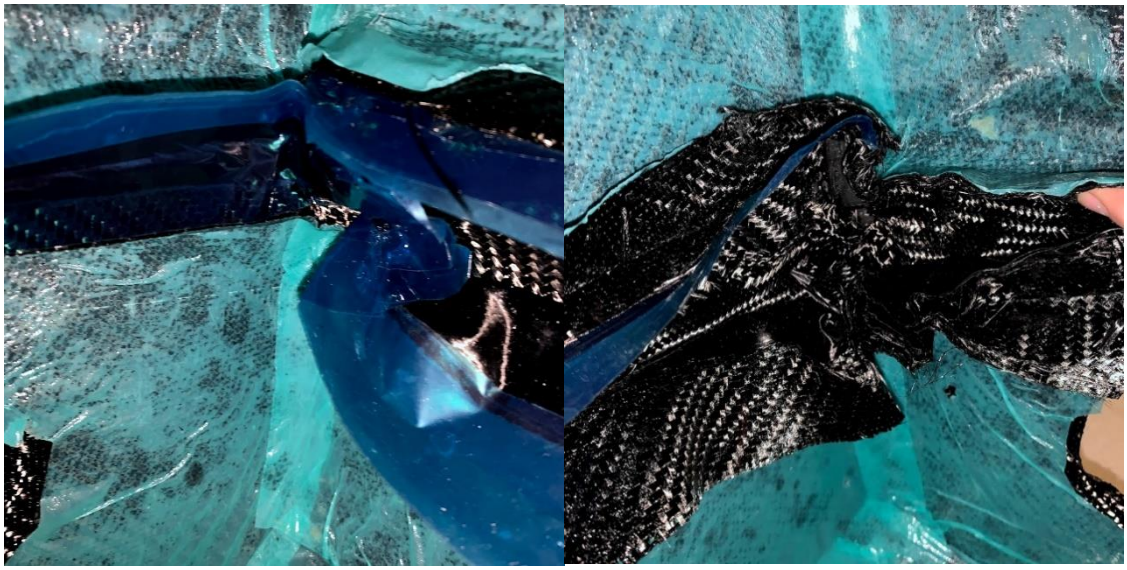

Figure 163. Front bulkhead/front bulkhead support corner before (left) and after (right) pulling the flash tape. Interweaving plies in corners was particularly difficult.

However, the rear quarters proved to be much easier to mate since there were less plies to interweave. Once the left and right quarters were mated, the front half was mated to the rear, shown in **Figure 164**.

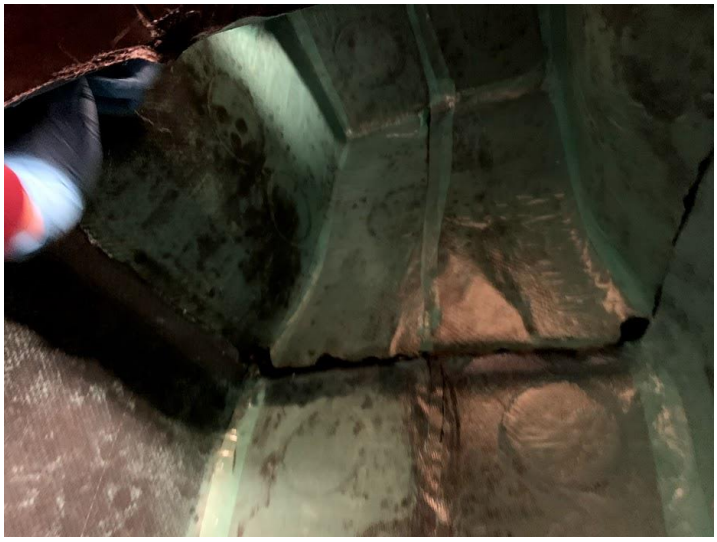

Figure 164. Mating front and rear molds.

Once the quarters were mated, the whole mold was debulked using the "donut" bag method. Core was then applied to all surfaces. Unfortunately, by debulking the whole outer skin with the film adhesive applied, the film adhesive got contaminated from the release ply and bagging materials, rendering it much more difficult to keep core attached to surfaces. To combat this problem, the film adhesive was heated with heat guns, and hot glue was used to bond core pieces to the adhesive. This is shown in **Figure 165**.

Figure 165. Heating the film adhesive (left) after contaminating the film adhesive from debulking (right).

The core templates were not made precisely enough, as trimming had to occur to make all the core pieces fit together. In addition, some templates did not properly line up, so thick pieces of core splice were used

to fill in the gaps, as shown in **Figure 166**. Approximately 1.75 lbs. of core splice was utilized, which is more than the expected value assuming one strip of core splice is placed between each set of edges.

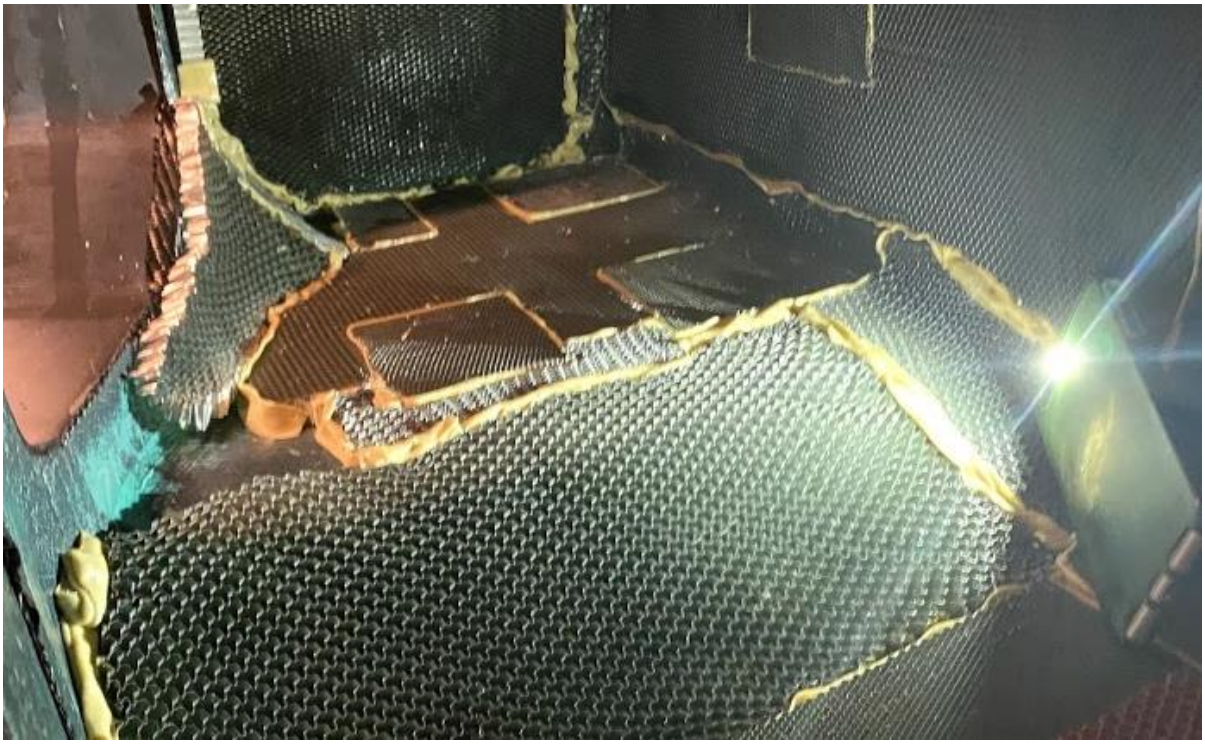

Figure 166. Core splice between sections. Some core templates did not fully span the geometry, so patches were created to mitigate gaps in the core layer.

Once all of the core was applied, the inner hardpoint pad-ups were applied, and the first ply of the inner skin was laid up. A subsequent debulk was completed to ensure sufficient compaction and bonding between the core and first inner skin. However, due to the nature of the donut vacuum bag, it could not be adjusted easily, leading to bridging issues near the floor transition section. The final plies were then laid up, and release ply and breather were applied to all surfaces. As expected, adjusting all the release ply and breather to cover every surface took longer than expected, and an acceptable vacuum bag configuration was achieved, shown in **Figure 167**.

Figure 167. The bag was routed through the rear access hole (left) and had plenty of excess material to remove internal bridging (right).

Because the bag was so large and susceptible to scraping on various sharp corners on the mold exterior and ground, a lot of pinholes were produced, so achieving full vacuum was difficult. Three vacuum ports were used to ensure sufficient compaction in all areas of the chassis.

Once cured, past strategies for releasing the part were used, including plastic Home Depot wedges and an inflatable bladder. Unfortunately, some of the flanges delaminated due to wedges getting between the plies. To release the part, wedges were first used to separate each mold flange. The FL mold was the first mold to come off, carefully worked via wedges between the part and mold at the cockpit cutout/SIS section. Once most of the SIS surface was released, team members pulled the mold off using the mold flanges, exposing the part shown in **Figure 168**.

Figure 168. Removal of the FL mold piece. The plasticine used the seal the corner around the FLCA surface insert baked onto the chassis structure.

With the FL side exposed, wedges were used at the chassis side in an attempt to remove the RL mold, pictured in **Figure 169**. Stacks of two wedges were used at a time, as three wedges caused too much local deformation, deforming the molds instead of releasing them from the part surface.

Figure 169. Wedging under the RL (left) and released surface (right).

Shown in **Figure 170**, the Bondo applied to fill in surface impurities ended up sticking to the part, causing much of the difficulty in mold removal. With two molds left, the RR mold was worked off with wedges at every edge.

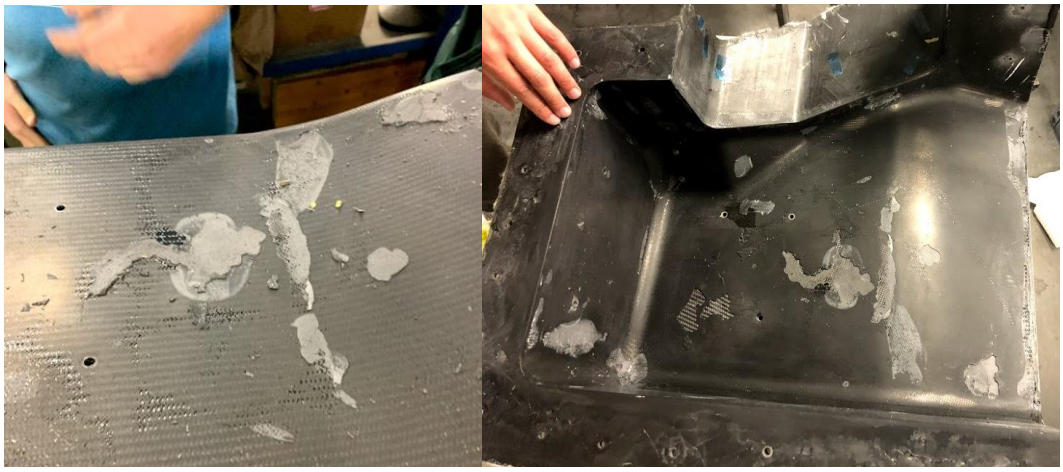

Figure 170. Bondo stuck to chassis surface (left) and resulting void in mold surface (right).

Due to some carelessness, the combustion vehicle chassis was damaged in the RR mold removal process. While trying to remove one of the rear mold pieces, a wedge was hammered in between the RR mold and chassis too close to a corner. Due to the tight geometry and location of the wedge, it was extremely difficult to extract. Left in place overnight, the laminate failed locally, leading to permanent deformation of the chassis, shown in **Figure 171** and **Figure 172**.

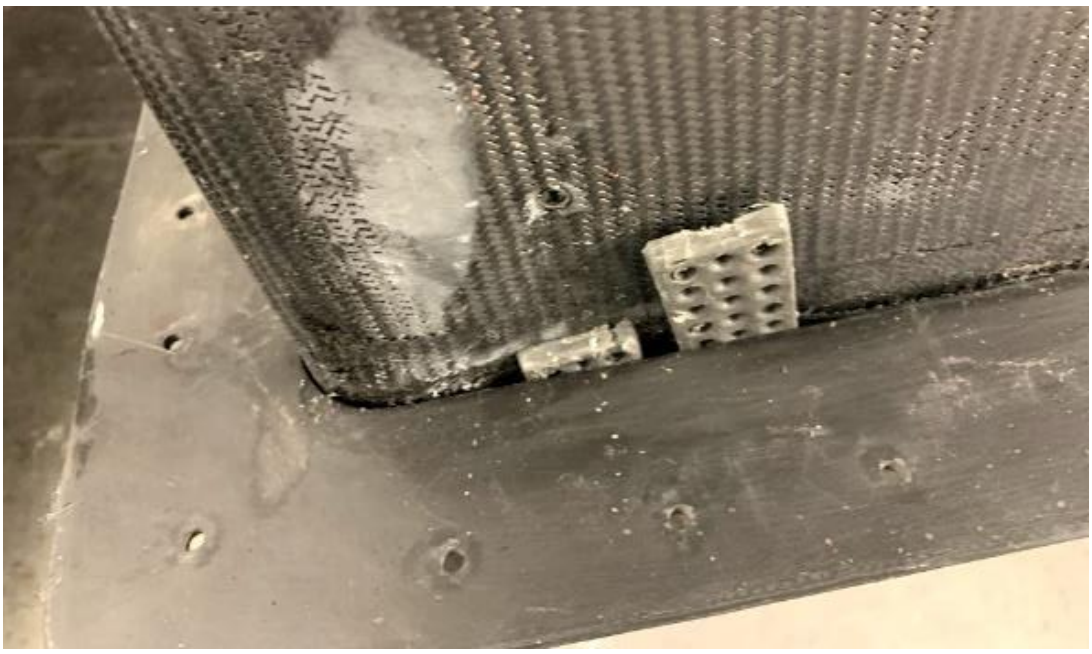

Figure 171. Wedges stuck between monocoque and RR mold.

With more hours of wedging and some WD-40, the RR mold released from the part. The FR mold came off easily after that, with plenty of free edges accessible for wedging. Once finally removed, the untrimmed monocoque weighed in at 39 lbs., the lightest monocoque the CPFSAE team has manufactured.

Based on this release, it is recommended to always take wedges out of the mold-monocoque interface when pausing between extraction, as the actual part or mold could fail, as shown in **Figure 172**. To repair this section, the failed area was identified and carefully cut out and replaced with a carbon patch wetted using structural adhesive.

Figure 172. Dented chassis wall (left) and the outer skin removed (right) in order to perform a wet layup repair.

Overall, the final monocoque result was better than in previous years, as evident in **Figure 173**. By eliminating the strap joint at the mid section of the chassis, post processing time and weight were minimized.

Figure 173. FBHS surface of combustion vehicle chassis.

Unfortunately, due to a lack of compaction in certain plane changes and improper core forming, in particular near the main hoop mount vertex, delamination between the outer skin and core occurred, shown in **Figure 174**. To repair this, a mix of microballoon, cabosil, and West Systems resin was used to fill in the area.

Figure 174. Delamination between core and outer skin (left) and a portion of subsequent repair (right).

For the electric vehicle monocoque layup, several techniques were altered in an attempt to make manufactuirng easier and to reduce time based on lessons learned from the first layup. Instead of using flash tape to line the mold mating edge, fluorinated ethylene propylene (FEP) fabric was used since it does not have an adhesive side. This made mating the quarters together easy, reducing mating time from 3 hours to 45 minutes.

In addition, the seams themselves were better interweaved. The majority of the front bulkhead plies were also laid up once the molds were assembled, making the mating progress at sharp corners easier. Furthermore, the whole outer skin was debulked without the film adheisve, making core application smoother. Lastly, all inner plies were cut such that they spanned across the left-right mating surface, reducing weight due to a lack of overlap.

In the future, better template design should be employed such that the plies do not have the same length at all seams, as this is the cause of the "bump" shown in **Figure 175**.

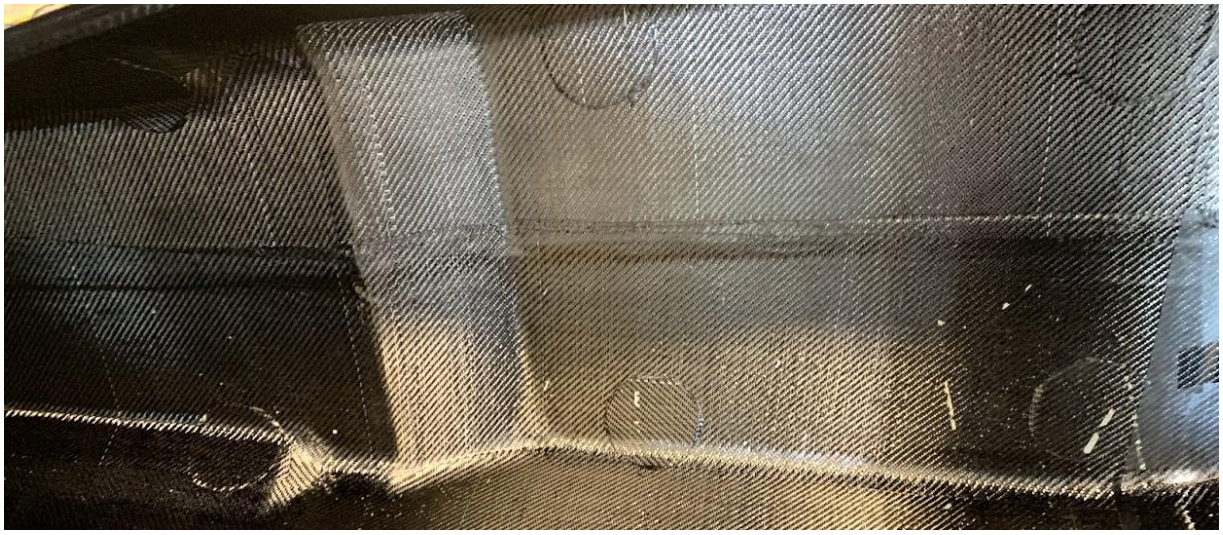

Figure 175. Seam down the centerline of the monocoque floor.

Staggering ply lengths should be used to prevent buildup in one section, which requires various configurations of a template for a given section.

Design Verification

To verify the design of the monocoque, it must pass all Formula SAE rules including geometric requirements and a structural equivalency test. The monocoque must also satisfy the given performance goals of torsional stiffness and total chassis weight. Before manufacturing, the geometric requirements were tested using chassis CAD and representative rules templates. Additionally, structural equivalency tests were performed to verify that the monocoque would be as strong as or stronger than a steel tube frame.

After manufacturing, performance tests were planned to measure the torsional stiffness and weight of the chassis. A mock technical inspection was also planned to ensure the monocoque meets all Formula SAE rules. Due to the outbreak of COVID-19, these tests could not be performed.

Geometry Verification

For every chassis geometry iteration, a line-by-line sweep through the 2019 Formula SAE rules followed to make sure that the chassis would be rules compliant. These rules, located under section T.3, require two templates to be placed in the driver's cell [7]. They keep the vehicle from getting too small, which could pose an accessibility and safety hazard for a driver. The templates are shown in **Figure 176**. The cockpit opening template is held horizontally and must pass from the top of the main hoop to 350mm from the floor of the chassis, pictured in **Figure 177**. In one instance, it was found that the roll hoop geometry interfered with the cockpit opening template, requiring the chassis to get wider as a result. The cross-section was easily changed, and the rules were once again swept through to ensure that the new geometry did not adversely affect any of the other requirements.

The cross-section template is used in the pedal box area of the chassis, shown in **Figure 178**. It must be positioned vertically and pass through the driver cell horizontally. To avoid the steering column, it may be flipped and re-positioned around the column, as well as shifted up and down.

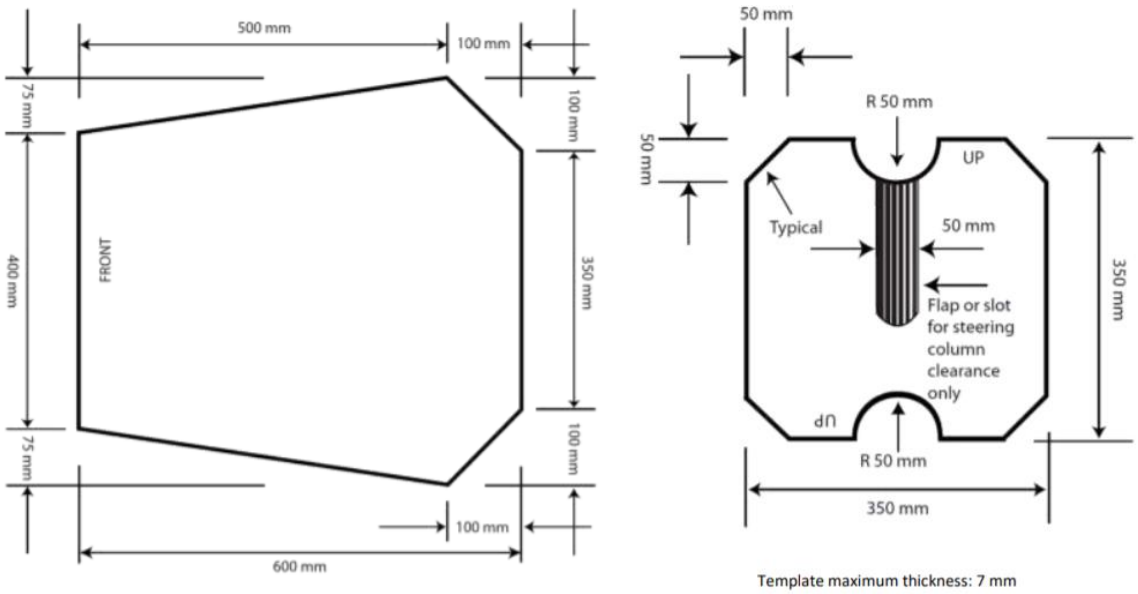

Figure 176. Cockpit opening template (left) and cross-section template (right) as specified in the 2020 Formula SAE rules.

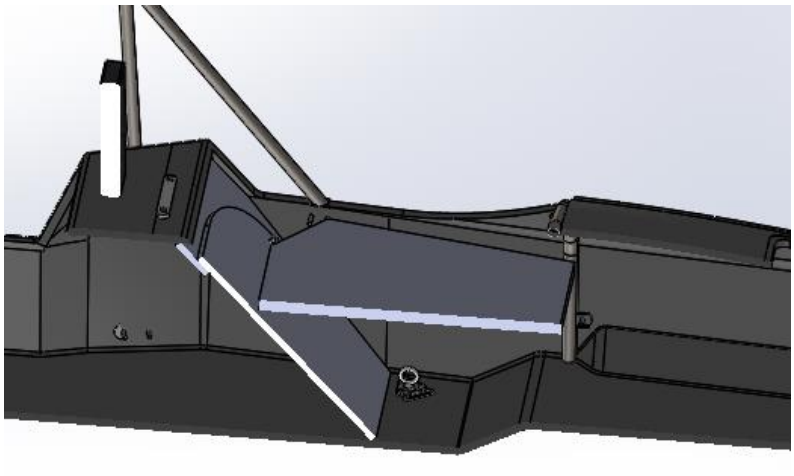

Figure 177. Chassis cockpit opening template (horizontal grey plane). Template must be lowered to a height of 350mm above the ground plane (pictured) without interfering with the chassis or the roll hoops.

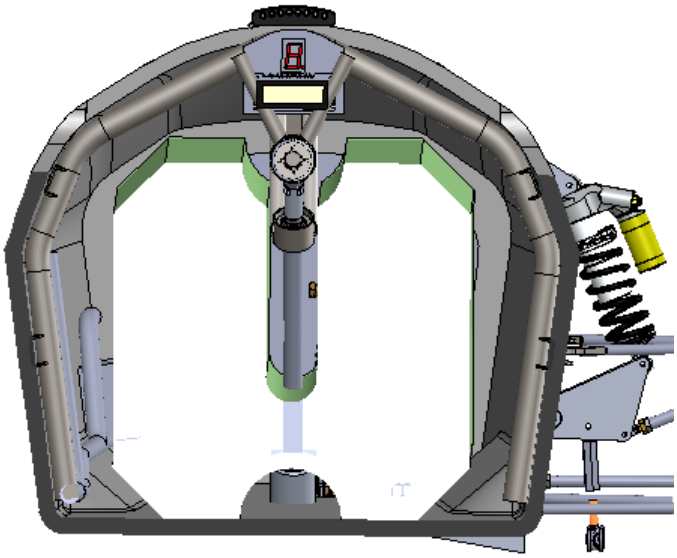

Figure 178. Chassis internal cross-section template (white). Template is allowed to move vertically as needed but must not interfere with any vehicle components.

Structural Equivalency Testing and Summary

Per Formula SAE rules, the monocoque must have equal or greater structural properties than the steel tube baseline [7]. The rules break up the chassis into many sections, such as the front bulkhead (FBH), front bulkhead support (FBHS), or side impact structure (SIS), and each must be tested for equivalency to match the benchmark steel tubes. The detailed background of SES testing and compliance is discussed in the Structural Equivalency Spreadsheet section of this report.

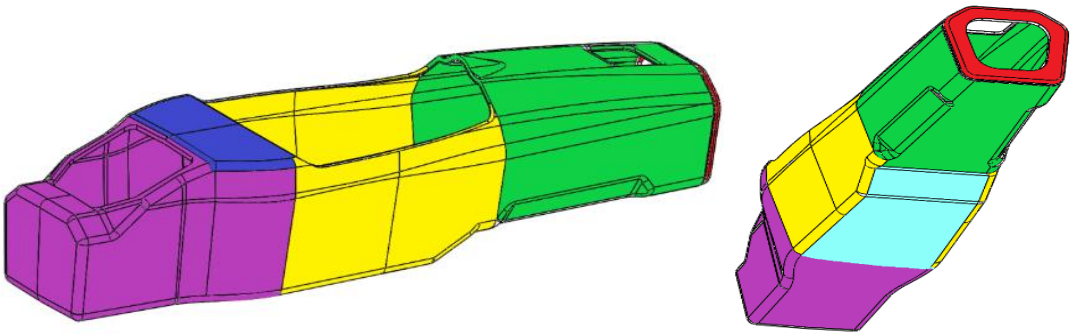

Figure 179. Breakdowns of different areas of the monocoque. Green contains FBHS, yellow contains SIS, blue contains driver harness mounting, purple contains main hoop mounting and fuel system protection (CP19C) and tractive system protection (CP19E).

For the MCD team, both tests can be performed on the ME Department Instron testing equipment, which yields displacement and force required to fail each test sample.

In the early stages of SES testing, it was desirable to validate the local 3-point bend failure models so that they could be used to predict laminate performance instead of blindly testing laminae. The focus of this model was to develop a better tool for selecting panel top skins, as these were typically the weakest structural element of the panel itself, with core coming in a close second. Because the 3-point bend models were not usable due to a lack of validity, the team iterated through layups and checked results in SES for compliance. The baseline laminate for the monocoque was based off the layup schedules used in 2017 but was altered by removing plies from the inner skin, with iterations listed in **Table 13.**

Table 13: SES Test Layups

Description	Layup Schedule
General	[45c/0/0c/0.5 Core/0c/45c]
SIS Floor	[45c/0/0/0c/0c/0.5 high density core/0c/45c]
SIS Side	[45c/0/0/0c/0c/.7 core/0c/45c]
FBHS Try 1	[45c/0/0/C/0c]
FBHS Try 2	[45c/0/0c/core/0c/45c]
SIS Try 1	[45c/0/0/0/C/0/0c]
SIS Try 2	[45c/0/0/C/0/0c]
SIS Try 3	[45c/0/0/0/C/0c]
SIS Try 4	[45c/0/0/0c/core/0c/45c]

General, FBHS, and SIS were predicted to have passed after testing, but FBHS and SIS were not compliant after further investigation. 3-point bend and perimeter shear results are shown in **Figure 180** and **Figure 181**, respectively.

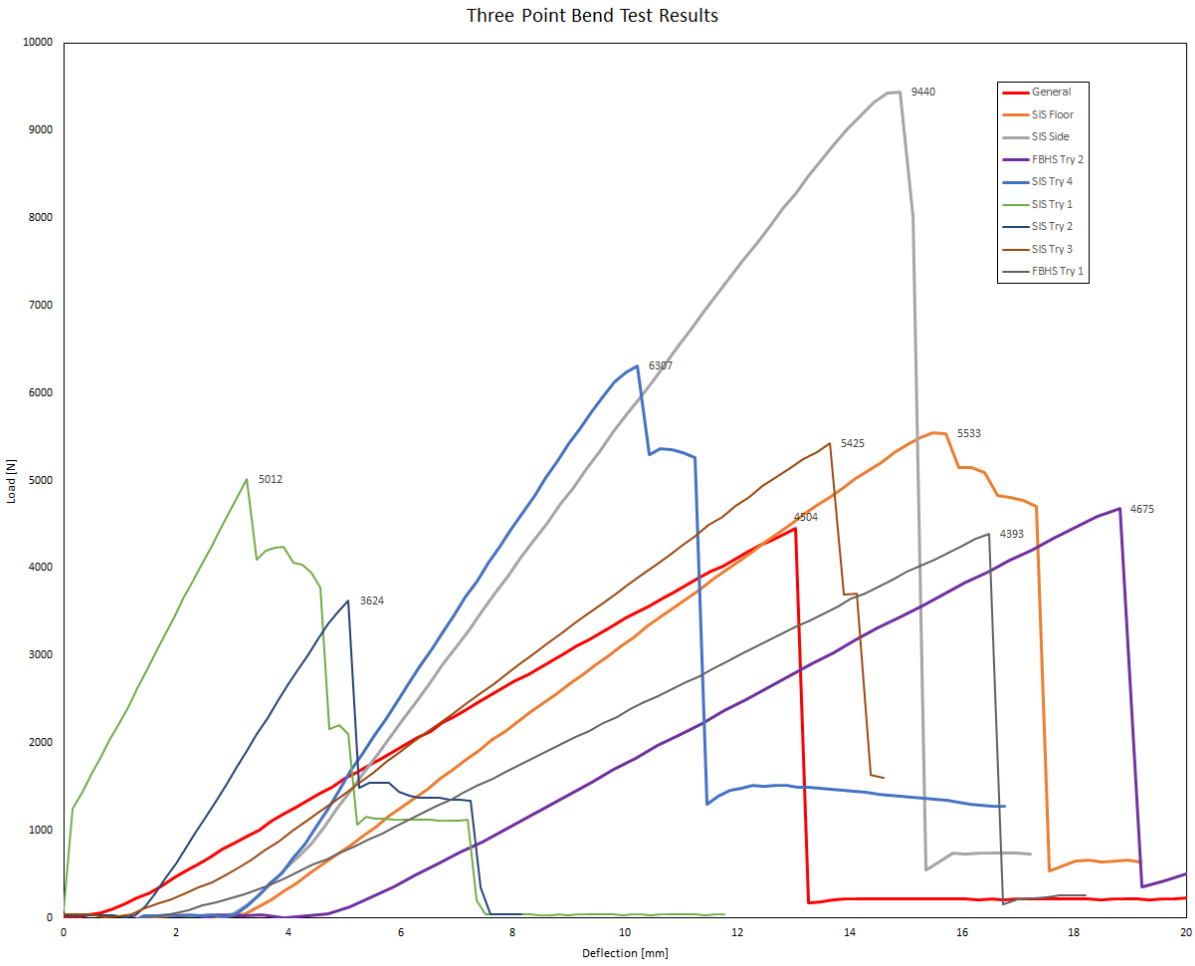

Figure 180. 3-point bend results from initial layup iterations.

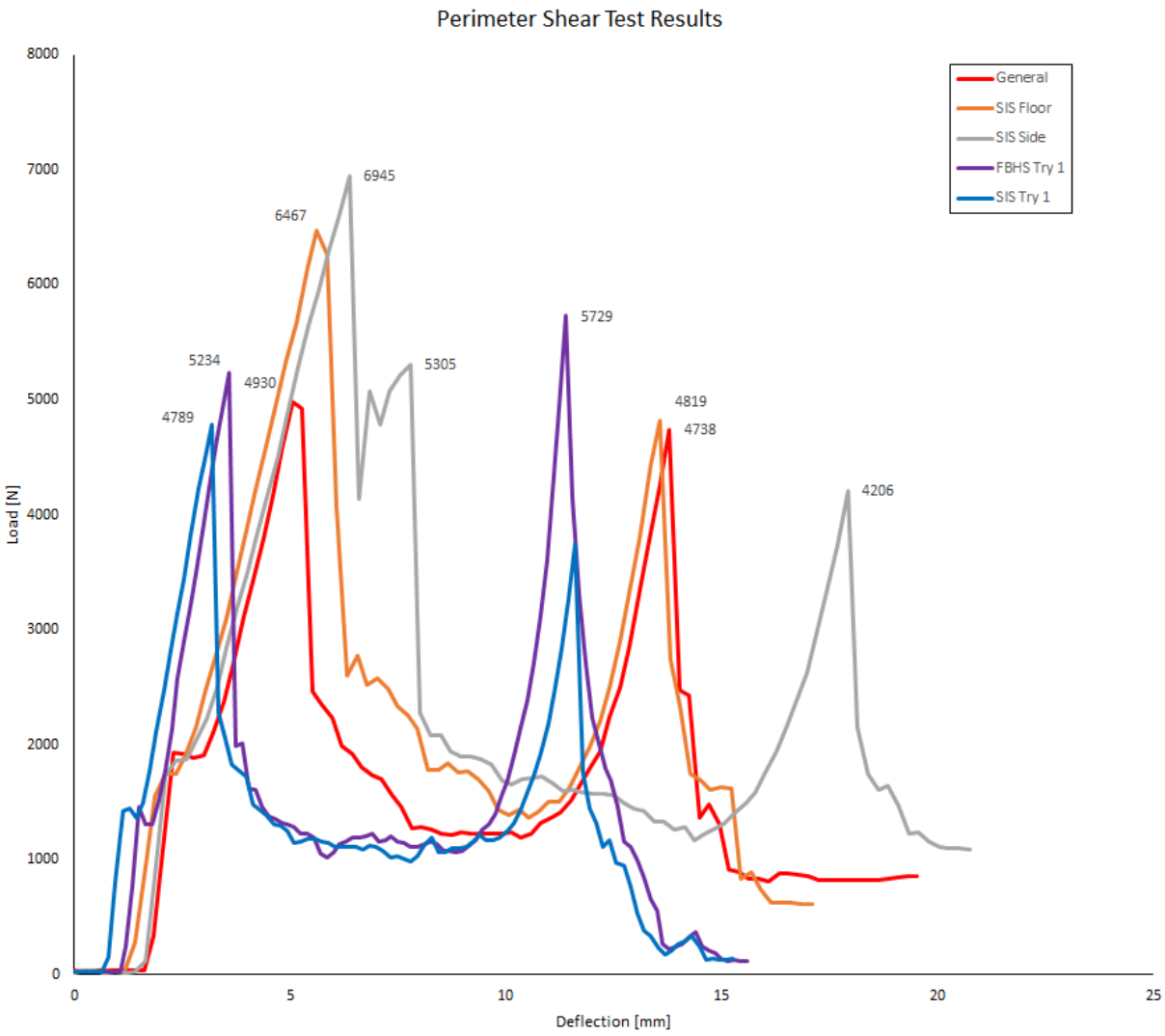

Figure 181. Perimeter shear test results for the initial layup iterations.

When checked in SES, laminate information was only inputted into the F.4.3 section, which only checked 3-point bend compliance. Once entered in the general F.7 tab, the FBHS and SIS laminates did not pass the buckling modulus and bending cells under F.3.4.2a, displayed in **Figure 182**.

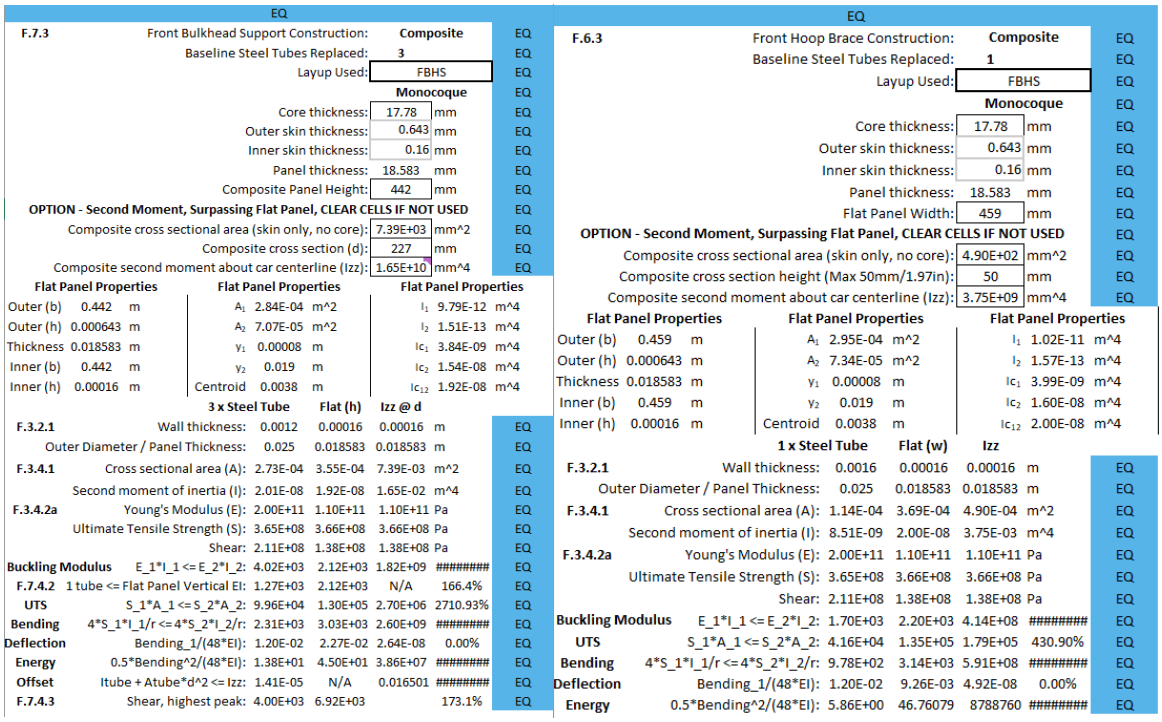

EQ								
F.7.3	Front Bulkhead Support Construction:			Composite			EQ	
	Baseline Steel Tubes Replaced:			3			EQ	
	Layup Used:			FBHS			EQ	
				Monocoque			EQ	
	Core thickness:			17.78	mm		EQ	
	Outer skin thickness:			0.643	mm		EQ	
	Inner skin thickness:			0.16	mm		EQ	
	Panel thickness:			18.583	mm		EQ	
	Composite Panel Height:			442	mm		EQ	
	OPTION - Second Moment, Surpassing Flat Panel, CLEAR CELLS IF NOT USED						EQ	
	Composite cross sectional area (skin only, no core):			7.39E+03	mm^2		EQ	
	Composite cross section (d):			227	mm		EQ	
	Composite second moment about car centerline (Izz):			1.65E+10	mm^4		EQ	
	Flat Panel Properties			Flat Panel Properties			Flat Panel Properties	
	Outer (b)	0.442	m	A_1	2.84E-04	m^2	I_1	9.79E-12 m^4
	Outer (h)	0.000643	m	A_2	7.07E-05	m^2	I_2	1.51E-13 m^4
	Thickness	0.018583	m	y_1	0.00008	m	Ic_1	3.84E-09 m^4
	Inner (b)	0.442	m	y_2	0.019	m	Ic_2	1.54E-08 m^4
	Inner (h)	0.00016	m	Centroid	0.0038	m	Ic_{12}	1.92E-08 m^4
				3 x Steel Tube	Flat (h)	Izz @ d		
F.3.2.1	Wall thickness:			0.0012	0.00016	0.00016	m	EQ
	Outer Diameter / Panel Thickness:			0.025	0.018583	0.018583	m	EQ
F.3.4.1	Cross sectional area (A):			2.73E-04	3.55E-04	7.39E-03	m^2	EQ
	Second moment of inertia (I):			2.01E-08	1.92E-08	1.65E-02	m^4	EQ
F.3.4.2a	Young's Modulus (E):			2.00E+11	1.10E+11	1.10E+11	Pa	EQ
	Ultimate Tensile Strength (S):			3.65E+08	3.66E+08	3.66E+08	Pa	EQ
	Shear:			2.11E+08	1.38E+08	1.38E+08	Pa	EQ
Buckling Modulus	E_1*I_1 <= E_2*I_2:			4.02E+03	2.12E+03	1.82E+09	########	EQ
F.7.4.2	1 tube <= Flat Panel Vertical EI:			1.27E+03	2.12E+03	N/A	166.4%	EQ
UTS	S_1*A_1 <= S_2*A_2:			9.96E+04	1.30E+05	2.70E+06	2710.93%	EQ
Bending	4*S_1*I_1/r <= 4*S_2*I_2/r:			2.31E+03	3.03E+03	2.60E+09	########	EQ
Deflection	Bending_1/(48*EI):			1.20E-02	2.27E-02	2.64E-08	0.00%	EQ
Energy	0.5*Bending^2/(48*EI):			1.38E+01	4.50E+01	3.86E+07	########	EQ
Offset	Itube + Atube*d^2 <= Izz:			1.41E-05	N/A	0.016501	########	EQ
F.7.4.3	Shear, highest peak:			4.00E+03	6.92E+03		173.1%	EQ

EQ								
F.6.3	Front Hoop Brace Construction:			Composite			EQ	
	Baseline Steel Tubes Replaced:			1			EQ	
	Layup Used:			FBHS			EQ	
				Monocoque			EQ	
	Core thickness:			17.78	mm		EQ	
	Outer skin thickness:			0.643	mm		EQ	
	Inner skin thickness:			0.16	mm		EQ	
	Panel thickness:			18.583	mm		EQ	
	Flat Panel Width:			459	mm		EQ	
	OPTION - Second Moment, Surpassing Flat Panel, CLEAR CELLS IF NOT USED						EQ	
	Composite cross sectional area (skin only, no core):			4.90E+02	mm^2		EQ	
	Composite cross section height (Max 50mm/1.97in):			50	mm		EQ	
	Composite second moment about car centerline (Izz):			3.75E+09	mm^4		EQ	
	Flat Panel Properties			Flat Panel Properties			Flat Panel Properties	
	Outer (b)	0.459	m	A_1	2.95E-04	m^2	I_1	1.02E-11 m^4
	Outer (h)	0.000643	m	A_2	7.34E-05	m^2	I_2	1.57E-13 m^4
	Thickness	0.018583	m	y_1	0.00008	m	Ic_1	3.99E-09 m^4
	Inner (b)	0.459	m	y_2	0.019	m	Ic_2	1.60E-08 m^4
	Inner (h)	0.00016	m	Centroid	0.0038	m	Ic_{12}	2.00E-08 m^4
				1 x Steel Tube	Flat (w)	Izz		
F.3.2.1	Wall thickness:			0.0016	0.00016	0.00016	m	EQ
	Outer Diameter / Panel Thickness:			0.025	0.018583	0.018583	m	EQ
F.3.4.1	Cross sectional area (A):			1.14E-04	3.69E-04	4.90E-04	m^2	EQ
	Second moment of inertia (I):			8.51E-09	2.00E-08	3.75E-03	m^4	EQ
F.3.4.2a	Young's Modulus (E):			2.00E+11	1.10E+11	1.10E+11	Pa	EQ
	Ultimate Tensile Strength (S):			3.65E+08	3.66E+08	3.66E+08	Pa	EQ
	Shear:			2.11E+08	1.38E+08	1.38E+08	Pa	EQ
Buckling Modulus	E_1*I_1 <= E_2*I_2:			1.70E+03	2.20E+03	4.14E+08	#########	EQ
UTS	S_1*A_1 <= S_2*A_2:			4.16E+04	1.35E+05	1.79E+05	430.90%	EQ
Bending	4*S_1*I_1/r <= 4*S_2*I_2/r:			9.78E+02	3.14E+03	5.91E+08	#########	EQ
Deflection	Bending_1/(48*EI):			1.20E-02	9.26E-03	4.92E-08	0.00%	EQ
Energy	0.5*Bending^2/(48*EI):			5.86E+00	46.76079	8788760	#########	EQ

Figure 182. SES sheet showing FBHS compliance. Laminates can pass via flat panel or second moment of inertia.

Luckily, one of the iterations of SIS test panels passed for FBHS, so that laminate was applied. SIS was finally compliant after adding several plies to the inner skin to reduce deflection. Due to poor quality of the load applicator manufacturing, the MCD team ran into several issues with testing, and had to retest several panels due to a lack of alignment with the testing setup. The load applicator was not perfectly square to the panel for some tests, so the tested peak loads were lower than the panel's true capability.

Once most of the laminate was finalized, testing was conducted for the upper and lower harness mounts. A jig was manufacturing for the lower harness and a representative panel was made with the harness layup and hardware, shown in **Figure 183**.

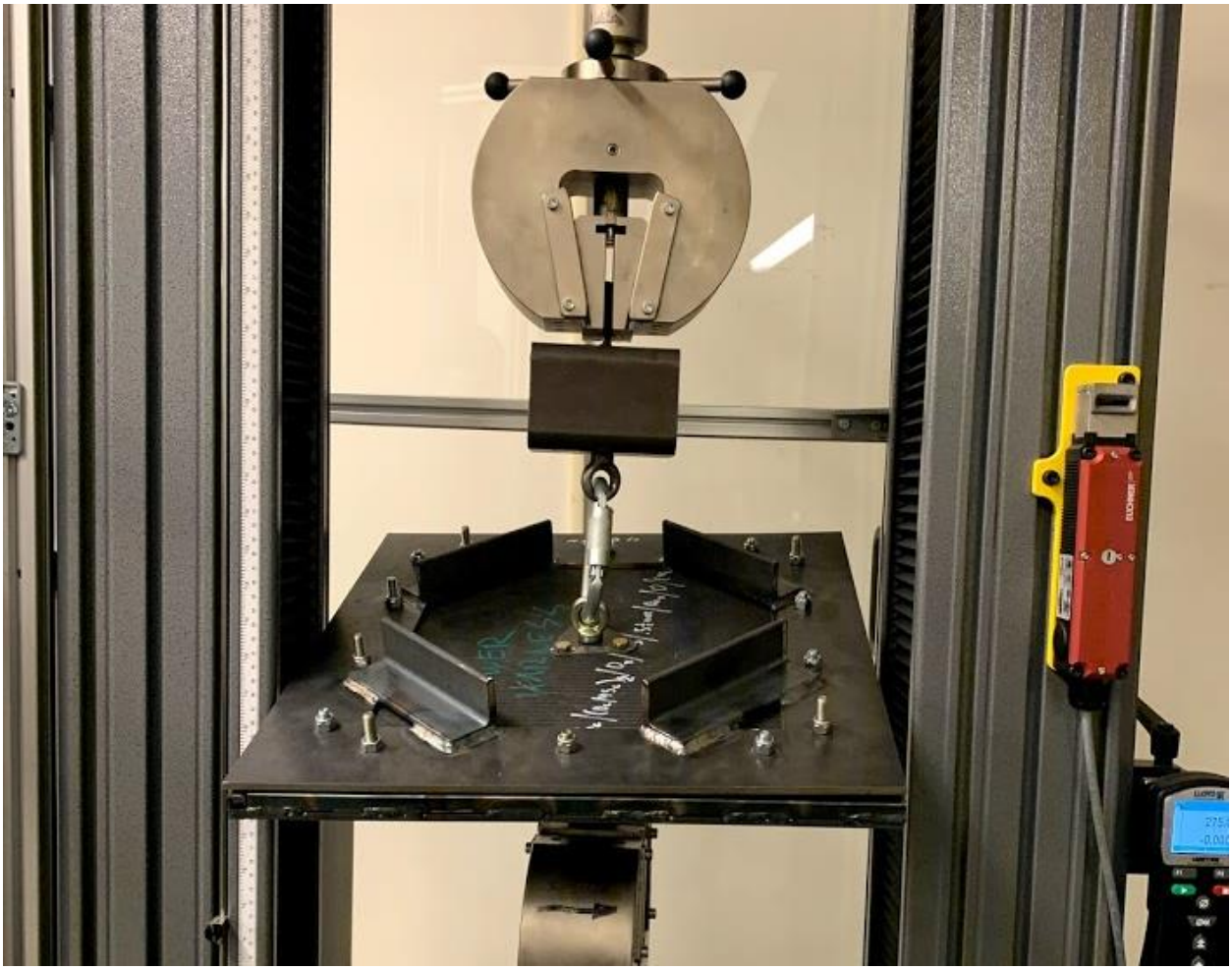

Figure 183. Lower harness being tested.

This test ran smoothly, and the laminate passed first try, with the laminate comprised of the SIS layup schedule and hardpoint pad-ups. However, the MCD ran out of time to develop a light laminate for the upper harness mounts, so a similar laminate was used to pass. In the future, a new upper harness jig should be developed to simulate on-vehicle conditions, as the current jig limits the performance of the sample panel. Because of the current jig geometry, the simulated firewall flange is limited in length, which reduces stiffness of the panel and can lead to premature core failure. The old upper harness jig is shown in **Figure 184**.

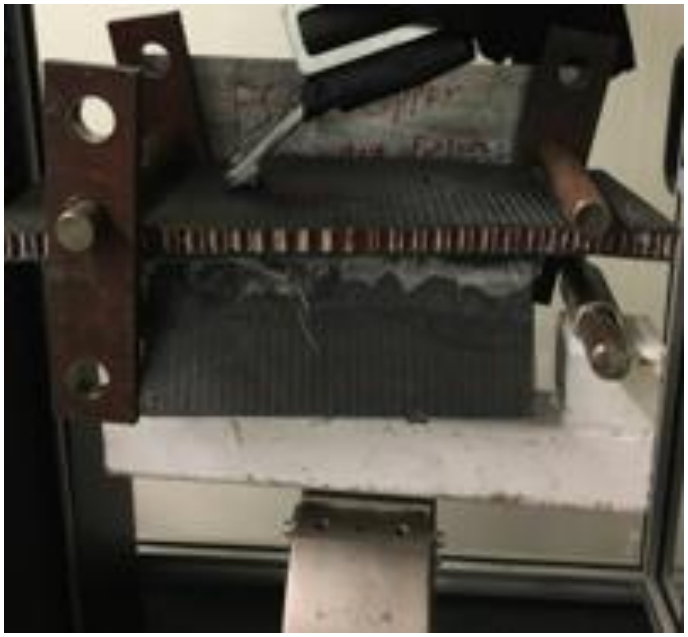

Figure 184. Upper harness inverted 3-point bend test jig.

After testing all the panels and ensuring compliance, SES was submitted on time, with the full, finalized layup schedule detailed in **Table 14**.

Table 14: Final SES Layup Schedule

	Laminate	Core	Core Thickness [in]
FBHS	$[45_c/0_2/0_{c2}/\text{Core}/0_c/45_c]$	3/16” 3.1 pcf Aluminum	0.7
Front Bulkhead	$[(45_c/0/0_c)_5/\text{Core}/(0_c/0/45_c)_4/0_c/45_c]$	3/16” 3.1 pcf Nomex	0.5
SIS	$[45_c/0_3/0_{c3}/\text{Core}/0_{c2}/0/45_c]$	1/8” 4.4 pcf Aluminum	0.7
Upper Harness	$[(45_c/0_c)_4/\text{Core}]_s$	3/16” 3.1 pcf Fiberglass	0.5
Rear/General	$[45_c/0/0_c/\text{Core}/0_c/45_c]$	3/16” 3.1 pcf Aluminum	0.5
Lower Harness	$[45_c/0_3/0_{c3}/(45_c/0_c)_2/\text{Core}/(0_c/45_c)_2/0_{c2}/0/45_c]$	1/8” 4.4 pcf Aluminum	0.7

Chassis Performance Testing

Following the manufacturing of the chassis, tests were planned to determine the torsional stiffness and weight of the final part. To test the torsional stiffness, the MCD team planned to utilize the frame stiffness jig and instructions provided by the *Torsional Stiffness of a Race Car* 2019 senior project [12]. The setup requires the chassis to be assembled with roll hoops, suspension links, and rigid links in place of the spring-damper unit. Then the frame stiffness jig is fastened to the uprights where the wheels would attach. The rear jig would be fixed to a table, and the front jig would be used to load one side of the car, as shown in **Figure 185**.

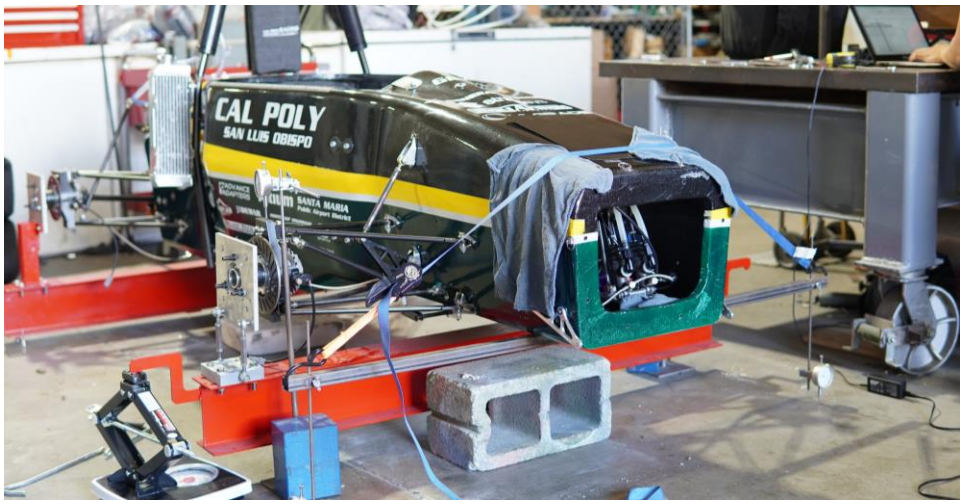

Figure 185. Chassis torsional stiffness test rig. Notice the scissor jack applying load to the FR jig, while a dial indicator measures the displacement of the FL jig.

Since this method of testing the torsional stiffness of the car includes the loaded deflection of the suspension members and their mounting to the chassis, the torsional stiffness output in ft-lb/deg will be less than just the torsional stiffness of the chassis. While this value is not something that is completely monocoque dependent, it does represent the chassis-suspension system, which is much more representative of stiffness values as they pertain to overall vehicle performance.

In addition, powertrain serviceability needed to be assessed. For this, we would record the amount of time it takes to remove and disassemble the drivetrain, with the target time being 45 minutes. Servicing the drivetrain is important to reliable vehicle performance, so it is important to minimize the difficulty of this process. Removal of the drivetrain will also require the removal of the intake and electronic components, which could complicate this.

After the vehicle is fully built, a full technical review would be performed to check the rules compliance of the monocoque. All important and governing chassis rules as of Winter 2020 are listed in **Appendix H**. This rules check, in addition to a properly completed SES, is critical to producing a car that will be allowed to run in the Formula SAE Competitions. This full technical inspection consists of many regulations and specifications for other systems and components that use the chassis as a reference, typically by defining the outside of the chassis as the “primary structure” and restricting the position of certain vital or sensitive components to be entirely inside this structure. While it is outside the scope of this senior project to generate solutions for components that may not pass their specific rules, it does fall within the monocoque team’s responsibility to advise on potential modifications or packaging changes that may be required to resolve a rules non-compliance issue. Examples of this include making sure that the fuel tank is fully enclosed within the “primary structure” and shielded from rear and side impacts as well as ensuring the proper clearance between the front bulkhead and anti-intrusion plate and the control pedals.

Project Management

At the beginning of this project, specific roles and responsibilities were developed to aid in the success of this project. These also helped the team complete work in a timely manner. As mentioned in the Objectives portion of this report, the MCD team followed the CPFSAE design season timeline. Also included in this section is a summary of the costs incurred by the team for the duration of the project.

Roles and Responsibilities

Each team member has been assigned a role in managing the team's progress. This division of labor was used to ensure all project requirements and deadlines were met in a timely manner. In addition to the responsibilities outlined in **Table 15**, members were also responsible for a specific scope when designing the chassis. These subsystems encompassed the majority of that member's work, but members were expected to help out wherever needed.

Table 15: Team Roles

Team Member	Role	Responsibilities	Subsystem
KC Egger	Communications Officer	*See note 1 below*	Analysis/Geometry
Brian Ford	Scribe	*See note 2 below*	Manufacturing
Kyle Nagao	Planning and Operations	*See note 3 below*	Structural Equivalency/Testing
Neal Sharma	Treasurer	*See note 4 below*	Structural Equivalency/Testing
Donovan Zusalim	Secretary	*See note 5 below*	Geometry/Manufacturing

Note 1:

- Main point of communication with sponsor and CPFSAE team
- Facilitate meetings with relevant CPFSAE team leads

Note 2:

- Maintain information repository for team (e.g. team binder, Google Docs site)
- Record meeting minutes
- Take pictures of manufacturing and testing

Note 3:

- Maintain group focus and is responsible for guiding de-railed meetings
- Maintain group's progress towards goals

Note 4:

- Maintain team's food budget
- Maintain team's materials budget

Note 5:

- Conduct and lead team meetings
- Organize meeting minutes and estimate meeting duration

Safety, Repair, and Maintenance

Since Formula SAE race cars are open-top and student-built, safety is a nontrivial issue. Fortunately, the competition is regulated by strict rules that set safety standards for all the cars. In addition to having SES for monocoques, the Formula SAE rulebook includes other precautionary requirements such as accounting for heat-transfer between the firewall and cockpit, covering up sharp objects in the cockpit, and ensuring the roll hoop envelope safely covers all drivers. Because of this, Formula SAE-related injuries are uncommon. Potential failures that can result in injury are listed in **Appendices I** and **J**, which are the Design Hazard Checklist and Failure Modes and Effects Analysis, respectively.

However, the manufacturing processes can be dangerous to those who are untrained. All of the labs on campus, including the Hangar, Mustang ’60, and Composites lab, have strict guidelines that students agree to follow when they are working on the premises. The composites lab guidelines ensured that only certified individuals can operate the oven and testing equipment.

The CPFSAE team will be responsible for any repairs and maintenance required for operation of the vehicle, including the chassis. However, the MCD team will assist them wherever possible. In the past, chassis-specific repairs have included fixing delamination, insert failures, and mis-drilled holes. Common maintenance items include ensuring the chassis is detailed before public events and cleaning the cockpit.

Cost Summary

The total documented cost of the project was $2208.40. This number includes the total amount officially spent by the CPFSAE team and the members of this project. However, this number is not entirely accurate due to undocumented purchases of small or inexpensive items such as sandpaper or tongue depressors that were not worth submitting a reimbursement for. It is estimated that these items total no more than $300. This number also does not include the total worth of the goods and services donated to the team from our various industry sponsors. Even considering the cost of undocumented items, the total cost of this project is still less than the $2500 budget requirement previously specified. A detailed cost breakdown is included in **Appendix F** of this report. Many of the consumables used to do the layup such as peel ply and breather were purchased using the Materials subsystem budget and not the Chassis subsystem budget, but they are nevertheless included in **Appendix F** for reference as a no-cost item.

Conclusions and Recommendations

By the closure of the Cal Poly Campus due to the outbreak of COVID-19 on March 20th, 2020 two chassis were delivered to the CPFSAE team. Of the two chassis, one had already completed post-processing and was in the process of being painted, shown in **Figure 186**, and the other had just started post-processing. A render of the final, completed CP20C vehicle is included in **Figure 187**.

Figure 186. The combustion car chassis being painted before campus closure.

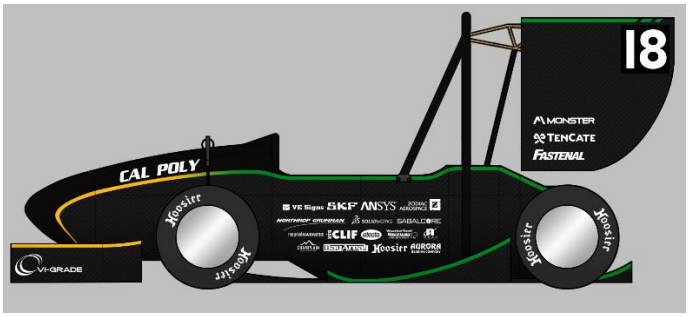

Figure 187. Render of intended final chassis with livery.

In April, SAE International made the decision to hold a virtual Formula SAE design competition in place of Formula SAE California 2020, meaning that no cars would compete dynamically in the 2019-2020 race season. Though most designs were unvalidated, CPFSAE still competed in the virtual design event and received positive feedback for the chassis design and analysis. The CPFSAE team maintains all records of the design event feedback.

As previously mentioned, no physical design validation tests besides weighing the unpainted chassis could be performed due to COVID-19. However, certain chassis specifications were measurable in CAD, and

others were determined from documentation kept by the MCD team. All design specifications that could be measured are summarized in **Table 16**.

Table 16: Achieved Chassis Specifications

Spec #	Design Parameter	Target	Tolerance	Achieved
1	Torsional Stiffness	1700 ft-lbf/deg	+/- 200 ft-lb/deg	Unknown*
2	Weight	45 lb	+/- 5 lb	41.4 lb**
3	Rear Packaging	3 ft^3	+/- 0.5 ft^3	3.62 ft^3
4	Camber Compliance	0.4 deg/g	+/- 0.05 deg/g	Unknown*
5	Toe Compliance	0.02 deg/g	+/- 0.005 deg/g	Unknown*
6	Material Cost	$2500	Max	$2208
7	Manufacturing Time	1000 man-hours	+/- 200 man-hrs	1900 man-hours***
8	Rules-Compliant	Pass	N/A	Unknown*

*Not validated due to COVID-19 pandemic **Weighed before painting ***Estimated

Future Improvements

Though this project was mostly successful, smaller failures along the way took considerable time and energy to overcome. To aid the future design, analysis, and manufacturing of future chassis, the MCD team has compiled the key takeaways and areas of improvement for this project.

In terms of design, four piece modular molds were a successful concept and should be implemented for ease of redesign in the future. Future iterations should always be kept in mind when designing global geometry since poor design decisions will most likely carry over for several years, such as the 2017 rear rocker flats. For suspension mounting locations, boss inserts should be designed and used so that chassis geometry can change each year to meet kinematic point locations. In addition, all surfaces should be made planar so that simple mounting schemes can be employed by other subsystems. Specific to CAD structure, mold and plugs should be created as configurations under original chassis model to allow for easy geometry updates. Furthermore, thorough model verification should be employed to identify and remove artifacts like knife-edges and discontinuities as these will cause errors when attempting to build the feature tree.

For analysis, all models need to be correlated to test data to produce accurate performance predictions for future designs. Specifically, all material properties must be correlated to test data. The 3-point bend model could be modeled with a set of nonlinear load functions instead of a physical the load applicator body, as that will simplify the model and eliminate any solver convergence issues. Furthermore, if test data does not correlate to the 3-point bend model, the cells could be modeled using shell elements to capture local deformation. With respect to the hardpoint sizing model, the FEM should be altered to include structural adhesive, which is an important member in the load path from suspension links to global chassis laminate. For the torsional stiffness model, the suspension mounts should be modeled for additional fidelity along

with their corresponding joint stiffnesses. All cutouts should be included, and the chassis edges should be constrained to simulate edge closeouts.

Despite the usefulness of finite element modeling, the use of basic spreadsheet models should still be used to predict panel failure modes, specifically based on the ESA handbook ([10]), as this can drive a lot of preliminary design decisions. When checking panel performance in SES, all sections should be filled out to ensure all rules are passed. The SES test rig should also be manufactured with attention to detail to ensure that the load applicator is perfectly square to the panel edges.

In terms of manufacturing, if new plugs are made, foam boards should be glued in small batches with more than enough clamps/weights used for each board. Copious amounts of gorilla glue should be used to avoid delamination. Once the plugs are machined, they should be lightly sanded to avoid sanding through primer. During the mold layup process, surface coat should be applied before inserting drill bushings onto the male pins, so they are covered in surface coat and do not become a mold surface. Furthermore, special care should be taken to the laminate surrounding each bushing. Each bushing should have extra material such as additional plies or chopped fiber to ensure sufficient bond between the bushing and the laminate. This will prevent bushings from falling out during use. Surface coat should be mixed slowly and painted onto the plug using sturdy brushes, applied in thin layers (0.030” thick). Once the surface coat is applied, the surface should be inspected for air bubbles, as those need to be filled or removed to prevent any blemishes on the surface. To prevent flange delamination, the first ply on the flange should extend 3” from the flange boundary so it can be used as a closeout. Film adhesive should be utilized for bonding core despite the initial room temperature cure. Since the molds are be post-cured in the oven, the film adhesive will undergo its typical cure cycle, thus will function correctly as a bond from core to facesheet.

During the chassis layup, the outer skin should be laid up with the molds in four separate quarters for ease of accessibility and good compaction during debulking stages. The front bulkhead should also be laid up once the molds are mated since it has a significant number of plies and can be difficult to interweave if laid up while the molds are separated. In addition, FEP should be used to separate plies for interweaving when mating the molds together. Separate carbon ply templates should be designed for each section such that the plies have different overlapping locations across seams to prevent thick stack-ups in one area. All plies and core pieces should be cut beforehand to minimize the actual layup time, as this preparation will streamline the process. Film adhesive should never be the exposed surface when debulking as that will reduce the adhesion of the material, making the core extremely difficult to lay up.

To release the monocoque once it is cured, inflatable bladders and plastic wedges should be used to evenly apply a separating force while releasing CFRP structures without bending fragile sections. Releasing the monocoque should be done with a lot of care, as too much applied force can damage the molds or the part. If the releasing process is completed over multiple days, wedges should always be removed to prevent permanent failure in the part or mold. Wedges should never be placed close to corners when initially releasing the part, as they will get stuck and damage the mold or part. If the molds are damaged during monocoque removal, voids can be filled using PTM&W Poly Filler HT or a similar product in favor of its quick cure time and easy sanding. Surface coat should not be used to fill voids as it is too durable and can bubble.

If you, the reader, intend to produce a new chassis, please see our Statement of Disclaimer. From our team to yours, we wish you luck and forethought to thwart the issues that we saw during our chassis production run. Thank you for reading.

References

[1] Eimon, F., et. al. “Carbon Fiber Monocoque Chassis Platform for Formula SAE and Formula SAE Electric Race Cars” 2017.

[2] “HexWeb™ Honeycomb Sandwich Design Technology” Hexcel Composites, 2000. Available: https://www.hexcel.com/user_area/content_media/raw/Honeycomb_Sandwich_Design_Technology.pdf

[3] Hagan, M., et. al. “Formula SAE Hybrid Carbon Fiber Monocoque/Steel Tube Frame Chassis” 2014.

[4] Brooks, R., et. al. “Frame Engineering Associates Cal Poly SAE Formula Electric Chassis” 2015.

[5] Savage, G. “Formula 1 Composites Engineering” *Engineering Failure Analysis*, vol. 17, no. 1, 2010, p. 92-115. Elsevier Ltd.

[6] Shu-yi, Pang et al. “Research of Chassis Torsional Stiffness on Vehicle Handling Performance.” 2010 WASE International Conference on Information Engineering 3 (2010): 253-256.

[7] “Formula SAE Rules 2019” SAE International, 2019. Available: https://www.fsaeonline.com/cdsweb/gen/DownloadDocument.aspx?DocumentID=64b861c2-980a-40fc-aa88-6a80c43a8540

[8] “The basics of bonded sandwich construction” Hexcel Composites, 1987. Available: https://engineering.purdue.edu/AAE450s/structures/sandwichstructure.pdf

[9] Sun, C.T. et al. “Comparative Evaluation of Failure Analysis Methods for Composite Laminates.” 1996.

[10] “Insert Design Handbook.” ESA PSS-03-1202 Issue 1. June 1987.

[11] Budynas, Richard G, J K. Nisbett, and Joseph E. Shigley. *Shigley's Mechanical Engineering Design.* New York: McGraw-Hill, 2011.

[12] Deng, R., et. al. “Chassis Torsional Stiffness Jig” 2018.

Appendix A: Chassis Architecture Decision Matrix

Decision Matrix		AF Steel Spaceframe (Control)		SES Steel Spaceframe		Aluminum Spaceframe		Hybrid-Partial 'Coque		Full Monocoque Mold		Full Monocoque Cut and Fold	
	Weight	Unweighted	Weighted	Unweighted	Weighted	Unweighted	Weighted	Unweighted	Weighted	Unweighted	Weighted	Unweighted	Weighted
Weight	7	0	0	-1	-7	1	7	0	0	1	7	1	7
Stiffness	6	0	0	0	0	0	0	1	6	1	6	1	6
Manufacturing Time	9	0	0	0	0	-1	-9	-1	-9	0	0	1	9
C-car Accessibility/Packaging	8	0	0	0	0	0	0	0	0	-1	-8	-1	-8
E-car Accessibility/Packaging	8	0	0	0	0	0	0	0	0	1	8	1	8
Ergonomics/Driver Comfort	5	0	0	0	0	0	0	-1	-5	-1	-5	-1	-5
FSAE Rule Adherance/Material Testing	4	0	0	1	4	0	0	1	4	1	4	1	4
Cost to Team	3	0	0	0	0	-1	-3	0	0	1	3	-1	-3
Adaptability (Future Years)	7	0	0	0	0	0	0	-1	-7	-1	-7	-1	-7
Aesthetics	2	0	0	0	0	0	0	1	2	1	2	-1	-2
Above and Beyond Safety	1	0	0	0	0	0	0	1	1	1	1	1	1
			0		**-3**		**-5**		**-8**		**11**		**10**

Appendix B: House of Quality

Correlations	
Positive	+
Negative	−
No Correlation	

Relationships	
Strong	●
Moderate	○
Weak	▽

Direction of Improvement	
Maximize	▲
Target	◇
Minimize	▼

									Column #	1	2	3	4	5	6	7	8	9	10						
	WHO: Customers								Direction of Improvement	▲	▼	▼	▼	▼	◇	◇	◇	▲	◇	NOW: Current Product Assesment - Customer Requirements					
Row #	Weight Chart	Relative Weight	Customer 1	Customer 2	Customer 3	Customer 4	Customer 5	Maximum Relationship	HOW: Engineering Specifications / WHAT: Customer Requirements (explicit & implicit)	Torsional Stiffness [ft-lb/deg]	Weight [lb]	Compliance [in/g]	Time [man-hr]	Cost [USD]	[Pass/Fail]	[Pass/Fail]	[Pass/Fail]	Volume [ft^3]]	[Pass/Fail]	Our Current Product (CP17)	Competitor #1: *(Ecurie Aix)*	Competitor #2: *(USNA)*	Competitor #3: *(CP16)*	Competitor #4: (UW)	Row #
1		17%	10	9	9	10	9	9	Increased Torsional Stiffness	●	○	○	▽							1	5	3	2	3	1
2		18%	9	10	10	9	10	9	Decreased Weight	○	●									3	5	5	4	4	2
3		10%	8	4	3	5	8	9	Localized Suspension Stiffness	○	○	●	▽							1	4	2	2	3	3
4		13%	5	8	8	6	7	9	Decrease Manufacturing Time				●		▽					2	5	4	3	3	4
5		3%	3	1	1	1	1	9	Lower Material Cost					●						4	2	5	4	3	5
6		10%	4	7	6	4	6	9	S.E.S.		▽		○		●					4	5	4	4	5	6
7		5%	1	5	4	3	2	9	Template							●			○	4	5	5	5	5	7
8		5%	2	2	5	2	3	9	Safety						○		●			5	5	3	3	5	8
9		11%	7	6	7	8	5	9	Rear Packaging	▽	▽							●		2	3	3	5	4	9
10		7%	6	3	2	7	4	9	Ergonomics (95% Male, 5% Female)		▽								●	2	4	3	2	3	10

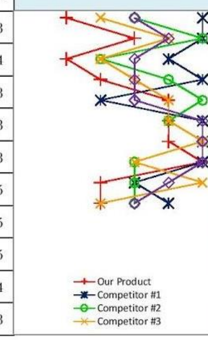

	1	2	3	4	5	6	7	8	9	10
HOW MUCH: Target	1700 ft-lb/deg	45 lb	0.004 in/g	1000 man-hours	$3,000	Pass	Pass	Pass	13 ft^3	Pass
Max Relationship	9	9	9	9	9	9	9	9	9	9
Technical Importance Rating	247.27	270	144.55	173.18	24.545	123.18	49.091	49.091	102.27	77.727
Relative Weight	20%	21%	11%	14%	2%	10%	4%	4%	8%	6%
Weight Chart										
Current Product Assesment - Engineering Specifications										
Our Product	1	3	1	2	4	4	4	5	2	2
Ecurie AIX	5	5	4	5	2	5	5	5	3	4
USNA	3	5	2	4	5	4	5	3	3	3
CP16	2	4	2	3	4	4	5	3	5	2
UW	3	4	3	3	3	5	5	5	4	3

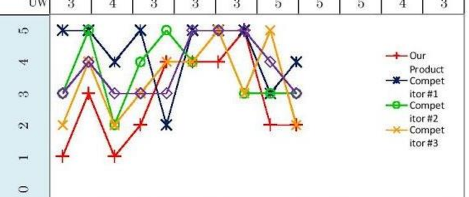

Column #	1	2	3	4	5	6	7	8	9	10

Appendix C: Material Technical Data Sheet Links

HexPly® 8552, Hexcel Corporation, 2020. [Online]. Available: https://www.hexcel.com/user_area/content_media/raw/HexPly_8552_us_DataSheet.pdf

Loctite® Frekote® B-15™, Henkel Corporation, 2013. [Online]. Available: http://www.aero-consultants.ch/view/data/3285/Produkte/Weitere%20Produkte/FREK%20B15-EN.pdf

Loctite® Frekote® 710-LV™, Henkel Corporation, 2015. [Online]. Available: https://tdsna.henkel.com/americas/na/adhesives/hnauttds.nsf/web/F1CAF99ADC9BC54F852574180042917E/$File/FREK710-LV-EN.pdf

PT1995 Graphite Filled High Temperature Epoxy Surface Coat, PTM&W Industries, Inc., 2010. [Online]. Available: https://www.ptm-w.com/technical-library/product-bulletins/Epoxy%20Tooling%20Materials%20Bulletins/PT1995%20Bulletin%2017Nov10.pdf

PT2520 Unfilled High Temperature Epoxy Laminating Resin, PTM&W Industries, Inc., 2010. [Online]. Available: https://www.ptm-w.com/technical-library/product-bulletins/Epoxy%20Tooling%20Materials%20Bulletins/PT2520%20Bulletin%2009Dec10.pdf

Tenax® Filament Yarn, version 27, Teijin Carbon Europe, 2018. [Online]. Available: https://www.teijincarbon.com/fileadmin/PDF/Datenbl%C3%A4tter_en/Filament-Product_programm__EU__v27_2018-06-27_EN.pdf

Appendix D: Local Failure Modes Spreadsheet

		Description	Thickness	Unit	E_1	E_2	v_12	v_23							
	Carbon	TC250/M46J	0.006	in	2.88E+10	7.86E+08	0.2257	0.87							
		TC275/HTS40	0.008	in											
		TC275/T700	0.006	in											
						compression			strong		weak		trans		
		Description	Thickess	cell size	density	strength	modulus	crush stren	strength	G ksi	strength	G ksi	G psi	E 1	E 2
		5052 3/16 3.1	0.5	3/16	3.1	410	97	170	265	45	150	20	4.46	99	44
		5052 3/16 3.1 (Tested)	0.5	3/16	3.1	410	97	170	1.45	44961	0.9	22945	333.59	46	89
		Location	Ply 1	Ply 2	Ply 3	Ply 4									
	Layup	Top	HTS40	M46J	M46J	HTS40									
		Bottom	HTS40	HTS40											
		Parameter	Value	Unit											
		Span, L	15.748	in	15.758 in is 400mm										
		Width, b	12	in	Max panel width according to SES is 500mm, or 19.66 in										
		Skin Thickness Top, t_f1	0.056	in											
	Lengths	Skin Thickness Bottom, t_f2	0.056	in											
		Core Thickness, t_c	0.7	in											
		Cell Size, S	0.1875	in											
		Total Thickness	0.812												
		Centroid Distance, h	0.406	in											
		Facing Poisson's Ratio, mu	0.2257	-											
		Lambda	0.9490595	-											
		Bending Deflection Constant, Kb	0.02083	-											
		Shear Deflection Constant, Ks	0.25	-											
		Moment of Inertia, I	0.1107697												
		Core Shear Modulus, G_c	4.50E+04	psi											
		Core Compression Modulus, E_c	9.70E+04	psi											
		Facing Modulus Top, E_f	2.50E+06	psi											
		Facing Modulus Bottom, E_f	1.05E+06	psi											
		Panel Modulus, E1	2.35E+06	psi											
		Panel Stiffness, D	8.37E+06												
		Total Load, P	1200	lb											
		Max Shear, Vmax	600	lbs											
		Max Moment, Mmax	4724.4	in-lbs											
		Facing Yielding	6597.4665	psi											
		FS, Facing Yielding		-											
		Core Shear Stress	46.921276	psi											
		FS, Core Shear Stress	5.6477577												
		Beam Deflection	1.78E-01	inch											
		Facing Dimpling, Top	2.88E+06	psi											
		FS, Facing Dimpling													
		Facing Wrinkling, Top	1.14E+05	psi											
		FS, Wrinkling, Top													
		Beam Deflection	3.32E-02												

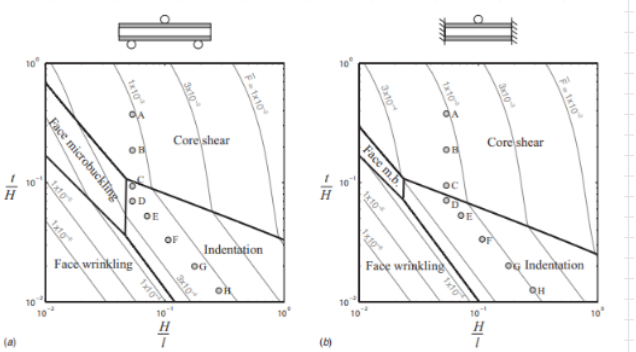

Fig. 7 Collapse mechanism maps for the (a) simply supported and (b) clamped sandwich beams with a square honeycomb core of relative density $\bar{\rho}$=0.1. The beams have n=5 walls across the width b of the beams. The geometries tested in this study are marked on the map along with contours of the nondimensional collapse load $\bar{F}$.

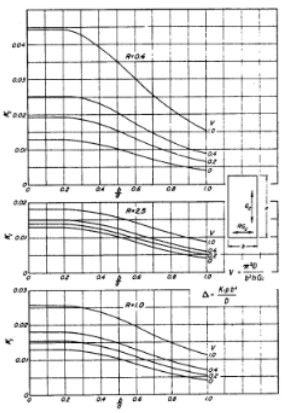

Figure 8 -- K_1 for determining maximum deflection, Δ, of flat rectangular sandwich panels a > b

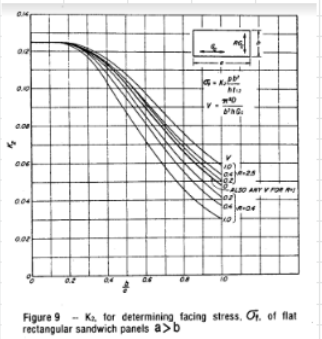

Figure 9 -- K_2 for determining facing stress, σ_f, of flat rectangular sandwich panels a > b

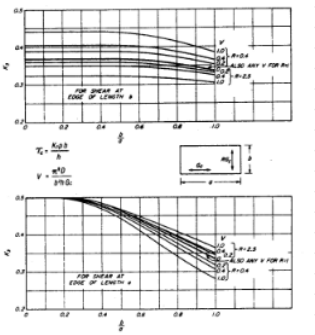

Figure 10 -- K_3 for determining core shear stress, τ_c, for flat rectangular sandwich panels a > b

Appendix E: Chassis Weight Calculator

Material	HTS40/TC275-1 Cloth	AS4C/TC250 Cloth	M46J/TC250 Uni
Average Ply Thickness [in]	0.01	0.017	0.012
Ply Area Weight [lb/in2]	0.00049	0.00092	0.00048
Ply Area Weight [gsm]	346	644	334

Material	Area Weight [lb/in^2]	Area Weight [lb/ft^2]
HTS40/TC275-1 Cloth	0.00064	0.09260
AS4C/TC250 Cloth	0.00108	0.15559
T700 Uni	0.00023	0.03326
NB102 Film Adhesive	0.00021	0.03024
0.7 thick 3.1 honeycomb	0.00126	0.18144
0.5 thick 3.1 honeycomb	0.00090	0.12960
HD 0.5" 4.4 cell alum core	0.00127	0.18333
0.7 thick F80 4.3 flexcore	0.00174	0.25056
0.5 thick F80 4.3 flexcore	0.00124	0.17856
.5 Nomex core	0.00052	0.07488

	Plies per Layup						
	SIS Side	SIS Floor	FBHS	General	FBH	Upper Harness	Lower Harness
HTS40/TC275-1 Cloth	7	7	4	4	20	7	
AS4C/TC250 Cloth	0	0	0	0	0	0	
M46J/TC250 Uni	4	4	2	1	9	2	
NB102 Film Adhesive	2	2	2	2	2	2	
0.7 thick 3.1 honeycomb	0	1	0	0	0	0	
0.5 thick 3.1 honeycomb	1	0	0	1	1	0	
HD 0.5" 4.4 cell alum core	0	0	1	0	0	0	
0.7 thick F80 4.3 flexcore	0	0	0	0	0	1	
0.5 thick F80 4.3 flexcore	0	0	0	0	0	0	
.5 Nomex core	0	0	0	0	1	0	
Total lb/ft^2	0.97135	1.02319	0.68075	0.59375	2.41638	1.02578	0.00000

Laminate	Surface Area ft^2	Total Weight lb
SIS side	8.496	8.252811486
SIS floor	3.314	3.390860197
FBHS	12.615	8.587416128
General	9.903	5.882909401
Front Bulkhead	1.204	2.909325565
Upper Harness	1.854	1.696647689
Lower Harness		
Total	37.190625	30.71977047
all measurements taken from outside face		
Ply Overlap Factor	1.2	
TOTAL ESTIMATE	43.63 lb	

Core Splice	
Weight Per Sheet [g]	191
Approx # of Sheets used	5
Splice Weight [g]	955
Splice Weight [lb]	**2.11**

Closeouts	
Length [in]	226.035
Plies	2.000
Width [in]	3.000
Area [in^2]	1356.2
Weight [lb]	**1.465**

Harness Hardpoints	
Area [ft^2]	0.196349540
Plies	8
Number	4
Weight [lb]	**0.5818**

Sus Hardpoints	
Area [in^2]	0.196349540
Plies	8
Number	8
Weight [lb]	**1.1637**

Powrtrain Hardpoints	
Area [in^2]	0.196349540
Plies	8
Number	2
Weight [lb]	**0.2909**

Hoop Hardpoints	
Area [in^2]	0.196349540
Plies	8
Number	8
Weight [lb]	**1.1637**

Appendix F: Expenses

Category	Product	Description	Supplier	Amount	QTY	Unit Price	Tax	Shipping	Subtotal	Discount (%)	Total	COMMENTS
Plugs	Tooling Foam - 20lb/ft^3 density	Foam to machine plug	Hangar	96" x 48" x 48"	1	$0.00	$0.00	$0.00	$0.00	100%	$0.00	Donated by General Polymer Solutions
	Alexit 343-55 Primer	Guide Coat	H20	As needed	1	$0.00	$0.00	$0.00	$0.00	100%	$0.00	Donated by Safran
	Chemlease MPP2180	Plug primer	Chemlease	As needed	1	$0.00	$0.00	$0.00	$0.00	100%	$0.00	Donated by Safran
	Axon APF-7	Polyester filler	Axon	As needed	1	$0.00	$0.00	$0.00	$0.00	100%	$0.00	Donated by Safran
	Bondo	Fix molds	Amazon	1 gal container	1	$0.00	$0.00	$0.00	$0.00	100%	$0.00	Used hangar/shed stock
	Gorilla Glue	Bond Foam	Home Depot	8 oz	30	$9.99	$1.50	$0.00	$299.70	0%	$344.66	Q'ty is +- a few bottles
Female Molds	Frekote B15	Final mold sealer	Henkel	2 gal container	1	$0.00	$0.00	$0.00	$0.00	100%	$0.00	Donated by Henkel
	Frekote 710LV Mold release	Mold release	Henkel	10 pack	10	$0.00	$0.00	$0.00	$0.00	100%	$0.00	Donated by Henkel
	Newplast Plasticine	For filling flange radius	Amazon	23 strips	1	$14.00	$2.10	$0.00	$14.00	0%	$16.10	Purchased by Brian via Amazon
	Vacuum bagging	Vac bagging material	Airtech	Assorted	1	$0.00	$0.00	$0.00	$0.00	100%	$0.00	Used hangar/shed stock/from Composites budget.
	Tacky tape	Seal vac bags	Airtech	Assorted	1	$0.00	$0.00	$0.00	$0.00	100%	$0.00	Used hangar/shed stock/from Composites budget.
	Breather	Breather	Airtech	Assorted	1	$0.00	$0.00	$0.00	$0.00	100%	$0.00	Used hangar/shed stock/from Composites budget.
	12K 2x2 Twill Fabric	Dry cloth for females	Chomorat	1 yard	50	$29.99	$4.50	$50.00	$1,499.50	100%	$0.00	Donated by Chomarat. Exact quantities unknown
	Locating pins and bushings	For bolting molds together	Safran	Assorted	1	$0.00	$0.00	$0.00	$0.00	0%	$0.00	Donated by Safran
	PTM&W 1995 A/B	Surface coat	PTM&W	1 gal pail	2	$186.69	$28.00	$0.00	$373.38	25%	$322.04	Ordering thru Christine
		Hi-temp resin for wet layup	PTM&W	1 gal	2	$129.79	$19.47	$0.00	$259.57	25%	$223.88	Ordering thru Christine
	PTM&W 2520 A/B1	Hi-temp resin for wet layup	PTM&W	5 gal pail	1	$489.16	$73.37	$0.00	$489.16	25%	$421.90	$500 from MESFAC.
	PTM&W 0828	Silicone Release Agent	PTM&W	1 gal	2	$74.36	$11.15	$0.00	$148.72	25%	$128.27	This was the decided upon release agent for the foam plug
	PTM&W Poly Filler HT	High temp bondo	PTM&W	1 quart	2	$18.90	$2.84	$31.00	$100.00	25%	$100.00	For repairing the female molds
	Mold flange washers	1/4" Screw Size, 9/32" ID, 5/8" OD, 0.065" Thick	Amazon	100 pack	2	$1.81	$0.00	$0.00	$3.62	0%	$3.62	Purchased by Don via Amazon
	Mold flange nuts	1/4"-20 Hex Nut	Amazon	100 pack	1	$5.95	$0.00	$0.00	$5.95	0%	$5.95	Purchased by Don via Amazon
	Mold flange bolts	1/4"-20 x 1" Bolt	Amazon	100 pack	1	$9.84	$0.00	$0.00	$9.84	0%	$9.84	Purchased by Don via Amazon
	Plastic sheeting for wet layups	10 ft. x 100 ft. Clear 4 mil Plastic Sheeting	Home Depot	1 roll	1	$65.67	$0.00	$0.00	$65.67	0%	$65.67	Purchased by KC, also includes some Acetone
	Sanding materials	100-1500 grit sandpaper, blocks, discs, etc	Misc	Assorted	1	$350.00	$0.00	$0.00	$350.00	0%	$350.00	Rough estimation, exact quantities unknown
Final Chassis	CR-III 3/16 5056 core	Honeycomb core	Hexcel	4 ft x 8 ft sheet	9	$0.00	$0.00	$0.00	$0.00	100%	$0.00	Donated. Exact quantities unknown
	HTS40/TC-275 3K 2x2 Twill	Prepreg cloth	Tencate	1 roll	6	$0.00	$0.00	$0.00	$0.00	100%	$0.00	Donated. Exact quantities unknown
	M46J/TC250 12K Uni	Prepreg uni	Tencate	1 roll	2	$0.00	$0.00	$0.00	$0.00	100%	$0.00	Donated. Exact quantities unknown
	Syringes	For potting inserts/bushings	Home Depot	1 Syringe	15	$24.77	$0.00	$0.00	$24.77	0%	$24.77	Used approx 15 total. Used hangar/shed stock first.
	CR-III 5052 core	Flexcore core	Hexcel	3 ft x 8 ft sheet	6	$0.00	$0.00	$0.00	$0.00	100%	$0.00	Donated. Exact quantities unknown
	Hysol EA9696 film adhesive	Adhere core to laminate	Henkel	500 ft^2	1	$0.00	$0.00	$0.00	$0.00	100%	$0.00	Donated. Exact quantities unknown
	Core splice	Splice core together	3M	1 Sheet	4	$0.00	$0.00	$0.00	$0.00	100%	$0.00	Used hangar/shed stock/from Composites budget.
	Loctite EA 9396	Potting inserts, repairs	Henkel	1 qt	2	$0.00	$0.00	$0.00	$0.00	100%	$0.00	Donated by Henkel
	Loctite EA 9309	Potting inserts, repairs	Henkel	1 qt	2	$0.00	$0.00	$0.00	$0.00	100%	$0.00	Donated by Henkel
SES	SES Size C Tubes	1" OD x 0.049" Wall x 0.9" ID Mild Steel Round Tube A513-Type 5 DOM	Online Metals	72"	1	$17.65	$2.65	$18.44	$17.65	0%	$38.74	Purchased by Kyle
	SES Size B Tubes	1" OD x 0.065" Wall x 0.87" ID Mild Steel Round Tube A513-Type 5 DOM	Online Metals	72"	1	$23.65	$3.55	$20.65	$23.65	0%	$47.85	Purchased by Kyle
	SES Size C and B Tubes	1.00" x 0.049" x 72" and 1.00" x 0.065" x 72"	Grainger	72"	1	$54.32	$8.15	$23.86	$54.32	0%	$86.33	Purchased by Kyle
	SES Size B Tubes	Unpolished (Mill) 1008-1010 Steel Round Tube, 1" Outer Diameter, 0.065" Wall Thickness, 0.8700" Inner Diameter	Amazon	72"	1	$16.34	$2.45	$0.00	$16.34	0%	$18.79	These are what we ultimately used for SES, were weakest
										Total	$2,208.40	

Appendix G: Manufacturing Drawings

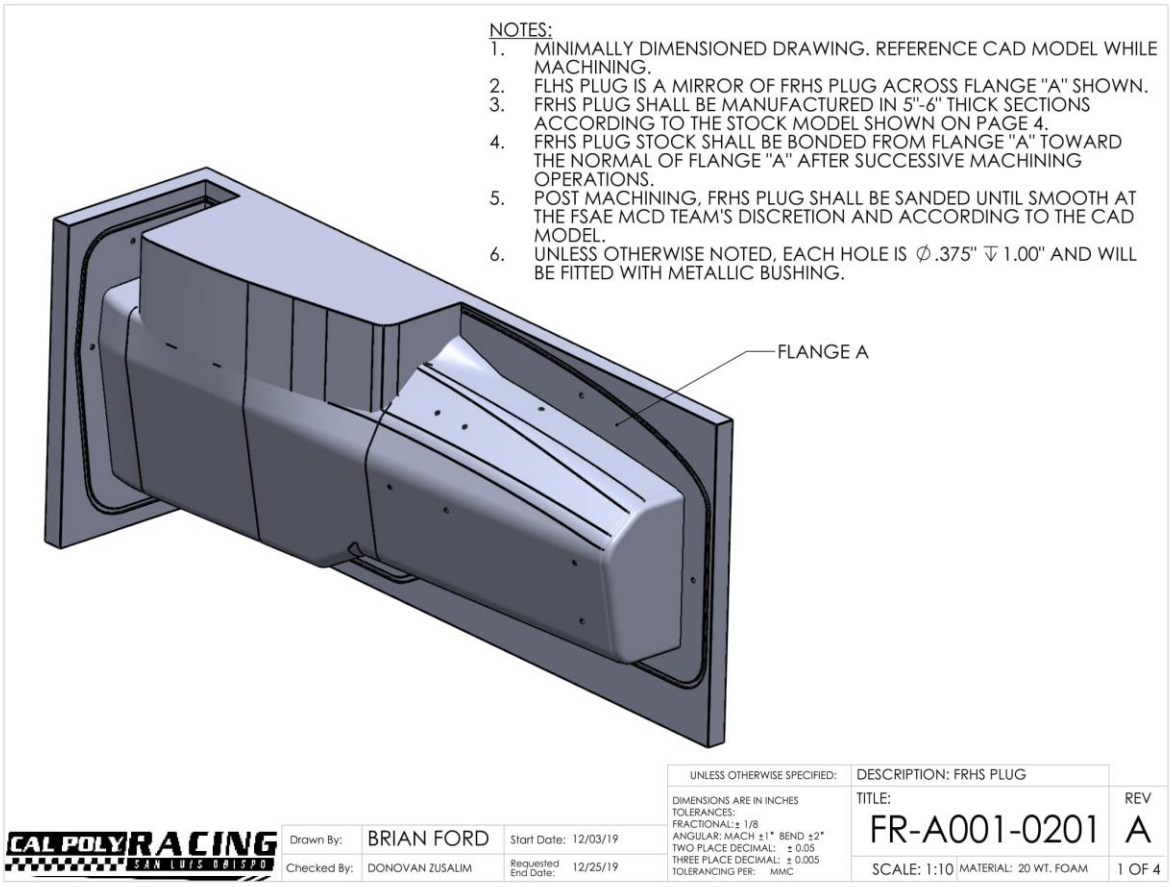

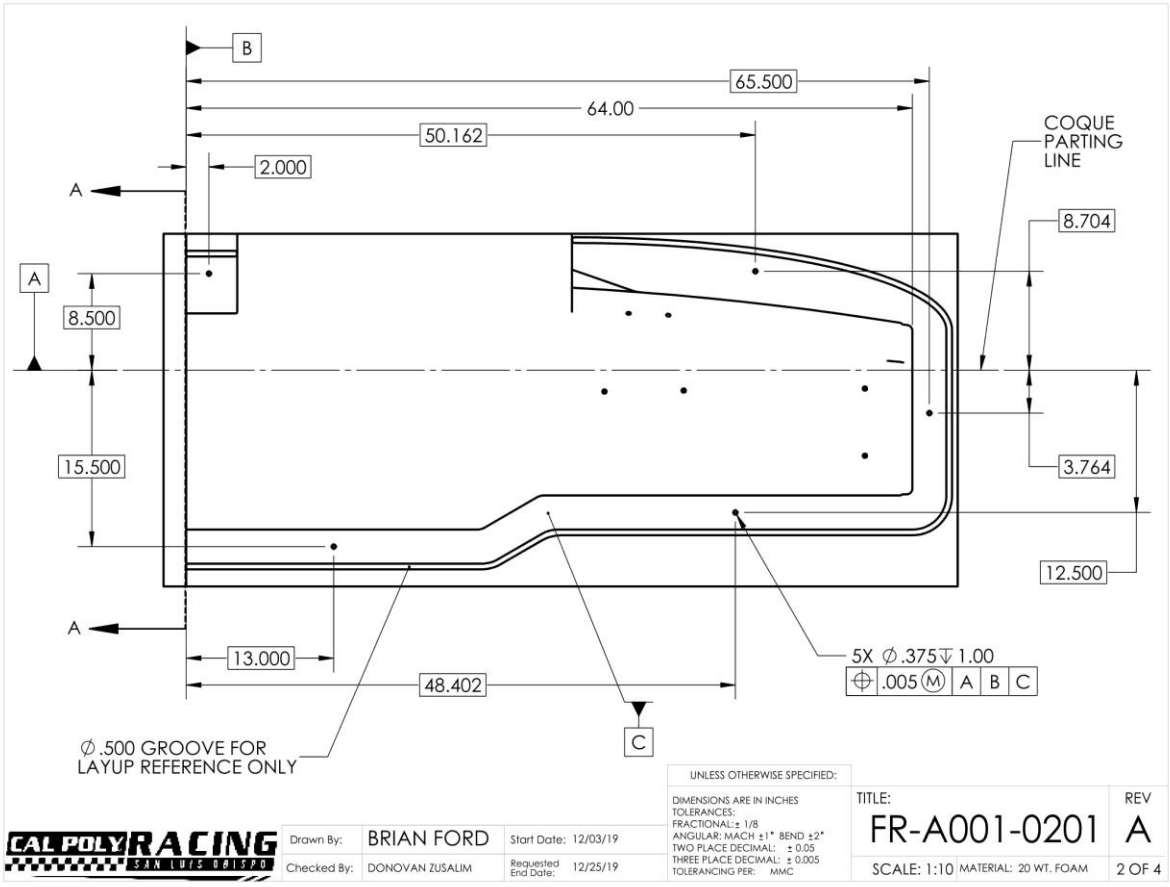

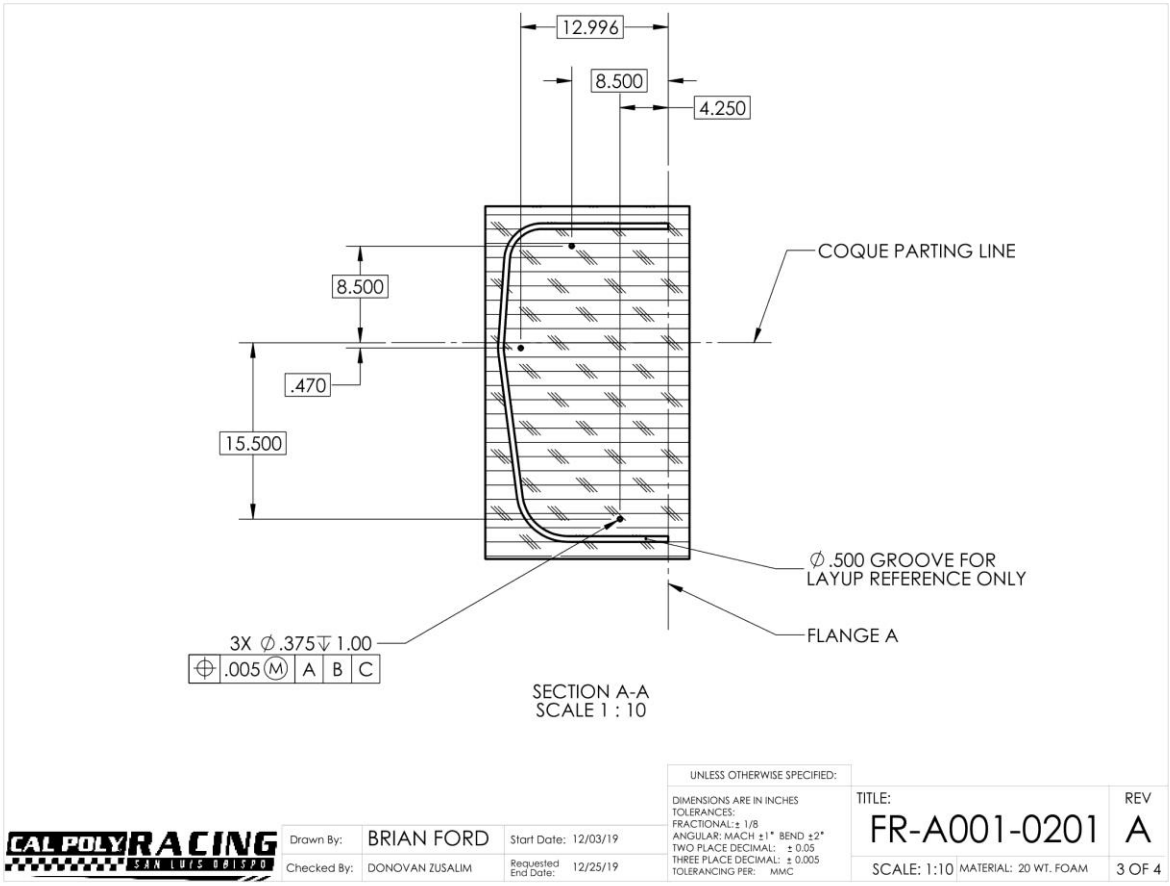

UNLESS OTHERWISE SPECIFIED:

DIMENSIONS ARE IN INCHES
TOLERANCES:
FRACTIONAL: ± 1/8
ANGULAR: MACH ±1° BEND ±2°
TWO PLACE DECIMAL: ± 0.05
THREE PLACE DECIMAL: ± 0.005
TOLERANCING PER: MMC

CAL POLY RACING SAN LUIS OBISPO

Drawn By:	BRIAN FORD	Start Date:	12/03/19
Checked By:	DONOVAN ZUSALIM	Requested End Date:	12/25/19

TITLE: FR-A001-0201

REV: A

SCALE: 1:10 MATERIAL: 20 WT. FOAM 3 OF 4

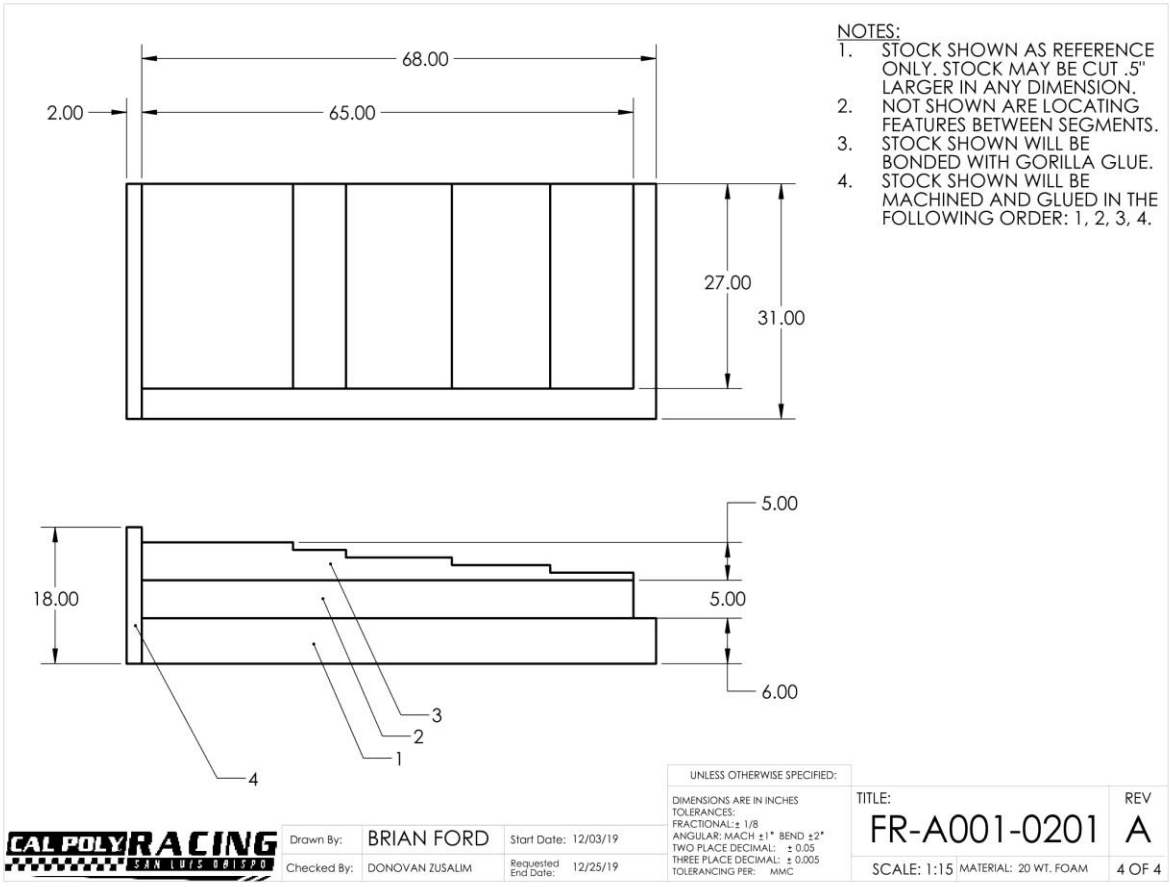

NOTES:
1. STOCK SHOWN AS REFERENCE ONLY. STOCK MAY BE CUT .5" LARGER IN ANY DIMENSION.
2. NOT SHOWN ARE LOCATING FEATURES BETWEEN SEGMENTS.
3. STOCK SHOWN WILL BE BONDED WITH GORILLA GLUE.
4. STOCK SHOWN WILL BE MACHINED AND GLUED IN THE FOLLOWING ORDER: 1, 2, 3, 4.

CAL POLY RACING SAN LUIS OBISPO

Drawn By:	BRIAN FORD	Start Date:	12/03/19
Checked By:	DONOVAN ZUSALIM	Requested End Date:	12/25/19

UNLESS OTHERWISE SPECIFIED:
DIMENSIONS ARE IN INCHES
TOLERANCES:
FRACTIONAL: ± 1/8
ANGULAR: MACH ±1° BEND ±2°
TWO PLACE DECIMAL: ± 0.05
THREE PLACE DECIMAL: ± 0.005
TOLERANCING PER: MMC

TITLE: FR-A001-0201
REV: A
SCALE: 1:15 MATERIAL: 20 WT. FOAM
4 OF 4

NOTES:

1. MINIMALLY DIMENSIONED DRAWING. REFERENCE CAD MODEL WHILE MACHINING.
2. RLHS PLUG IS A MIRROR OF RRHS PLUG ACROSS FLANGE "A" SHOWN.
3. RRHS PLUG SHALL BE MANUFACTURED IN 4"-6" THICK SECTIONS ACCORDING TO THE STOCK MODEL SHOWN ON PAGE 4.
4. RRHS PLUG STOCK SHALL BE BONDED FROM FLANGE "A" TOWARD THE NORMAL OF FLANGE "A" AFTER SUCCESSIVE MACHINING OPERATIONS.
5. POST MACHINING, RRHS PLUG SHALL BE SANDED UNTIL SMOOTH AT THE FSAE MCD TEAM'S DISCRETION AND ACCORDING TO THE CAD MODEL.
6. UNLESS OTHERWISE NOTED, EACH HOLE IS ⌀.375" ↧1.00" AND WILL BE FITTED WITH METALLIC BUSHING.

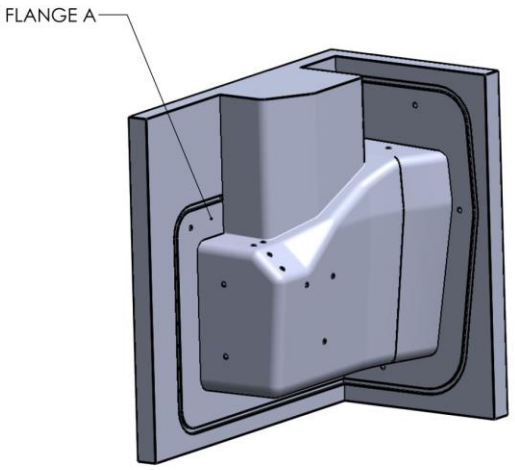

CAL POLY RACING SAN LUIS OBISPO

Drawn By:	BRIAN FORD	Start Date:	12/03/19
Checked By:	DONOVAN ZUSALIM	Requested End Date:	12/25/19

UNLESS OTHERWISE SPECIFIED:
DIMENSIONS ARE IN INCHES
TOLERANCES:
FRACTIONAL: ± 1/8
ANGULAR: MACH ±1° BEND ±2°
TWO PLACE DECIMAL: ± 0.05
THREE PLACE DECIMAL: ± 0.005
TOLERANCING PER: MMC

DESCRIPTION: RRHS PLUG

TITLE: FR-A001-0203

REV: A

SCALE: 1:10 MATERIAL: 20 WT. FOAM

1 OF 4

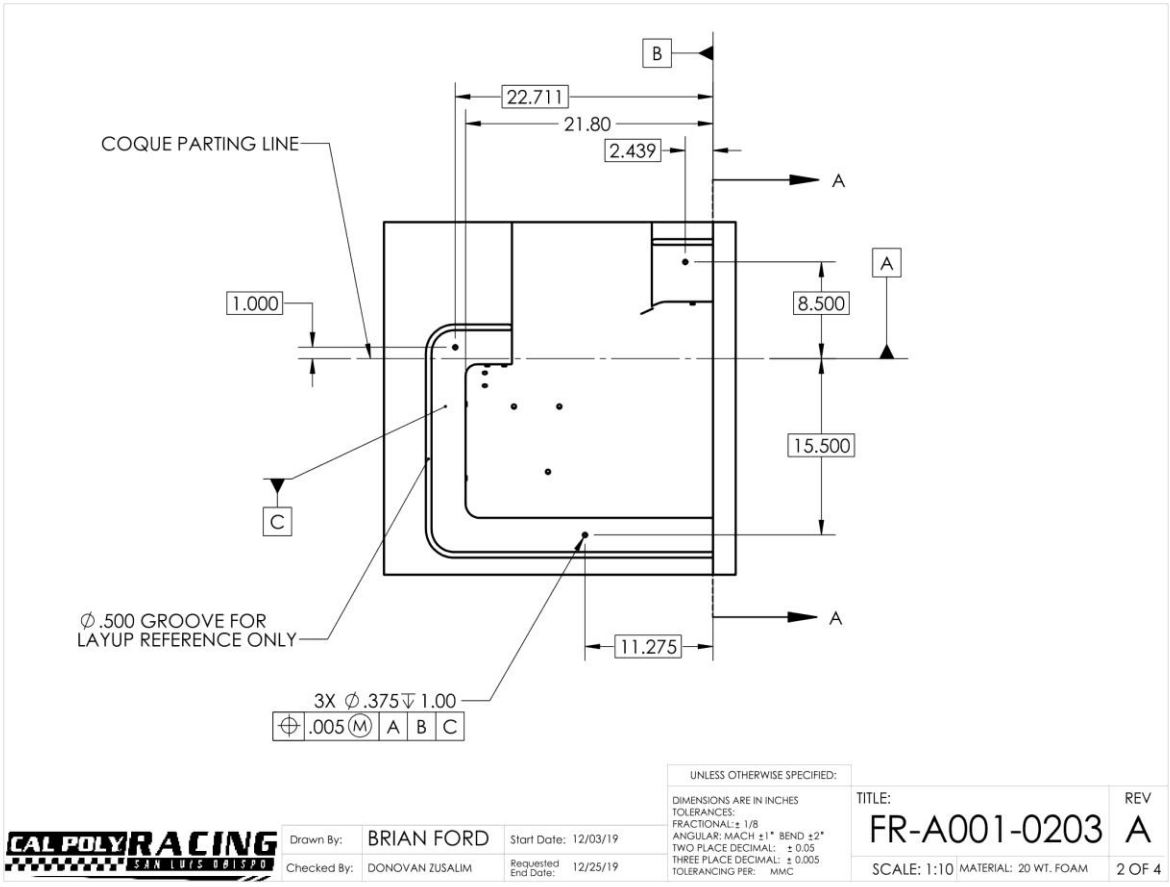

CAL POLY RACING SAN LUIS OBISPO	Drawn By:	BRIAN FORD	Start Date: 12/03/19	UNLESS OTHERWISE SPECIFIED: DIMENSIONS ARE IN INCHES TOLERANCES: FRACTIONAL: ± 1/8 ANGULAR: MACH ±1° BEND ±2° TWO PLACE DECIMAL: ± 0.05 THREE PLACE DECIMAL: ± 0.005 TOLERANCING PER: MMC	TITLE: FR-A001-0203 REV A
	Checked By:	DONOVAN ZUSALIM	Requested End Date: 12/25/19		SCALE: 1:10 MATERIAL: 20 WT. FOAM 2 OF 4

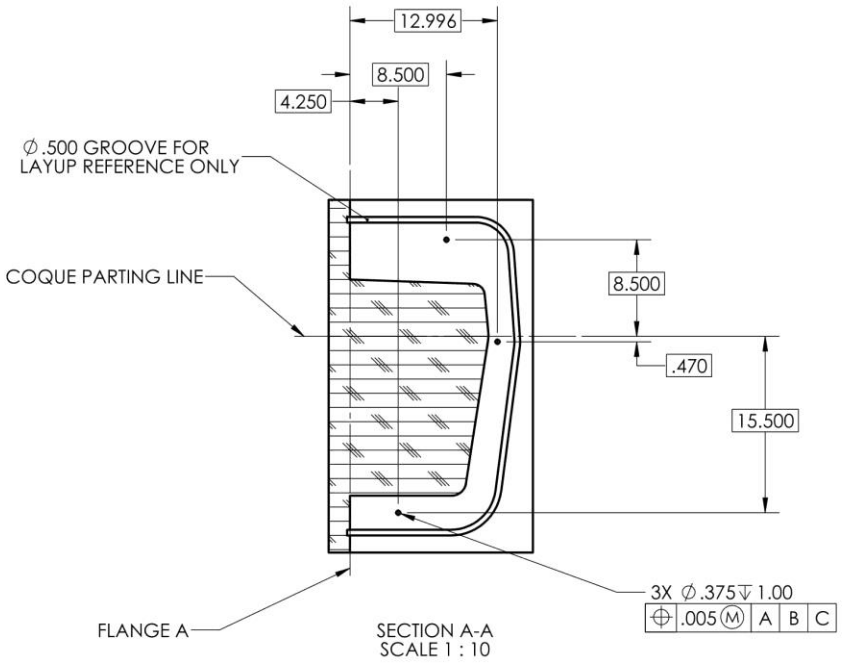

UNLESS OTHERWISE SPECIFIED:

DIMENSIONS ARE IN INCHES
TOLERANCES:
FRACTIONAL: ± 1/8
ANGULAR: MACH ±1° BEND ±2°
TWO PLACE DECIMAL: ± 0.05
THREE PLACE DECIMAL: ± 0.005
TOLERANCING PER: MMC

CAL POLY RACING SAN LUIS OBISPO

Drawn By:	BRIAN FORD	Start Date:	12/03/19
Checked By:	DONOVAN ZUSALIM	Requested End Date:	12/25/19

TITLE: FR-A001-0203 REV A

SCALE: 1:10 MATERIAL: 20 WT. FOAM 3 OF 4

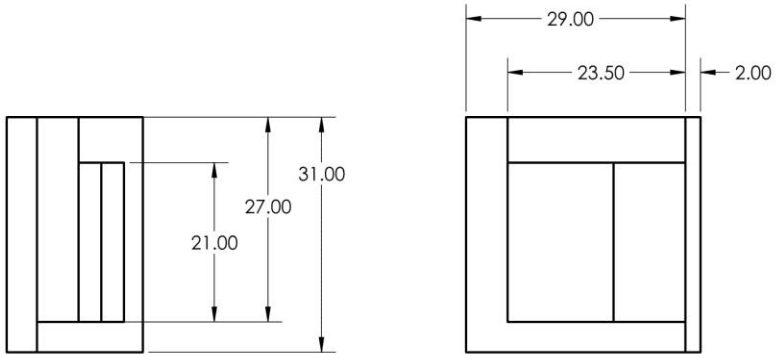

NOTES:
1. STOCK SHOWN AS REFERENCE ONLY. STOCK MAY BE CUT .5" LARGER IN ANY DIMENSION.
2. NOT SHOWN ARE LOCATING FEATURES BETWEEN SEGMENTS.
3. STOCK SHOWN WILL BE BONDED WITH GORILLA GLUE.
4. STOCK SHOWN WILL BE MACHINED AND GLUED IN THE FOLLOWING ORDER: 1, 2, 3, 4.

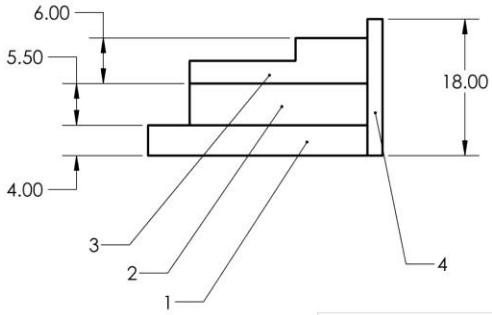

UNLESS OTHERWISE SPECIFIED:

DIMENSIONS ARE IN INCHES
TOLERANCES:
FRACTIONAL: ± 1/8
ANGULAR: MACH ±1° BEND ±2°
TWO PLACE DECIMAL: ± 0.05
THREE PLACE DECIMAL: ± 0.005
TOLERANCING PER: MMC

CAL POLY RACING SAN LUIS OBISPO

Drawn By:	BRIAN FORD	Start Date:	12/03/19
Checked By:	DONOVAN ZUSALIM	Requested End Date:	12/25/19

TITLE: FR-A001-0203

REV: A

SCALE: 1:15 MATERIAL: 20 WT. FOAM 4 OF 4

Appendix H: Design Verification Plan

Tests may be performed in the hangar wearing minimal PPE. Long pants, closed toed shoes, and safety glasses should be worn for all testin engineers, but the driver should wear full driver gear for the "broomstick test." Reference the FSAE 2020 Rules booklet while conducting tests.

I. SES Verification *as governed by the 2020 FSAE SES spreadsheet. To be completed by Dec 13, 2019.*			
	Requirement/Sub-Area	Test	Pass [Y/N]
	Prove that the monocoque is structurally equivalent or greater to a steel tube frame chassis. Each of the following areas shall be tested with a 3 Point Bend (3PB) test, Perimeter Shear (PS) test, or the weak side of a laminate has material properties at least 50% of those in the strong side. The tests are described in detail in the 2020 FSAE rules under: F.4.3.	-	-
	F.7.3. Front Bulkhead	3PB, PS, 50%	
	F.7.4 Front Bulkhead Support		
	F.7.5 Front Hoop Attachment F.7.5.1 The Front Hoop must be mechanically attached to the monocoque and must meet F.7.9.	Visual	
	F.7.6 Side Impact Structure F.7.6.1 Side Impact Zone - the region longitudinally forward of the Main Hoop and aft of the Front Hoop and vertically from 320 mm above the lowest point of the upper surface of the floor to the bottom surface of the floor of the monocoque	Measure height, 3PB, PS, 50%	
	F.7.7 Main Hoop Attachment F.7.7.1 The Main Hoop must be mechanically attached to the monocoque and must meet F.7.9. F.7.7.2 Mounting plates welded to the Roll Hoop must be 2.0 mm minimum thickness steel.	Visual	
	F.7.8 Roll Hoop Bracing Attachment Attachment of tubular Front or Main Hoop Bracing to the monocoque must comply with F. 7.9.		
II. Performance Goals *To be fully tested in February 2020, after manufacturing of the CFRP monocoque.*			
	Goal	Test	Result
	Torsional stiffness of the chassis. Total stiffness goal of 1700 ftlbs/deg.	Chassis torsional stiffness jig used in accordance to the use manual of 2019 senior project: "Torsional Stiffness of a Race Car."	
	Total weight of as manufactured chassis: 45 lb	Weigh chassis using human scales	
	Total weight of finished chassis: 50 lb		
	Servicability. Be able to remove the drivetrain assembly in under 45 minutes.	Time a full dissassembly of the drivetrain on EV and Combustion vehicle.	
III. Chassis Rules *as specified by 2020 FSAE rules booklet. To be completed in April 2020 after manufacturing of the FSAE vehicle.*			
Sub-Area	Requirement	Test	Pass [Y/N]
T.3.1 Cockpit Opening			
	T.3.1.1 The template shown below must fit into the cockpit opening	Use the 2D template according to T.3.1.2	
	T.3.1.2 The template will be held horizontally, parallel to the ground, and inserted vertically from a height above any Primary Structure or bodywork that is between the Front Hoop and the Main Hoop until it: a. Has passed below the top bar of the Side Impact Structure b. Is 350 mm above the ground for monocoque designs		
	T.3.1.3 Fore and aft translation of the template is permitted during insertion.		
	T.3.1.4 During this test: a. The steering wheel, steering column, seat and all padding may be removed. b. The shifter or shift mechanism may not be removed unless it is integral with the steering wheel and is removed with the steering wheel. c. The firewall must not be moved or removed. d. Cables, wires, hoses, tubes, etc. must not impede the template During inspection, the steering column, for practical purposes, will not be removed. The template may be maneuvered around the steering column shaft, but not the steering column supports.		

	F.5.5.3 Roll Hoop and Driver Position When seated normally and restrained by the Driver Restraint System, the helmet of a 95th percentile male (see V.2.1.1) and all of the team's drivers must: a. Be a minimum of 50 mm from the straight line drawn from the top of the Main Hoop to the top of the Front Hoop. b. Be a minimum of 50 mm from the straight line drawn from the top of the Main Hoop to the lower end of the Main Hoop Bracing if the bracing extends rearwards. c. Be no further rearwards than the rear surface of the Main Hoop if the Main Hoop Bracing extends forwards.	Perform broomstick test, where driver helmets must lie at least 50mm from the broomstick connecting the front and rear roll hoops.	
	IN.8.3.1 Inspection Scope The following items may be confirmed during inspection: a. Main hoop outer diameter and thickness where it protrudes above the monocoque b. Main hoop extends to the lowest part of the tub c. Mechanical attachment of main hoop to tub exists and matches the SES, at all points shown on the SES d. Front Hoop is installed, visually or by feel and that the mechanical attachment (if included) agrees with the SES	Visual	
	T.2.9 Roll Bar Padding Any portion of the roll bar, roll bar bracing or frame which might be contacted by the driver's helmet must be covered with a minimum thickness of 12 mm of padding which meets SFI Spec 45.1 or FIA 8857-2001.		
T.3.2 Internal Cross Section			
	T.3.2.1 A free internal cross section to allow the template shown below to pass through must be maintained through the cockpit.	Use the 2D template according to T.3.2.2	
	T.3.2.2 Conduct of the test: a. The template will be held vertically and inserted into the cockpit opening rearward of the rearmost portion of the steering column. b. The template will then be passed horizontally through the cockpit to a point 100 mm rearwards of the face of the rearmost pedal when in the inoperative position		
	T.3.2.3 During this test: a. If the pedals are adjustable, they must be in their most forward position. b. The steering wheel may be removed c. Padding may be removed if it can be easily removed without the use of tools with the driver in the seat d. The seat must remain in the cockpit e. Cables, wires, hoses, tubes, etc. must not impede the template		
T.3.3 Driver's Seat			
	T.3.3.1 The driver's seat must be protected by one of the following: a. In side view, the lowest point of the driver's seat must be no lower than the bottom surface of the lower frame rails b. A longitudinal tube (or tubes) that meets the requirements for Side Impact tubing, passing underneath the lowest point of the seat.	Visual	
	T.3.3.2 When seated in the normal driving position, adequate heat insulation must be provided to ensure that the driver will not contact any metal or other materials which may become heated to a surface temperature above 60°C.		
	T.3.3.3 Insulation may be external to the cockpit or incorporated with the driver's seat or firewall.		
	T.3.3.4 The design must address all three types of heat transfer between the heat source (exhaust pipe, coolant hose/tube) and the panel that the driver could contact (seat or floor): a. Conduction Isolation by one of the following: □ No direct contact between the heat source and the panel □ A heat resistant, conduction isolation material with a minimum thickness of 8 mm between the heat source and the panel. b. Convection Isolation by a minimum air gap of 25 mm between the heat source and the panel c. Radiation Isolation by one of the following: □ A solid metal heat shield with a minimum thickness of 0.4 mm (0.015 in) □ Reflective foil or tape when combined with conduction insulation.		
T.3.4 Floor Closeout			
	T.3.4.1 All vehicles must have a floor closeout to prevent track debris from entering	Visual	
	T.3.4.2 The closeout must extend from the foot area to the firewall		
	T.3.4.3 The panel(s) must be made of a solid, non brittle material.		
	T.3.4.4 If multiple panels are used, gaps between panels must not to exceed 3 mm.		
T.3.5 Firewall			

	T.3.5.1 A firewall must separate the driver compartment from all components of the fuel supply, the engine oil, the liquid cooling systems, any lithium batteries and any high voltage system.		
	T.3.5.2 The firewall must meet the following: a. A non permeable surface made from a rigid, fire resistant material. b. Extend sufficiently far upwards and/or rearwards such that any point less than 100 mm above the bottom of the helmet of the tallest driver must not be in direct line of sight with any part of the fuel system, the cooling system or the engine oil system. c. Seal completely against the passage of fluids (the firewall itself and edges) d. Pass through for wiring, cables, etc. may be used if grommets are used to seal the pass through. e. Seat belts must not pass through the firewall f. Multiple panels may be used to form the firewall but must be sealed at the joints	Visual, have multiple drivers tested and utilize a straight edge to visualize L.O.S. to fuel system	
T.3.6 Tractive System Firewall (EV only)			
	T.3.6.1 A firewall must separate the driver compartment from all tractive system components, including any HV wiring.	Visual	
	T.3.6.5 The firewall must be rigidly mounted.		
	T.3.6.6 Conductive parts (except for the chassis) must not protrude through the firewall or must be properly insulated on the driver side.		
T.3.7 Controls Accessibility			
	All vehicle controls, including the shifter, must be operated from inside the cockpit without any part of the driver, including hands, arms or elbows, being outside the planes of the Side Impact Structure defined in T.2.26 / T.2.34	Visual	
T.3.8 Visibility			
	T.3.8.1 The driver must have adequate visibility to the front and sides of the vehicle	Visual	
	T.3.8.2 When seated in a normal driving position, the driver must have a minimum field of vision of 100° to either side	Use traffic cones to determine driver F.O.V. Verify the F.O.V. using a string and a protractor.	
	T.3.8.3 If mirrors are required to meet this rule, they must remain in place and adjusted to enable the required visibility throughout all dynamic events.	Visual	
T.4.1 Harness – General			
	T.4.1.1 Definitions a. 5 point system – consists of two lap belts, two shoulder straps and one anti submarine strap. b. 6 point system – consists of two lap belts, two shoulder straps and two leg or anti submarine straps. c. 7 point system – consists of two lap belts, two shoulder straps , two leg or anti submarine straps and a negative g or Z belt. d. Upright Driving Position - with a seat back angled at 30° or less from the vertical as measured along the line joining the two 200 mm circles of the template of the 95th percentile male as defined in T.2.10.4 and positioned per T.2.10.5 e. Reclined Driving Position - with a seat back angled at more than 30° from the vertical as measured along the line joining the two 200 mm circles of the template of the 95th percentile male as defined in T.2.10.4 and positioned per T. 2.10.5 f. Chest to groin line - the straight line that in side view follows the line of the shoulder belts from the chest to the release buckle.	-	-
T.4.2 Harness Requirements			
	T.4.2.1 The vehicle must use a 5, 6 or 7 point restraint harness meeting at least one of the following specifications: a. SFI Specification 16.1 b. SFI Specification 16.5 c. FIA specification 8853/98	Visual	
	T.4.2.2 The belts must have the original manufacturers labels showing the specification and expiration date		
	T.4.2.3 The harness must be within the year of expiration shown on the labels. Harnesses expiring on or before Dec 31 of the competition year are permitted.		
	T.4.2.4 The harness must be in new or like new condition, with no signs of wear, cuts, chaffing or other issues.		
	T.4.2.5 Vehicles with a Reclined Driving Position must have: a. A 6 point or 7 point harness b. Anti submarine belts with tilt lock adjusters (“quick adjusters”) OR two sets of anti submarine belts installed.		
	T.4.2.6 All lap belts must incorporate a tilt lock adjuster (“quick adjuster”). Lap belts with “pull-up” adjusters are recommended over “pull-down” adjusters.		

	T.4.2.7 The shoulder harness must be the over the shoulder type. Only separate shoulder straps are permitted. “Y” type shoulder straps are not allowed. The “H” type configuration is allowed.		
	T.4.2.8 All harness hardware must be threaded in accordance with manufacturer’s instructions.		
	T.4.2.9 All harness hardware must be used as received from the manufacturer. No modification (including drilling, cutting, grinding, etc) is permitted.		
T.4.3 Belt, Strap and Harness Installation - General			
	T.4.3.1 The lap belt, shoulder harness and anti submarine strap (s) must be securely mounted to the Primary Structure		
	T.4.3.2 Any guide or support for the belts must meet the minimum requirements of T.2.5 OR T.2.6 OR T.2.7		
	T.4.3.3 The tab or bracket to which any harness is attached must: a. Have a minimum cross sectional area of 60 sq mm of steel to be sheared or failed in tension at any point of the tab b. Be 1.6 mm (0.063 inch) minimum thickness c. Be aligned such that it is not put in bending when the attached part of the harness is put under load. d. Where lap belts and anti submarine belts use the same attachment point, there must be a minimum cross sectional area of 90 sq mm of steel to be sheared or failed in tension at any point of the tab. e. Not cause abrasion to the belt webbing	Visual. Utilize calipers to measure critical dimensions.	
	T.4.3.4 Attachment of tabs or brackets must meet the following: a. Where brackets are fastened to the chassis, no less than two 6 mm or 1/4” minimum diameter Critical Fasteners, see T.10.2 and T.10.3 or stronger must be used to attach the bracket to the chassis. b. Where a single shear tab is welded to the chassis, the tab to tube welding must be on both sides of the base of the tab. Double shear attachments are preferred. Tabs and brackets for double shear mounts should be welded on both sides.		
	T.4.3.5 Harnesses, belts and straps must not pass through a firewall. All harness attachment points must be on the driver’s side of any firewall.		
T.4.4 Lap Belt Mounting			
	T.4.4.1 The lap belts must pass around the pelvic area below the Anterior Superior Iliac Spines (the hip bones).		
	T.4.4.2 The lap belts must not be routed over the sides of the seat. The belts must come through the seat at the bottom of the sides of the seat and continue in a straight line to the anchorage point.		
	T.4.4.3 The seat must be rolled or grommeted where the belts or harness pass through a hole in the seat		
	T.4.4.4 In side view, the lap belt must be capable of pivoting freely by using either a shouldered bolt or an eye bolt attachment.	Visual	
	T.4.4.5 Lap belts must not be mounted by wrapping them around frame tubes.		
	T.4.4.6 With an Upright Driving Position, in side view the lap belt must be at an angle of between 45° and 65° to the horizontal. The centerline of the lap belt at the seat bottom should be between 0 – 75 mm forward of the seat back to seat bottom junction.		

Appendix I: Design Hazard Checklist

ME 428/429/430 Senior Design Project 2019

DESIGN HAZARD CHECKLIST

Team: FSAE MONOCOQUE CHASSIS DEVELOPMENT Faculty Coach: Dr. JOSEPH MELLO

- CHASSIS ONLY, NO OTHER VEHICLE SYSTEMS

Y	N	
☐	☑	1. Will any part of the design create hazardous revolving, reciprocating, running, shearing, punching, pressing, squeezing, drawing, cutting, rolling, mixing or similar action, including pinch points and sheer points?
☐	☑	2. Can any part of the design undergo high accelerations/decelerations?
☐	☑	3. Will the system have any large moving masses or large forces?
☐	☑	4. Will the system produce a projectile?
☑	☐	5. Would it be possible for the system to fall under gravity creating injury?
☐	☑	6. Will a user be exposed to overhanging weights as part of the design?
☑	☐	7. Will the system have any sharp edges?
☐	☑	8. Will any part of the electrical systems not be grounded?
☐	☑	9. Will there be any large batteries or electrical voltage in the system above 40 V?
☐	☑	10. Will there be any stored energy in the system such as batteries, flywheels, hanging weights or pressurized fluids?
☐	☑	11. Will there be any explosive or flammable liquids, gases, or dust fuel as part of the system?
☐	☑	12. Will the user of the design be required to exert any abnormal effort or physical posture during the use of the design?
☑	☐	13. Will there be any materials known to be hazardous to humans involved in either the design or the manufacturing of the design?
☐	☑	14. Can the system generate high levels of noise?
☑	☐	15. Will the device/system be exposed to extreme environmental conditions such as fog, humidity, cold, high temperatures, etc?
☐	☑	16. Is it possible for the system to be used in an unsafe manner?
☐	☑	17. Will there be any other potential hazards not listed above? If yes, please explain on reverse.

For any "Y" responses, add (1) a complete description, (2) a list of corrective actions to be taken, and (3) date to be completed on the reverse side.

Figure 4: Design Hazard Checklist, Page 1

Description of Hazard	Planned Corrective Action	Planned Date	Actual Date
AFTER CHASIS MANUFACTURING, THE FINISHED CHASSIS WILL NEED TO BE POST-PROCESSED TO ALLOW FOR INTEGRATION WITH OTHER VEHICLE SYSTEMS THIS INCLUDES CUTTING AND DRILLING, AND IS TYPICALLY DONE WITH CHASSIS RESTING AT STANDING HEIGHT	WHEN SUPPORTING CHASSIS ON A WORK SURFACE, OR ANY OTHER ELEVATED POSITION WHERE IT HAS THE POTENTIAL TO FALL OFF, HAVE THE CHASSIS SUPPORTED WITH APPROPRIATE BLOCKS, TIE DOWN STRAPS, AND ENSURE THAT ALL INDIVIDUALS WORKING IN THE VICINITY OF THE ELEVATED CHASSIS ARE WEARING THE PROPER SAFETY EQUIPMENT.	N/A	
BEING A CARBON FIBER PART, THERE IS ALWAYS THE POSSIBILITY FOR FIBER SPLINTERS, AND OTHER HAZARDS CAUSED BY THE SHARD NATURE OF INDIVIDUALLY CURED FIBERS, MOST TYPICAL TO BE FOUND NEAR EDGES AND JOINTS.	AFTER THE MANUFACTURING AND POST PROCESSING OF THE CHASSIS, ALL ROUGH OR SHARP EDGES SHOULD EITHER BE SANDED SMOOTH, OR SEALED AWAY AND COVERED WITH AN EPOXY FILLER. THIS IS ALSO USED TO SEAL CORE EDGES, TO PROTECT FILM ADHESIVE FROM FLUIDS SUCH AS ENGINE OIL AND GASOLINE	N/A	
THE MANUFACTURE OF THIS CHASSIS REQUIRES THE USE OF EPOXY RESINS, AS WELL AS THE USE OF ACETONE AS A SURFACE CLEANER AND THE SANDING, CUTTING AND DRILLING OF CURED CARBON, PRODUCING FINE CARBON DUST, AMASKIN, EYE AND LUNG IRRITANT	ALL INDIVIDUALS ASSISTING WITH THE MANUFACTURE OF THE CHASSIS, WHETHER IT IS MOLD MANUFACTURING OR CUTTING AND DRILLING OF THE FINISHED, CURED PART, WILL BE REQUIRED TO WEAR THE NECESSARY PROTECTIVE EQUIPMENT. INCLUDING, BUT NOT LIMITED TO: GLOVES, EYE PROTECTION, COVERALLS, CLOSED TOE SHOES, RESPIRATORS	2/1/2020	
THE EXHAUST AND COOLING COMPONENTS FOR THE COMBUSTION POWERTRAIN GENERATE A SIGNIFICANT AMOUNT OF HEAT, ENDANGERING THE EFFECTIVENESS OF BONDED CONNECTIONS, AS THESE TEMPERATURES CAN EXCEED THE GLASS TRANSITION TEMPERATURE OF THE RESIN, POTTING COMPOUND AND FILM ADHESIVE	ADEQUATE COOLING AND HEAT SHIELDING METHODS WILL BE REQUIRED TO ENSURE THE STRUCTURAL INTEGRITY OF THE CHASSIS AND ITS HARDPOINT MOUNTING.	N/A	

Figure 5: Design Hazard Checklist, Page 2

Appendix J: Failure Modes and Effects Analysis

Product: FSAE CHASSIS

Design Failure Mode and Effects Analysis

Prepared by: DONOVAN ZUSMAN

Team: MONOCOQUE CHASSIS DEVELOPMENT

Date: 10/03/19 (orig)

System / Function	Potential Failure Mode	Potential Effects of the Failure Mode	Severity	Potential Causes of the Failure Mode	Current Preventative Activities	Occurence	Current Detection Activities	Detection	Priority	Recommended Action(s)	Responsibility & Target Completion Date	Action Results: Actions Taken	Action Results: Severity	Action Results: Occurence	Action Results: Criticality
structure / support driving loads	structural failure, loss of stiffness	loss of performance, inability to continue driving	8	core fatigue, delamination, poor manufacturing, incorrect layup, improper prediction of loads	FEA model, validation through testing	7	structural inspections	7	392						
structure / mounting	structural failure	damage to other systems, inability to continue driving	7	core fatigue, delamination, poor manufacturing, incorrect layup, improper prediction of loads	FEA model, validation through testing	7	structural inspections	4	196						
structure / support impact loads	structural failure	injury to driver, damage to other systems, failure to comply with structural regulations	9	core fatigue, delamination, poor manufacturing, incorrect layup, improper prediction of loads	FEA model, validation through testing	8	structural inspections, design feedback (SES judge)	1	72						
driver cell / protect driver	structural failure	injury to driver	10	core fatigue, delamination, poor manufacturing, incorrect layup, improper prediction of loads	FEA model, validation through testing	1	driver feedback	1	10						
driver cell / provide driver comfort	driver uncomfortable	driver fatigue, injury to driver, loss of vehicle performance	5	Poorly designed for humans. Lack of real world input.	Driver input, ergonomics studies	5	driver feedback	1	25						
chassis / aesthetics	chassis is visually unappealing (looks like blord)	loss of design points, lower competition standings	4	lack of effort, poor surface prep	planar geometry, aesthetic design considered	5	visual inspection	2	40						
geometry / subsystem integration	subsystem packaging limited	inadequate system design, poor system interaction	6	lack of effort, poor design	collaboration with subsystems	6	subsystem feedback	2	72						
chassis / lightweight	chassis heavy	loss of performance	6	lack of effort, poor design, improper prediction of loads, overly conservative design	FEA model, validation through testing	6	measure chassis weight	2	72						
chassis / minimize drag	high chassis drag	loss of performance, effect on other systems (aero)	3	poor design	CFD modeling, scale model wind tunnel testing	6	CFD, aero pressure tap data	5	90						
mold / release part	release failure	longer manufacturing times, unhappy workers, poor part quality	5	improper manufacturing, lack of effort, chemical incompatability	chemical trials, refining surface prep techniques	7	check part release during manufacturing	1	35						
mold / reference features	reference misalignment	poor location of important systems, loss of vehicle performance, poor part quality	6	poor referencing, poor locating, equipment limitations	industry input, using capable machines	4	CMM	2	48						

Product: _____

Design Failure Mode and Effects Analysis

Prepared by: _____

Team: _____

Date: _____ (orig)

												Action Results			
System / Function	Potential Failure Mode	Potential Effects of the Failure Mode	Severity	Potential Causes of the Failure Mode	Current Preventative Activities	Occurence	Current Detection Activities	Detection	Priority	Recommended Action(s)	Responsibility & Target Completion Date	Actions Taken	Severity	Occurence	Criticality
mold / ridgidity	unsupportive mold	poor part quality, loss of vehicle performance	5	lack of effort, poor design	industry input, research	5	Visual inspection, Inspect final part for warping	3	75						